2010

Yersinia pestis VIRULENCE FACTOR YopM UNDERMINES THE FUNCTION OF DISTINCT CCR2$^+$Gr1$^+$ CELLS IN SPLEEN AND LIVER DURING SYSTEMIC PLAGUE

Zhan Ye
University of Kentucky, yezhan7477@gmail.com

ABSTRACT OF DISSERTATION

Zhan Ye

College of Medicine

University of Kentucky

2010

Yersinia pestis VIRULENCE FACTOR YopM UNDERMINES THE FUNCTION OF DISTINCT CCR2$^+$Gr1$^+$ CELLS IN SPLEEN AND LIVER DURING SYSTEMIC PLAGUE

ABSTRACT OF DISSERTATION

A dissertation submitted in partial fulfillment of the
requirements of the degree of Doctor of Philosophy in the
College of Medicine at the University of Kentucky

By
Zhan Ye

Lexington, Kentucky

Director: Dr. Susan C. Straley, Professor of Microbiology

Lexington, Kentucky

2010

ABSTRACT OF DISSERTATION

Yersinia pestis VIRULENCE FACTOR YopM UNDERMINES THE FUNCTION OF DISTINCT CCR2$^+$Gr1$^+$ CELLS IN SPLEEN AND LIVER DURING SYSTEMIC PLAGUE

Yersinia pestis, the infective agent of bubonic and pneumonic plague, is classified as a category A agent of bioterrorism. YopM, a protein toxin of *Y. pestis*, is necessary for full virulence in a systemic plague mouse model with ambient-temperature grown bacteria. We used this model to identify the cells undermined by YopM. Natural killer (NK) cells were previously reported to be lost in spleen and blood in a YopM-associated way; however, NK cell depletion was found not to occur in liver, and ablation of NK cells had no effect on bacterial growth, indicating that NK cells are redundant for the YopM-mediated virulence mechanism. In mice either ablated for Gr1$^+$ cells or lacking the chemokine receptor CCR2, wildtype growth was at least partially restored to the *ΔyopM Y. pestis* in both spleen and liver. In a mouse model of bubonic plague, CCR2 also was shown to be required for the *ΔyopM Y. pestis* to show wildtype growth in skin. These data pointed towards Gr1$^+$CCR2$^+$ cells, which include polymorphonuclear leukocytes (PMNs), inflammatory monocytes and inflammatory dendritic cells (iDCs), as key cellular components in controlling the *in vivo* growth of the *ΔyopM Y. pestis*. Recruitment of Gr1$^+$CCR2$^+$ cells into both organs was not YopM-dependent, except iDCs, whose influx from blood into spleen was blocked by the YopM-producing *Y. pestis* parent strain, but not the *ΔyopM* mutant. Ablation of PMNs, another main subset of Gr1$^+$CCR2$^+$ cells, relieved the growth limitation of the *ΔyopM Y. pestis* in liver, but not in spleen. Taken together, the data imply that YopM disables the recruitment of CCR2$^+$Gr1$^+$ iDCs into spleen but compromises the function of CCR2$^+$Gr1$^+$ PMNs in liver. These results were recapitulated when the infecting ambient-temperature-grown bacteria received 3 hours of incubation at 37°C. However, the appearance of the *ΔyopM* mutant phenotype was postponed at least 24 hours, indicating that some virulence property of *Y. pestis* that was induced by the temperature transition compensated for the loss of YopM in the *ΔyopM* strain at an early stage of the infection. In general, these findings provide a framework for focusing future research to identify YopM's direct molecular targets.

KEYWORDS: YopM, CCR2, Gr1, PMNs, iDCs

Zhan Ye

10/04/2010

Yersinia pestis VIRULENCE FACTOR YopM UNDERMINES THE FUNCTION OF DISTINCT CCR2$^+$Gr1$^+$ CELLS IN SPLEEN AND LIVER DURING SYSTEMIC PLAGUE

By

Zhan Ye

Susan C. Straley

Director of Dissertation

Beth A. Garvy

Director of Graduate Studies

10/04/2010

Date

RULES FOR THE USE OF DISSERTATIONS

Unpublished dissertation submitted for the Doctor's degree and deposited in University of Kentucky Library are as a rule open for inspection, but are to be used only with due regard to the rights of the authors. Bibliographical references may be noted, but quotations or summaries of parts may be published only with the permission of the author, and with the usual scholarly acknowledgements.

Extensive copying or publication of the dissertation in whole or in part also requires the consent of the Dean of the Graduate School of the University of Kentucky.

A library that borrows this dissertation for use by its patron is expected to secure the signature of each user.

Name   Date

_____

_____

_____

_____

_____

_____

_____

_____

_____

_____

_____

DISSERTATION

Zhan Ye

College of Medicine

University of Kentucky

2010

Yersinia pestis VIRULENCE FACTOR YopM UNDERMINES THE FUNCTION OF DISTINCT CCR2$^+$Gr1$^+$ CELLS IN SPLEEN AND LIVER DURING SYSTEMIC PLAGUE

DISSERTATION

A dissertation submitted in partial fulfillment of the
requirements of the degree of Doctor of Philosophy in the
College of Medicine at the University of Kentucky

By
Zhan Ye

Lexington, Kentucky

Director: Dr. Susan C. Straley, Professor of Microbiology

Lexington, Kentucky

2010

For my loving wife, Guangfan

ACKNOWLEGEMENTS

This dissertation would not have been written without the contribution from many people. I owe my gratitude to all those people who have made this dissertation possible and because of whom my graduate experience has been one that I will cherish forever.

My deepest gratitude is to my mentor, Dr. Susan Straley. I have been amazingly fortunate to have an advisor who gave me the guidance to recover when my steps faltered and also gave me the freedom to explore by my own. Her patience and support helped me to overcome many crisis situations and finish this dissertation. I am also indebted to the past and present members of Straley Lab, Clarissa Cowan, Amanda Gorman, Tanya Myers-Morales, Annette Uittenbogaard, Christine Wulff-Strobel, for their generous helps in my experiments and providing a great working atmosphere in the lab.

I would like to thank the members of my committee, Dr. Donald Cohen, Dr. Sarah D'Orazio, Dr. Alan Kaplan, Dr. Rebecca Kellum and Dr. Jerold Woodward. Their insightful comments and constructive criticisms at different stages of my research were thought-provoking and helped me to complete my dissertation. In particular, I am deeply grateful to Dr. Kaplan and Dr. Cohen, who served as co-mentors in my committee, for their guidance and advice in the design of my experiments. They have been always ready to discuss difficulties in my research and help me to sort out the technical problems in my work. Additionally, I would also like to thank Dr. Isabel Mellon for her willingness to serve as my outside examiner.

TABLE OF CONTENTS

LIST OF TABLES

LIST OF FIGURES

Chapter One: Introduction

A. Plague and *Yersinia pestis* natural history

a) **Natural history and major clinical forms of plague**

Plague, a deadly infectious disease caused by the gram negative bacterium, *Yersinia pestis*, has caused widespread loss of human life during recurrent pandemics. Three pandemics in human history were recorded. The first pandemic, named the Justinian plague (541–767 A.D.) killed 100 million people in Europe and Asia. The second pandemic, named the Black Death (1346-19th century), spread over 3 major continents including Asia, Europe and Africa and reduced the world's population from 450 million to between 350 and 375 million. The third pandemic began in China in 1855 and for the first time was recognized to be transmitted by two different sources: bubonic plague transmitted through infected rats and fleas and pneumonic plague with direct person-to-person transmission. This modern plague became a global threat after the bacteria from the high-mortality 1894 epidemic in Hong Kong were disseminated by marine shipping to Hawaii and finally reached San Francisco. After more than one century of effort since Alexandre Yersin and Shibasaburo Kitasato isolated the bacterium of the Hong Kong epidemic, plague is believed to be curable and only draws some historical interest. However, plague's geographic range has expanded greatly, and *Y. pestis* poses new threats in previously unaffected regions, including the western United States (Figure 1.1). Epidemics still occur frequently in developing countries where people live in unsanitary, rat-infested environments, for example, the 1994 pneumonic plague outbreak in India and ongoing outbreaks in South America and Africa (92, 106, 315) . The concern about the

potential use of *Y. pestis* as a bioterrorism weapon is increasing because *Y. pestis* can be used in an aerosol attack that causes an outbreak of pneumonic plague. Further, because of the delay between exposure to *Y. pestis* and becoming sick, infected people could travel over a large area and possibly spread the bacteria to others, which makes controlling the disease more difficult. A bioweapon carrying *Y. pestis* is possible because the bacterium is available and could be isolated and grown in quantity in a laboratory, even though manufacturing an effective weapon using *Y. pestis* would require advanced knowledge and technology.

Clinically, there are three major forms of plague, bubonic, pneumonic and septicemic.

Bubonic plague is a rodent-associated, flea-borne zoonosis. *Xenopsylla cheopis* (the oriental rat flea) is considered the classic vector because of its role in the last pandemics. However, over 31 species of flea have been proven to be vectors of plague, and their importance in *Y. pestis* transmission depends on the region. For example, *Oropsylla montana* (the rock squirrel flea) is more potent than *X. cheopis* in the western US (245).

When a flea leaves its dead host and bites a human, the bacteria will enter into the skin tissue through regurgitated blood from the flea (Figure 1.1). Even when phagocytosed by macrophages, *Y. pestis* can survive and reproduce inside the cells. After adaptation to the microenvironments in flea bite sites, the bacteria can enter the lymphatic system until they reach a lymph node, where they stimulate severe haemorrhagic inflammation that causes the lymph nodes to expand. The expansion of lymph nodes is the cause of the characteristic "bubo" associated with the disease (251).

The bacteria rapidly enter into the bloodstream via the lymphatics so that they can travel to anywhere in the body. At this stage, bubonic plague progresses to septicemic

plague (142, 245). In septicemic plague, bacterial endotoxins can induce disseminated intravascular coagulation (DIC). Some of these clots can clog the vessels and cut off blood supply to various organs such as the liver, brain, or kidney. These organs will then stop functioning. Over time, the clotting proteins are consumed, and bleeding into the skin and other organs occurs, which manifests as a red and/or black patchy rash and hemoptysis (coughing up or vomiting of blood). While septicemic plague is usually secondary to lymphadenitis, patients with septicemic plague sometimes have no history of a bubo, and this clinical form has been termed primary septicemic plague. Untreated septicemic plague is usually fatal and the patients often die on the same day symptoms first appear.

The third form is pneumonic plague that can be caused by two ways, primary and secondary (138, 245). Secondary pneumonic plague is the typical one and develops secondarily to either bubonic or septicemic plague. Primary pneumonic plague is rare and caused by person-to-person transmission through a bacteria-containing aerosol. The incubation period for pneumonic plague is usually between two and four days, but can be as little as a few hours. The initial symptoms are fever, weakness and headache, which make it indistinguishable from viral flu. However, this disease can rapidly progress to pneumonia with shortness of breath, chest pain, cough and hemoptysis. Without diagnosis and treatment, the patient will die from respiratory failure and shock in one to six days; mortality in untreated cases is approximately 100%.

b) Clinical diagnosis and treatment

Because of the rapid progression of the disease, a clinical diagnosis of plague is

generally based on the symptoms and exposure history. For example, if a patient has a history of contact with rodents or other wild animals in the southwestern area of the United States and developed a painful, swollen lymph node and high fever, bubonic plague should be suspected. Septicemic plague and pneumonic plague are more difficult to diagnose because they display non-specific gram-negative septicemia and pneumonia symptoms, respectively, instead of the distinctive "bubo" in bubonic plague. As soon as plague is suspected, different samples, such as blood, bubo aspirates, sputum, and scrapings from skin lesions, should be obtained for laboratory diagnosis. However, treatment should start immediately while waiting for the laboratory results.

A laboratory diagnosis of plague includes tests based on bacteriologic and serological evidence (245). Staining techniques such as the Gram, Giemsa, Wright, or Wayson stain can provide supportive but not presumptive or confirmatory evidence of a plague infection. A new rapid diagnostic test that uses fluorescent antibody against the fraction 1 (F1) antigen, a pilus antigen expressed predominantly at 37ºC, has recently shown promise for early detection of plague. Alternative methods for diagnosing plague have been developed, including enzyme linked immunosorbent assays (ELISA), PCR analysis, and DNA hybridization. However, none of these techniques has been developed sufficiently and evaluated to be used routinely by clinical laboratories. To confirm a diagnosis of plague, it is necessary to isolate the organism from the samples collected from the patient. *Y. pestis* grows slowly and may require more than 48 hours to form visible colonies. The optimal growth occurs at 28°C. Blood culture results are positive in 85-96% of patients, and bubo aspirate culture results are positive in 80-85% of patients, while sputum culture results are positive only if lung involvement is present.

All patients suspected of having bubonic plague should receive supportive care, such as crystalloid infusion and administration of oxygen, as well as isolation for at least 48 hours after starting antibiotic treatment to prevent the potential spread of the disease in case the patient develops secondary plague pneumonia. Early administration of antibiotics is essential. Drugs that cover *Y. pestis* should be given empirically to any patient with predisposing risk factors and signs and symptoms of plague. The antibiotics usually used in anti-plague treatment include gentamicin, streptomycin sulfate, chloramphenicol**,** doxycycline**,** ciprofloxacin**,** tetracycline and co-trimoxazole. Antibiotic treatment duration should be 10 days. In severe cases, a 2-drug regimen should be used. The tetracyclines are popular antibiotics for plague prophylaxis (211, 245).

c) Vaccines

Although plague can be cured these days, the potential for rapid spread still raises a concern for public health. Meanwhile, the individuals who might be exposed to *Y. pestis*, e.g. veterinarians, scientists engaged in research with *Y. pestis* and individuals who are travelling to parts of the world where the disease is endemic, are at high risk for the disease and should be vaccinated. Therefore, in the long term, prophylactic vaccination against this disease holds the brightest prospect for its control.

Both live and killed vaccines have been used. The live vaccine was derived from an attenuated strain (EV76), while a killed vaccine (named USP) used a formalin-fixed virulent strain of *Y. pestis* and relied on the *Y. pestis*-specific F1 fibril protein as the principal immunogen (212). The killed vaccine was used in people from the late 1890s and although evidence indicates that these formulations reduced the incidence of bubonic

5

plague (62), there is no evidence that they are effective against pneumonic plague in humans (67). While the live EV76 vaccine conferred greater protection against infection with WT *Y. pestis*, this vaccine caused severe adverse reactions (198, 275), not to mention the quick waning of the protective responses induced by this vaccine (245).

Therefore there is need to seek new plague vaccines. The virulence factors produced by the plague bacterium have been studied because of their potential immunogenic and protective properties. Foremost amongst these have been the F1 proteins and V antigen plus Yops (Yersinia outer proteins), which will be described in the next section. As potential vaccine candidates, F1 and V antigen have been studied separately (11, 184, 227) and a combination of them has been formulated (126, 358). The latter candidate showed not only significantly greater protective efficacy than the killed vaccine, but also protected against pneumonic plague in a murine model (359).

B. The virulence properties and transmission properties of *Y. pestis*

a) The Transmission Cycle of *Y. pestis*

As shown in Figure 1.2, *Y. pestis* is maintained in nature through transmission between hematophagous adult fleas and certain rodent hosts including wild and domestic rodents (106). Humans are dispensable in the maintenance of *Y. pestis*. Fleas acquire *Y. pestis* from an infected blood meal and the bacteria are restricted to the digestive tract of the flea. The organisms multiply in the midgut (stomach) of the flea, and the stomach exhibits clusters of brown specks containing *Y. pestis* after 2 days.

A bacterial biofilm, which is a dense aggregate of microorganisms embedded in an extracellular matrix (ECM) and usually attached to a surface, is formed by *Y. pestis* on

the flea spines that line the interior surface of its proventriculus, a valve guarding the entrance to the midgut (149). Growth and consolidation of the biofilm interferes with the patency of the proventricular valve as well as the passage of blood into the midgut (22, 245). Between days 3 and 9 after the infected blood meal, the bacterial masses may completely block the duct between the stomach and the esophagus; then no further blood meal can access the stomach. Blocked fleas make frequent, persistent attempts to take a blood meal before they die from starvation. The blood sucked by the hungry flea is mixed with the bacteria and regurgitated as aggregates coated with polysaccharide (bacterial biofilm) into the mammalian host. It is worth noting that the unblocked flea also can transmit *Y. pestis*, although fleas with a completely blocked proventriculus make prolonged and repeated attempts to feed, which increases the opportunity for transmission (92).

When the infected flea bites a human, the bacteria in the regurgitated blood are injected into the dermis layer of skin (289). Due to the lower temperature (<28ºC) in the flea gut, *Y. pestis* cells released from fleas are readily phagocytosed by polymorphonuclear leukocytes (PMNs) and monocytes, although these bacteria can express some antiphagocytic properties such as insecticidal-like toxins complex (343). Cells phagocytosed by PMNs are largely destroyed, while those engulfed by resident mononuclear cells such as macrophages are believed to grow intracellularly and develop resistance to further phagocytosis (63, 185).

Then *Y. pestis* spreads from the flea bite site to the regional lymph nodes and multiplies there to high numbers, causing formation of a bubo. After that the infection spreads into the bloodstream, liver, spleen and other organs, which means that bubonic

plague progresses to septicemic plague (245). In 5% of human cases, *Y. pestis* spreads hematogenously to the lungs and causes pneumonic plague (289). Bubonic plague does not transmit directly between human patients; however, pneumonic plague is easily spread from one patient to another through aerosols containing *Y. pestis*. Meanwhile, since the bacterium transmitted this way comes from the mammalian hosts, the infecting *Y. pestis* is fully armed with thermally up-regulated virulence properties. The immunosuppressive bias of the lung and absence of acute inflammation for 36-48 h after infection allow rampant bacterial proliferation (173). Therefore, the incubation time is shorter and the mortality rate is much higher than those in bubonic plague.

Yersinia pestis was evolved from the oral-fecal pathogen *Yersinia pseudotuberculosis* (2). At least three human pathogenic biovars of *Y. pestis* were identified through metabolic and genomic studies, based mainly on their abilities to ferment glycerol and reduce nitrate. These three biovars, named Antiqua, Medievalis, and Orientalis, were thought to be associated with the three plague pandemics (1, 2). However, there is no direct evidence connecting any of the biovars with historical plague. Furthermore, the correlations between geography and history are based exclusively on the three classical biovars and do not take into account isolates of "atypical" *Y. pestis* that do not fit into the classical biovars, i.e. so-called pestoides and microtus (13, 372). It is suggested that *Y. pestis* should be subdivided into populations based on molecular groupings, rather than biovars. Eight populations, which do not correspond directly to classical biovars, were recognized (1).

Y. pestis cycles between a mammal and a flea vector and expresses distinct subsets of genes in its two hosts. Products encoded by the genes specifically required to infect and

cause disease in the mammalian host are referred to as virulence factors and the properties in *Y. pestis* that enable it to be transmitted by flea are termed transmission factors. Five transmission factors of *Y. pestis*, murine toxin (MT), F1 capsule, plasminogen activator (Pla), hemin storage locus *(hms)* encoding enzymes and insecticidal toxin compex that are involved specifically in flea-borne transmission have been identified, and their properties are listed in Table 1.1. It is worth noting that *Y. pestis* diverged from its *Y. pseudotuberculosis* ancestor only within the last 10,000-20,000 years and *Y. pseudotuberculosis* is transmitted through the oral-fecal route only between mammalian hosts. Therefore, some of these transmission factors were acquired during the evolution from *Y. pseudotuberculosis* to *Y. pestis* (for example, pMT and Pla (58), F1 (66) and biofilm (95)). Their functions favor the growth of bacteria in the internal environment of the flea (such as MT and biofilm), promote transmission and dispersal (F1), and promote the dissemination of the bacteria in the mammalian host after inoculation by a flea bite (such as Pla). Meanwhile, some of these factors (MT and biofilm) are sensitive to the culture temperature, which means that they are highly expressed at the temperature in the flea (26°C) and downregulated at the internal temperature of the mammalian host (37°C). Both transmission and virulence factors will be discussed below in detail.

b) Major Chromosomal Virulence Factors of *Y. pestis*

In humans, half of the iron is in hemoglobin and one-tenth is in cellular proteins that use iron for important cellular processes like storing oxygen (myoglobin) and performing energy-producing redox reactions (cytochromes). A small amount of iron circulates

through the plasma, bound in transferrin. Some iron in the body is stored. Physiologically, most stored iron is bound by ferritin molecules; the largest amount of ferritin-bound iron is found in liver hepatocytes, the bone marrow and the spleen. Macrophages of the reticuloendothelial system store iron as part of the process of breaking down and processing hemoglobin from engulfed red blood cells. The mammalian host has developed many mechanisms to inhibit the amplification of the invading pathogens by limiting the nutrients necessary to their growth. Iron sequestration by mammalian proteins is one of the most important ones (56). Therefore the ability of a bacterium to compete with the host for iron should be important to its virulence.

Analysis of the KIM genome has identified 16 putative iron transport systems (103). The 16 systems can be divided into 4 categories: siderophore-dependent systems, ABC iron transporters, non-ABC iron transporters, and hemin transporters.

A siderophore is a small compound that is synthesized and secreted by the bacterium to acquire iron from the environment. The yersiniabactin (Ybt) system is the only one with a clear function in this category. The Ybt system is essential for virulence of *Y. pestis* from infection by subcutaneous routes and important for iron acquisition in early stages of the bubonic plague in mice (29). The genes encoding the Ybt system are located in the pigmentation locus (*pgm*), which is a large unstable area of *Y. pestis* chromosomal DNA (102-kb) (99). The *pgm* locus is composed of a ~35 kb iron acquisition segment linked to a ~68 kb pigmentation segment (55). This iron acquisition segment is considered to be a high-pathogenicity island (HPI) (59) and contains a cluster of genes encoding the iron-regulated proteins (*irp),* yersiniabactin siderophore biosynthetic and transport proteins (*ybt*) and the pesticin/yersiniabactin outer membrane receptor (*psn*)

which are involved in the iron-regulated biosynthesis and transport of the Yersiniae siderophore Ybt. *Δpgm* cultures are bacteria highly attenuated in mice inoculated via peripheral routes, while they are fully virulent by the intravenous (IV) route of infection because they can get iron from blood (99).

The second category, ABC transporters, is generally composed of a solute-binding protein in the periplasm along with an inner membrane permease and an inner membrane-associated ATPase. Yfe, an ABC transporter for both manganese and iron, has been found to be important for full *Y. pestis* virulence in a bubonic plague mouse model (30). Other ABC transporters for iron (Yfu and Yiu) and hemin transporters (Hmu, encoded by *hmu* (hemin uptake locus)) have been functionally characterized, but were not found to be required for virulence in the mouse model (115, 160, 334).

In *Y. pestis,* the iron acquisition and transport systems are under the regulation of a ferric uptake regulation (Fur) protein encoded by the *fur* gene located in another area of the chromosome outside the iron acquisition segment (312).

The second important component of *pgm* is the *hms* locus, which is located in the pigmentation segment of *pgm* and is responsible for binding hemin and Congo red, causing the so-called pigmented phenotype (Pgm$^+$) of colonies grown on Congo red-agar plates (55). The *hms* locus contains a 4-gene operon, *hmsHFRS*. There are also two unlinked genes not in the *pgm* locus, *hmsT* and *hmsP*, which are essential for the normal pigmentation phenotype. HmsH and HmsF were characterized as surface exposed outer membrane proteins, and HmsR, and HmsT contain transmembrane domains and appear to be inner membrane proteins. The function of the *hms* gene products are similar to glycosyl transferase and polysaccharide deacetylase enzymes in other bacteria that are

11

required to produce extracellular polysaccharides (134). Therefore, hms gene products mediate the production of biofilm which blocks the foreguts of vector fleas, as described in B a) **The Transmission Cycle of *Y. pestis*** (135). Grown at ambient temperature in the flea or *in vitro*, *Y. pestis* synthesizes an ECM of poly-β-1,6-linked *N*-acetyl-D-glucosamine (β-1,6-GlcNAc) that is essential for biofilm formation. Biofilm formation is sensitive to the culture temperature and is downregulated at mammalian internal temperature (37°C) (95, 149).

c) Major Plasmid Virulence Factors of *Y. pestis*

All of the *Y. pestis* strains contain three plasmids of 9.5, 70 to 75, and 100 to 110 kb. In strain KIM derivatives, these three plasmids are termed pPCP1 (Pesticin, Coagulase, Plasminogen activator), pCD1 (Calcium Dependence), and pMT1 (245), respectively.

The multicopy pPCP1 encodes three proteins: Pla, the bacteriocin pesticin (Pst), and the pesticin immunity protein (Pim) (245, 303). Loss of the 9.5-kb plasmid results in greatly decreased ability of *Y. pestis* to cause its usual systemic infection following subcutaneous inoculation or intraperitoneal injection and attenuates *Y. pestis* by a millionfold in a subcutaneous infection model (51, 303, 304). Pst is a muramidase that can slowly hydrolyze murein in the bacterial wall and convert bacterial cells into stable spheroplasts (350). Whereas Pim is located in the periplasma and inactivates the Pst before it degrades murein of the Pst producing bacterium (248). Studies on rats infected through flea transmission or intradermal (ID) injection showed that the *pla* gene is not only one of the most highly expressed genes in the bubo but also indispensable for the establishment of bubonic plague (289, 290). However, primary septicemic plague does

not depend on Pla (289), and Pla is not required for virulence (lethality) of *Y. pestis* in pneumonic plague but it is required for the bacterial colonization of the lung (174).

Pla is a highly abundant integral outer membrane protein expressed more strongly at 37°C than 26°C. As a proteinase, the main virulence function of Pla is to convert plasminogen (Plg) to plasmin (Pln) through cleavage. It also increases the activities of plamin by inactivating the main Pln control protein α2-antiplasmin (164). The major function of plasmin is fibrinolysis which may support bacterial dissemination and evasion of innate immune surveillance systems (80). Meanwhile, Pla is also thought to promote bacterial spread by digesting laminin of basement membranes and activating collagenases and gelatinases, which further damage the tissue barriers (169). Pla has nonproteolytic functions in adhesion of *Y. pestis* to extracellular matrix components such as laminin, the major glycoprotein in basement membranes, and it can promote invasion of *Y. pestis* into epithelial cells *in vitro* (75, 170, 322). These effects could underlie its colonization role in the lung in pneumonic plague. Further, Pla promotes invasion of alveolar macrophages by binding to c-type lectin receptor, DEC-205 (CD205), and this interaction promotes bacterial dissemination from lung to spleen in pneumonic plague (371). Thus, Pla is multifunctional but its predominant role in bubonic plague is thought to be to promote hemorrhagic dissemination of the bacteria from the primary site of infection. Meanwhile, it is believed that the major late pathologic manifestation of untreated human plague is related to the plasmid-encoded plasminogen activator activities (303).

The 70-kb plasmid pCD1 encodes the Yop virulon, which is comprised of three components: the Yop effector virulence proteins, the Ysc (Yop secretion) system , i.e. Yop translocon and injectisome for secreting Yops out of the bacterial cell, and the

injectisome tip complex of so-called translocator Yops which is necessary for injecting the effector Yops into host cells (73, 245) (Figure 1.3).

Before contact with eukaryotic target cells, *Yersinia* bacteria incubated at the temperature of their mammalian host (37°C) build several syringe-like Ysc injectisomes at their surface (74). These are protein pumps spanning the peptidoglycan layer and the two bacterial membranes and topped by a stiff needle-like structure protruding outside the bacterium. The whole organelle is comprised of 27 proteins. The internal part contains 10 proteins, which include an essential part of the pump, the ATPase (YscN). The part of the injectisome that spans the bacterial outer membrane is a homomultimeric ring-shaped structure. The Ysc injectisome ends with a needle formed by the polymerization of monomers of the YscF protein (Figure 1.3). Through the Ysc injectisome effector Yops can be efficiently targeted into the host cytosol without "leaking" into the extracellular space. The six injected effector Yops favor the growth of invading bacteria in mammalian hosts through several mechanisms, such as disrupting phagocytosis, blocking the production of proinflammatory cytokines and perturbing the dynamics of the cytoskeleton (337) (Figure 1.4, see further discussion below).

The largest plasmid pMT contains the gene encoding the so-called murine toxin (Ymt) and the structural gene for the F1 protein fibrillar capsule (245). Murine toxin refers to two forms of a protein (native polymers of 240 and 120 kDa) toxic only for mice and rats but not to other animals (136, 283). Murine toxin was shown in early studies to have β-adrenergic blocking ability (48) and its toxic function was manifested by hypotension and vascular collapse when it was released from lysing bacteria at the terminal stage of septicemic plague (283). However, this toxin later was found to be a phopholipase D and

to be more important for the growth of the bacteria in the flea gut (136) instead of in mice, since deletion this *ymt* gene does not significantly increase the lethal dose in mouse infection (137).

The *caf1M1A1* operon in pMT encodes a pilus called F1 and referred to in the plague literature by the misnomer "capsule". The production of F1 is strongly dependent on the temperature, which must be at least 35°C (89). Therefore, no F1 capsule is detected in the flea gut, whereas *caf1* is one of the most highly expressed genes during infection of the mammal. A coating of F1 fibrils encapsulates *Y. pestis* in vivo and causes interactions with host cells to be inefficient, thereby protecting the bacteria from phagocytosis and contributing to virulence in systemic plague (49, 89). The F1 fibrils are highly immunogenic (65, 290), which makes F1 antigen a promising candidate for plague vaccine development (11). Interestingly, the virulence of *Y. pestis* is not affected by the deletion of the *caf1* gene in ID or IV infected mice. However, F1 capsule is indispensable for full virulence in the flea-transmitted bubonic plague model (288), indicating the importance of F1 in the natural transmission of *Y. pestis.*

C. Delivery of Yops by Type III Secretion System (T3SS)

a) T3SS

The T3SS is an export machine used by pathogenic Gram-negative bacteria to deliver proteins straight into the eukaryotic cytosol with the aim to subvert the host cell defense (41, 107). Made up of more than 20 proteins, the T3SS is among the most complex protein secretion systems known in Gram-negative bacteria. Its structure shares many similarities with bacterial flagella (long, rigid, extracellular structures used for motility)

and some of the proteins participating in the T3SS share amino-acid sequence homology with flagellar proteins. The basic structure of the T3SS consists of the membrane-embedded basal body, the needle and the tip structure, except the flagellar translocon (the ancestral T3SS) that does not have a needle or function for injecting into eukaryotic cells. As the central component of the typical T3SS, the needle complex is a supramolecular structure that mediates the passage of the secreted proteins through the multi-membrane bacterial envelope. There are two hallmarks of the T3SS: the protein substrates are selected by the system through recognition of an N-terminal recognition sequence of amino acid and/or mRNA codons without cleavage; then these proteins pass through two bacterial membranes without a periplasmic intermediate (bypassing Sec system). The T3SS is used by Gram-negative bacteria to secrete proteins that help the bacteria infect multicellular, eukaryotic organisms. The proteins are secreted directly from the bacterial cell into the cells of the organism to be infected (the host) using a needle-like structure which is the hallmark of the T3SS.

The T3SS proteins can be grouped into three categories: (1) structural proteins building the base, the inner rod and the needle (2) effector proteins secreted into the host cell to promote infection (3) chaperones binding effectors in the bacterial cytoplasm and protecting them from aggregation and degradation and directing them towards the needle complex. Secretion by the T3SS is triggered by contact of the needle with a host cell. T3SS effectors manipulate host cells in several ways, such as antiphagocytosis and induction of apoptosis (74, 132).

b) The signals for secretion of effector Yops

The internal diameter of the needle-like injectisome is not large enough for the fully folded effector Yops to pass through (73); thus the Yops must transit in a partially unfolded state and there must be some signals mediating the translocation of Yops, although no classical signal sequence has been found in the amino acid sequence in those Yops (214). Fifteen codons at the N-terminus have been confirmed necessary for Yop secretion (307); however, changes in the amino acid sequence by point or frameshift mutations could not block the secretion of YopE, YopN and YopQ (8, 9) and led to the idea that the 5' end of the mRNA is the true signal for secretion; thus secretion was hypothesized to occur concomitantly with Yop mRNA translation.

This hypothesis could be true for the late phase of interaction of a yersinia with a host cell but is problematic in the early phase, in which antiphagocytic responses mediated by Yops happen very fast and cannot be explained by this co-translational translocation model. Meanwhile, export and translocation of some antiphagocytic Yops, such as YopE and YopH, have been proven to be controlled at the posttranslational level (39, 114); and the mutation of the first 11 codons without alteration of the amino acid sequence does not block the secretion of YopE (188). Therefore, the signal for the initial secretion is likely to be in the amino acid sequence, instead of in the Yop mRNA.

Another group of proteins named Syc (Specific Yop Chaperone) are also necessary for the secretion of some (but not all) Yops by keeping these Yops in a "secretion competent" state (unfolded or partially folded conformation which is easy to pass through the injectisome) (36, 314, 356, 357). Each Syc protein binds only to a specific partner Yop, for example, SycE specifically binds YopE (Figure 1.4), and in general, the gene encoding each Syc protein is located beside the gene encoding the corresponding Yop.

The Syc proteins are indispensable because the secretion of each Yop is significantly impaired without its specific Syc.

c) Contact between bacterium and eukaryotic cell

Once the bacteria enter into the mammalian host and reach a temperature of 37°C, the injectisomes start to be assembled and the bacteria begin to synthesize Yops. However, before the bacterium contacts a eukaryotic host cell, Yops stay in the cytosol instead of being expelled into the extracellular space. Actually, to avoid the deleterious effect of excessive Yops on the bacterium itself, the production of Yops is also closely controlled before the physical contact between bacterium and host cell is established (72).

The required contact is not accomplished by the injectisome itself but by the interaction between bacterial outer membrane proteins called adhesins and host molecules at the surface of a target cell (Figure 1.4). Potential adhesins expressed by *Y. pestis* are Pla, pH 6 antigen (Psa) and attachment-invasion locus (Ail). Pla is encoded by pPCP1 and its function has been described in detail in section **Major Plasmid Virulence Factors of *Y. pestis***.

A fimbrial adhesin, *Y. pestis* pH 6 antigen, whose encoding gene is located on chromosome (186), was named for its regulated expression because it is expressed only when the bacteria grow between pH 5 and 6.7 at temperatures of 35 to 41 $^{\circ}$C. It is reported that Psa is involved in the binding of *Y. pestis* to target cells to allow effective intracellular delivery of Yops (316). More recent studies showed that Psa uses the phosphorylcholine moiety of phosphotidylcholine as a receptor to mediate bacterial binding to pulmonary surfactant and alveolar epithelial cells (108). *Y. pestis* lacking the

fimbrial subunit PsaA is deficient in dissemination during bubonic plague and, to a lesser degree, during pneumonic plague (61).

However, a pH 6 antigen mutant only has a modest decrease in virulence via the IV, subcutaneous (SC), or intranasal (IN) routes of infection (61, 173, 186), and the expression of pH 6 antigen is greatly downregulated in a mouse model of pneumonic plague due to fully virulent *Y. pestis* (173). Thus, other adhesins may be required for *Y. pestis* Yop delivery. The Ail outer-membrane protein, which binds host fibronectin (339), was found to be the predominant adhesin for Yop delivery *in vitro* when the *Y. pestis* strain KIM5 was grown at 28 ^{o}C, and deletion of *ail* from KIM5 increased the LD$_{50}$ ca. 3000 fold in Swiss Webster mice (98).

Yaps *(Yersinia* Autotransporter Proteins), another potential group of adhesins, were also found recently. Autotransporters are a family of proteins secreted by the type V secretion mechanism, in which the secreted protein contains all of the necessary information to mediate translocation across the bacterial outer membrane after passing through the inner membrane via the Sec system (129). The autotransporter YadA, which is indispensable in *Y. pseudotuberculosis* and *Y. enterocolitica*, does not contribute to *Y. pestis* virulence since it is only a pseudogene in *Y. pestis* (302). However, another autotransporter, YapE, has been proven to be important in efficient *Y. pestis* CO92 colonization in C57B/6 mice, as well as for the binding of *Y. pestis* to eukaryotic cells (177).

d) Effector Yops injected into eukaryotic cells by translocators

The injectisome, as described here, is sufficient for bacteria to secrete Yops into their

surrounding environment but it is not sufficient for the injection of Yops into target animal cells. A group of proteins, or translocators, include YopB, YopD, and LcrV, and form a transient pore structure in the eukaryotic cell membrane. YopB and YopD contain hydrophobic regions that are predicted to function as transmembrane domains (73). However, only YopB is actually detected in the host cell membrane, and LcrV may act like a chaperone for YopB and YopD. YopD may act to facilitate insertion of YopB in the host cell membrane (74).

Interestingly, LcrV (low calcium response protein V, the V antigen mentioned earlier in the context of plague vaccines) lacks a predicted transmembrane domain and exists as a soluble dimer in solution. Unlike Yops B and D, LcrV is a multifunctional protein. As a structural component of the translocon within the bacterial cytoplasm, LcrV permits Yops secretion by forming a stable complex with a negative regulatory protein, LcrG (199). Before the bacterium contacts a eukaryotic cell or when *Y. pestis* is cultured in the presence of millimolar calcium, the level of LcrV in the cell is low so that LcrG blocks the Ysc from the cytoplasmic face of the inner membrane. As soon as the physical contact between bacterium and host cell is established or calcium is removed from the medium, levels of LcrV are increased and the excess LcrV titrates LcrG away from the Ysc, allowing secretion of Yops to occur.

In addition, LcrV is released in large amounts into the surrounding medium and may silence host immune cells which do not contact *Yersinia* directly (10, 227, 246). LcrV may bind a Toll-Like Receptor (TLR)2/6 complex and elicit production of the anti-inflammatory cytokine interleukin (IL)-10 (50, 84). Further, unlike effector Yops, LcrV can enter cells by a novel T3SS-independent mechanism after *in vitro* infection. LcrV co-

localizes with endosomal proteins between 10–45 min of infection, followed by lysosomal protein(s) between 1– 2 h. After 2.5–3 h of infection, V was observed in conjunction with mitochondrial proteins, and subsequently with Golgi protein(s) between 4–6 h of infection (87, 100). However, its activity and interactions inside host cells are not known.

e) The functions of the effector Yops

The T3SS delivers the set of six Yop effector proteins into host cells once the bacteria contact host target cells at mammalian body temperature. Enzymatic and cell biological mechanisms of five of the Yops, YopH, YopE, YopT, YpkA/YopO and YopJ/YopP, have been elucidated.

YopJ inhibits activation of MAP kinase kinases (MKKs) and nuclear factor-κB (NF-κB) signaling through acetyltransferase or ubiquitin-like cysteine protease activities (228, 234) (Figure 1.5) but is not required for virulence in either a mouse model of systemic plague (317) or mouse and rat models of bubonic plague (180, 369). *Y. pestis* was found to suppress the secretion of tumor necrosis factor-α (TNF-α) and phosphorylation of mitogen-activated protein kinase (MAPK) in a YopJ specific manner in *in vitro* infected macrophage cells as efficiently as enteropathogenic *Yersinia*, but was less able to activate caspases, suppress NF-κB activation, and induce apoptosis in macrophages than the high-virulence *Y. enterocolitica* WA O:8 strain. The lower efficiency of translocation of *Y. pestis* YopJ into the host cell than that of the corresponding *Y. enterocolitica* effector YopP was shown to be related to the above differences (367). Paradoxically, the lower cytotoxicity due to *Y. pestis* YopJ correlates with the increased virulence in bubonic

plague by minimally stimulating innate and adaptive immune responses (368).

In tissue-culture infection models, YopH, YopE, YopT, and YopO have been shown to antagonize focal complex formation and activity of Rho family GTPases and synergistically inhibit phagocytosis by mammalian cells (73, 349). Phagocytosis is a complicated process involving many cytoskeletal molecules. Each of three major family members of Rho GTPases, RhoA, Rac-1, and Cdc42, control the formation of individual cytoskeletal elements: stress fibers by RhoA, lamellipodia by Rac-1, and filopodia by Cdc42. When bound to GTP, the GTPase is active and allows interaction with downstream effectors, while the inactive GDP-bound conformation blocks the pathway. Three main regulatory molecules tightly control the GTP-binding and hydrolytic cycle. Guanine nucleotide-Exchange Factors (GEFs) activate Rho proteins by GDP/GTP exchange, and GTPase-activating proteins (GAPs) inactivate them through inducing GTP hydrolysis. The third one is a negative regulator, GDP dissociation inhibitor (GDI), which binds the inactive, GDP-bound form of the Rho protein, inhibits the exchange of GDP for GTP (which would reactivate the Rho protein) and delivers it to its original membrane.

YopE is important for full virulence of *Yersinia pestis* and deletion of *yopE* increases the LD_{50} at least 10^4-fold in a systemic plague model (245). As shown in Figure 1.5, YopE plays a role as a GAP to inhibit Rho proteins by accelerating hydrolysis of GTP. In addition to anti-phagocytosis, YopE may also function to counteract proinflammatory cytokine production, presumably through downstream effects of inhibiting Rho GTPases (349).

It is essential for Rho proteins to attach to the inner side of the cell plasma membrane by the C terminus in order to gain their normal function. Therefore, when YopT, a

cysteine protease, cleaves RhoA, Rac, and Cdc42 near their C terminus and releases them from the membrane, cytoskeleton dynamics maintained by these Rho proteins are interrupted (296, 349).

After a translocation channel (YopB) is inserted into the plasma membrane, a transient pore is formed but there is no membrane lysis. Meanwhile, pore formation in the membrane only can be detected when the infecting bacteria lack some Yops, indicating that these Yops can counteract the pore-forming function of YopB (73). It was reported that YopE and YopT inhibit pore formation through GAP activity and releasing the GTPase from the membrane, respectively (Figure 1.5) (348).

YopO (YpkA in *Y. pseudotuberculosis*) is an autophosphorylating serine-threonine kinase that shows some sequence and structural similarity to RhoA-binding kinases (349). YopO binds to GDP- or GTP-bound RhoA or Rac-1 with similar affinity without affecting GDP/GTP exchange. YopO is activated by actin binding, and actin can also function as an *in vitro* substrate of the kinase. Although binding of YopO to actin and to RhoA and Rac-1 are clearly relevant to phagocytosis inhibition, the kinase target and the exact mode of action of YpkA/YopO are still unknown.

YopH is a highly active protein tyrosine phosphatase (PTP) that antagonizes several signaling pathways associated with phagocytosis (97), as well as other immune response pathways in host cells, for example, the production of Monocyte Chemoattractant Protein-1 (MCP-1); also called CCL2 (Chemokine (C-C motif) ligand 2) in mouse macrophages (281). Although the studies of the YopH virulence mechanism have been mainly done on *Y. pseudotuberculosis* and *Y. enterocolitica*, YopH has been shown to be crucial for lethality in a mouse model of systemic plague (IV infection), and a Δ*yopH*

strain is attenuated for both bubonic and pneumonic plague (54).

The function of YopM is the focus of this dissertation and the background on research on its function is discussed below.

D. YopM is necessary for *Y. pestis* growth in a systemic plague model by counteracting innate defenses

The sixth effector Yop, YopM, is the only effector Yop that does not have an enzymatic activity. YopM is essential for virulence in the mouse model of systemic plague: in C57BL/6 mice, a YopM⁻ strain of *Y. pestis* KIM5 is reduced in lethality by at least 4 orders of magnitude (183).

a) Structure and intracellular trafficking of YopM

YopM is a 46.2-kDa acidic protein that is 409 residues in length and made up almost entirely of fifteen repeats of a 19-residue leucine-rich repeat (LRR) motif (184). The YopM monomer is horseshoe-shaped and has the potential to form tetramers in which the monomers stack together to form a hollow cylinder with an inner diameter of 35 A˚; however the form that YopM assumes within the mammalian cell is not known (96) (Figure 1.6).

Similarly to the other five effector Yops, YopM is injected by the T3SS into the eukaryotic cell (Figure 1.7). However, it is the only one proven to be transported into the nucleus (300). After delivery to the host cell cytoplasm, YopM localizes to the nucleus in a process that is facilitated by vesicular trafficking (Figure 1.7). Among the cytosolic proteins identified as being able to bind YopM, such as α-thrombin (183), α1-antitrypsin

(131), and the serine/threonine kinases ribosomal S6 protein kinase 1 (RSK1) and PRK2 (202), the two kinases have drawn more attention because they were proven to be activated by this interaction.

RSK1 is a substrate of extracellular signal-related kinase (ERK) in the Ras/MAPK signal transduction pathway and plays an important role in cell survival and growth (105). However, nuclear localization of YopM is not dependent on its RSK1 interaction (201). PRK2 is a member of the protein kinase C family involved in cytoskeletal changes, receptor tyrosine kinase signaling, and activation of translation after it is activated by the GTPase RhoA, phospholipids and MEK kinase 2, and interacts with the tyrosine kinase adaptor proteins Nck and Grb2 (202).

Two groups recently studied the interaction between YopM and RSK1 or PRK2 by serial deletion of YopM domains or LRRs (201, 204). They identified a C-terminal domain of YopM (from LRR12 to the C-terminus) and an internal portion encompassing LRR6-15 that are required for interaction with RSK1 and PRK2, respectively. However, there is no visible effect of delivery of YopM into cultured cells, and microarray analysis of macrophage-like cell lines infected with *Y. enterocolitica* having or lacking YopM also has not yielded any clue to YopM's mechanism of action (139, 282).

b) Mechanism of YopM's Function in *in vivo* infection

Although the precise cellular mechanism of YopM remains to be established, there is no doubt YopM is an important *Yersinia* virulence factor. A *Y. enterocolitica ΔyopM* mutant was unable to establish a systemic infection following oral challenge of mice (338), and virulence of a *Y. pseudotuberculosis ΔyopM* mutant was significantly

attenuated in mice via the IV route of infection (204). The LD_{50} value for a *Y. pestis*

ΔyopM mutant was at least 10^5-fold higher than that of the parental strain in mice

challenged intravenously. The *Y. pestis ΔyopM* mutant proliferates in spleen and liver of

mice for several days following IV infection but is then rapidly eliminated from these

organs, and this growth limitation of *ΔyopM Y. pestis* is retained in severe combined

immunodeficiency (SCID) mice, indicating that YopM is important for resistance to

innate immunity (159).

YopM was shown to promote virulence of *Y. pseudotuberculosis* by altering the

balance of key cytokines in serum on d 4 post infection (p.i.), for example, decreased

production of IFN-γ and increased levels of IL-18 and IL-10, and the PRK2 and RSK1

interaction domains of YopM were both required for IL-10 induction *in vivo* (204).

Meanwhile, the mutation of RSK1 binding sites on YopM increased the recruitment of

monocytes as well as inhibited colonization in spleen during septicemic *Y.*

pseudotuberculosis infection, which implicates RSK1 as a potential molecular target of

YopM in the cytosol (201). However, the pathway from RSK1 to YopM's effects on

cytokine expression during infection has not yet been delineated.

Because *in vitro* approaches to defining the pathogenic mechanism of YopM in *Y.*

pestis infection have not been fruitful, we have begun to characterize YopM's effects *in*

vivo. Previously Kerschen et al. found that YopM was still required for lethality in IV

infected SCID mice, showing that YopM's virulence mechanism does not require B or T

cells and indicating that early in systemic plague, YopM's main function is to counteract a

component of innate immunity (159). A striking YopM-specific effect during systemic

plague in normal C57BL/6 mice was the depletion of natural killer (NK) cells from

spleen and a reduction of NK cell numbers in blood, suggesting that YopM might cause a loss of the NK cell compartment during systemic plague. Correlated with this effect, there was a YopM-associated loss of mRNA for IFN-gamma by NK cells in infected spleens and diminished expression of mRNAs in splenic macrophages for cytokines that are required for viability and activation of NK cells (IL-15, IL-18 and IL-12). These findings supported the hypothesis that YopM may function to inhibit IFN-mediated activation of macrophages through the depletion of NK cells (159).

E. Thermal regulation of major virulence factors and transmission factors

When *Y. pestis* is transmitted by flea to mammals, the expression of virulence and transmission factors is altered due to the change of the surrounding temperature. As described in **B a),** production of biofilm and MT is downregulated once the bacteria move from the ambient temperature (26°C) to the internal temperature of a mammal (37°C). Pla synthesis is not temperature-dependent, but its plasminogen activator activity that leads to fibrinolysis is much greater at 37°C than at temperatures below 28°C (203).

When the bacteria enter into a mammalian host, insecticidal toxin complex proteins made in the flea may provide some immediate protection to the bacteria by inhibiting phagocytosis (343). Meanwhile, the bacteria need to activate their T3SS through establishment of contact with the eukaryotic cells. As discussed in **C c)**, several adhesion factors including Pla, pH 6 antigen, Ail and Yaps are involved in this process. *Y. pestis* pH 6 antigen is expressed only when the bacteria grow between pH 5 and 6.7 at temperatures of 35 to 41°C, which means it is absent in the flea and present in the mammal (61). Through binding to phosphotidylcholine in the host cell membrane, pH 6

antigen promotes bacterial dissemination in bubonic plague and pneumonic plague. Ail protein is expressed at both ambient temperature and 37 ^{o}C, and mediates two distinct different host-parasite interactions. By binding host fibronectin (339), Ail is the major adhesin to facilitate Yop delivery *in vitro* in bacteria grown at 28 ^{o}C prior to the assay (98), whereas it is responsible for the constitutive serum-resistance of *Y. pestis* in a mammal (37 ^{o}C) (28), which will be discussed further in **F b)**. The last group of adhesins is the Yaps that belong to the autotransporter family. One member of the Yap family, YapE, has been proven to mediate the binding of *Y. pestis* to eukaryotic cells and play an important role in efficient *Y. pestis* CO92 colonization in C57B/6 mice (177). Apparently YapE functions at 37 ^{o}C, but it is not known whether its expression is temperature-dependent.

Once shifted to 37°C, the expression of the T3SS and Yops is upregulated. The injectisomes start to be assembled and the synthesis of Yops is upregulated (226), which have been discussed in **C d) and e)**. The production of F1 fibrils, which contribute to the antiphgocytosis activity of *Y. pestis* in concert with the T3SS, is also induced by the shift of temperature; however its anti-phagocytosis function needs 4-5 hours to be detected (89).

Another important temperature-dependent virulence factor of *Y. pestis* is lipopolysaccharide (LPS). LPS consists of three portions: O-antigen, core oligosaccharide and Lipid A. *Y. pestis* has a rough-type LPS that lacks an O-specific chain (301), which favors efficient plasminogen activation by Pla (165). Another important component is Lipid A, which interacts with the host LPS receptor complex consisting of TLR4 and its coreceptor MD-2 to induce cellular responses. The number and length of acyl side chains

of Lipid A are critical for TLR4 signaling in humans. Hexa-acylated Lipid A maximally stimulates immunological responses in humans, whereas altering the number or length of the attached fatty acids reduces the magnitude of the response (215). The Lipid A obtained from bacteria cultivated at ambient temperature is normally a typical hexa-acylated LPS. However, after the temperature transition from 26°C to 37°C, *Y. pestis* immediately begins to produce LPS with tetra-acylated Lipid A, which is not only nonstimulatory for TLR4 but also acts as an antagonist to the stimulatory hexa-acylated form of LPS (91, 223).

F. Host responses to *Y. pestis*: innate and adaptive responses

a) Innate and adaptive immune responses

The innate immune response is the first line of host defense against pathogens in a non-specific manner, which means that the cells of the innate system recognize and respond to pathogens in a generic way. However, unlike the adaptive immune system, the innate immune system provides immediate but not long-lasting defense against infection. The innate immune system includes barrier structures, phagocytic cells including PMNs, macrophages and monocytes, DCs, NK cells, platelets, mast cells and molecules such as complement proteins, cytokines, and antimicrobial peptides.

The adaptive immune system is composed of highly specialized systemic cells and processes that eliminate or prevent pathogenic challenges. The adaptive immune response provides organism-specific protection that frequently has a long-lasting immunological memory. In most cases, the bacterium will be eliminated from the host by the synergistic effect of both innate and adaptive immunity.

To survive inside of the host and maintain a persistent infection, *Y. pestis* uses a variety of mechanisms to evade or overcome the host immune system, especially the innate immune system (Figure 1.8) (185).

b) Preparation of *Y. pestis* in the flea to overcome incoming mammalian host defenses

The first threat from the host immune system to *Y. pestis* is complement attack because the bacteria must survive and/or grow in blood to be transmitted between its insect vector and mammalian hosts and in the transudate at the foci of infection which also contains complement proteins. The ability of *Y. pestis* to escape complement attack is termed serum resistance (245).

The enteropathogenic yersiniae (*Y. enterocolitica* and *Y. pseudotuberculosis*) are fully resistant to complement when they are grown at 37°C but not when they are grown at 26°C (12, 40, 245). In contrast, *Y. pestis* is resistant to complement at both 26 and 37°C (12), which favor its growth in both flea and mammalian host. Resistance to complement in *Y. enterocolitica* has been studied in detail and has been shown to involve YadA, Ail, and LPS O antigen, with YadA playing a dominant role (35).

However, *Y. pestis* does not express YadA and expresses only rough LPS (245). Previous studies have suggested that *Y. pestis* LPS may mediate serum resistance (245); however, there is no evidence of a direct role for LPS in serum resistance. The *Δail Y. pestis* strains are extremely sensitive to complement. It is currently suggested that Ail might be the sole complement resistance factor due to its requirement for full protection of *Y. pestis* from complement-mediated lysis *in vitro* (28). Alteration in the structure of

LPS may also interfere with the expression and the surface exposure of Ail.

Another possible early host response against *Y. pestis* could be induced by TLR4-mediated activation, which is inhibited when *Y. pestis* Lipid A changes from the hexa-acylated form to tetra-acylated one after the temperature transition (91, 223).

c) *Y. pestis* **escapes from immune attack at an early stage of infection**

Y. pestis is believed to exist predominantly in an extracellular location *in vivo*, although initially the bacteria might invade resting tissue phagocytes such as macrophages and DCs, based on assays of mouse spleens in the systemic phase of bubonic plague (192). The intracellular vs. extracellular location of *Y. pestis* during the peripheral phases of plague in skin or lung have not yet been studied.

Phagocytes including macrophages and PMNs are the major players in the first surveillance line for bacterial infection. These cells recognize invading pathogens and engulf and destroy them. At the early stage of infection, the first immune cells encountered by *Y. pestis* in skin probably are dermal macrophages and DCs at the infection site. To avoid clearance at this stage, *Y. pestis* develops several different mechanisms to block phagocytosis, such as insecticidal toxin complex YipA and YipB (expressed while the bacteria are in the flea) and F1 fibrils and effector Yops. However, the antiphagocytosis function of *Y. pestis* is not equally efficient against the various host cell types; and even for any one cell type it is not 100% effective. Evidence has shown that *Y. pestis* is resistant to phagocytosis by PMNs but not monocytes by 3 h of growth *in vivo* at 37°C (prior to F1 fibrils expression). After 3 to 5 h, the bacteria are resistant to uptake by both types of phagocytes (245). Meanwhile, histological evidence indicates

that *Y. pestis* is killed within PMNs, and analyses of the cell association, intra- vs extra-cellular localization, and viability of *Y. pestis* in spleen following SC infection indicate that at up to 2 days p.i. host PMNs are able to control *Y. pestis* growth (192).

Unlike PMNs, macrophages provide a protected environment for *Y. pestis* to survive and proliferate, as well as avoid contact with other components of the host immune system. *Y. pestis* proliferates in the phagolysosome of macrophages, acquires the ability to evade phagocytosis and expresses various virulence determinants (253, 319), which are essential for pathogenesis. Further, the bacteria within macrophages can be trafficked to the local draining lymph node (254). Between 4 and 5 days p.i., the numbers of *Y. pestis* increase rapidly *in vivo*, and the bacteria can escape from macrophages into the extracellular compartment. The two-component system PhoP/PhoQ may regulate one or more genes important for the intracellular survival of *Y. pestis* in macrophages (237). These include ones for synthesis of 4-aminoarabinose and its addition to lipid A, a modification that confers resistance to cationic antimicrobial peptides (261, 360).

d) *Y. pestis* modulates innate immune responses

After *Y. pestis* accommodates to conditions within the mammalian host, the environmental factors that are different from those in the flea, such as high temperature (37°C) and physical contact with host cells, stimulate the expression of *Y. pestis* virulence factors including the T3SS and Yops, F1 pilus, Psa and high activity of pla. They no longer express polysaccharide biofilm (95) and their lipid A is tetra-acylated. Hence the bacteria surface is radically different from that initially present upon injection by flea bite. At 1 to 2 days p.i., disturbance of the host immune responses by the virulence factors

become detectable (245).

Phagocyosis at this stage is inhibited by three mechanisms. While within macrophages, *Y. pestis* plasmid pMT starts to encode F1 protein which forms a gel-like fibrillar coating around the bacterium. This capsule increases bacterial resistance to engulfment by both macrophages and PMNs, probably through masking the bacterial ligands from the receptors on phagocytic cells (89). In an acidic environment like the phagolysosome of macrophages and necrotic lesions, expression of pH6 antigen will be induced, which has a fimbrial structure and acts as adhesin to establish the contact between bacterium and host cells without triggering engulfment (316). Meanwhile, purified pH6 antigen has been found to selectively bind to apolipoprotein B (apoB)-containing lipoproteins in human plasma, mainly LDL. This interaction could prevent recognition of the pathogen by the host defense systems (195). The third mechanism is the effector Yops. As described in Section **C. e) The functions of the effector Yops,** YopH, YopE, YopT, and YopO synergistically inhibit phagocytosis by mammalian cells through inhibiting multiple pathways that govern actin mobilization.

In addition to antiphagocytosis, effector Yops also modulate innate immune responses through other mechanisms. For instance, YopH can suppress the production of reactive oxygen intermediates by macrophages and PMNs (116) and YopM depletes NK cells from spleen in the systemic plague model (159), which will be discussed in detail in this work.

Cytokines and chemokines are the bridge connecting the innate and adaptive immune systems. Through negative regulation of major signal pathways in the infected cells, effector Yops inhibit the production of many cytokines. YopJ/YopP has been shown to

inhibit TNF-α release by macrophages and IL-8 release by epithelial and endothelial cells (44). YopM causes decreased expression of TNF-α, IL-1β, IL-12, IL-18, IL-15, and IFNγ, which are cytokines that activate innate immune cells including macrophages, DCs, NK cells, and PMNs (159, 276). Another component of the T3SS, LcrV, is also found to trigger the release of the suppressive cytokine IL-10 (349).

Besides cytokines, effector Yops also inhibit the expression of some important chemokines or adhesion molecules and in turn block the recruitment of key immune cells. Examples include the inhibition of the expression of MCP-1 by YopH (281) and reduced production of adhesion molecules, such as intercellular adhesion molecule-1 (ICAM-1) and E-selectin, by YopJ/YopP (43).

e) *Y. pestis* paralyzes DCs without affecting their maturation

DCs are key players at the interface of innate and adaptive immunity. Circulating precursor DCs enter tissues as immature DCs, where they can directly encounter pathogens that induce secretion of cytokines (e.g. IFN-α), which in turn can activate eosinophils, macrophages, and NK cells. Contact with the microorganisms also triggers a series of programmed events that include migration of immature DCs to lymphoid organs and conversion of immature DCs into mature ones, together with the degradation of pathogens within the phagosome and the presentation of microbial antigens by the major histocompatibility complex (MHC) molecules. This in turn causes DCs to activate T cells by an MHC-specific manner, and activated T cells promote terminal maturation of the DCs (23, 24). In addition to the control of the costimulatory pathway, DCs seem to contribute to T-cell activation by overcoming suppression mediated by CD4 and CD8

regulatory T cells by secretion of IL-6 (178). Activated T lymphocytes migrate to the injured tissue. Helper T cells (CD4$^+$) secrete cytokines, which permit activation of macrophages, NK cells, and eosinophils. Cytotoxic T cells (CD8$^+$) eventually lyse the infected cells. B cells become activated after contact with T cells and DCs and then migrate into tissues where they mature into plasma cells and produce antibodies that neutralize the initial pathogen (23, 24).

Many pathogens have developed a variety of mechanisms to disarm host defenses, such as impairing DC maturation, promoting apoptosis of DCs, and inhibiting cytokine secretion. *Y. enterocolitica* was found to induce apoptosis of murine DCs as well as inhibit the expression of MHC-II; major adhesion molecules such as CD54 (ICAM-1), CD 80, and CD86; and cytokines including KC, TNF-α, IL-10 and IL-12 by DCs (94). During infection by *Y. pestis*, DCs are one of the early targets of *Y. pestis* (197, 370). However, instead of a negative effect on DC viability and maturation, the most pronounced effect of *Y. pestis* on DCs appears to be the paralysis of DC movement by impairing cytoskeletal rearrangement, and this effect seems to be mediated by the products encoded by pCD1 (347). Paralysis of DCs also results from the compromised TLR4-dependent induction of IL-12(p40)$_2$ by DCs in *Y. pestis* infection (268)

f) *Y. pestis* reduces host adaptive immunity by both influencing the induction of cytokine expression and acting directly on immune cells

The adaptive immune response is characterized by selective and clonal expansion of immune cells (T and B cells) to recognize antigens from a pathogen, providing specificity and long-lasting immunological memory. Given the very short incubation time of plague,

35

the protection an infected person receives during the primary infection from the adaptive immune system may be limited. However, studies about the modulation of adaptive responses by this bacterium will facilitate vaccine development and understanding that may apply to the pathogenesis of other facultative intracellular bacteria.

Yersinia has the ability to influence adaptive immunity by directly suppressing T cell activation as well as inducing the mitochodrially regulated apoptosis of T cells. One of the effector Yops, YopH with tyrosine phosphatase activity, exerts both of these effects in a cell culture model (6, 52). For example, YopH was found to block *in vitro* T cell antigen receptor (TCR) signaling at its very first step by dephosphorylating LcK (leukocyte-specific protein tyrosine kinase), which associates with the cytoplasmic tails of the CD4 and CD8 co-receptors on T helper cells and cytotoxic T cells, respectively, and then transmits signaling from the TCR complex (6). A recent study also reported that that primary human cytolytic T cells respond to *Y. pestis* pCD1-encoded virulence proteins that are presented by infected monocytes and dendritic cells, and T cell responses to non-*Yersinia* antigen are maintained (278).

So far I have not found any study showing a direct inhibitory effect of *Y. pestis* on T cells *in vivo*. However, some *in vivo* studies of the cellular immune responses to *Y. pestis* showed the possible importance of T cells in the defense against *Y. pestis*. Parent et al. vaccinated B-cell-deficient μMT mice intranasally with live replicating *Y. pestis* and found that vaccination dramatically increased survival of μMT mice that were subsequently IN challenged with a lethal *Y. pestis* dose(239). The vaccine significantly reduced bacterial growth in lung, spleen and liver and elevated the number of pulmonary T cells. T cell ablation abolished this vaccine-mediated protection, and the transfer of *Y.*

pestis-primed T cells to naive μMT mice protected against lethal intranasal challenge. Meanwhile, IFN-γ, TNF-α and inducible NO synthase (iNOS), key products of cellular immunity, perform critical protective functions during humoral defense against lethal pulmonary *Y. pestis* challenge (240). And a more recent paper reported that mice vaccinated with live attenuated *Y. pestis* (KIM5 *Δpgm*) are synergistically protected by primed CD4 and CD8 T cells from lethal pulmonary *Y. pestis* infection (247).

Serum samples collected from mice infected IP with *Y. pestis* can transfer passive protection to IN infected C57BL/6 mice (240), indicating that humoral immunity plays an important role against *Y. pestis* challenge. Two major immunogenic proteins, F1 and LcrV (V antigen), provide a high degree of protection, and subunit vaccines based on these proteins have demonstrated efficacy in small animal models (11, 184, 227). Classical humoral immune mechanisms could directly combat extracellular *Y. pestis* organisms and simultaneously aid cell-mediated immunity by neutralizing surface-exposed *Y. pestis* virulence factors that dampen cellular responses, thereby promoting T-cell activation. At the same time, classical cell-mediated immune mechanisms may aid humoral defense by eradicating intracellular *Y. pestis* reservoirs. Thus, the two major components of the adaptive immune system could act synergistically to protect the host against *Y. pestis*.

G. Current animal model for *Y. pestis* study

Corresponding to each of the three natural forms of plague, there is usually more than one animal model used to study plague. Here I focus on the mouse models related to the *Y. pestis* strains used in this study, which are *Δpgm* strain KIM5 and the fully virulent strain CO92.

To establish bubonic plague, the best and most natural way is to infect the mice with a *Y. pestis* infected flea, *X. cheopis* (150, 289). *X. cheopis* fleas are infected by feeding them with blood containing *Y. pestis*. Then a mesh-covered capsule containing infected *X. cheopis* is applied to a shaved area on the dorsolateral surface of restrained mice for a certain time. However, since the *Y. pestis* used in this model is usually the fully virulent strain, this infection model needs several specially designed instruments, such as the artificial feeding system with strict temperature and humidity as well as a mouse restrainer in a biosafety level 3 (BSL3) Lab.

The convenient way to mimic the natural bubonic plague is to inject *Y. pestis* into the skin of mice. Traditionally this was done by injecting the bacteria SC. However, Sebbane et al. showed that fleas initially deposit *Y. pestis* into dermal tissue, and not SC, because the infection that develops at the bite site is ID and the flea mouthparts are not long enough to penetrate through the dermis (289). Therefore, in our study *Y. pestis* CO92 was injected ID into the shaved skin on the back at the base of the tail to set up a bubonic plague model in BSL3 containment. Histopathological analysis showed that inflammation was limited to the dermis and epidermis at the early stage of infection (Figure 3.3, panel C and D).

There are two ways to set up a pneumonic plague model, IN inoculation of *Y. pestis* or exposure of the mouse to aerosol containing *Y. pestis*. The lungs from mice infected by both methods developed acute inflammation and contained a large amount of bacteria in the histopathological analysis (3, 173). Since the aerosol-mediated infection model needs a special mouse restrainer and nebulizer in a BSL3 lab, we chose the simpler method, which is IN inoculation in BSL3 containment.

Systemic plague can be caused by infecting mice in BSL2 containment with the attenuated *Δpgm* strain KIM5, since the *Δpgm Y. pestis* is fully virulent for the IV route of infection through which they can get iron from blood (99). Bacteria can be injected into the vein of mice through the tail vein or retro-orbital plexus which was chosen in this study. And in IV-infected C57BL/6 mice, *ΔyopM Y. pestis* KIM5 show growth limitation in liver and spleen, which is a strong YopM-specific virulence phenotype that greatly facilitates sorting out the key players in YopM's pathogenic effects.

Since the goal of this study was to identify the immune responses compromised by YopM, parent strains (KIM5 or CO92) containing YopM and *ΔyopM* mutant strains were used to develop the systemic, bubonic and pneumonic plague models. The infection doses were chosen between the LD_{50} of the parent and mutant strains in order to display the possible effects of YopM on the host immune system.

H. Hypothesis and rationale for the overall experimental approach in these studies

To characterize YopM's effects *in vivo*, we sought to determine how YopM modulates the function of immune cells to favor *Y. pestis* growth in the host. There was no information yet on the target cells or relative importance of Yops other than YopH in pneumonic or bubonic plague. Since we already knew that the growth limitation of *ΔyopM* mutant *Y. pestis* was maintained in SCID mice (159), which lacked normal T and B cell function, we focused our work on the innate immune system. The hypothesis was that YopM undermines a function of at least one innate immune cell.

The YopM-dependent NK cell depletion in spleen and blood during infection made

NK cells the first candidate to study (159). mRNA analysis by RT-PCR had shown YopM-associated loss of mRNA for IFN-γ by NK cells in infected spleens and diminished expression of mRNAs in splenic macrophages for cytokines that are required for viability and activation of NK cells (IL-15, IL-18 and IL-12). These findings supported the hypothesis that YopM may function to inhibit IFN-γ-mediated activation of macrophages through the depletion of NK cells. To test this hypothesis, C57BL/6 mice with depletion of NK cells from spleen and liver were used. If NK cells are critical for controlling *ΔyopM Y. pestis*, the absence of this cell population in mice should relieve the growth defect of the *ΔyopM* strain. Meanwhile since the growth defect of *ΔyopM Y. pestis* also exists in liver, the dynamics of NK cells in liver during the infection with both parent and mutant strains should be examined.

It is believed that tissue macrophages, DCs and PMNs are early target cells for Yops delivery *in vivo*, because these cells are present before or soon after infection begins and function to initiate the innate defenses that are undermined by Yops. Consistent with this hypothesis, *Y. pestis* has been found in association with alveolar macrophages early during lung infection of mice (46) and likewise in association with macrophages, DCs, and PMNs in spleens of mice infected IV, and YopM can be injected into these cells (197).

We characterized the dynamics of macrophage, DC, and PMN populations in both liver and spleen during systemic plague in mice and identified any YopM-associated recruitment of these immune cells into both organs. We hypothesized that the recruitment of these cells into organs may be inhibited by YopM because the growth limitation of the *ΔyopM Y. pestis* could be explained if these bactericidal cells were present in the *ΔyopM*

40

Y. pestis-infected organs but not the parent strain infected ones.

To test whether the above immune cell populations are responsible for the growth limitation of *ΔyopM Y. pestis* in spleen and liver, mice ablated for different immune cells were used. For ablation of both PMNs and monocytes, anti-Gr1 antibody was injected IP into the mice; and liposome-clodronate was used to remove the resident macrophages and DCs as well as the inflammatory monocytes in the circulation and tissue. To specifically deplete PMNs, anti-Ly6G was injected IP into the mice. Finally mouse strains lacking the major chemokine CCL2/MCP-1 or its receptor Chemokine (C-C motif) Receptor 2 (CCR2) were used to study the inflammatory monocytes and a newly discovered class of DCs, Tip DCs. The rationale was that if any of these cell types played a critical role in YopM's virulence mechanism, the absence of this cell population should relieve the growth defect of the *ΔyopM* mutant. Since spleen and liver contain different microenvironments and responses to infection; the infection dynamics and distribution of leukocytes in both of the organs were studied and compared in every ablation model.

If there was any cell type identified as a key player responsible for the growth defect of *ΔyopM Y. pestis* mutant, the effects of YopM on functions of this cell type should be studied.

The major animal model used in this study was the systemic model with IV injection of the *Δpgm Y. pestis* KIM5, because we already knew the growth defect of the *ΔyopM* strain in this model. However, systemic or septicemic plague is almost always secondary to bubonic or pneumonic plague. And it is becoming clear that spleen and lung present distinctly different inflammatory environments when infected by *Y. pestis*, with PMNs migrating rapidly into spleens infected by the IV route but not appearing in lungs until 36

h after IN infection (173, 318). Accordingly, some virulence properties required for lethality of systemic plague are not required in pneumonic plague. Examples are the capsular fibril F1 and the antiphagocytic adhesin PsaA (49, 61, 79). Therefore, to understand how YopM modulates the host immune responses in natural plague, it was worth checking the role of YopM in both bubonic and pneumonic plague, in which the pgm^+ strain must be used.

The bacteria used in the systemic model were cultured at 26°C overnight before the infection to identify host responses and the role of YopM in an infectious process like the one that occurs after flea bite. However, natural systemic plague usually occurs secondarily to bubonic plague, which means the bacteria have already adapted to the internal environment in the mammalian host before they seed in spleen and liver. At the body temperature of the mammalian host (37°C), the T3SS of *Y. pestis* is activated so the Yops can be injected into the host cells, whereas the infecting bacteria grown at 26°C have to hide in the resident macrophages or DCs for a while to activate this system. To mimic the natural systemic plague model, we used pre-induced bacteria, which grew at 26°C overnight and were transferred to 37°C three hours before infection. We hypothesized that the growth defect of the *ΔyopM* strain would be maintained after that pre-induction. The infection dynamics and distributions of leukocytes during systemic plague in wild-type (WT) C57BL/6 mice, anti-Ly6G treated mice and CCR2 knock-out (KO) mice were tested and compared between infection by non-induced *Y. pestis* grown at 26°C and by pre-induced bacteria which received 3 hours stimulation at 37°C before the infection.

Table 1.1. *Y. pestis* transmission Factors

Factors	Gene	Location of Gene	Expressing Specie(s) of *Yersinia*	Function and Role in Transmission
Murine Toxin (Phospholipase D)	*ymt*	pMT (plasmid)	*Y. pestis*	Bacterial survival in flea midgut
F1 capsule	*caf1M1A1*	pMT (plasmid)	*Y. pestis*	Prevents autoaggregation
Pla	*pla*	pPCP1 (plasmid)	*Y. pestis*	Cleavage and activation of plasminogen to promote dissemination of bacteria from fleabite site
Enzymes (e.g., Polysaccharide deacetylase and glycosyl transferase)	*hms*HFRS operon	*hms* locus in *pgm* locus (chromosome)	*Y. pestis* *Y. pseudotuberculosis*	biofilm formation to block the proventriculus
Insecticidal toxin complex	*yitRABC operon, yipAB operon*	*chromsome*	*Y. pestis* *Y. pseudotuberculosis,* Some *Y. enterocalitica*	Phagocytosis resistance immediately after transmission

Summarized and modified from reference (133, 134, 288, 343)

Figure 1.1 World Distribution of Plague and the bubonic plague vector *Xenopsylla*

cheopis

World Distribution of Plague, 1998

Countries that reported plague, 1970-1998

Regions where plague occurs in animals
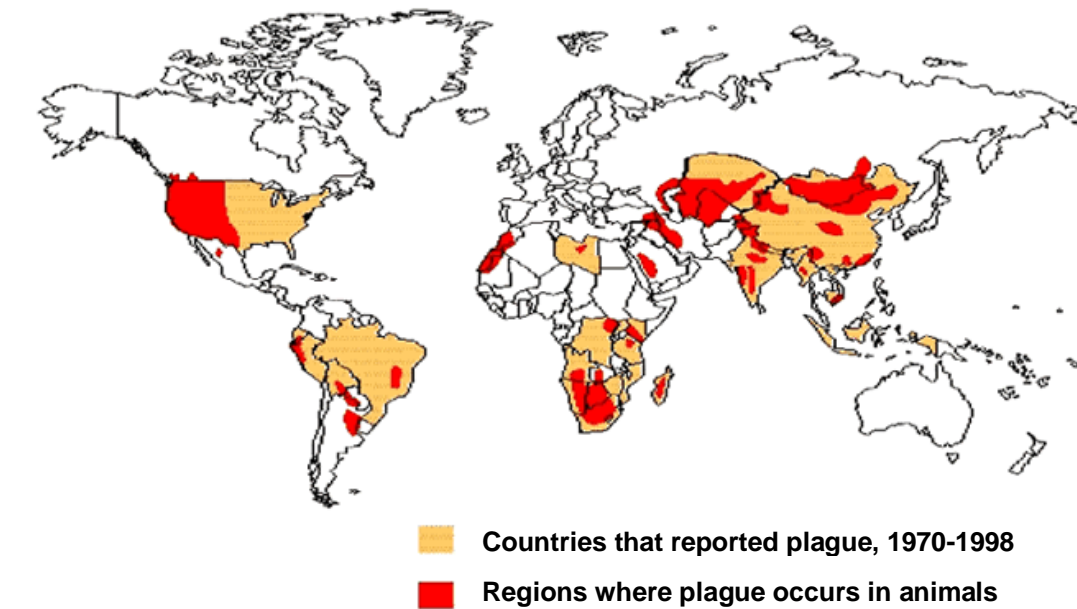
Male *Xenopsylla cheopis* engorged with blood. Both male and female fleas can transmit the infection.

From the Centers for Disease Control and Prevention (CDC) website

Figure 1.2 The Transmission Cycle of *Y. pestis*
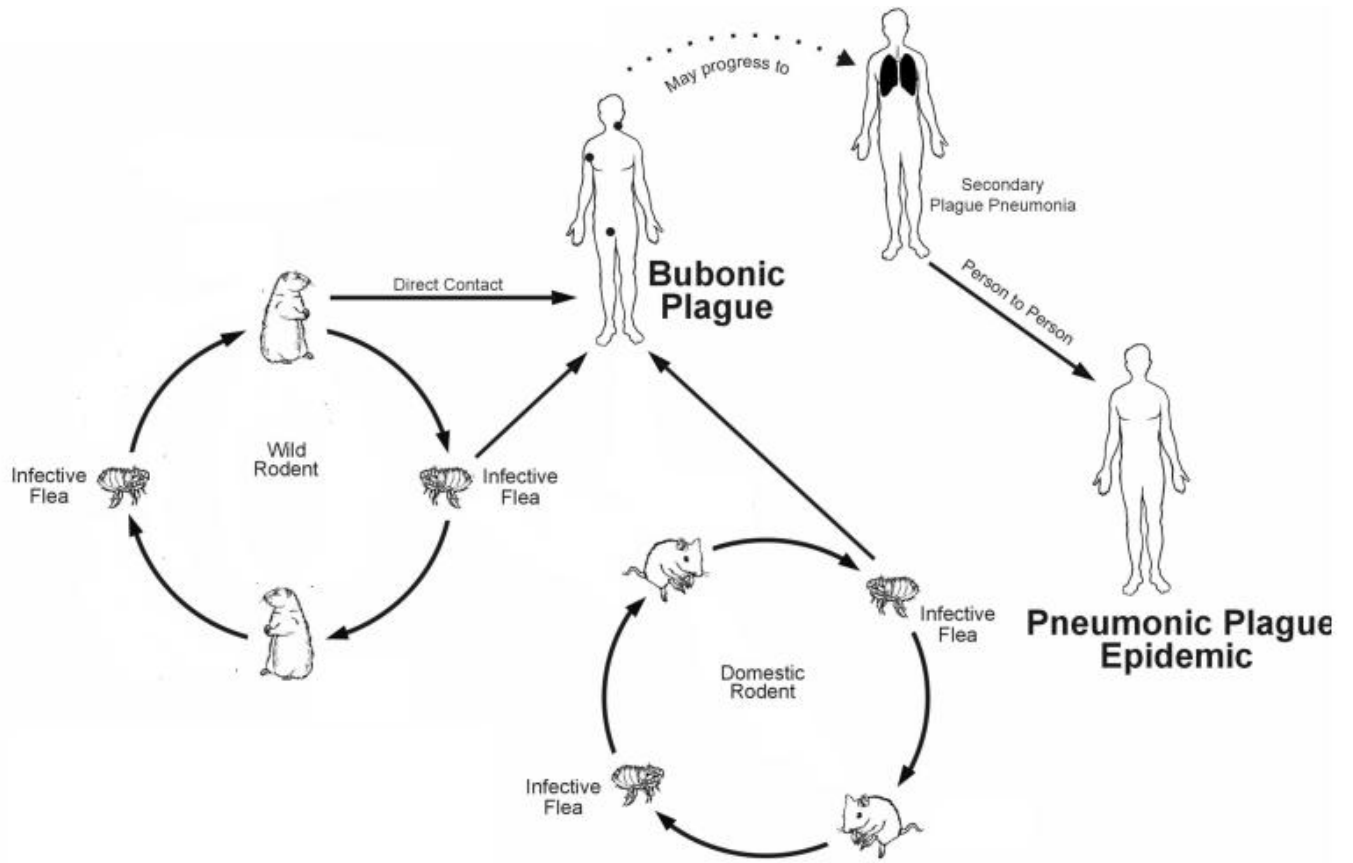
Simplified from Dr. Neal R. Chamberlain's figure.

(http://www.unbc.ca/nlui/wildlife_diseases_bc/plague_cycles.gif)

Figure 1.3 The Ysc Injectisome
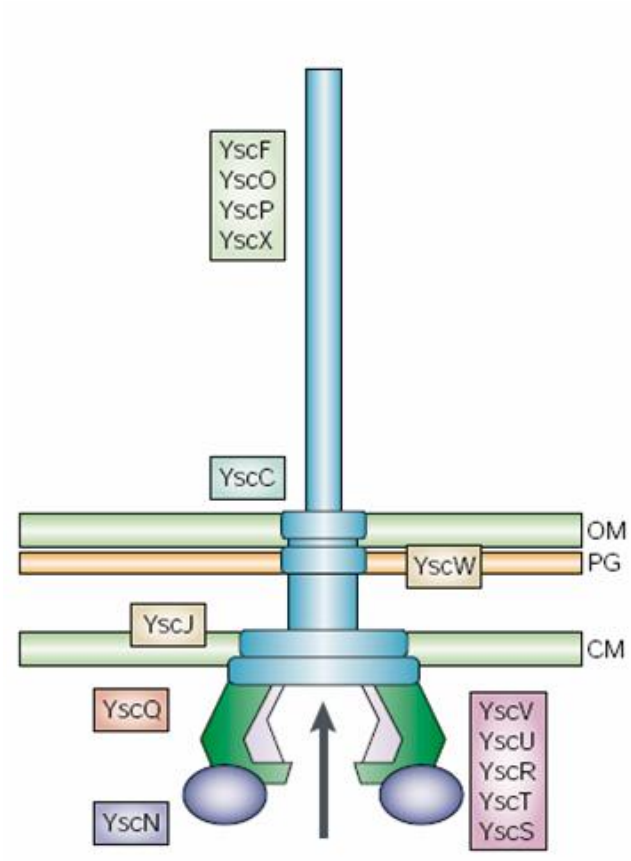
Ysc injectisome spanning the outer membrane (OM), the peptidoglycan layer (PG) and the cytoplasmic membrane (CM) of the bacterium. The ring in the OM is made of the secretin YscC, assisted by the lipoprotein YscW. YscF, YscO, YscP and YscX are external parts of the injectisome. YscF is the main constituent of the needle structure. YscV, YscU, YscR, YscT and YscS are proteins of the basal body that are in contact with the CM. YscN is the ATPase of the translocon. Not shown is the tip complex that creates a pore in the host cell plasma membrane. (74)

Figure 1.4 Secretion of Yops by the Ysc injectisome and translocation across the target cell membrane
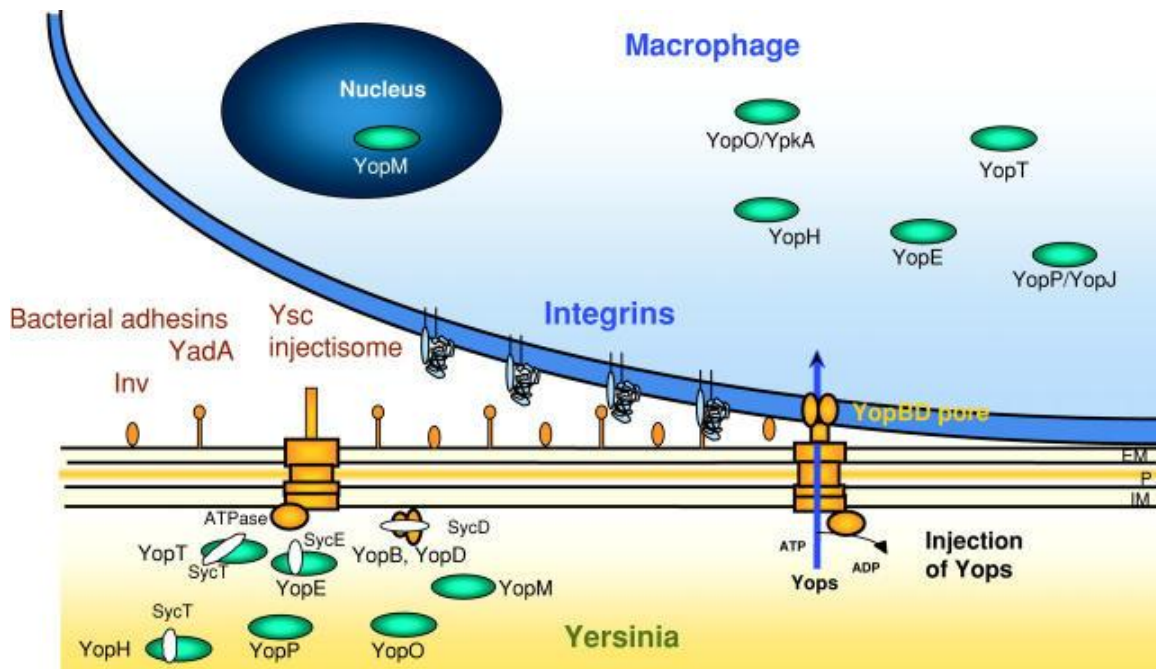
At 37°C, *Yersinia* assembles its Ysc injectisome. The secretion channel opens and Yops are exported after a stable contact is established between a eukaryotic target cell and the bacterium through the interaction of the bacterial adhesins YadA or Inv in enteropathogenic Yersiniae with integrins; and pH 6 antigen, Pla and Ail in *Y. pestis* with Phosphatidylcholine (108), CD205 (371) and Fibronectin (339) on the eukaryotic cell surface. YopB with the aid of YopD forms a pore in the target cell plasma membrane, and the effector Yops are translocated across this membrane into the eukaryotic cell cytosol. YopM is the only Yop migrating to the nucleus. EM, outer membrane; P, peptidoglycan; IM, plasma membrane. (73)

Figure 1.5 Modulation of host signaling pathways by Yops
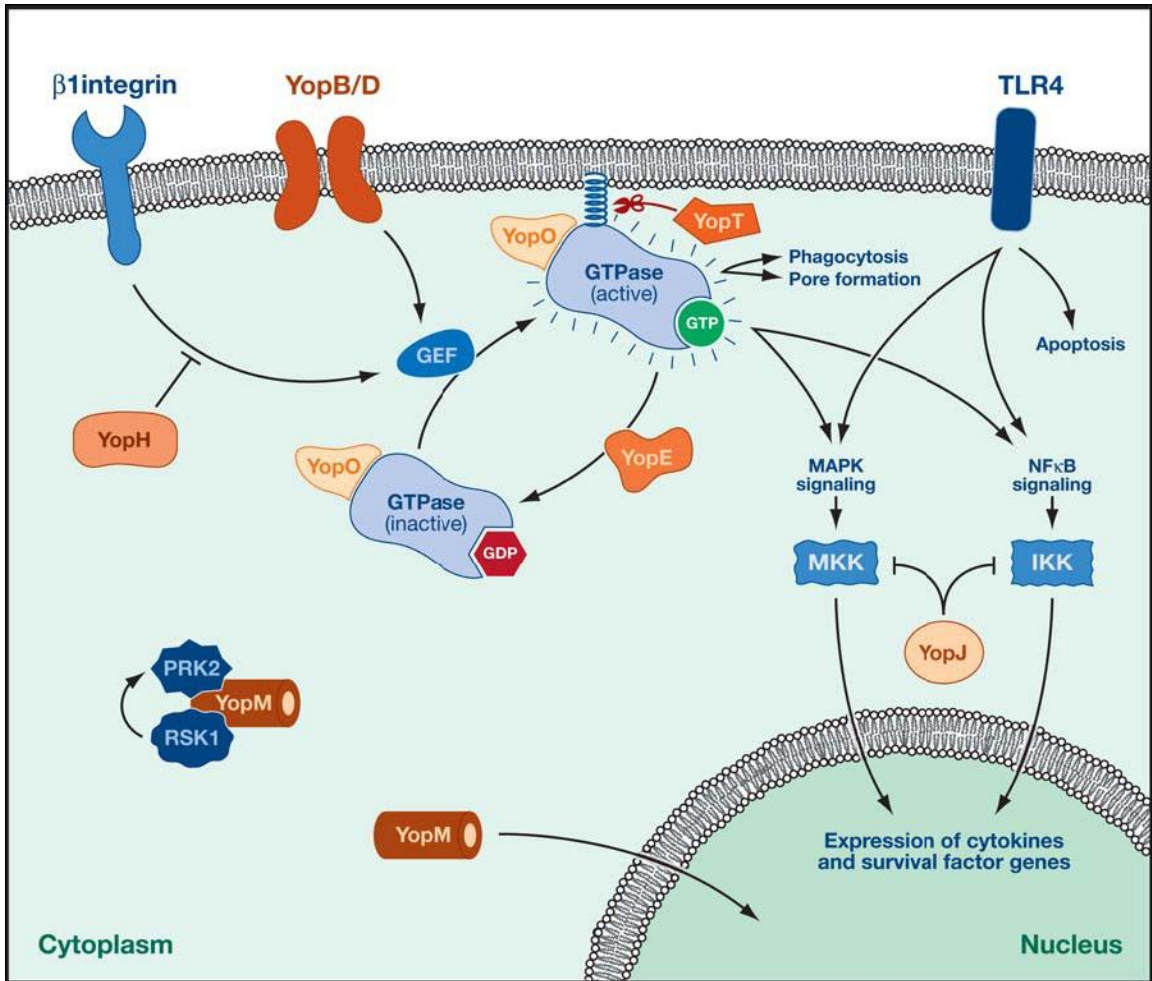
YopH, YopE, YopT, and YopO antagonize focal complex formation and activity of Rho family GTPases, whose activation triggers phagocytosis in the case of the β1 integrin signaling pathway, or pore formation (leakiness after insertion of the Ysc tip complex) in the case of the translocator pathway. YopE and YopT inhibit phagocytosis by acting as a GAP (YopE) and cleaving the C-terminal isoprenyl cysteine from RhoA, which releases the GTPase from the membrane (YopT). YopO binds to the active or inactive Rho GTPase and counteracts signaling and phagocytosis by an unknown mechanism. The PTP activity of YopH inhibits early steps in the β1 integrin signaling pathway to counteract

phagocytosis. Rho GTPase activation also stimulates gene transcription via the MKK and NF-κB pathways, leading to the production of cytokines and survival factors. YopJ acetylates serine and/or threonine residues in the activation loops of MKK and inhibitor-κB kinase (IKK). YopM enters into the nucleus by unknown mechanism, as well as forms a complex with two serine/threonine kinases, protein kinase C-related kinase 2 (PRK2) and ribosomal S6 protein kinase 1 (RSK1) in the cytosol. (349)

Figure 1.6 Schematic representation of the YopM structure
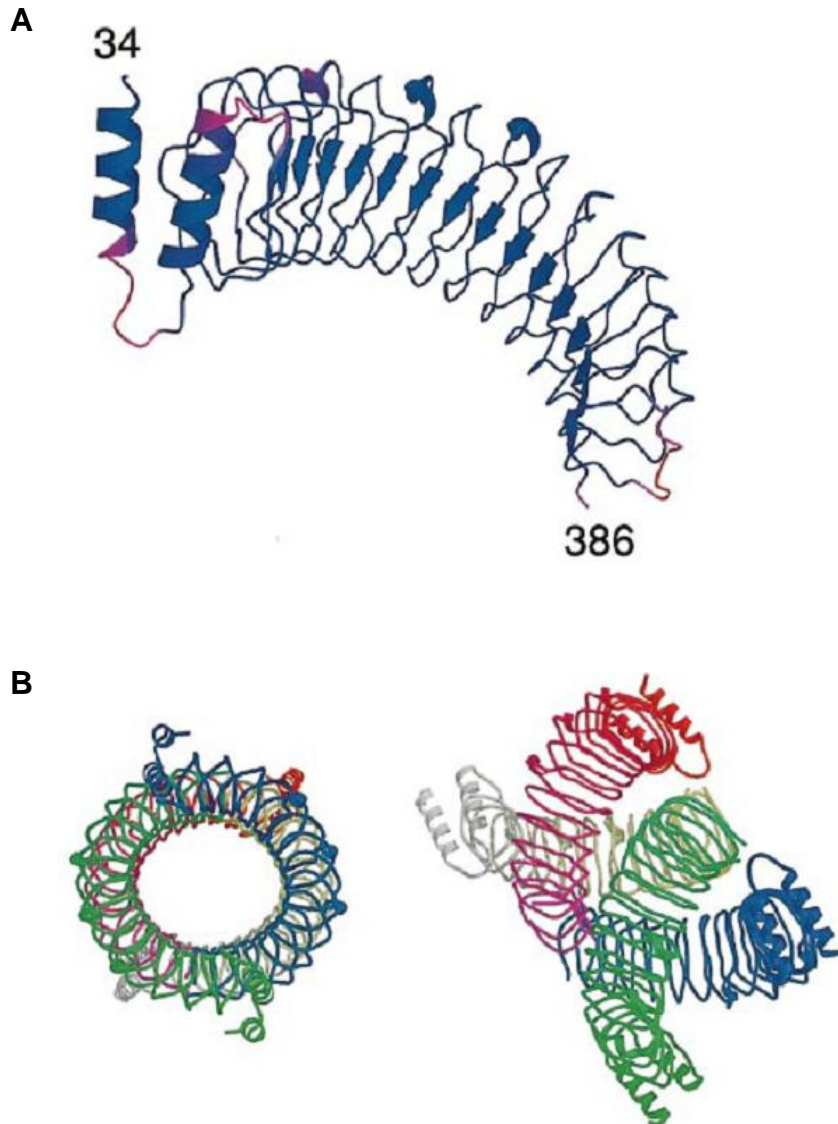
Panel A, YopM monomer. The N and C-terminal residues that were observed in the crystal structure are labeled. Panel B, Two views of the YopM tetramer. (96)

Figure 1.7 Model for YopM's cellular trafficking
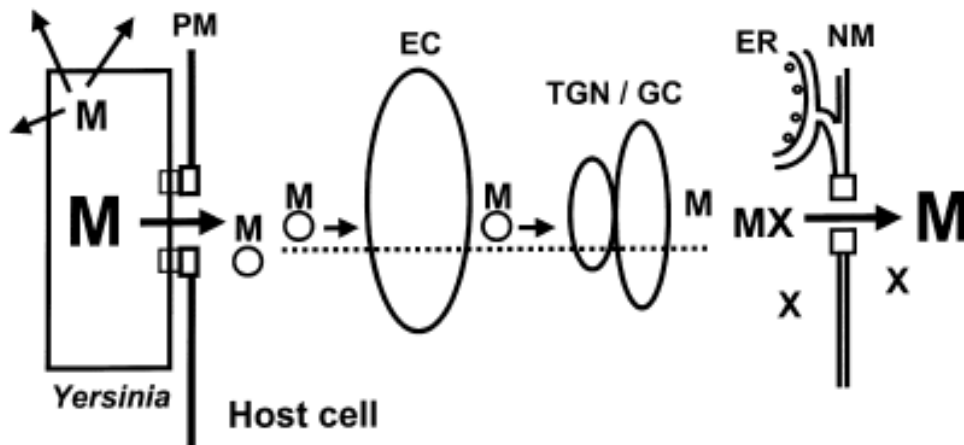
YopM (M) is injected by the T3SS into the eukaryotic cell through the pore in the plasma membrane (PM) formed by translocator YopB and binds to the surface of a vesicle, which then carries YopM to the endosomal compartment (EC). YopM's endosomal trafficking is microtubule dependent. At some point, YopM is released from the surface of the vesicle and interacts with the hypothetical component X, which chaperones YopM through the nuclear pore. Microtubules are shown schematically as a dotted line. GC, Golgi compartment; ER, endoplasmic reticulum; NM, nuclear membrane. (300)

Figure 1.8 *Y. pestis* modulates host immune responses to survive
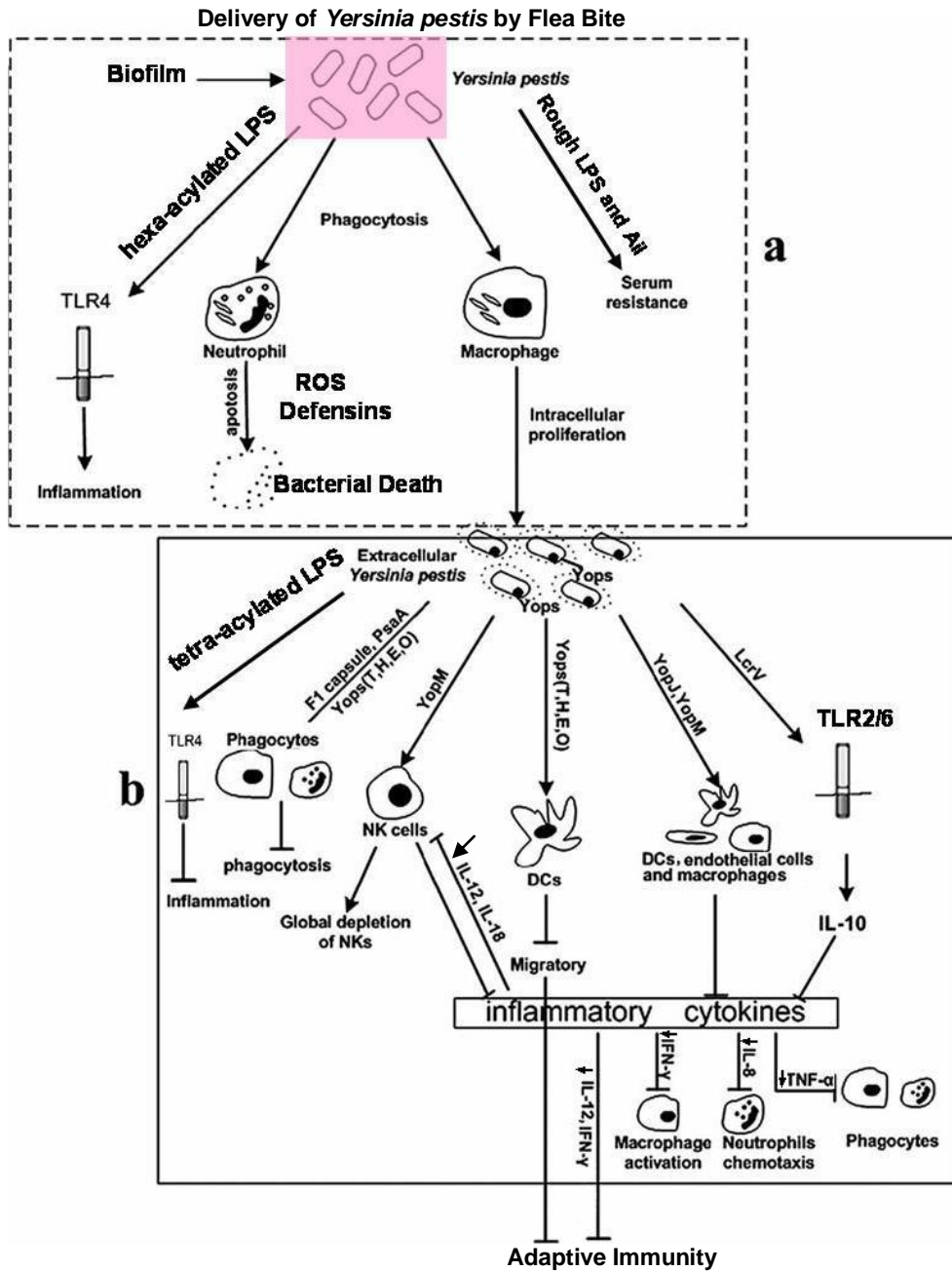
Y. pestis defense mechanisms against host innate immunity. (a) Defense mechanisms at the early stage of infection. (b) Defense mechanisms after the release of *Y. pestis* from macrophages. The figure was modified from the reference (185).

Chapter Two: Methods and Materials

A. Bacterial strains and *in vitro* cultivation

Bacterial strains and plasmids used in this study are listed in Table 2.1. This study employed strains from the two most recently evolved groups of *Y. pestis* populations (1), *Y. pestis* KIM5 (Kurdistan Iran Man, molecular grouping 2.MED), an isolate from Iran, and *Y. pestis* CO92 (1.ORI), isolated in the USA. The genomes of both strains have been sequenced (82, 241). *Y. pestis* KIM5 and its derivatives lack the chromosomal *pgm* locus and are conditionally virulent: they are attenuated from peripheral routes of infection but are virulent by the IV route of infection, which bypasses the requirement for the Ybt siderophore-based iron-acquisition mechanism encoded in this locus (159, 341). KIM5-3002, the *ΔyopM-1* derivative of KIM5, was created by deletion of the entire *yopM* gene, from −2 bp before the initiating Met codon through the stop codon by an allelic exchange method (159). The Δ*lacZ* Y. *pestis* KIM5-3003 was created in the *Y. pestis* KIM5 background by allelic exchange followed by sucrose selection to cure the suicide plasmid pLacZ as described previously (42). *Y. pestis* CO92.S6 and CO92.S19 were created by Christine Wulff in our lab (104, 363). *Y. pestis* CO92.S6 is fully virulent and *Y. pestis* CO92.S19 is the Δ*yopM-2* derivative of strain CO92.S6. CO92.S19 and CO92.S6 were handled only in BSL3 containment with select agent security.

Y. pestis KIM5-derived strains were routinely grown at 26ºC or 26ºC plus 3 hours pre-induction at 37ºC (26/37ºC) for pre-induction in Heart Infusion Broth (HIB, Difco Laboratories) without calcium and harvested in exponential phase at A620 = 0.8 to 1.2. Cells were centrifuged at 23,281 x g and 4ºC for 5 min, washed and diluted in PBS.

Samples from the dilutions were plated on tryptose blood agar (TBA, Difco Laboratories) (241) and incubated at 30°C for 2 d to determine the actual dose. To distinguish KIM5-3003 from the mixture of KIM5 and KIM5-3003, bacterial mixtures were plated on TBA plus 40 μg/ml X-Gal (Research Organics) and incubated at 30°C for 2 d. *Y. pestis* CO92-derived strains were grown at 28°C or 37°C as indicated in HIB supplemented with 2.5 mM $CaCl_2$ and 0.2% xylose; when the CO92 Lcr plasmid pCD2 was present, 50 μg/ml carbenicillin (Cb) also was present. Prior to infecting mice, the cultures were diluted in PBS. Samples of the doses and appropriate serial dilutions were plated on supplemented HIB + Cb and the number of colony forming units (CFUs) was determined after incubation for 2 d at 28°C. The presence of the pigmentation locus (245) in all Pgm[+] strains was confirmed by the formation of red colonies on Congo red agar (323) at 28°C. The presence of a functional Lcr virulence plasmid was confirmed by absence of growth at 37°C on supplemented HIB agar containing 0.2 M $MgCl_2$ and 0.2 M sodium oxalate (MgOx plates) and by the low calcium response growth and Yop secretion phenotypes (245) in the defined medium TMH (317).

pCD2Ap *ΔyopM-2* was created by Christine Wulff in our lab. The *yopM* ORF and 197 upstream bases containing the *yopM* promoter (265) were deleted from pCD2Ap of the *Y. pestis* CO92 derivative *Y. pestis* CO99-3015.S6. Briefly, primers LF up 5' ACATTAGAGCTCTGCCTGTCTCCGTTGTTG 3' and LF down 5' TACTATCTGCAGTGTATGGCCGCAGAGT 3' were used to copy 1180 bp of DNA upstream of the deleted locus by PCR, and primers RF up 5' TGCTGCAGACGCA-AGAGCGTTCAT 3' and RF down 5' ATCTCTCGAGACGCCACCGTTGATTA 3' were used to copy 1230 bp of downstream DNA. The upstream and downstream DNAs were

cloned into pLD55 as respective *Sac*I/*Pst*1 and *Pst*I/*Xho*I PCR products to create the allelic exchange plasmid p*ΔyopM-2* in *Escherichia coli* DH5αλ*pir*. The deletion was moved into pCD2Ap by allelic exchange as previously described (210, 233). The deletion did not remove any ORFs other than *yopM*, and its upstream boundary was 196 bp downstream from the stop codon of the nearest potential ORF (265). The deletion extended 1 bp downstream of the *yopM* stop codon (similarly to the *ΔyopM-1* mutation in *Y. pestis* KIM, which deletes the stop codon but no downstream bases). The resulting *yopM* deletion was confirmed by PCR. The absence of YopM expression in the *ΔyopM-2* strain but normal expression and secretion of YopH and LcrV with appropriate regulation by calcium in the medium was confirmed by immunoblot analysis of whole cells and culture supernatants. The two mutations, *ΔyopM-1* in the KIM5 background and *ΔyopM-2* in the CO92 background, are believed to have the same phenotypes because they are both well separated from upstream and downstream ORFs; but because they are not identical, we have given them different allelic designations.

B. Infection of mice and measurement of bacterial viable numbers in tissues

All animal experiments in this work were reviewed and approved by the University of Kentucky Institutional Animal Care and Use Committee. For studies with *Y. pestis* KIM5, KIM5-3002 and KIM-3003, 6 to 8 week old female C57BL/6N.HSD mice (Harlan Sprague Dawley, Inc) or female CCR2$^{-/-}$ and CCL2$^{-/-}$ C57BL/6J mice (obtained from Jayakrishna Ambati M.D., Department of Ophthalmology and Visual Sciences, University of Kentucky and bred by Annette Uittenbogaard in our lab (7)) ranging from 6 to 15 weeks of age were anesthetized with an isoflurane-oxygen mixture by a rodent

anesthesia machine. 100 µL (400 CFU) of bacterial suspension was injected into each mouse IV via the retro-orbital plexus. This was above the LD_{50} for the parent strain and below that for the $\Delta yopM$-1 mutant. At designated times after infection, groups of three or four mice per strain per time point were humanely killed by CO_2 inhalation followed by cervical dislocation, and their spleens and livers were weighed, transferred to a sterile bag containing 5 ml of PBS, and placed on ice. The tissues were homogenized in a Stomacher 80 lab blender (Tekmar Co.) for 60 s with high speed. The liver and spleen homogenates were diluted in PBS and plated to measure the bacterial burden in the organs. When studying the distribution of bacteria in mice, bone marrow from femurs was flushed by 1 ml sterile PBS, and the intestine was harvested and minced finely before homogenization. In most of the experiments, TBA plates were used, whereas Yersinia selective agar (YSA; Difco Laboratories) was used to recover *Yersinia pestis* from the intestine.

To study the function of peritoneal cells, C57B/L6 mice were IP injected with the designated dose in 100 µl sterile PBS. At harvest timepoints, 5 ml ice-cold PBS was injected into the peritoneal cavity of each mouse immediately after it was killed by CO_2 inhalation. The peritoneal lavage fluid was harvested by using a 10 ml syringe with an 18 gauge needle after thorough massage of the abdomen.

For infection with *Y. pestis* CO92 strains, the mice were anesthetized with ketamine (100mg/kg, IVX Animal Health) and xylazine (10mg/kg, Butler Co.) given IP. Bacterial doses were made in 100 µl of PBS for ID infection and administered with a 1-ml tuberculin syringe fitted with a retractable 26 gauge needle (Becton, Dickinson and Company). For IN infection a 20 µl volume of bacteria in PBS was instilled into the nares from a plastic micropipette tip. The effect of xylazine was then reversed by subcutaneous

injection of yohimbine (2mg/kg, Ben Venue Laboratories), at a different site than used for infection) and the mice were treated with an optical lubricant before being returned to their cages. At designated times after infection, the mice were humanely killed by IP injection of 100 µl of Beuthanasia-D (minimum of 150 mg/kg) followed by thoracic puncture, and the spleen and a patch of skin surrounding the infection site were recovered. Spleens were minced, and taken into a 3-ml syringe along with 1 ml of sterile distilled water (dH_2O). A second syringe equipped with a 20-gauge emulsifying needle was attached, and the sample was passed back and forth 20 times to further disrupt the tissue and release the bacteria. The piece of skin was minced and transferred to a 50-ml conical tube containing 2 ml sterile PBS, collagenase (40,000 U/ml), dispase protease (224 U/ml), and DNase (16,000 U/ml). The tubes were then agitated for 30 min in an upright position at 250 rpm on a gyrotory platform at 37°C. The resulting digest was taken into a 5-ml syringe and emulsified as above through an 18-gauge emusifying needle. The resulting spleen and skin suspensions were then serially diluted in PBS and plated in duplicate to determine CFUs.

C. Tests of virulence in mice

To determine LD_{50} values, groups of 8 mice were infected IV, IN, ID or IP with 10-fold or 3-fold increasing doses of YopM[+] parent or Δ*yopM* strains as indicated. The mice were monitored daily for 14 d for signs of illness and mortality. Mice were humanely killed if deemed unlikely to survive to the next observation and counted as though they were dead at the next observation. Criteria for humane killing were loss of the righting reflex or immobility accompanied by hunched posture, ruffled fur, and heavy breathing.

D. Innate immune cell ablation

NK cell ablation was mediated by anti-NK1.1 mAb PK136 that had previously been prepared by injecting the B cell hybridoma PK136 clone (American Type Culture Collection) IP into pristane-primed BALB/c mice and was a gift from Donald A. Cohen, Ph.D. in our Department. Ascites was clarified by centrifugation and stored at -20 $^{\circ}$C. Before use in mice, antibodies were again centrifuged and then filtered through a 0.22 μM pore-size low-protein-binding membrane (Millipore). Anti-NK1.1 mAb or rat IgG (Sigma-Aldrich Chemical Co.) was injected IP at 1 mg/mouse on d −1, 1 and 3 of *Y. pestis* infection.

Ablation of Gr1$^+$ cells was done as described previously (272). Briefly, anti-Gr1 mAb had been prepared from B cell hybridoma line R6-8C5 (DNAX Research Institute) and partially purified using ammonium sulfate precipitation. It was provided for this work by Donald A. Cohen Ph.D. in our Department. Anti-Gr1 mAb or rat IgG was injected IP at 100 μg/mouse on d −1 and 1 of *Y. pestis* infection.

Systemic ablation of macrophages/DCs was mediated by liposome-encapsulated clodronate (Cl$_2$MDP). The liposomes were prepared as previously described (346). Liposomes containing clodronate (clodronate liposome) or PBS (PBS liposome) were purchased from Nico van Rooijen Ph.D., Department of Molecular Biology, Vrije Universiteit Medical Center. Mice in ablation groups or control groups were injected IV via the retro-orbital plexus with 200 μL clodronate liposomes or PBS liposomes 18 h prior to Y. pestis infection and on d 1 p.i..

PMNs were ablated with the PMN-specific anti-Ly6G mAb (mAb 1A8; Bio X Cell)

or rat IgG (Sigma) injected IP at 200 µg/mouse on d −1 and 1 of *Y. pestis* infection. The extent of ablation in these and in mock-treated mice was assessed by flow cytometry with detection via fluorochrome-tagged anti-Ly6G and anti-CD11b antibodies.

To test the importance of recruitment of inflammatory monocytes into foci of infection, two KO mice strains were used. CCR2$^{-/-}$ and CCL2$^{-/-}$ strains were generated as described previously (168, 191). To create the CCR2 KO strain, the entire CCR2 coding region was replaced by insertion of a neomycin-resistance expression cassette, while CCL2/MCP-1 KO mice were created through targeted disruption of CCL2/MCP-1 gene. Although the original KO strains were generated on a mixed C57BL/6 × 129/Ola genetic background, the mice used in this study represent the progeny of the eighth generation backcross of the KO mutations to inbred C57BL/6 animals. Therefore C57BL/6 mice were used as control to the ablated mice.

Two tests employed transgenic Macrophage Fas-induced apoptosis (MaFIA) mice on a C57BL/6 background (57). These mice were bred and confirmed by PCR to be homozygous for the inducible suicide transgene before use in experiments. Mice were between 5 and 8 weeks old, and both sexes were used, distributed equally among treatment groups. These mice can be ablated for cells of the macrophages/DCs lineage by treatment with the dimerizer drug AP20187 (gift of Ariad Pharmaceuticals, Inc. to Donald A. Cohen Ph.D.). Seven days prior to infection, the ablation regimen was initiated by IV injection of 10 mg/kg of dimerizer drug or mock injection solution (water containing 4% [vol/vol] ethanol, 10% [wt/vol] PEG-400, and 1.7% [vol/vol] Tween-20). Injection was done within 30 min of dilution of dimerizer into the injection solution, and the volume, adjusted by body weight, averaged 100 µl per mouse. The mice received daily injections

of drug or mock solution for 5 days and then were allowed to rest two days before being infected with *Y. pestis* KIM5.

E. Flow cytometry

Cells isolated from livers and spleens were analyzed in a FACSCalibur flow cytometer (Becton Dickinson FACS Systems). Briefly, spleens were placed in sterile bags containing 5 ml PBS and then processed with the Stomacher 80 lab blender for 60 s at high speed. The homogenate was centrifuged (913 x g and 10 min) and resuspended in 2 ml RBC lysis buffer (150 mM NH_4Cl, pH 7.2). After 2 min, the reaction was terminated by addition of 8 ml of PBS. The cell suspensions were filtered through a 40μm-pore-size cell strainer (Becton, Dickinson and Company) to remove connective tissue, centrifuged (913 x g for 10 min), and resuspended in PBS containing 1% (wt/vol) BSA and 0.1% (wt/vol) sodium azide (PBS-BSA-azide).

To process livers, finely minced livers were placed into sterile bags containing 10 ml RPMI 1640 (Life Technologies Inc.) with 10% FBS (ATCC) and processed with the Stomacher 80 lab blender for 60 s at high speed. The homogenates were incubated with DNase I (160 U/ml, Sigma-Aldrich) and collagenase (400 U/ml, Invitrogen) for 30 min in a 37°C water bath with shaking at 125 rpm. After filtration through a 40 μm-pore-size cell strainer, cell suspensions were washed once with ice-cold PBS-BSA-Azide and resuspended with 5 ml 33.8% Percoll (Amersham Bioscience, GE Healthcare) followed by a 12-min centrifugation at 693 x g. The cells in the bottom layer were collected, washed with PBS and treated with RBC lysis buffer. Nonlysed cells were resuspended in PBS-BSA-azide.

In some experiments, blood was obtained by cardiac puncture using a syringe containing 30 μl of 1000 units/ml heparin (Elkins-sinn, Inc). Approximately 200 μl of blood was harvested from each mouse and then mixed with 5 ml of PBS. The mixture was carefully overlaid on 5 ml Lympholyte-Mammal (Cedarlane Labs), and then centrifuged at 600 x g for 20 min at room temperature. The leukocytes were obtained from the interface and washed twice in PBS-BSA-Azide. When harvesting the leukocytes from bone marrow, two femurs were isolated from each mouse. Bone marrow from every femur was flushed by 1 ml sterile PBS and the leukocytes were obtained after washed twice with PBS-BSA-Azide.

The antibodies and compounds used in flow cytometry staining are listed in table 2.2. The following antibodies were purchased from BD Pharmingen, Inc.: allophycocyanin (APC)-conjugated anti-CD11c, APC-conjugated anti-NK1.1, APC-conjugated anti-CD62L, Fluorescein isothiocyanate (FITC)-conjugated anti-CD3, FITC-conjugated anti-CD11b, FITC-conjugated DX5 (anti-CD49b), Phycoerythrin (PE)-conjugated anti-B220, PE-conjugated anti-CD8, PE-conjugated DX5, PE-conjugated anti-Ly6G, PE-conjugated anti-NK1.1, PE-conjugated anti-CD86 and PE-conjugated anti-$I_A{}^b$. To gate out apoptotic or dead cells, ethidium monoazide (EMA, Sigma) was used for viability staining. To evaluate NKT cells, mCD1d/PBS57 (APC conjugated) was used (provided by the NIH Tetramer Core Facility).

Prior to staining, the cells were counted, and samples were adjusted to 5×10^5 cells per 100 μl and treated with Fc Block™ for 15 min. All samples were stained with EMA to identify dead cells. In the presence of the appropriate combinations of antibodies and EMA, the cells were incubated on ice for 30 min, with the last 10 min being in the light.

After being washed in PBS, the cells were resuspended in ice-cold PBS containing 4% (wt/vol) paraformaldehyde, pH 7.4 and treated at least 30 min before flow cytometric analysis.

To detect intracellular iNOS and TNFα in particular cell types, cells were processed with BD Cytofix/Cytoperm™ Plus Fixation/Permeabilization Kit (BD Biosciences). Briefly, cells were treated with GolgiPlug™ (1 μl per ml of cell suspension) for 4 hours at 37°C followed by surface marker staining described above. Then the cells were incubated with Fixation/Permeabilization solution for 20 min at 4 $^{\circ}$C. After being washed with Perm/Wash™ buffer, the cells were stained with appropriate antibodies at 4°C for 1 hour in the dark. Then they were sent for flow cytometric analysis after washes and resuspended in PBS-BSA-Azide.

Flow cytometric processing was performed by the Flow Cytometry Core Facility at the University of Kentucky. Software WinMDI (Version 2.7; Joseph Trotter, Salk Institute for Biological Studies, La Jolla, CA [available at http://facs.Scripps.edu/software.html]) was used to analyze the data. To measure the expression level of each cellular surface marker, mean fluorescence intensity (MFI) of the fluorochrome conjugated to this marker's monoclonal antibody was used. Typical leukocyte populations obtained by these methods from non-infected mice are given in Table 2.3. The numbers of total leukocytes harvested from spleen and liver did not change significantly after infection (data not shown). Therefore, the percentages, not the absolute numbers, of individual immune cell type in the total live leukocytes were reported in this dissertation excepte in Figure 8.4.

F. Giemsa Staining to test the cellular contents of the peritoneal lavage in IP infection

Peritoneal cells harvested from the IP infected mice were pelleted (913 x g for 10 min), resuspended with ice-cold PBS and counted. 200 uL cell suspensions (4×10^5 cells/ mL) was loaded into the assembled cytospin cartridge (Shandon) and centrifuged at 700 rpm for 7 min. Slides then were collected and air-dried for 10 min at room temperature. The cells then underwent 2 min fixation with LeukoStat Fixative Solution (Fischer Diagnostics), 25 sec of staining with Diff Quick Solution 1 (Baxter) and 1 min of staining with Diff Quick Solution 2 (Baxter). After 2x washes with double-distilled water, the slides were air-dried and sealed by Permount (Fischer Diagnostics) and coverslips, and then were ready for reading under the microscope.

G. Measurement of Reactive Oxygen Species (ROS) and nitric oxide (NO) production in leukocytes from infected spleen or peritoneal lavage

To study the splenic leukocytes, spleens were homogenized with the Stomacher 80 lab blender for 60 seconds at high speed and treated with 300U/ml collagenase (Invitrogen) at 37°C for 30 minutes. To study their stimulability, those cells were treated with 200 nM Phorbol Myristate Acetate (PMA, Cell Signaling Technology) or PBS as control at 37°C for 1 hour after RBC lysis. Then the cells were stained with 2',7'-dichlorodihydrofluorescein diacetate (DCFDA) and 4-amino-5-methylamino-2',7'-difluorofluorescein (DAF) (Invitrogen) (5 µM in 1x Hanks salt solution (GIBCO)) at 37°C for 30 minutes. DCFDA and DAF powder was dissolved by pure (H_2O free) dimethyl sulfoxide (DMSO) to make 5 mM stock solution and kept in lightproof

container at -20°C as 10 uL aliquot. As soon as DCFDA or DAF was added, the cells were incubated or transported in lightproof container.

Finally those splenic leukocytes were stained with antibodies against appropriate surface markers and EMA for 30 minutes. After two washes, the samples were analyzed by the Flow Cytometry Core Facility at the University of Kentucky immediately.

Peritoneal cells were harvested by peritoneal lavage as described in Section 2.F. The cells were washed with ice-cold PBS twice, resuspended with 1x Hanks salt solution, and counted. $1x10^5$ cells were loaded into each well of 96-well plate. After treatment with 200 nM PMA or PBS for 1 hour at 37°C, the cells were incubated with DCFDA or DAF (5 µM in 1x Hanks salt solution) for 30 minutes. The relative fluorescence units (RFUs) were read by microplate reader (Molecular Devices Corporation).

H. Histopathology

Lobes of liver were harvested from C57BL/6 mice infected IV with either *Y. pestis* KIM5 or *Y. pestis* KIM5-3002. In the BL3 facility, skin patches at the infection sites were excised from C57BL/6 or CCR2$^{-/-}$ mice ID infected with either *Y. pestis* CO92.S6 or *Y. pestis* CO92.S19. In the pneumonic plague model, portions of lung were harvested from C57BL/6 mice IN infected with either *Y. pestis* CO92.S6 or *Y. pestis* CO92.S19. All of the above tissues were fixed for 24 h at room temperature in 10% buffered formalin and processed through graded alcohol and xylene, followed by embedment in paraffin (performed in the Histology Laboratory in Department of Pathology and Laboratory Medicine at the University of Kentucky). Sections stained with hematoxylin and eosin were examined and photographed with an Axiophot microscope (Carl Zeiss, Inc.).

I. Statistical analysis

With few exceptions (note in the text), all experiments were conducted at least twice with at least 3 replicate mice per group. Then the data from the replicate experiments were pooled for analysis of significance. Significance of differences among groups was assessed by the Student's unpaired 2-tailed t test. Values for $P < 0.05$ were considered significant. Data are presented as the mean value ± standard deviation and the numbers of mice used for each datum point are given in the figure legends. Virulence tests measuring lethality were conducted at least twice with four to eight mice per group and three or four dosage groups. Probit analysis was applied to log-transformed pooled data (17; implemented through BioStat 2008 5.1.1.0 [by A. Simachov at AnalystSoft]). Pairwise comparison of data groups with nonparametric distributions was made with the Wilcoxon two sample test. Four frequently used notations for significance in this dissertation are listed in Table 2.4. The less-used notations are described in individual figures.

Table 2.1 Bacterial strains and plasmids used in this study

Strain	Relevant properties	Source or Reference
Y. pestis		
KIM5	Pgm$^-$ Lcr$^+$; pCD1 pMT1 pPCP1; conditionally virulent Δ*pgm* 2.MED strain; also called KIM D27	R. R. Brubaker
KIM5-3002	Δ*yopM-1* derivative of KIM5; *yopM* coding sequence deleted from 2 bp upstream of Met through the translational stop codon.	(159)
KIM5-3003	Δ*lacZ* derivative of KIM5; created by allelic exchange followed by sucrose selection to cure the suicide plasmid pLacZ	(42)
CO99-3015.S6	CO92 Ap^r Δ*pgm* Lcr$^+$ pFra, pPCP1; contains pCD2Ap	Spencer Leigh; (104)
CO92.S6	CO92 Ap^r Pgm$^+$ Lcr$^+$ pFra, pPCP1; reconstituted virulent strain made by introduction of pCD2Ap into CO92.S1.	(104)
CO92.S19	Reconstituted Lcr$^+$ Δ*yopM-2* strain made by introducing pCD2Ap Δ*yopM-2* from CO99-3015.S11 into CO92.S1.	(363)
E. coli		

DH5α*λpir*	*recA1 endA1 gyrA96 thi-1 hsdR17 supE44 relA1 deR* Δ(*lacZYA-argF*)U169 *λpir*+	Lab stock
Plasmids		
pLD55	Suicide vector with *ori*$_{R6K\gamma}$ and fusaric acid selection; Ap^{r}Tc^r	(210)
pΔ*yopM-2*	pLD55 containing the 1180 bp left flank DNA upstream of the Δ*yopM-2* locus fused to the 1230 bp right flank DNA downstream of Δ*yopM-2*	This Study

Table 2.2 Antibodies and compounds used in flow cytometry staining

Fluorochrome	Antibodies or Compounds	Sources
FITC	CD3	BD Pharmingen, Inc.
	DX5	BD Pharmingen, Inc.
	CD11b	BD Pharmingen, Inc.
	iNOS	BD Pharmingen, Inc.
	Gr1	BD Pharmingen, Inc.
PE	Ly6G	BD Pharmingen, Inc.
	TNF-alpha	BD Pharmingen, Inc.
	CD19	BD Pharmingen, Inc.
	Mac3	BD Pharmingen, Inc.
	CD8	BD Pharmingen, Inc.
	B220	BD Pharmingen, Inc.
	NK1.1	BD Pharmingen, Inc.
	DX5	BD Pharmingen, Inc.
APC	CD11c	BD Pharmingen, Inc.
	NK1.1	BD Pharmingen, Inc.
	Gr1	BD Pharmingen, Inc.
	mCD1d/PBS57	NIH Tetramer Core Facility
Compound	EMA	Sigma
Compound	DCFDA	Invitrogen
Compound	DAF	Invitrogen

Table 2.3 Average populations of total leukocytes, PMNs, MDMs, NK cells, DCs and iDCs obtained from the spleens and livers of uninfected mice.

	Total Number per Organ (10^6)	
Cells	Spleen	Liver
Total leukocytes	110.7 ± 9.5	8.9 ± 0.3
PMNs (Ly6G$^+$ CD11b$^+$)	9.3 ± 0.5	0.29 ± 0.03
MDMs (Ly6G$^-$ CD11b$^+$)	5.5 ± 2.9	0.79 ± 0.05
NK cells (NK1.1$^+$ DX5$^+$ CD3$^-$)	7.4 ± 1.5	0.73 ± 0.08
DCs (CD11c$^+$)	4.5 ± 0.9	1.2 ± 0.25
iDCs (CD11b$^+$CD11c^{int})	2.1 ± 0.2	0.21 ± 0.007

Table 2.4 Notations for the significance

A.

Infecting Strains	Comparison Between Different Groups of Mice	Notation
ΔyopM strain (KIM5-3002)	NK-ablated and mock-ablated mice	
	Gr1+ cell ablated and mock-ablated mice	†, P<0.05; ††, P<0.01
	PMN ablated and mock-ablated mice	
	MDM-ablated and mock-ablated mice	
	CCR2 KO and WT mice	
	CCL2 KO and WT mice	
Parent strain (KIM5)	NK-ablated and mock-ablated mice	
	Gr1+ cell ablated and mock-ablated mice	#, P<0.05; # #, P<0.01
	PMN ablated and mock-ablated mice	
	MDM-ablated and mock-ablated mice	
	CCR2 KO and WT mice	
	CCL2 KO and WT mice	

B.

Mice	Comparison Between *Y. pestis* strains	Notation
Immune cell mock-ablated mice		
WT mice	*ΔyopM* strain (KIM5-3002) and parent strain (KIM5)	*, P < 0.05; **, P < 0.01
NK-ablated mice		
Gr1+ cell ablated mice		
PMN ablated mice	*ΔyopM* strain (KIM5-3002) and parent strain (KIM5)	δ, P < 0.05; δδ, P < 0.01
MDM-ablated mice		
CCR2 KO mice		
CCL2 KO mice		

RESULTS

Chapter Three: Characterizing Different Plague Models

In most experiments of this study, we used a systemic plague model, which means direct injection of bacteria into the retro-orbital plexus of mice to infect the spleen and liver. The bacteria used in this model were *Δpgm Y. pestis* KIM5 so they were virulent from the IV route but not the ID route. The bacteria were inoculated and cultured in HIB medium at 26ºC or 26/37ºC, then diluted to the target concentration before infection. The bacteria seed spleen and liver within 30 min of infection (57). Therefore this model offered the strong advantage of a synchronous infection that can be readily quantified under BSL2 conditions to provide insight on host responses to simulated flea-grown (26ºC) or mammal adapted (26/37ºC) *Y. pestis*.

Other models in this study were ID and IN infections. Fully virulent *Y. pestis* CO92 was used. In the BSL3 lab, CO92 was cultured at 28ºC and diluted before infection. These bacteria have the *pgm* locus so they are not iron-dependent and can multiply in skin and lung tissue, where the Ybt iron acquisition system is important to obtain iron for bacterial growth. These ID and IN routes of infection mimic the real diseases, bubonic and pneumonic plague, respectively.

To check the role of YopM in the virulence, the first step was to measure the effect of this protein on lethality (LD_{50}) of *Y. pestis*. Based on the LD_{50}, bacterial doses were chosen and the growth patterns of the bacteria with or without YopM were plotted.

A. *Y. pestis* **mainly disseminates into spleen and liver in the systemic model**

It is important to know where the injected bacteria seed because the seeding sites, especially early seeding sites, are the microenvironment in which bacteria contact the host immune system. As shown in Figure 3.1A, a high dose of *Y. pestis* KIM5 (5000 CFU/mouse) was injected retro-orbitally and different organs, including spleen, liver, intestine, gallbladder, lung, kidney, cervical lymph nodes and bone marrow, were harvested after 6, 24 and 48 hours. The homogenate was plated onto TBA or YSA plates, and CFUs were counted after 2 days incubation at 30 °C. The percentages of recovered CFU in each organ with respect to the infecting dose were calculated and plotted.

Surprisingly, only less than 30% bacteria could be recovered after 6 hours, mainly in spleen and liver (Figure 3.1B), and no bacteria were detected from other organs except a few from intestine. Thus, over 70% of the infecting bacteria were cleared and the actual percentage could be even higher, since the bacteria kept multiplying in that 6 hours. The viable numbers of bacteria recovered from spleen and liver at 24 and 48 hours p.i. were much higher than those at 6 hours p.i., and bacteria were recovered from all of the other organs, although the number was much lower than in the spleen and liver (Figure 3.1 C and D). This finding helped us to focus our work on spleen and liver as the major target organs.

B. **YopM is required for the virulence of *Y. pestis* in this systemic plague model and compromises the proinflammatory response in liver**

First, we measured the LD_{50} of *ΔyopM-1 Y. pestis*. A serial dilution of *ΔyopM-1 Y. pestis* was injected IV into C57BL/6 mice and those mice were observed closely for 2

weeks. The actual doses were obtained by plating dilutions of the infecting suspension and the death of mice was recorded. Through the software Biostat, we derived the LD_{50} of the *ΔyopM-1* mutant (26ºC, table 3.1). Compared to the known LD_{50} of the parent strain KIM5 (Table 3.1) (159), we found the LD_{50} of the *ΔyopM-1 Y. pestis* KIM5-3002 to be 4000-fold higher. This showed that YopM is indispensable for the full virulence of *Y. pestis* in this systemic model.

Next we compared the growth pattern of the parent and *ΔyopM-1* strains. The design of this experiment is shown in Figure 3.2A. Groups of 3 or 4 mice were infected with 400 CFU of the parent strain KIM5 or the *ΔyopM-1* strain KIM5-3002. A group of mice infected with each strain was euthanized daily from d 1 to d 5 p.i. and bacteria were recovered from spleens and livers. The growth curves (Figure 3.2B) displayed the pattern of both strains in spleen and liver. In spleen, the parent strain showed an early rapid growth before d 2 p.i. and a subsequent brief plateau. A second growth spurt occurred between d 3 and d 4 p.i., followed by the second plateau and death of the mice. The *ΔyopM-1* strain grew in spleen similarly to the parent strain until d 2 p.i. and remained at the same level until d 4 p.i., followed by clearance. The parent strain showed a similar growth pattern in liver to that in spleen, whereas the plateau of the *ΔyopM-1* growth curve in liver only lasted until d 3 p.i. and was followed by clearance. The difference between two strains became significant in both spleen and liver after d 2 p.i..

Together with the LD_{50} data, this finding showed that the absence of YopM not only increases the lethal dose but also inhibits the multiplication of *Y. pestis* in the host at an early stage of the infection.

To check YopM's effect on the inflammatory response at the early stage of plague, we did histopathological analysis of the livers from the mice infected with these two strains. The lesions in the mice infected with parent *Y. pestis* were found to be dominated by resolving acute inflammation on d 3 p.i., whereas those from mice infected with the *ΔyopM-1* mutant contained large numbers of PMNs and macrophages (Figure 3.2C). We hypothesized that the difference in the acute inflammatory response between the parent and mutant strains may be responsible to their different growth characters in this model.

C. YopM is necessary for the pathogensis of bubonic plagues, but not for pneumonic plague and probably functions to counteract inflammation

To mimic the natural infection, we used other two models: a bubonic plague model and a pneumonic plague model. Fully virulent Pgm$^+$ *Y. pestis* CO92.S6 and its *ΔyopM-2* mutant CO92.S19, in which YopM and its promoter were deleted from the CO92.S6 background, were given to mice. In the bubonic model, fully virulent *Y. pestis* grown at 28ºC were injected ID at the site just above the base of the tail to mimic flea bites (289). In the pneumonic plague model, the mice were infected with the 37ºC-grown bacteria through the nasal cavity. As in the systemic model, we also checked the role YopM by measuring the LD$_{50}$ and by histopathological analysis.

The LD$_{50}$ of the *ΔyopM-2* mutant CO92.S19 by the IN route was similar to that for CO92.S6 (Table 3.1), indicating that YopM is not a virulence factor for pneumonic plague. However, by the ID route, the *ΔyopM-2* strain was reduced in lethality by 25-fold compared to *Y. pestis* CO92.S6 (Table 3.1). These results showed that YopM is required for full virulence in bubonic plague but not pneumonic plague.

Influx of inflammatory cells does not occur into lungs before 36 to 48 h p.i. in pneumonic plague (173), but it was not known whether there is a rapid inflammatory response in bubonic plague. We addressed this question in the experiments of Figure 3.3. We harvested the skin surrounding the infection site at 8, 24 48 and 72 h p.i. for histopathological analysis. For comparison, lungs of mice infected IN were also evaluated. There was no inflammation present in the lungs after 24 h p.i. (Figure 3.3C and 3.3D, lower panels). Marked hemorrhage as well as numerous inflammatory cells appeared by 48 h p.i. in the IN infection of either strain (Figure 3.3E). In contrast, a robust influx of inflammatory cells was underway as early as 8 h p.i. in the skin of mice infected ID with either *Y. pestis* strain but limited in epidermis by 24 h p.i. (Figure 3.3C and 3.3D, upper panels), while the inflammatory response expanded into the dermis at 48 h p.i. (Figure 3E, upper panel). Although there was no difference between the parent and the *ΔyopM-2* strains seen in the pathological appearance of the cutaneous infection sites, these strains differed in their virulence (LD_{50}, Table 3.1) in this bubonic model. These findings are consistent with an indispensable role of YopM in *Y. pestis* virulence being its function in modulation of the early inflammatory responses. Because there is no early inflammatory response in pneumonic plague, YopM is not needed for full virulence in that disease, whereas YopM is required for bubonic plague, to overcome the rapid inflammatory response.

Table 3.1 Virulence in 6 to 8-week female C57BL/6 mice of *Y. pestis* strains used in this study.

Y. pestis Strain	Key Properties	Culture Temperature	Route	LD$_{50}$ (Reference)
KIM5 (D27)	Δ*pgm*	26 ºC	IV	<50 (159)
			IP	6×10^4 (this study)
KIM5-3002	Δ*yopM-1* Δ*pgm*	26ºC	IV	2.08×10^5 (this study)
			IP	$\geq 10^7$ (this study)
KIM5-3002	Δ*yopM-1* Δ*pgm*	26/37ºC[a]	IV	5.4×10^4 (this study)
CO92.S6	Pgm$^+$	28 ºC	IN	14 (363)
			ID	17 (this study)
CO92.S19	Δ*yopM-2* Pgm$^+$	28 ºC	IN	39 (363)
			ID	409 (this study)

a. 26/37ºC means the bacteria were cultured at 26 ºC overnight and transferred to 37 ºC for 3 hours before processed for infection.

Figure 3.1 Distribution of KIM5 *Y. pestis* in mice at early stage of the infection

A

B

C

D

48 Hours Post KIM5 Infection
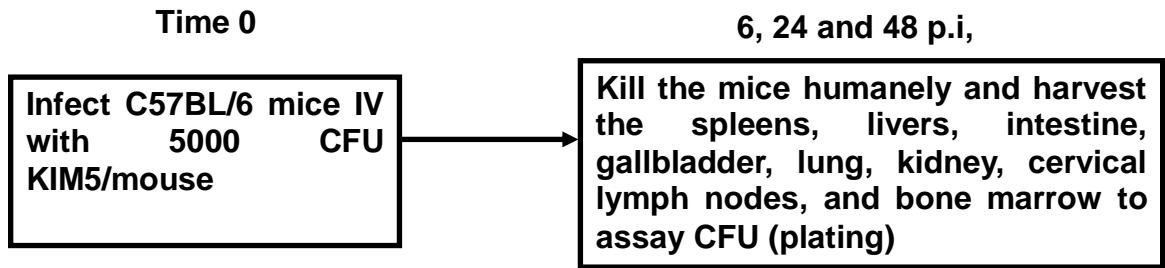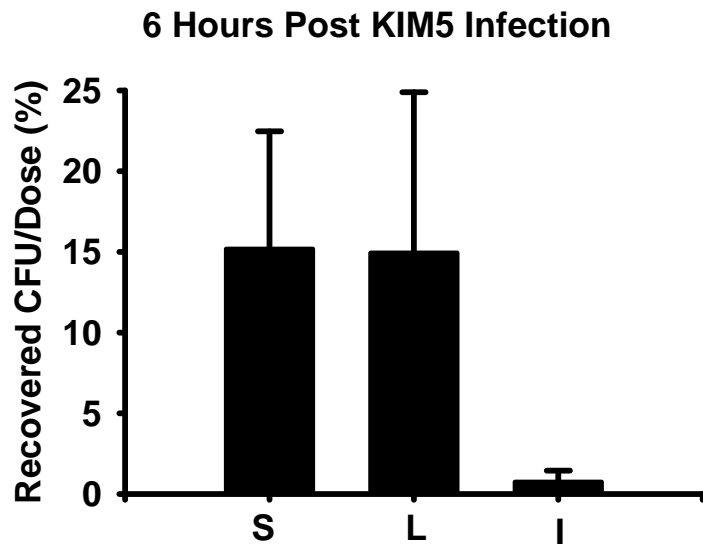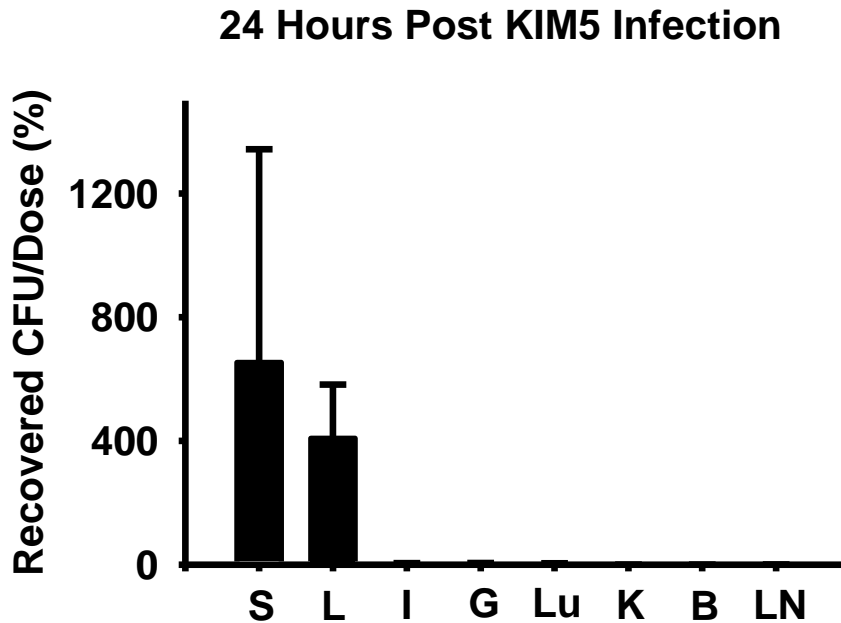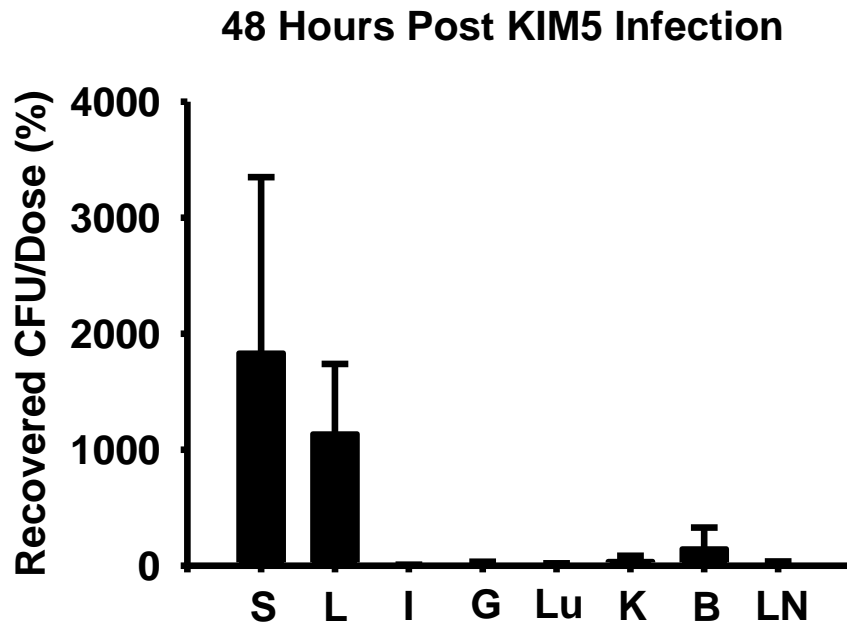
C57BL/6 mice were infected IV with 5000 CFU *Y. pestis* KIM5 (the parent strain) that had been grown at 26°C. At the indicated times, groups of mice were analyzed for bacterial viable numbers (CFU) in different organs. Panel A, experimental design. Panel B, the ratio of recovered CFU in spleens, livers and intestine to the infecting dose (expressed as percentage). Each datum point represents the average of values from 6 mice. S, Spleen; L, liver; I, intestine; G, gallbladder; Lu, lung; K, kidney; B, bone marrow; LN, cervical lymph node.

Figure 3.2 Comparisons of bacterial CFUs and histopathological responses in C57BL/6

mice infected with *ΔyopM-1 Y. pestis* KIM5-3002 or the parent strain KIM5 *Y. pestis*

A

Day 0

Day 1, 2, 3, 4 and 5 p.i

| Infect the C57 BL/6 mice IV with 400 CFU/mouse *ΔyopM-1* mutant KIM5-3002 or KIM5 | → | Kill the mice humanely and harvested the spleens and livers for CFU (plating) and histopathological analysis |

B

C
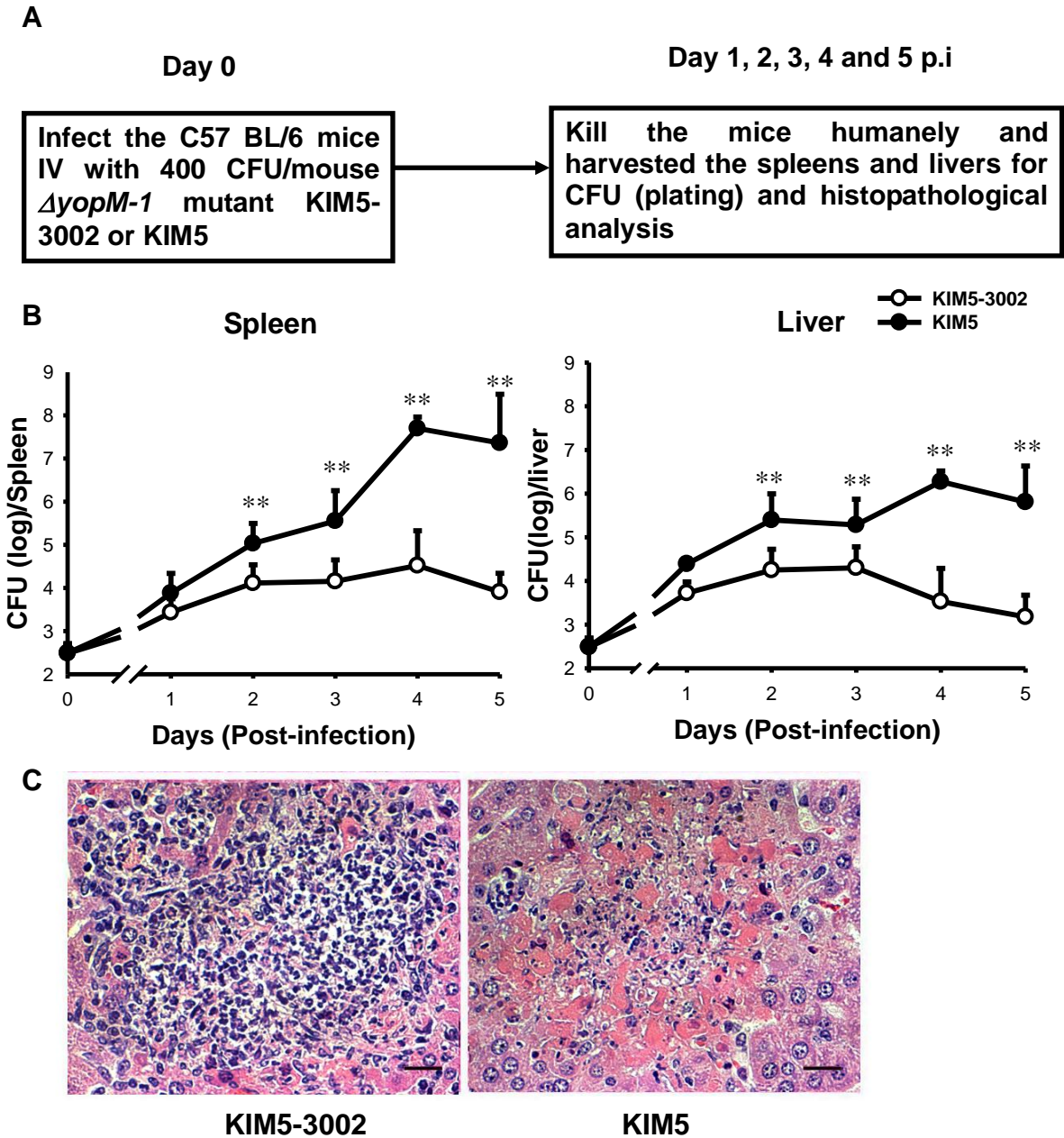
KIM5-3002   **KIM5**

Mice were infected IV with 400 CFU of KIM5-3002 or KIM5 *Y. pestis*. At the indicated

times p.i., spleens and livers of mice were analyzed for bacterial viable numbers (CFU)

and histopathology. Panel A, experimental design. Panel B, CFUs of KIM5-3002 (open

circles) or KIM5 (closed circles) *Y. pestis* from spleens and livers. The data represent the average plus SDs (error bars) for 29 mice (pooled from groups of 3 or 4 mice) per datum point. The day 0 points give the total bacterial doses as determined by plating the inocula. Values that are significantly different between KIM5-3002 and KIM5 infected groups are indicated (**, $P < 0.01$). Panel C, histopathology on d 3 p.i. in liver of mice infected with KIM5-3002 (left) or KIM5 (right) (Bars: 20 μm) (H&E staining).

Figure 3.3 Histology in skin after ID infection and in lung after IN infection with

ΔyopM-2 Y. pestis CO92.S19 or the parent strain CO92.S6

A

Day 0	8, 24, 48 and 72 hours p.i.

B

C

D

E
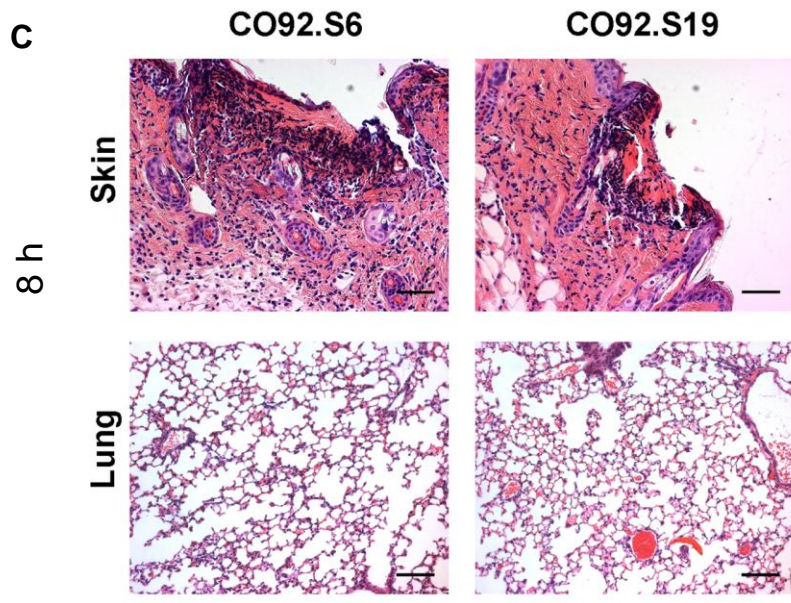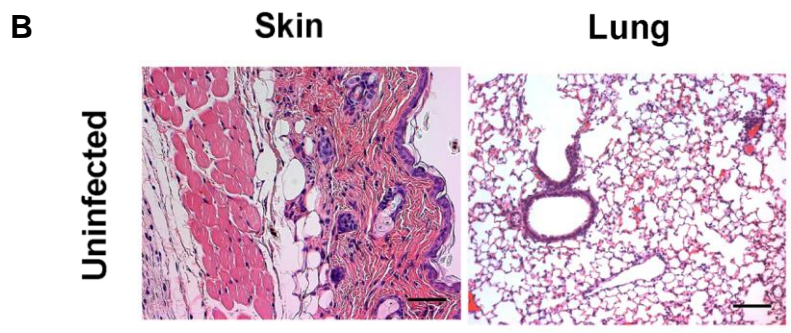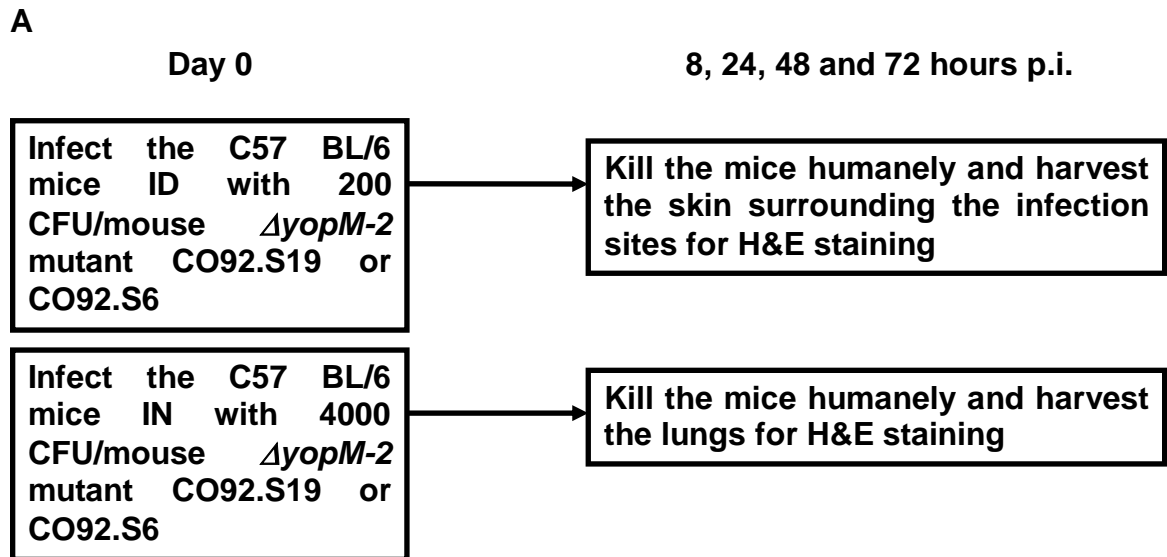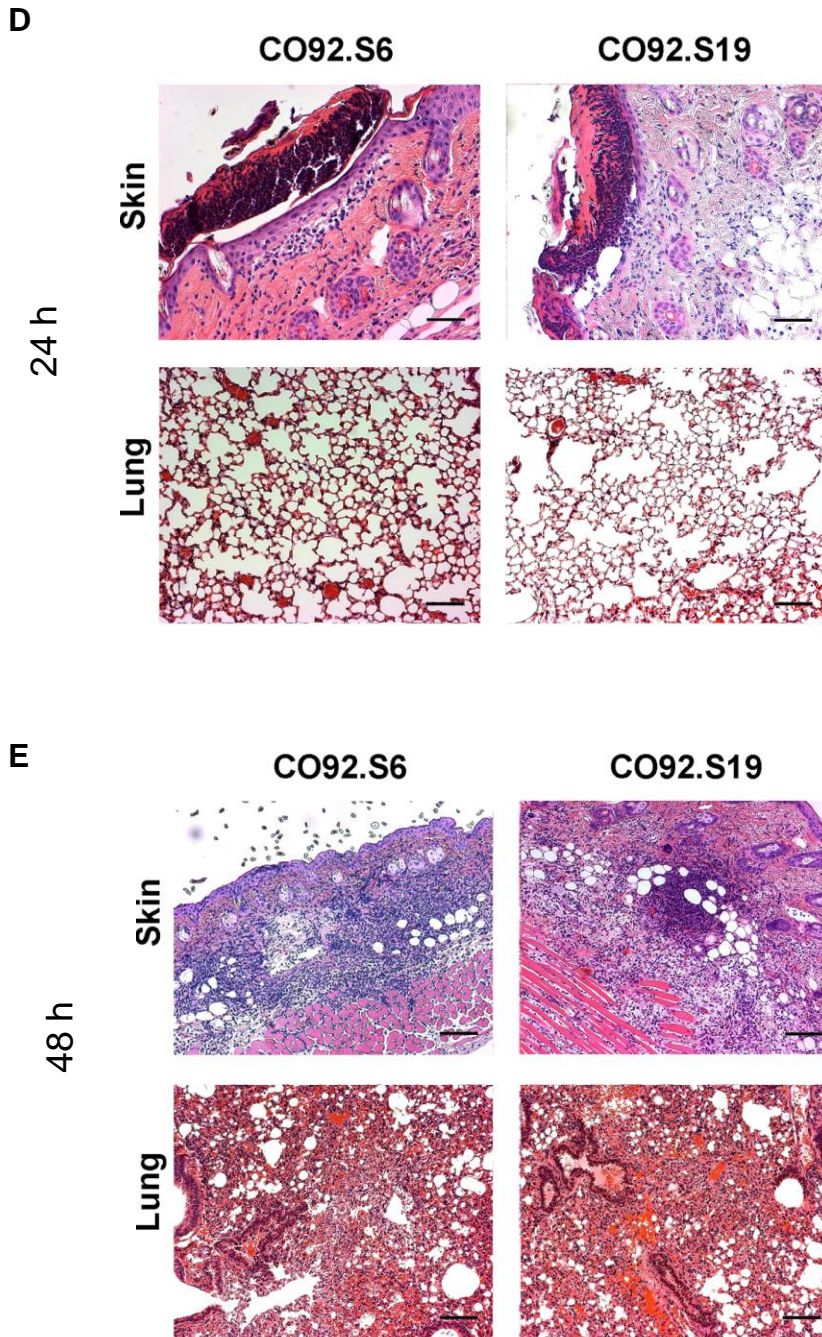
Tissue samples were harvested from uninfected mice and the mice infected by the fully virulent *Y. pestis* CO92.S6 (the parent strain) or the Δ*yopM-2* derivative at 8, 24 and 48 h post ID infection with ca. 200 CFU (actual doses: CO92.S6 = 216 and CO92.S19 = 163 CFU) or post IN infection with 5100 CFU of CO92.S6 and 4000 CFU of CO92.S19.

Panel A, experimental design. Panel B, skin and lung from uninfected mouse. Panel C, D and E skin near the infection sites and lungs harvested from the mice 8, 24 and 48 h post infection, respectively. Bars in the panels of skin: 50 µm in panel B, C and D; 100µm in panel E. Bars in the panels of lung: 100 µm.

RESULTS

Chapter Four: NK cells are not a key target of YopM

The time course for the growth of the parent *Y. pestis* KIM5 is similar in liver and spleen of mice with systemic plague; and the timing of the growth and clearance of the *ΔyopM-1* mutant KIM5-3002 are also similar for the two organs although clearance begins earlier in liver (Figure 3.2B). It was hypothesized that the host mechanisms that control the growth patterns are similar in the two organs. In previous work (159), several leukocyte populations had been characterized in spleens and blood of mice with systemic plague, and NK cells showed a YopM-dependent pattern of influx into spleen. However, none of these cell types had been tested in liver and their roles in limiting the growth of the *ΔyopM-1* mutant also needed to be clarified. In this work we checked the recruitment of NK cells into liver and their requirement for controlling growth of *ΔyopM-1 Y. pestis* in liver as well as in spleen.

A. YopM-containing *Y. pestis* depleted the NK1.1$^+$CD3$^-$ NK subgroup in spleen, whereas the splenic NK1.1$^+$CD3$^+$ (NKT) subgroup was intact

There are two major surface markers on NK cells in C57BL/6 mice: NK1.1 (clone: PK136) and CD49b (clone: DX5). NK1.1 is unique to NK cells, whereas CD49b is expressed by NK cells and some T cells (224). Meanwhile, some NK1.1$^+$ cells also express TCR and CD3, which are usually on the T cell surface. These cells are called NKT cells and are a potent source of immunoregulatory cytokines, including IL-4, IFN-γ and TNF. A specific stain to detect NKT cells is mCD1d/PBS-57 (113). PBS57 is a

fluorescent analogue of α-galactosylceramide, which is loaded onto a MHC-like molecule mCD1d, which is the ligand for the specific double-negative αβ- TCR on NKT cells. There are two main subsets of mCD1d-dependent NKT cells: NK1.1$^+$ and NK1.1$^-$ NKT cells. The majority of NKT cells express NK1.1 on their surface and these cells produce higher levels of IFN-γ and lower levels of IL-4 than their NK1.1$^-$ counterparts. Therefore, the relevant NKT cells in our study should be the NK1.1$^+$ NKT cells (34, 113). Meanwhile, almost all the mCD1d/PBS-57$^+$ cells in our experiments were positive for CD3 and NK1.1 simultaneously (Figure 4.1B).

According to above surface markers, classical NK cells were defined as NK1.1$^+$DX5$^+$CD3$^-$ and NK1.1$^+$DX5$^-$CD3$^-$, while NKT cells were simply defined as CD3$^+$ NK1.1$^+$. In order to cover all possible NK-like cells, a subset of DX5$^+$ cells, DX5$^+$NK1.1$^-$CD3$^-$, with unknown function was also checked (Table 4.1). Representative flow-cytometric scatter plots of the different cell types considered in this dissertation are shown in Figure 4.2.

Groups of 3 or 4 C57BL/6 mice were infected IV with 400 CFU of *Y. pestis* KIM5 or KIM5-3002. Spleens were harvested for flow cytometric analysis on d 2, 4 and 5 p.i.. The design of this experiment is shown in Figure 4.1A. YopM-dependent loss of splenic NK1.1$^+$ (DX5$^+$ or DX5$^-$) CD3$^-$ NK subgroups was observed during infection as previously reported (159) (Figure 4.1C). Neither NK1.1$^+$CD3$^+$ NKT cells nor DX5$^+$NK1.1$^-$CD3$^-$ cells showed any YopM-dependent changes, although the percentages of these latter cells dropped by ca. 2-fold between d 2 and d 4 p.i. in mice infected by either *Y. pestis* strain (Figure 4.1D).

B. There was no YopM-associated depletion of either classic NK cells or NKT cells in liver

We then tested whether the YopM-specific NK cell depletion seen previously in spleen was truly a global effect, which means that ablation occurred in the two major organs (liver and spleen, Figure 3.1B) colonized by *Y. pestis* early in systemic plague. Groups of 3 or 4 C57BL/6 mice were infected IV with 400 CFU/mouse of *Y. pestis* KIM5 or KIM5-3002. Livers were harvested for flow cytometric analysis on d 2, 4 and 5 p.i..

The staining of splenic leukocytes by all of three antibodies (anti-NK1.1 and DX5/anti-CD49b) was consistent and reproducible. However, the staining with DX5 was not consistent in liver so only anti-NK1.1 was used. As with spleen, representative flow-cytometric scatter plots of different cell types in liver are shown in Figure 4.2.

Figure 4.1E shows the dynamics of the influx of major NK populations (NK1.1$^+$CD3$^-$ NK cells and NK1.1$^+$CD3$^+$ NKT cells) into infected livers. In contrast to the results in spleen, there was no YopM-related depletion of any NK cell population in liver. These data indicated that YopM-specific depletion of NK cells is not systemic, and contrary to our hypothesis, YopM modulates immune responses through different mechanisms in spleen and liver.

C. Ablation of NK cells by anti-NK1.1 (PK136) did not relieve the growth defect of the *ΔyopM-1* mutant in spleen and liver

Although we confirmed that YopM in the parent strain cannot deplete NK cells from livers, it did not mean that NK cells were not key cells to control growth of the Δ*yopM-1* mutant, because splenic NK cells still showed YopM-dependent depletion. The best way

to test the role of NK cells in the YopM virulence mechanism is to compare the infection in mice lacking NK cells to that in mice with an intact NK cell population. If NK cells are responsible for growth restriction of the Δ*yopM-1* mutant *Y. pestis*, this growth limitation should be relieved in mice lacking NK cells.

As shown in Figure 4.3A, we tested this hypothesis by comparing the growth of parent and Δ*yopM-1* mutant *Y. pestis* in mice ablated for NK cells by antibody anti-NK1.1. On d 1 prior to infection and d 1 and 3 p.i. we injected PK136 mAb (anti-NK1.1) or rat-IgG to each mouse IP in the ablation groups or mock groups, respectively. Mice were then infected IV with 400 CFU and killed humanely on d 2, 4 and 5 p.i. for analysis of CFU, leukocyte populations, and histopathology in spleen and liver.

Since DX5$^+$ cells include some T cells, DX5 was not the best antibody to test the efficiency of PK136 treatment. We decided to use anti-NK1.1 to detect the residual NK cells. To avoid false ablation, i.e., a situation in which some NK cells were bound by the PK136 used for ablation and hence masked for detection with PK136 but were not actually ablated, we used the isotype control antibody anti-IgG2a to detect any PK136 bound live NK cells. The result showed that very few IgG2a$^+$ cells were present after PK136 treatment (Figure 4.3B).

About 90% of NK1.1$^+$CD3$^-$ cells were ablated from both spleen and liver by the initial antibody treatment and the subsequent treatments maintained very low levels of NK cells during the experiment (Figure 4.3D, dashed and dotted lines). However, successful NK cell ablation failed to relieve the restricted growth of Δ*yopM-1 Y. pestis* KIM5-3002 in either organ (Figure 4.3E, dashed lines).

D. NK ablation did not convert the pathological appearance of the Δ*yopM-1* mutant-infected livers to that of parent strain-infected ones

Histopathological analysis of the livers (d 4 p.i.) in both the KIM5-3002-infected mock-treated or NK cell-ablated mice showed lesions that were similar in character and number (Figure 4.3C). The histopathological appearance was typical of the proinflammatory response that precedes micro-granuloma formation in C57BL/6 mice that are curbing net growth of the *ΔyopM-1* mutant (Figure 3.2C).

Although it is possible that the less than 10% of NK1.1$^+$ cells remaining in the anti-NK1.1 mAb-treated mice could be sufficient to exert full growth-limitation of the *ΔyopM-1* mutant, we consider it more likely that YopM-dependent NK cell depletion may be a side effect caused by the compromised function of other cell types such as PMNs, macrophages and DCs in spleen.

Table 4.1 Surface markers on different leukocytes in flow cytometric analysis

Cell Type	Markers	Staining combinations
NK cells	DX5, NK1.1 and CD3	$NK1.1^+DX5^+CD3^-$ (Spleen)
		$NK1.1^+DX5^-CD3^-$ (Spleen)
		$NK1.1^+CD3^-$ (Liver)
NKT cells	mCD1d/PBS57, DX5, NK1.1 and CD3	$mCD1d/PBS57^+\ CD3^+$
		$NK1.1^+CD3^+$
PMNs	Ly6G, CD11b and Gr1	$Ly6G^+CD11b^+$
		$Ly6G^+Gr1^+$
MDMs	Ly6G, CD11b	$Ly6G^-CD11b^+$
iDC	CD11b, CD11c	$CD11b^+CD11c^{int}$
DCs	CD11c, CD11b, CD8 and B22	$CD11b^+CD11c^+$
		$CD8^+CD11C^+$
		$B220^+CD11c^{Low}$

Figure 4.1 Comparisons of bacterial CFUs and NK cell percentages of live leukocytes in spleens and livers after infection of C57BL/6 mice with *ΔyopM-1* Y. pestis KIM5-3002 or the parent *Y. pestis* KIM5

A

B

C

D

Spleen

NK1.1-DX5+CD3- NK Cells

Spleen

NK1.1+CD3+ NKT Cells

E

Liver

NK1.1+CD3- NK Cells

Liver

NK1.1+CD3+ NKT Cells
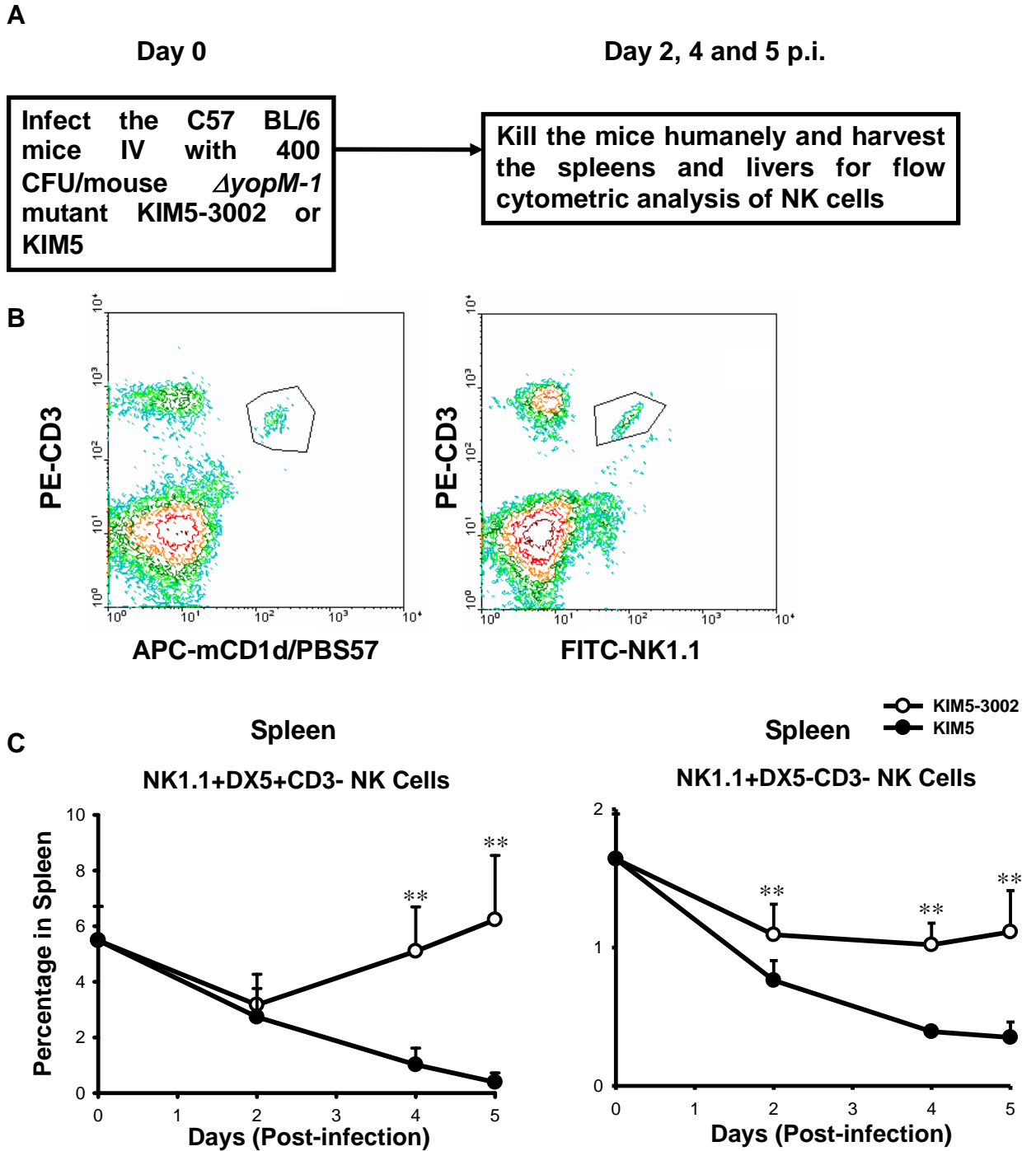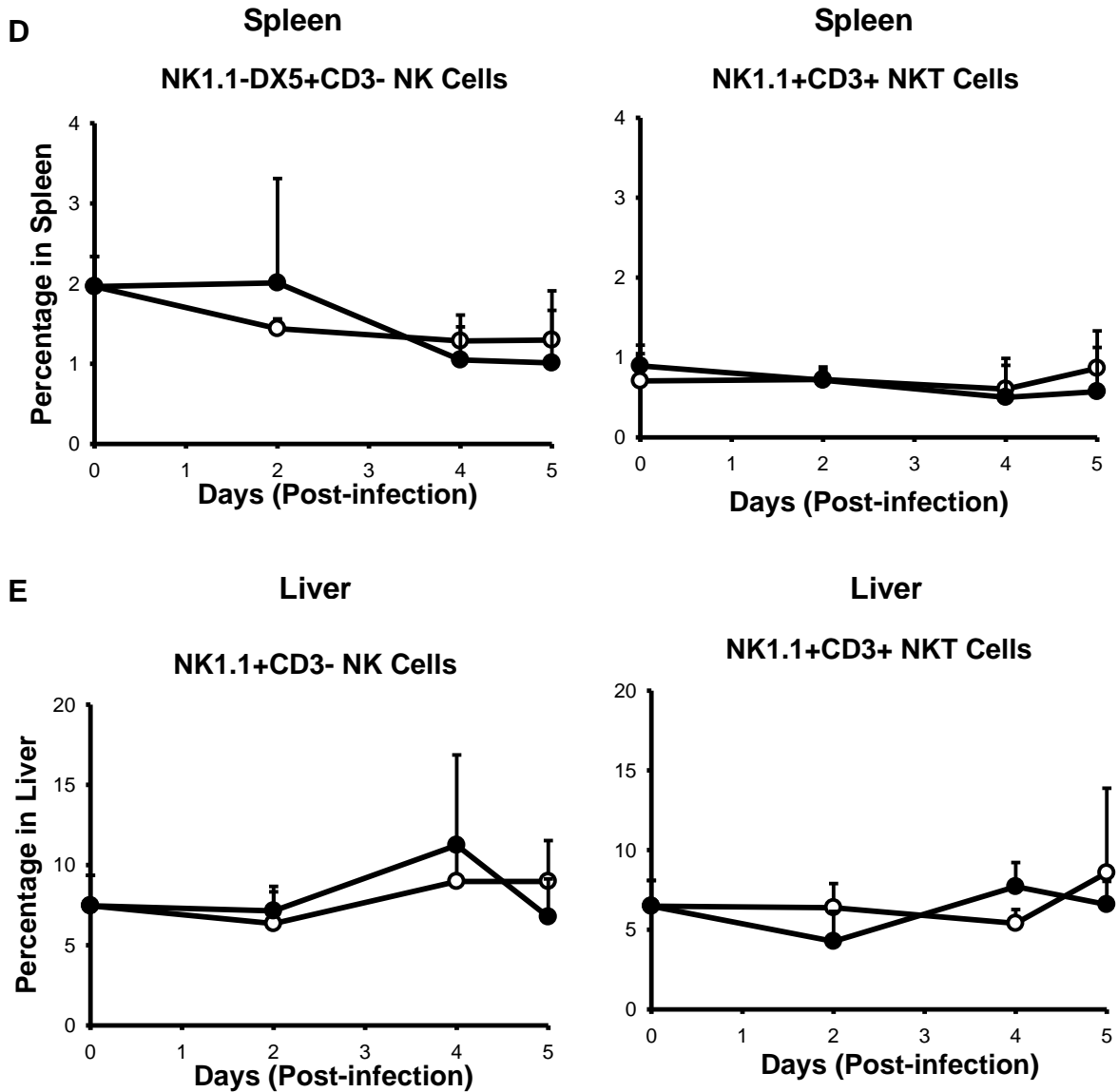
Mice were infected IV with 400 CFU of KIM5-3002 (open circles) or KIM5 (closed circles) *Y. pestis*. Panel A, experimental design. Panel B, flow cytometric scatter plots defining a population of mCD1d/PBS57$^+$CD3$^+$ cells recruited to spleen infected by *ΔyopM-1 Y. pestis* (left panel) and determining where those cells mapped in an analysis of NK1.1$^+$ CD3$^+$ cells in that sample (right panel). At the indicated times p.i., the percentages of different subgroups of NK1.1$^+$ cells in leukocytes from spleen (panel C

92

and D) or liver (panel E) were determined. The data represent the average plus SDs for 12 mice per datum point for spleen and 14 mice per point for liver, pooled from replicate experiments. Differences between KIM5-3002 and KIM5 infected groups (*, $P < 0.05$; **, $P < 0.01$) are indicated.

Figure 4.2 Representative Flow-cytometric Scatter Plots
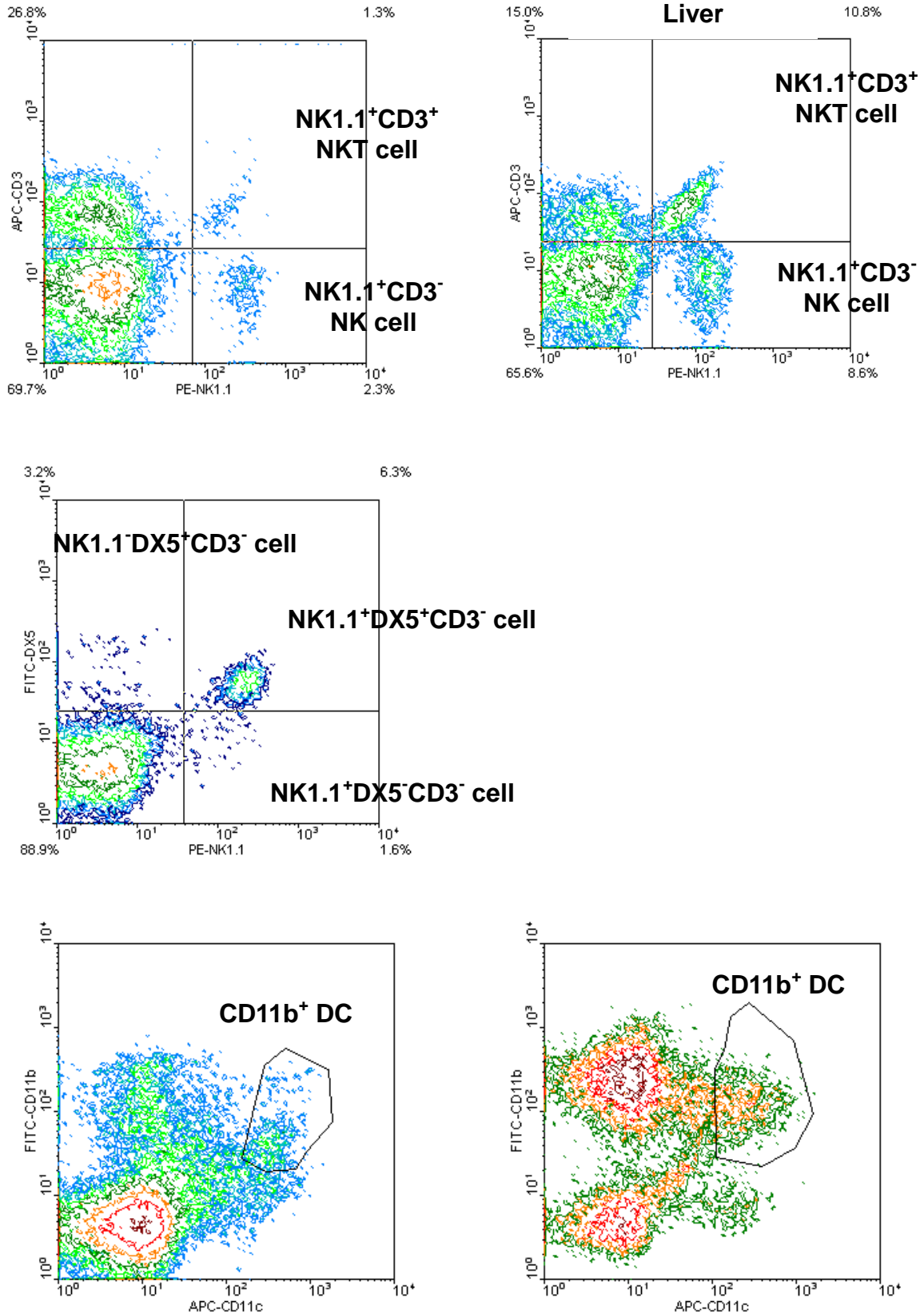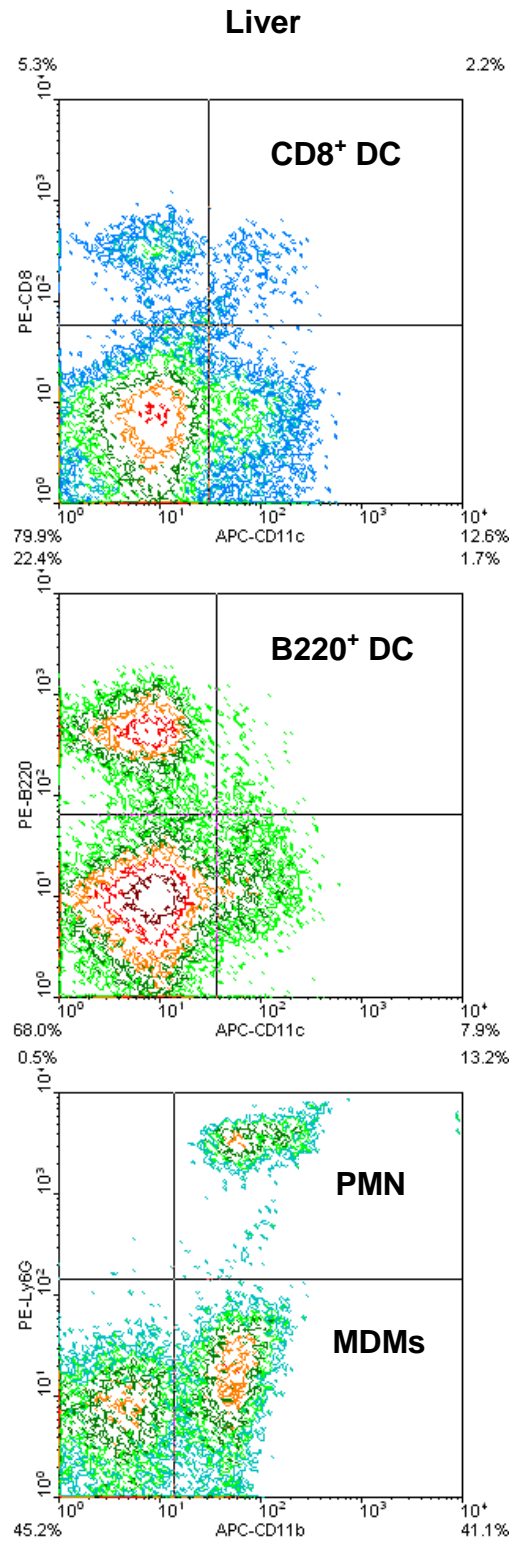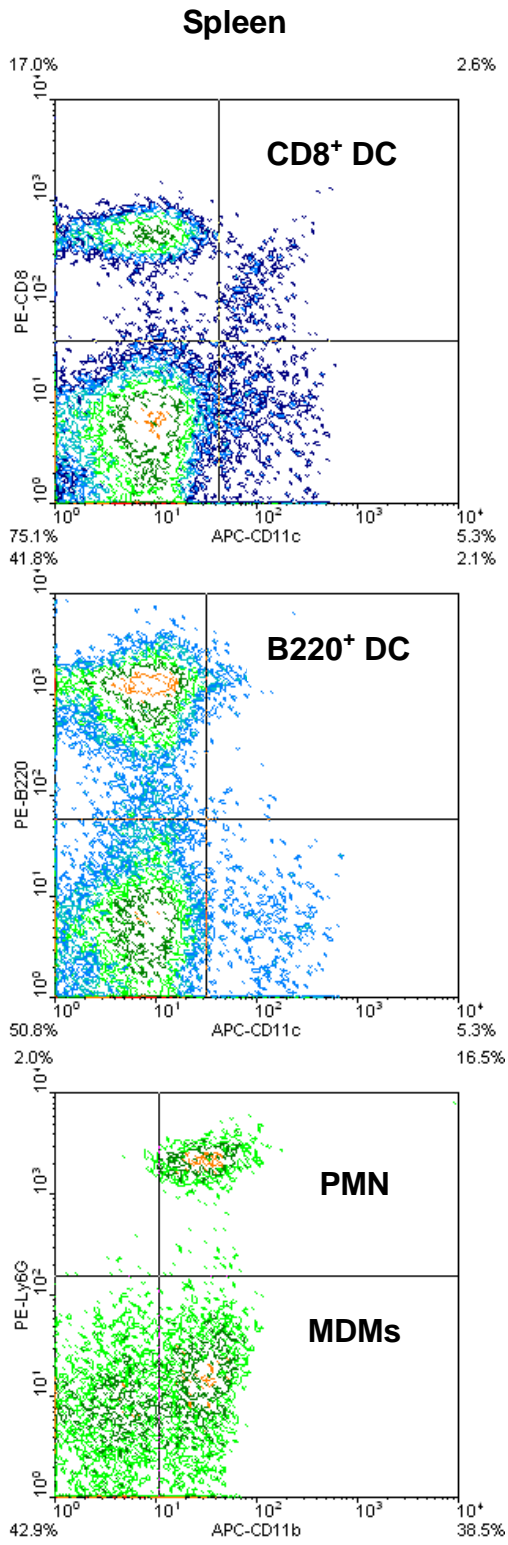
Spleen

Liver

Spleen
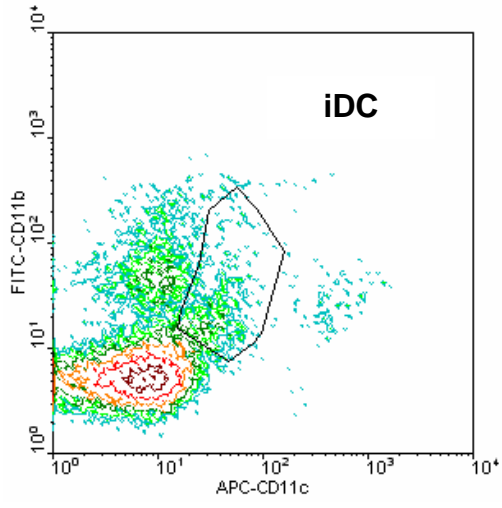
Liver
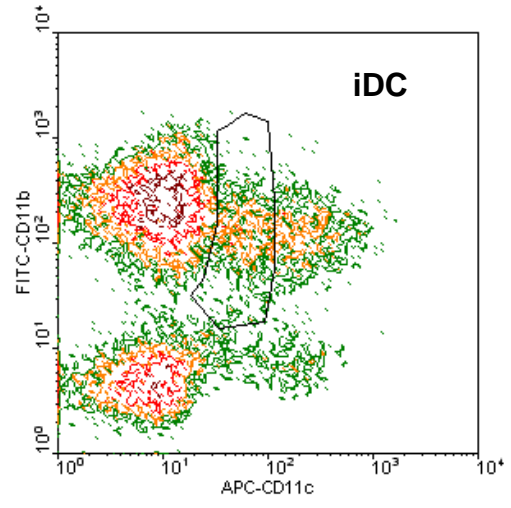
Figure 4.3 Anti-NK1.1 mAb-mediated NK cell ablation failed to relieve the growth

defect due to the *ΔyopM-1* mutation

C

Mock Ablation   NK Ablation

─□─ KIM5-3002 Mock Ablation
─■─ KIM5 Mock Ablation
─△─ KIM5-3002 NK Ablation
▲ KIM5 NK Ablation

Spleen   **Liver**

D

NK1.1+ CD3- NK Cells   NK1.1+ CD3- NK Cells

E

Days (Post-infection)   Days (Post-infection)

98
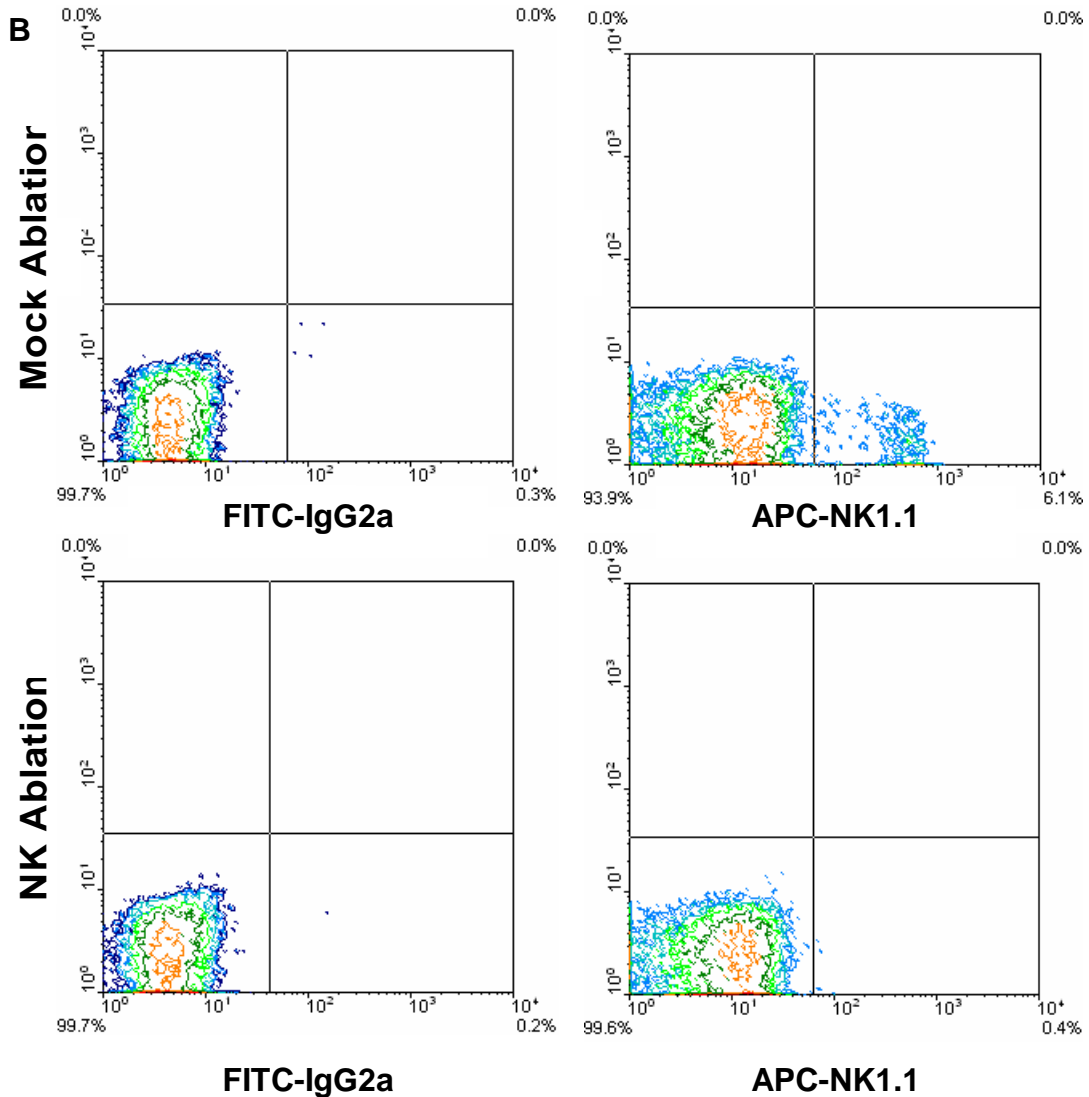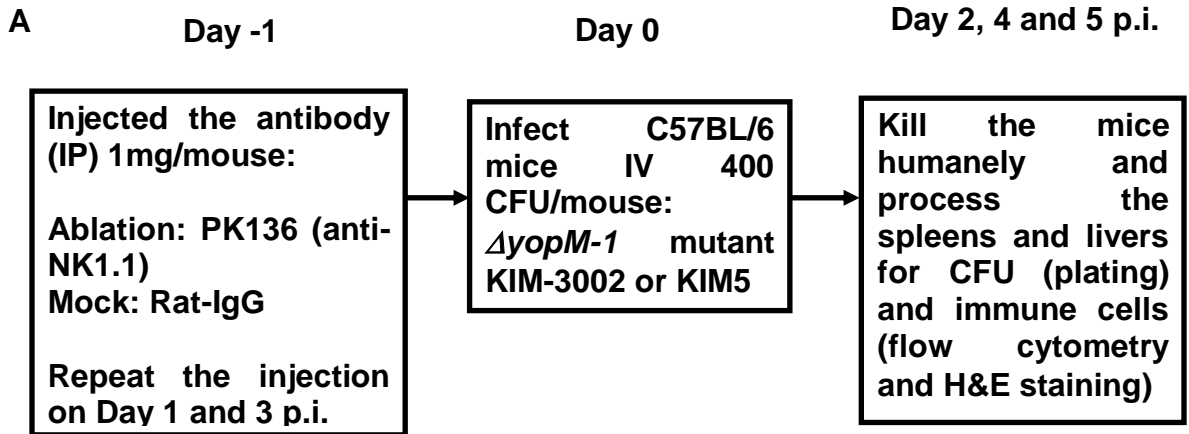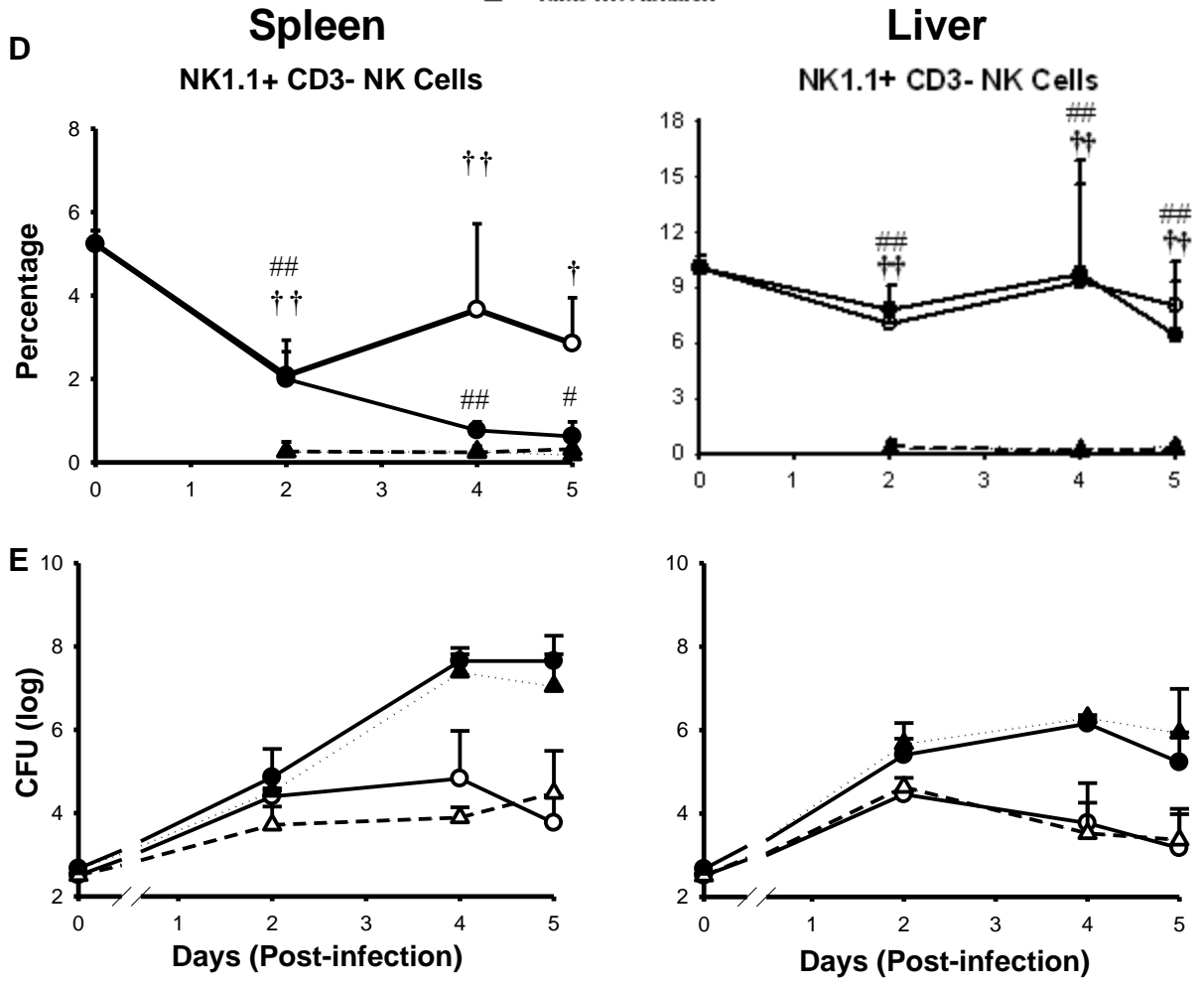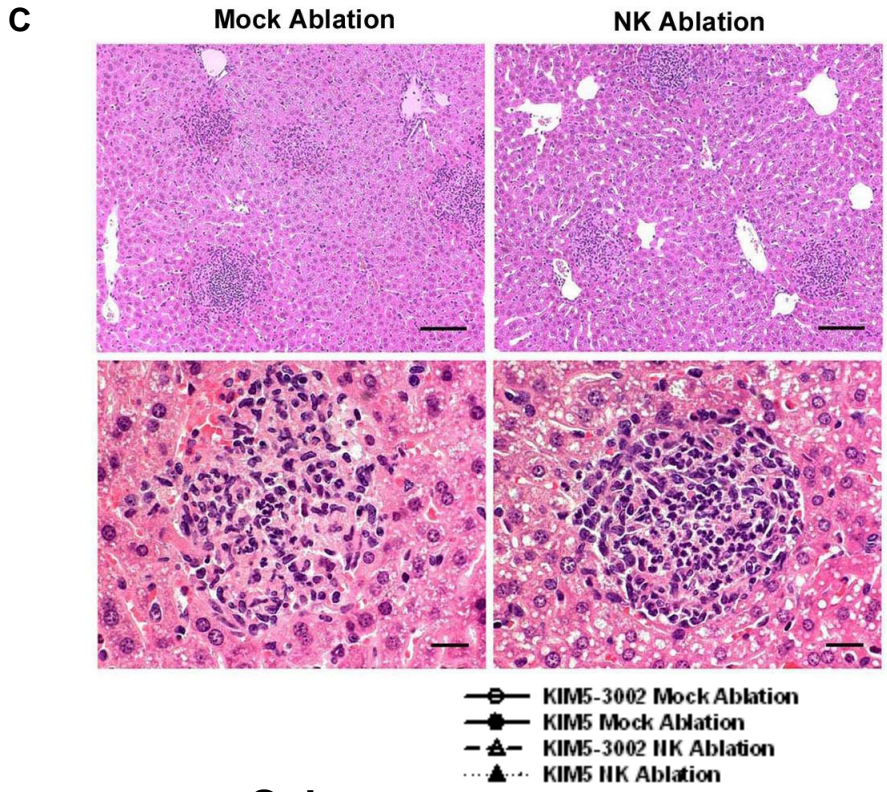
Mice were given anti-NK1.1 mAb (NK cell-ablated groups, dashed and dotted lines) or rat IgG (mock ablation groups, solid lines) IP one day before IV infection with 400 CFU of *ΔyopM-1 Y. pestis* KIM5-3002 (open triangles and dashed lines for NK cell ablation groups and open circles for mock-treated groups) or the parent strain KIM5 (solid triangles and dotted lines for ablation groups and solid circles for mock-treated groups). Panel A, experimental design. Panel B, flow cytometric scatter plots detecting IgG2a$^+$ cells present after PK136 (lower panel) or mock treatment (upper panel). Panel C, histopathology on d 4 p.i. liver of NK cell-ablated and mock-treated mice infected with KIM5-3002. The lower panels (Bars: 20 μm) and the upper panels (Bars: 100 μm) show typical lesions caused by KIM5-3002. The percentages of CD3$^-$ NK cells (panel D) and numbers of CFUs (panel E) in spleens and livers on d 2, 4, and 5 p.i. were determined. The data represent the average plus SDs (error bars) for 6 mice per datum point, pooled from replicate experiments. Values that are significantly different in the NK cell-ablated and mock ablation groups of mice infected with KIM5-3002 are indicated as follows: †, $P<0.05$; ††, $P<0.01$. Values that are significantly different in the NK cell-ablated and mock ablation groups of mice infected with KIM5 are indicated as follows: #, $P<0.05$; ##, $P<0.01$.

RESULTS

Chapter Five: With the exception of CD8$^+$ DCs, the numbers of classic DCs are not altered in a YopM-related way before day 4 p.i.

Since NK cells did not prove to be a target of YopM that was critical for virulence, we evaluated other leukocyte population dynamics for clues that would point toward cells that are responsible for the *in vivo* growth defect of *ΔyopM-1* mutant *Y. pestis*. From previous studies done by our lab with SCID mice, we already knew that adaptive immunity, which involves classic T and B cells, is not responsible for controlling the growth of Δ*yopM-1* mutant *Y. pestis* in the systemic plague model (159). Here we focused on innate immune cell types, such as DCs, PMNs and monocytes. DCs were the first cell type to be studied because they are present at portals of microbial infection and in reticuloendothelial organs colonized by *Y. pestis*, and their potent antigen-presentation and surveillance functions are important for both innate and adaptive defenses against invading microorganisms. Further, because of the large YopM-associated effect on NK cells in spleen, we performed this analysis in mice ablated for NK cells as well as in mock-treated mice to learn if the absence of this important but apparently non-critical cell would unmask an effect of YopM on other cell types.

A. In spleen, only the influx of CD8$^+$DCs was inhibited by YopM before day 4 p.i.

There are three major DC subgroups: myeloid DCs (CD11b$^+$CD11c$^+$), lymphoid DCs (CD8$^+$ CD11c$^+$) and plasmacytoid (CD11c^{Low} B220$^+$) (16, 187). According to their surface markers (Table 4.1), we used anti-CD11c to detect all DCs and anti-CD11b, anti-

CD8 and anti-B220 to distinguish different subgroups. Representative flow-cytometric scatter plots of the different cell types are shown in Figure 4.2.

As described in Figure 5.1A, groups of C57BL/6 mice were infected IV with 400 CFU/mouse the parent *Y. pestis* KIM5 or the *ΔyopM-1* mutant KIM5-3002. On d 2, 4 and 5 p.i., spleens were harvested for flow cytometric analysis. Figure 5.1B shows that in spleens (left panels) only CD8$^+$ DCs displayed a reproducible YopM-associated pattern of change in which the numbers of these DCs declined significantly by d 4 p.i. of infection by the parent *Y. pestis* strain but were maintained in the Δ*yopM-1* mutant. Other subgroups, CD11b$^+$ and B220$^+$ DCs, did not show any YopM-dependent change even on d 5 p.i.. Staining for surface activation markers of DCs, such as CD86 and IA^b (295), from infected spleens on d 1, 2 and 3 p.i. did not reveal any significant difference between *ΔyopM-1* mutant and parent *Y. pestis* infections as indicated by MFI (Figure 5.1C).

B. The three classical DC subgroups in liver showed YopM-associated influx on or after day 4 p.i., which was later than the appearance of the *ΔyopM-1* mutant growth limitation

Depletion of NK cells by YopM had been confirmed to occur in spleen but not in liver. This result indicated that the immune response to YopM is organ-specific, which makes sense because spleen and liver have different surveillance mechanisms for pathogens. Therefore, we also tested DC subgroups in liver of mice infected as described in Figure 5.1A. In contrast to spleen, in liver all of the three DC subgroups showed moderate YopM-related changes, which were significant on d 4 and 5 p.i. for CD8$^+$ DCs

and d 5 p.i. for CD11b$^+$ and B220$^+$ DCs (Figure 5.1B, right panels).

Considering the growth pattern of these two *Y. pestis* strains (Figure 3.2B), the growth curves of parent KIM5 and *ΔyopM-1* mutant always diverge by d 3 p.i. in liver and the net growth of the *ΔyopM-1* mutant is controlled thereafter. That indicates that the immune responses which are compromised by YopM must occur before d 3 p.i.. Therefore, at least based on their numbers, both CD11b$^+$DCs and B220$^+$ DCs did not as appear to be the key cells controlling the growth of the *ΔyopM-1* mutant in liver.

C. NK cell ablation did not affect the distribution of DCs in spleen and liver

There is extensive cross-talk between DCs and NK cells, for example, DCs could have a role in NK cell survival through cell-to-cell contact and production of cytokines including IL-15 (353). To test whether NK cell depletion in spleen affected DC recruitment, we compared all three DC subgroups in mock-treated mice to those in NK cell-ablated mice infected with the parent *Y. pestis* KIM5 or the *ΔyopM-1* mutant (experimental design described in Figure 4.3A). As shown in Figure 5.2, NK cell ablation did not affect the distribution of any of the DC subgroups in spleen and liver.

Although CD8$^+$ DCs showed a relatively early YopM-related change, the difference in cell number of these DCs was not significant at d 2 p.i., when the growth limitation of the *ΔyopM-1* strain was already apparent, and it was hard to believe that they were the major cell type controlling the *ΔyopM-1* mutant. Therefore, we extended our study to larger innate immune cell populations, such as PMNs and monocytes.

Figure 5.1 Comparison of 3 DC subgroups in liver and spleen between mice infected

with *ΔyopM-1 Y. pestis* KIM5-3002 or the parent *Y. pestis* KIM5

C

Ia^b of CD11c+ DCs in Spleen

MFI

Days (Post-infection)

CD86 of CD11c+ DCs in Spleen

Days (Post-infection)
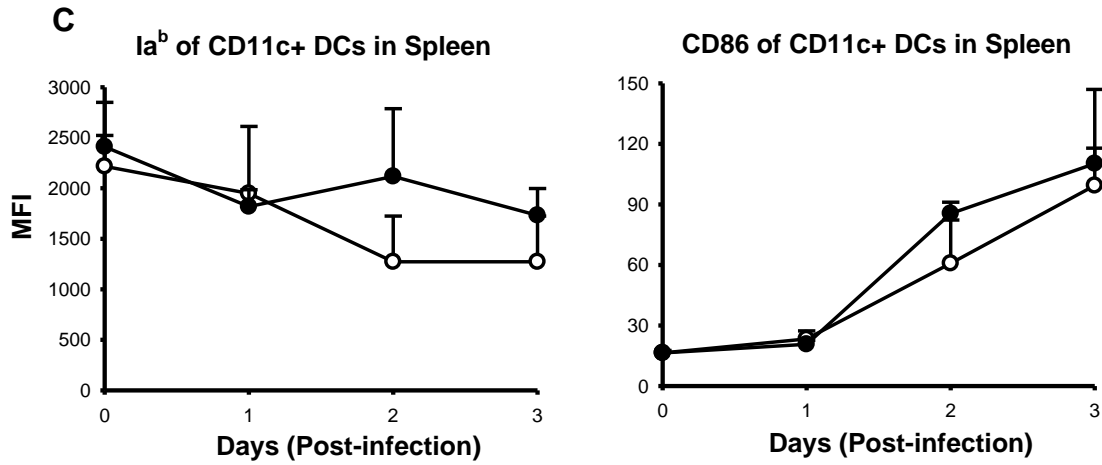
DCs were analyzed from the viable leukocyte populations obtained from *Y. pestis* KIM5 or KIM5-3002 infected spleens and livers. Panel A, experimental design. Panels B showes CD11b$^+$ DCs, CD8$^+$ DCs and B220$^+$ DCs (15 and 13 mice per datum point for spleen and liver, respectively) in spleen and liver. Panel C, MFI (mean fluorescence intensity) of the staining of surface activation markers, CD86 and Ia^b, on DCs from *Y. pestis* KIM5 or KIM5-3002 infected spleens. Values that are significantly different between *Y. pestis* KIM5-3002 and KIM5 infected groups are indicated (**, $P < 0.01$).

Figure 5.2 Effects of NK cell ablation on the distribution of three DC subgroups in liver and spleen between mice infected with *ΔyopM-1 Y. pestis* KIM5-3002 or the parent *Y. pestis* KIM5
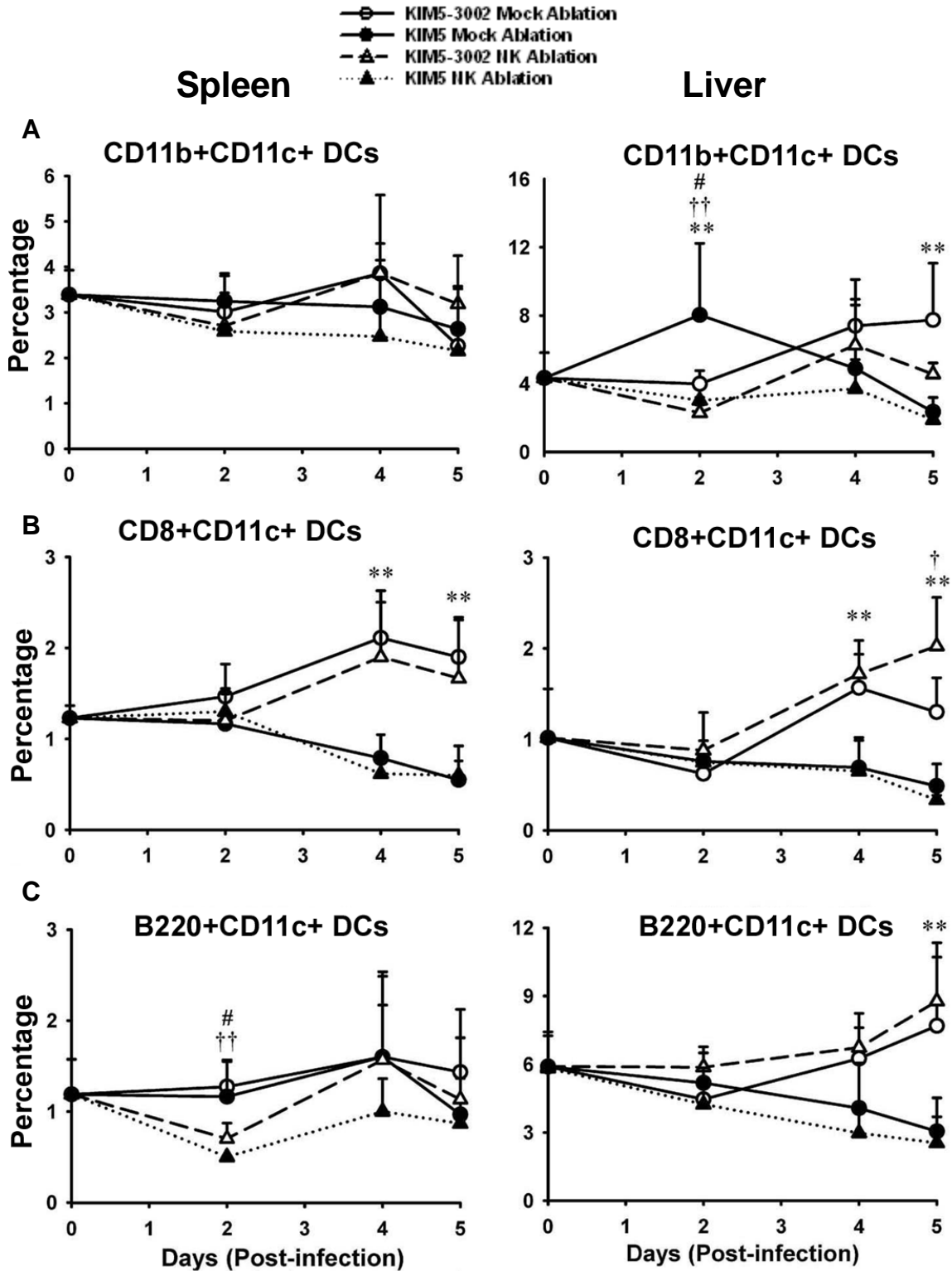
DCs were analyzed from the viable leukocyte populations obtained in the experiments of Figure 4.3; symbols and lines are the same as in Figure 4.3. Panels A, B and C show CD11b$^+$ DCs, CD8$^+$ DCs and B220$^+$ DCs (6 mice per datum point), respectively, in spleen and liver. The notations for statistical significance are the same as in Figure 4.3, with the addition of comparisons between groups of mock treated mice infected with *Y. pestis* KIM5 and KIM5-3002, where *, $P < 0.05$; **, $P < 0.01$.

RESULTS

Chapter Six: Gr1$^+$ cells are responsible for controlling the *ΔyopM-1* mutant in both spleen and liver

To evaluate the importance of PMNs and inflammatory monocytes in the pathogenic mechanism of YopM, we ablated these cells *in vivo* with anti-Gr1 (Ly6G/Ly6C) mAb given on d 1 prior to, and d 1 post, infection of C57BL/6 mice with the *ΔyopM-1* mutant or the parent *Y. pestis* strain and harvested organs in an early stage of disease, i.e., before d 3 p.i.. The design is shown in Figure 6.1A.

Gr-1 is expressed on mature granulocytes in bone marrow and peripheral tissues. It is also expressed transiently during monocyte differentiation in bone marrow and at low levels on plasmacytoid dendritic cells in lymphoid tissues. Anti-Gr1 reacts with Ly-6G, a 21–25 kDa GPI anchored specific cell surface protein on PMNs and less strongly with Ly-6C^{high} cells, which include inflammatory monocytes (130). Therefore, anti-Gr1 treatment actually ablated both PMNs and inflammatory monocytes.

A. Anti-Gr1 antibody successfully depleted most PMNs from spleen and liver, and the influx of inflammatory monocytes into spleen was also abolished

To measure the efficacy of anti-Gr1, spleens and livers were harvested for flow cytometric analysis. To detect PMNs, the staining combination of Ly6G and CD11b was used. CD11b, a 165-170 kDa integrin α_M, non-covalently associates with CD18 to form $\alpha_M\beta_2$ integrin (Mac-1) and binds to CD54 (ICAM-1), C3bi, and fibrinogen (33, 309, 311). CD11b is expressed on monocytes, macrophages, some DCs, and PMNs and functions in

various adhesive interactions as well as in mediating the uptake of complement coated particles (310). In flow cytomeric analysis, PMNs were defined as being Ly6G$^+$CD11b$^+$. Ly6G$^-$CD11b$^+$ cells were a mixture of inflammatory monocytes, macrophages and some DCs, termed MDMs (inflammatory monocytes/DCs, macrophages and myeloid DCs) in this study (Table 4.1). Representative flow-cytometric scatter plots of these different cell types are shown in Figure 4.2.

Figure 6.1B (dashed and dotted lines) shows that the ablation protocol removed over 90% of the PMNs from both liver and spleen. As shown in mock-treated groups (Figure 6.1C, solid lines), MDMs had a YopM-related pattern in spleen, which should be described as failure to be recruited by parent strain instead of depletion. However, the increase in MDMs in both organs was also abolished or delayed by anti-Gr1 treatment (Figure 6.1C, dashed and dotted lines). This phenomenon could result indirectly from the absence of PMNs caused by the anti-Gr1, or directly from depletion of MDMs by this antibody.

B. The *ΔyopM-1* mutant grew uncontrolled in spleen and liver from Gr1$^+$ cell depleted mice compared to mock-treated mice

In mock-treated mice, the YopM-associated growth defect was exhibited as expected at days 2 and 3 p.i. (Figure 6.1D. solid lines). Strikingly, the growth defect of the *ΔyopM-1* mutant strain in both spleen and liver disappeared in the mice treated with anti-Gr1 antibody, and growth of the parent strain was slightly enhanced (Figure 6.1D, dashed lines). This result indicated that Gr1$^+$ cells, including PMNs and some MDMs, are the major cells to clear the *ΔyopM-1* mutant in systemic plague.

C. The lesions in livers from anti-Gr1 treated mice morphologically mimicked those in the livers from the mock-treated mice

The lesions in livers of mock-treated mice infected with parent *Y. pestis* were dominated by dissipating acute inflammation on d 3 p.i., whereas those from mice infected with the *ΔyopM-1* mutant contained large numbers of PMNs and macrophages, as described previously (Figure 6.1E, upper panels; (231, 318)). However, this histological picture appeared to be in conflict with whole-organ flow cytometry which showed no significant difference in the percentage of intact PMNs and MDMs ("intact" means EMA⁻) in livers infected with the two strains of *Y. pestis* (Figure 6.1B and C, right panels). To address this issue, we visually scored all the lesions in the d 3 p.i. histopathological slides for number, size, and character. We found that infection by the *ΔyopM-1* strain caused fewer but larger foci than those by *Y. pestis* KIM5. The foci in livers of mice infected by the *ΔyopM-1* mutant always contained morphologically intact PMNs and MDMs, whereas livers from mice infected by the parent strain typically contained a mixture of morphologically intact cells and cellular debris (Figure 6.1F, bottom panels; illustrated in higher magnification by the upper panels in Figure 6.1E). The difference in the foci between the two strains was clear by d 2 p.i. (Figure 6.1F, upper panels), indicating that there was a YopM-associated difference in PMN and MDM integrity or function that correlated with the difference in growth for the parent and *ΔyopM-1* mutant strains.

After treatment with anti-Gr1, lesions in mice infected by the *ΔyopM-1 Y. pestis* morphologically mimicked those in mice infected with the parent strain (Figure 6.1E, lower panels), which had advanced to the bland necrosis typical of d 4 p.i. and later (159).

In general, ablation of Gr1$^+$ cells made the infection by the *ΔyopM-1* mutant resemble that by the parent strain and implicated these cells as cellular targets of YopM during its modulation of the host immune response.

Figure 6.1 Ablation of Gr1$^+$ cells relieved the growth defect of the *ΔyopM-1 Y. pestis*

KIM5-3002

D

E

F
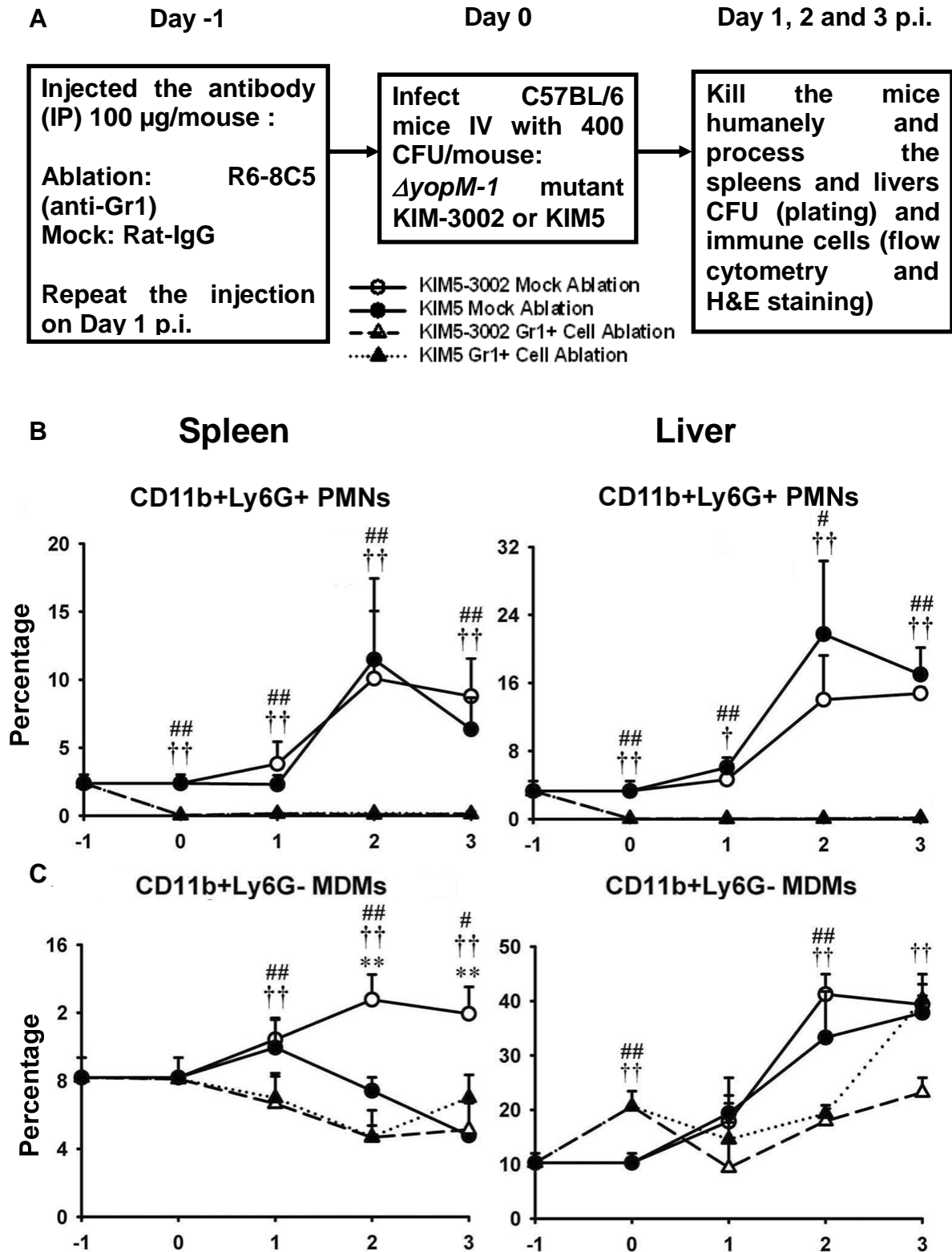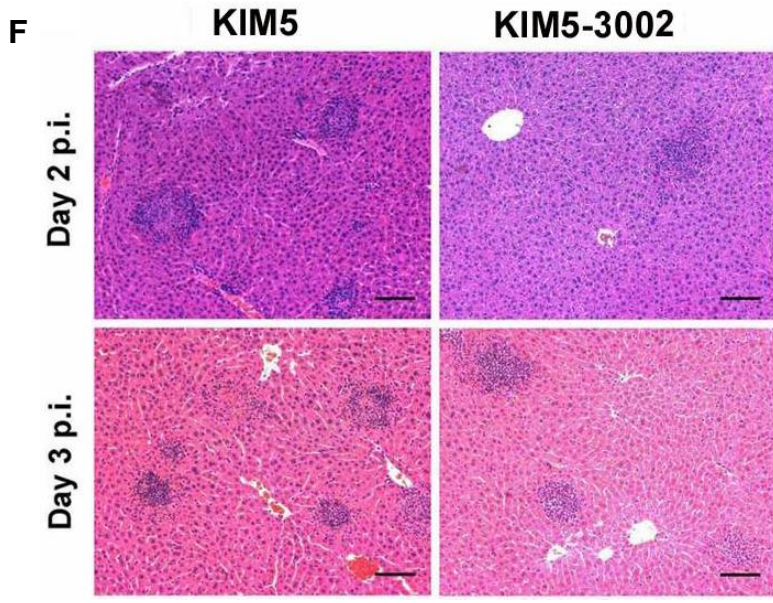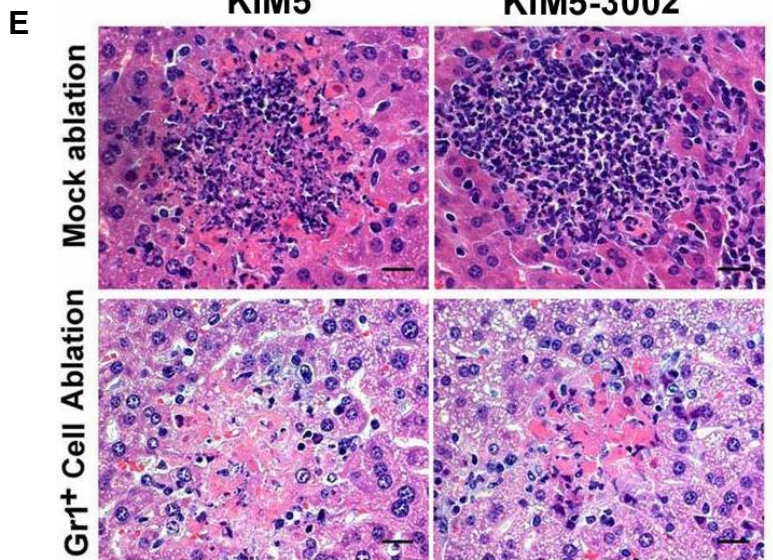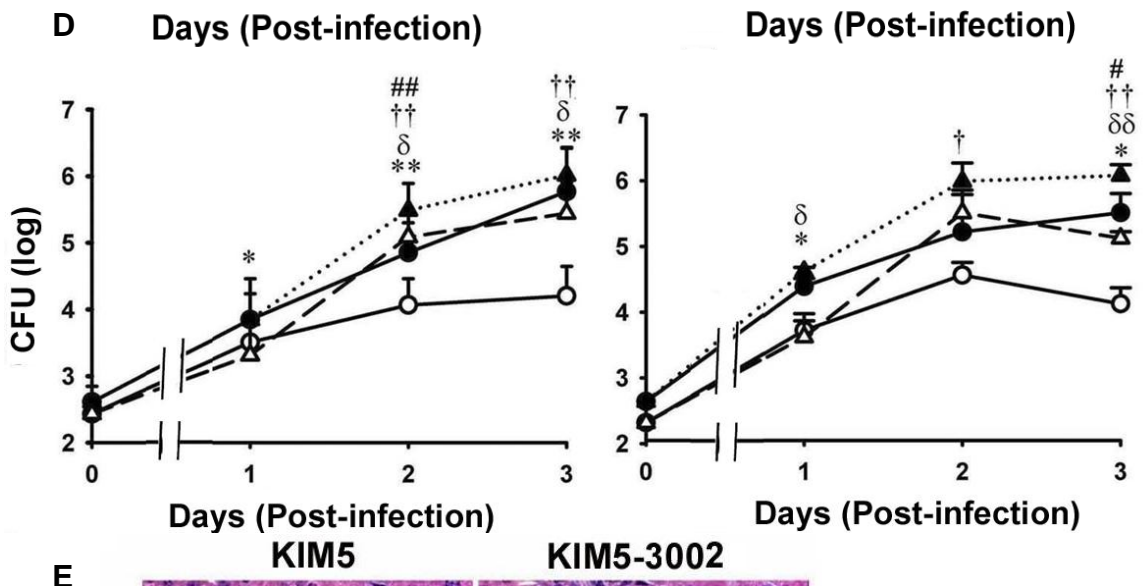
Mice were given anti-Gr1 (Ly6G/Ly6C) mAb IP (Gr1$^+$-cell ablated groups, dashed and dotted lines) or rat IgG (mock ablation groups, solid lines) one d before and one d after infection IV with 400 CFU of KIM5-3002 (open triangles and dashed lines for Gr1$^+$-cell ablation groups and open circles for mock-treated groups) or the parent strain KIM5 (solid triangles and dotted lines for ablation groups and solid circles for mock-treated groups). Panel A, experimental design. On d 1, 2, and 3 p.i., the percentage of PMNs (panel B) and MDMs (panel C) in viable leukocytes from spleens and livers and numbers of CFUs (panel D) in spleens and livers were determined. The data represent the average plus SD (error bar) for 6 mice per datum point for panels B and C and 9 mice per point for panel D, pooled from replicate experiments. Values that are significantly different for the Gr1$^+$-cell-ablated and mock ablation groups of mice infected with KIM5-3002 are indicated as follows: †, $P < 0.05$; ††, $P < 0.01$. Values that are significantly different for the Gr1$^+$-cell-ablated and mock ablation groups of mice infected with *Y. pestis* KIM5 are indicated as follows: #, $P < 0.05$; # #, $P < 0.01$. Values that are significantly different for mock-treated groups of mice infected with *Y. pestis* KIM5 and KIM5-3002 are indicated as follows: *, $P < 0.05$; **, $P < 0.01$. Values that are significantly different for Gr1$^+$-cell-ablated groups of mice infected with *Y. pestis* KIM5 and KIM5-3002 are indicated as follows: δ, $P < 0.05$; δδ, $P < 0.01$. Panel E and F: Histopathology in livers from mice that were ablated for Gr1$^+$ cells or mock-treated and infected with *Y. pestis* KIM5 or KIM5-3002. Panel E (Bars: 20 μm), shows lesions from d 3 p.i.. In panel F (Bars: 100 μm), differences in numbers and sizes of lesions caused by the two *Y. pestis* strains are illustrated for both d 2 and d 3 p.i..

RESULTS

Chapter Seven: The roles of PMNs in the controlling *ΔyopM-1 Y. pestis* growth in spleen and liver

As mentioned above, Gr1+ cells include PMNs and some MDMs, both are major immune cell populations during inflammation and among the first cell types encountering bacteria in *Y. pestis* infection. Since these cells have many distinct functions in the innate immune response and there is extensive cross-talk between them, it is necessary to identify their individual roles in YopM's immune-modulating mechanism. We firstly studied PMNs in their recruitment into organs and their activation in two different animal models. Further, anti-Ly6G, an antibody specific for PMNs, was used to ablate this cell type in the systemic plague model to distinguish its role from that of MDMs.

A. YopM-containing *Y. pestis* showed the same ability to recruit PMNs into spleen and liver as the *ΔyopM-1* mutant when the mice were infected by IV route

In this experiment, mice were IV-infected with the parent strain or the *ΔyopM-1* mutant, and spleens and livers were harvested on d 1, 2 and 3 p.i., as described in Figure 7.1A. Figure 7.1B shows that the percentage of PMNs ($Ly6G^+CD11b^+$) in the total live splenic or hepatic leukocytes increased during infection by both *Y. pestis* strains, peaking on d 2 p.i.. However, no YopM-associated difference between the two strains was found. Thus, there was no significant difference in the influx of PMNs from blood into both spleen and liver regardless of the presence of YopM in the infecting strain.

B. PMNs from the spleens of IV-infected mice did not display any YopM-dependent difference in ROS and NO production or altered ability to be stimulated ex vivo at 8, 16 and 45 hours p.i.

Since the recruitment of PMNs was not YopM related in systemic plague, we then tested the activation of these cells by measuring ROS and NO production. When bacteria are ingested or detected by phagocytic cells, such as PMNs and macrophages, serial defense mechanisms are activated in the cells to kill these pathogens. One of the most important ones is the generation of microbicidal oxidants from the activation of an NADPH oxidase–mediated oxidative burst (64). Another activation marker is NO, which is derived from the oxidation of the terminal guanidine nitrogen atom of L-arginine by iNOS (221).

The cell-permeant DCFDA is commonly used to detect the generation of reactive oxygen intermediates in PMNs and macrophages. Upon cleavage of the acetate groups by intracellular esterases and oxidation, the nonfluorescent DCFDA is converted to the highly fluorescent 2',7'-dichlorofluorescein (DCF) (148). DAF is commonly used to detect intracellular nitric oxide. Extracellularly applied DAF diacetate spontaneously crosses the plasma membrane and is cleaved by esterases to generate intracellular DAF, which is then oxidized by NO to a triazole product accompanied by increased fluorescence (163) .

To qualify the ROS and NO production in splenic PMNs, groups of mice were infected IV with high dose (10^6 CFU/mouse) of pre-induced (26/37°C) parent or *ΔyopM-1* mutant *Y. pestis*. Pre-induction was done by transferring the 26°C cultured bacteria to 37°C for 3 hours before infection. Pre-induction made the T3SS ready so that the bacteria

would inject their Yops into the host cells as soon as they contacted those cells. As showed in Figure 7.2A, spleens were harvested at 8, 16 and 45 h p.i.. With or without pre-treatment with PMA, an activator of protein kinase C to stimulate MΦs and PMNs *in vitro*, the splenic leukocytes were stained with antibodies against surface markers and DCFDA or DAF.

Activated PMNs were defined as $Ly6G^+Gr1^+DCFDA^+$ or $Ly6G^+Gr1^+DAF^+$. Since almost all of the $Ly6G^+Gr1^+$ cells are $DCFDA^+$ or DAF^+, we therefore used the MFI as a measure of the level of ROS or NO in PMNs. At 8 or 16 h p.i., in the absence of PMA, no differences were found in the percentages of $Ly6G^+Gr1^+DCFDA^+$ or $Ly6G^+Gr1^+DAF^+$ cells, as well as the MFIs of DCFDA or DAF between mice infected with the parent and mutant strains (Figure 7.2B and C). After PMA pre-treatment, although the MFI of DCFDA or DAF showed a slightly higher level than those without PMA treatment, no YopM-dependent ROS or NO production was found (Figure 7.2B and C). At 45 h p.i., both strains caused significantly less recruitment of PMNs into the spleens compared to those harvested at 8 or 16 h p.i. (Figure 7.2B, C and D, left panels). Meanwhile, those PMNs failed to be activated or stimulated by PMA (Figure 7.2D, right panels). This phenomenon could be related to the very high infection dose (10^6 CFU/mouse, compared to the much lower dose of 400 CFU/mouse used in most of our experiments), under which condition the cells from those spleens may be very vulnerable and undergoing apoptosis after 45 hour of infection. In summary, in either early or late stage infection, no YopM-dependent activation or stimulation in PMN were found in spleens from mice infected IV.

Only splenic PMNs were analyzed in the above experiments because the procedure to separate leukocytes from hepatocytes was long and contained some mechanical processes which may activate ROS and NO production by leukocytes.

C. Differential count of the peritoneal PMNs harvested from mice infected IP showed the same recruitment pattern regardless of the presence of YopM

Although spleen contains a large number of leukocytes, the MDMs and PMNs that are affected by YopM constitute less than 10% of them. Further, the long procedure to process spleen also raised a concern that transient changes in ROS and NO production in PMNs may have already disappeared when the cells were eventually ready to be stained. Therefore, we used another animal model to avoid the above problems. As described in Figure 7.3A, a range of doses ($5x10^4$, 10^6 or $5x10^7$ CFU/mouse) of *Y. pestis* was injected into the peritoneal cavity. Relatively high doses were used to ensure a large fraction of infected peritoneal cells. As in the previous set of experiments, 26/37ºC bacteria were used to ensure prompt delivery of Yops and detection of an effect of YopM after a short infection period. After 4, 6, 8 and 24 hours peritoneal lavage fluid was collected, and the cells were stained by Diff-Quick for differential count.

Before we measured the influx of PMNs into the peritoneal cavity, we tested the virulence of the two *Y. pestis* strains in this model. As shown in Table 3.1, the LD_{50} of the *ΔyopM-1* mutant is 200 fold higher than that of parent strain. That indicated that YopM modulated the immune responses to favor the lethality of the parent strain, as in the IV model.

Diff-Quick (Giemsa staining) was used to stain the peritoneal cells, and differential counting was done with the slides under the microscope according to the morphology of those cells. As shown in Figure 7.3B and C, before infection the majority of the peritoneal cells (PCs) was macrophages (ca. 80%), and lymphocytes counted for ca. 20% of total PCs (data not shown). Less than 1% PCs were PMNs before infection. However, PMNs became dominant (ca. 60% of total PCs) after infection and the percentage of macrophages decreased to ca. 30-40% (Figure 7.3C).

In order to find any possible difference in the influx of PMNs into peritoneal cavity, we tested different bacterial doses ($5x10^4$, 10^6 and $5x10^7$ CFU/mouse) and different time points (4, 6, 8 and 24 h p.i.). However, no significant YopM-dependent PMN recruitment to the peritoneal cavity was found from any of these experiments. Representative plots (10^6 CFU/mouse, 6 hours p.i.) of PMNs and macrophages are shown in Figure 7.3C. Consistent with the impression in Figure 7.3B, there was a change in the dominant cell type from macrophage to PMNs. Interestingly, the total numbers of the recovered PCs were similar between uninfected and infected mice (ca. 10^7 cells/mouse), which indicated that more than half of the macrophages had either left the peritoneal cavity or adhered to the peritoneum tightly after infection. This phenomenon is called the macrophage disappearance reaction (MDR) and will be discussed in the chapter **10. F b)**.

D. Peritoneal cells from mice infected IP by the *ΔyopM-1* mutant or the parent *Y. pestis* showed the same activation characteristics

The experiments to detect ROS and NO production in peritoneal cells were designed as shown in Figure 7.4A. Groups of mice were infected IP with a high dose ($5x10^4$, 10^6

and 5×10^7 CFU/mouse) of 26/37°C parent *Y. pestis* or *ΔyopM-1* mutant and PCs were harvested at 4, 6, 8 and 24 hours p.i.. Then the PCs were stained with DCFDA or DAF and the relative fluorescence units (RFUs) were read by microplate reader. Representative plots (10^6 CFU/mouse, 6 hours p.i.) of RFUs of DCFDA and DAF are shown in Figure 7.4B. As with MFI of DCFDA and DAF in splenic PMNs, no difference was found in the RFUs of DCFDA or DAF between parent and mutant strains at any dose or at any harvest time point, indicating that YopM produced by the infecting parent stain does not affect the activation of these PCs (mainly PMNs).

Figure 7.4B also showed that the RFUs of DCFDA and DAF staining were low and demonstrated no significant difference between the uninfected and infected mice. These results could result from the failure of those PCs (the mixture of PMNs, macrophages and some lymphocytes) from the infected mice to be activated by *Y. pestis* because these PCs could be stimulated by PMA (data not shown). However, some drawbacks of this IP infection model made the interpretation of these data more difficult. First, more than half of the peritoneal macrophages failed to be harvested, and those missing cells may contain intracellular bacteria and produce ROS and NO although most of these cells may not be fully activated. Second, the components of PCs from uninfected and infected mice are greatly different (Figure 7.3C). Therefore, the PCs from uninfected mice may not be the right control for those from infected ones (Figure 7.4B). The PCs from mice injected IP with casein could be used as alternative control. However, 90% of PCs from those mice were PMNs (data not shown) (considering that 50% of PCs from the infected mice were PMNs), raising the similar concerns to that from the uninfected mice.

E. Specific ablation of PMNs did not eliminate the difference in growth between the _ΔyopM-1_ mutant and parent strain in spleen but did reduce this difference in liver

Although we confirmed that YopM in the parent strain did not affect PMN influx into spleen, liver and peritoneal cavity, as well as the activation of splenic PMN or peritoneal cells, we still could not exclude PMNs as key cells in controlling the _ΔyopM-1_ mutant, especially in liver. Anti-Gr1 treatment had revealed a critical role of $Gr1^+$ cells, including PMNs and some MDMs, in the YopM virulence mechanism. Therefore, specific ablation of PMNs would test the hypothesis that PMNs do not mediate growth limitation of _ΔyopM-1 Y. pestis_ in liver or spleen. A commercial anti-Ly6G made these experiments possible. If PMNs are responsible for growth restriction of the _ΔyopM-1_ mutant _Y. pestis_, this growth limitation should be relieved in mice lacking PMNs.

As shown in Figure 7.5A, we compared the growth of parent and _ΔyopM-1_ mutant _Y. pestis_ in mice ablated for PMNs by antibody IA8 (anti-Ly6G). On d 1 prior to infection and d 1 p.i., IA8 mAb or rat-IgG was injected IP into each mouse in the ablation groups or mock-treatment groups, respectively. Mice were then infected IV with 400 CFU, and killed humanely on d 2 and 3 p.i. for analysis of CFU and leukocyte populations in spleen and liver.

More than 90% of $Ly6G^+CD11b^+$ PMNs were ablated from both spleen and liver by the initial antibody treatment, and the subsequent treatments maintained very low levels of PMNs during the experiment (Figure 7.5B). Consistent with data on PMN recruitment and PMN activation in spleen, successful PMN ablation failed to relieve the restricted growth of _ΔyopM-1 Y. pestis_ KIM5-3002 in spleen (Figure 7.5D). However, the growth

defect of the *ΔyopM-1* mutant strain in liver disappeared in the mice treated with anti-Ly6G antibody, and growth of the parent strain was slightly but not significantly enhanced in those mice (Figure 7.5D). This result indicated that PMNs could be one of the major cells to clear *ΔyopM-1* mutant in liver but not in spleen during systemic plague.

Figure 7.1 Comparisons of PMN percentages in spleens and livers after infection of C57BL/6 mice with *ΔyopM-1 Y. pestis* KIM5-3002 or the parent *Y. pestis* KIM5
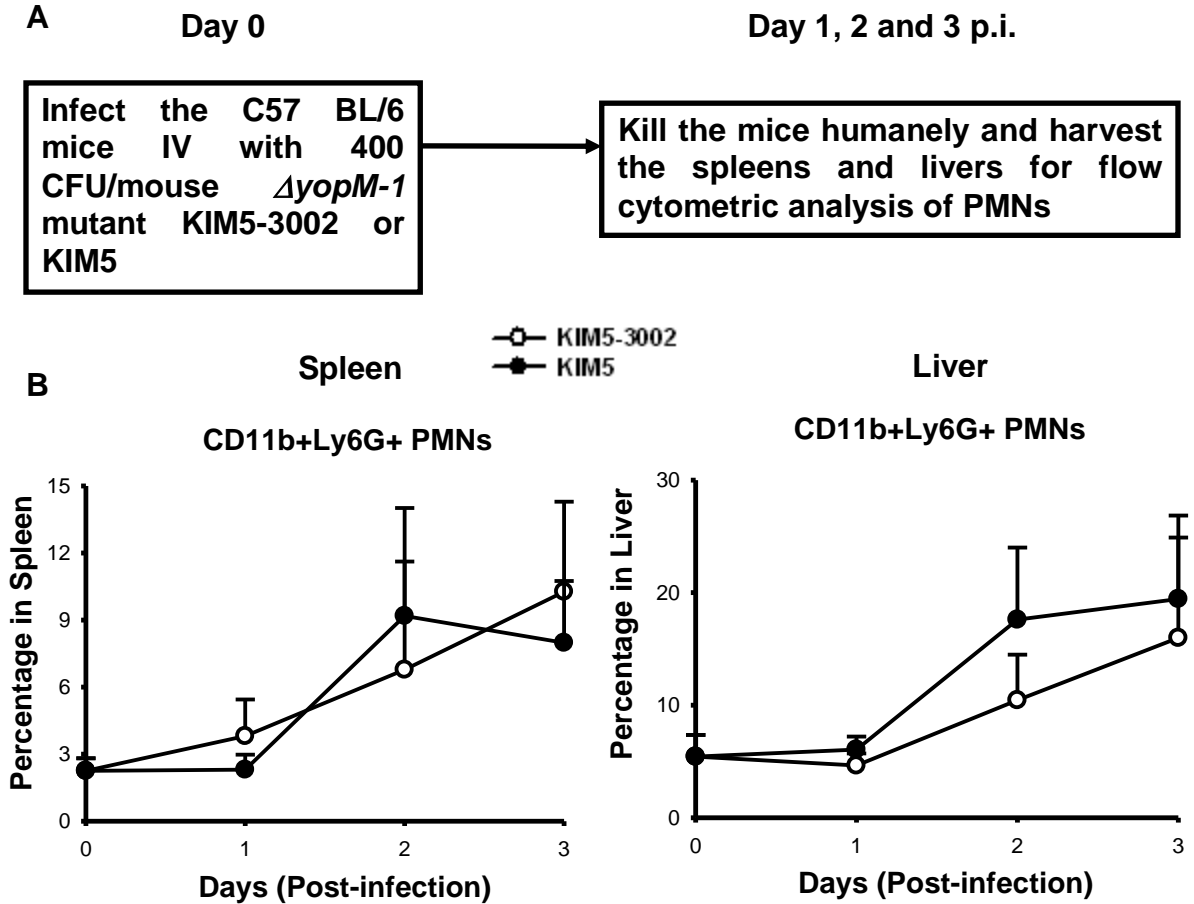
Mice were infected IV with 400 CFU of KIM5-3002 (open circles) or KIM5 (closed circles) *Y. pestis*. Panel A, experimental design. At the indicated times p.i., the percentages of $Ly6G^+CD11b^+$ PMNs in leukocytes from spleen or liver (panel B) were determined. The data represent the average plus SD for 19 mice per datum point for spleen and 15 mice per point for liver, pooled from replicate experiments.

Figure 7.2 Comparisons of ROS and NO production by the splenic PMNs from mice

infected with *ΔyopM-1 Y. pestis* KIM5-3002 or the parent *Y. pestis* KIM5

A

B

C

Ly6G+Gr1+DCFDA+ Cells 16 h p.i.

Ly6G+Gr1+DCFDA+ Cells 16 h p.i.

Ly6G+Gr1+DAF+ Cells 16 h p.i.

Ly6G+Gr1+DAF+ Cells 16 h p.i.

D

Ly6G+Gr1+DCFDA+ Cells 45 h p.i.

Ly6G+Gr1+DCFDA+ Cells 45 h p.i.

Ly6G+Gr1+DAF+ Cells 45 h p.i.

Ly6G+Gr1+DAF+ Cells 45 h p.i.

124
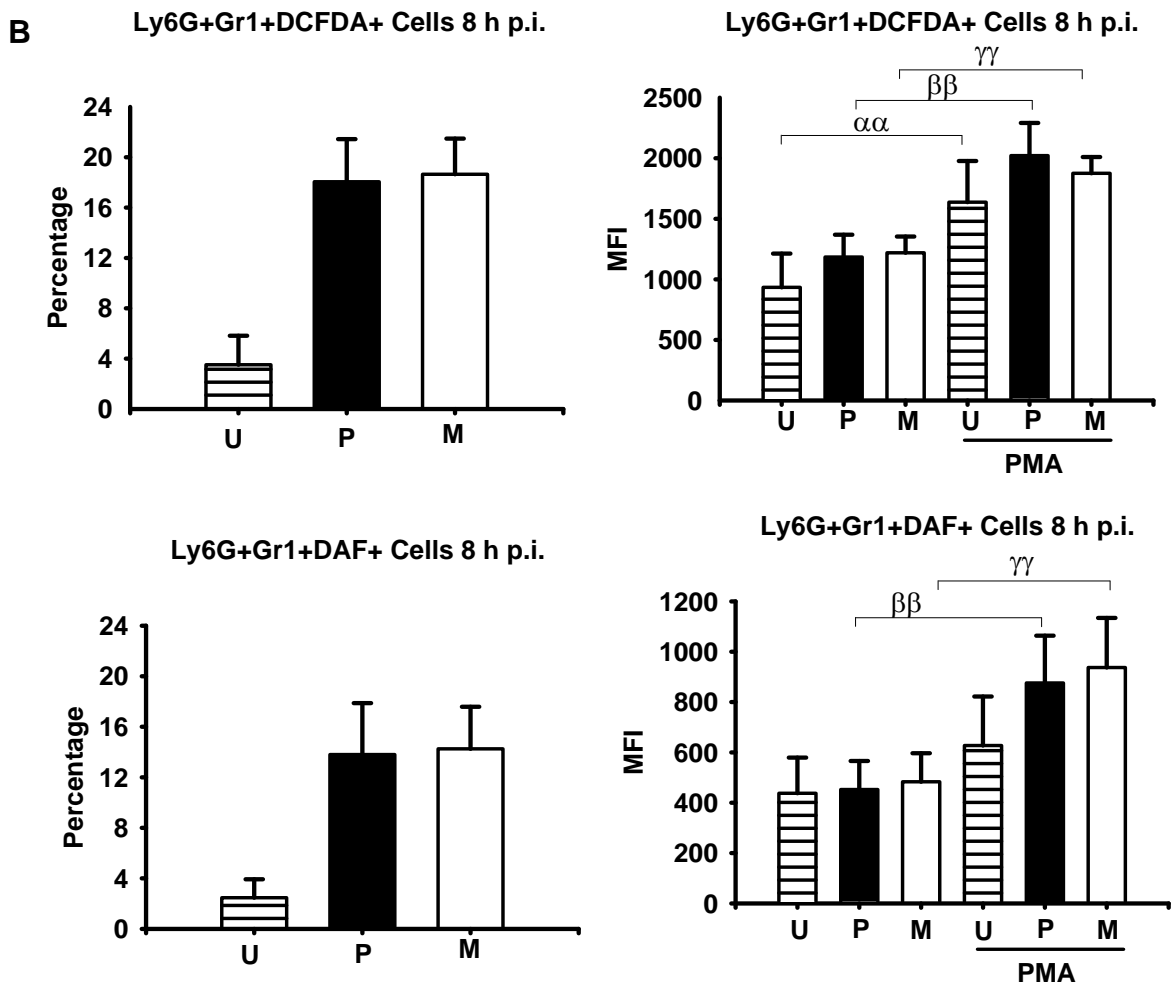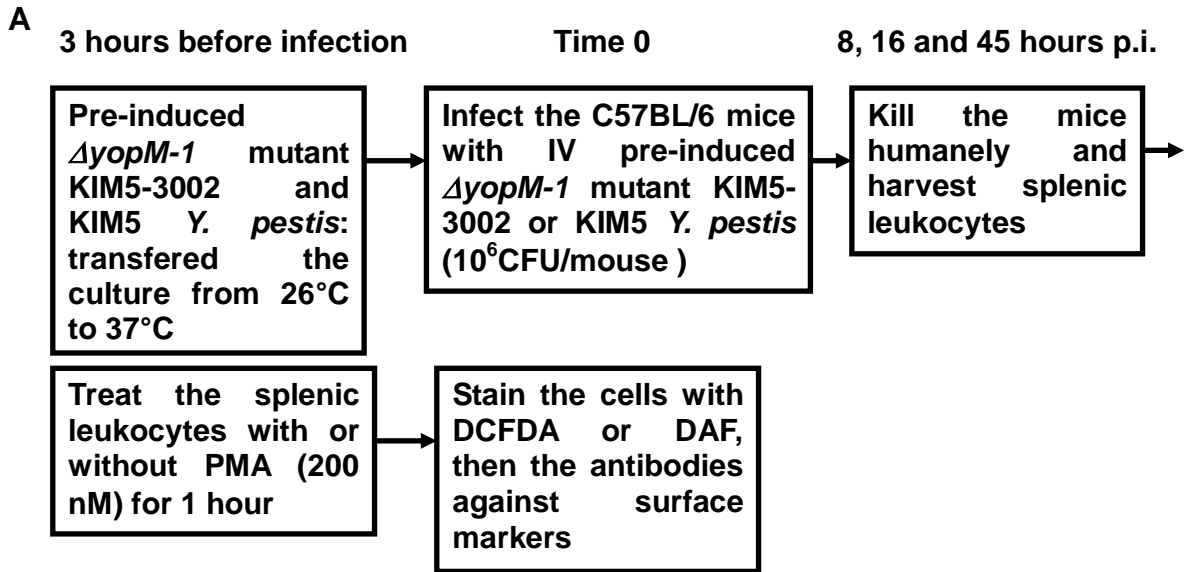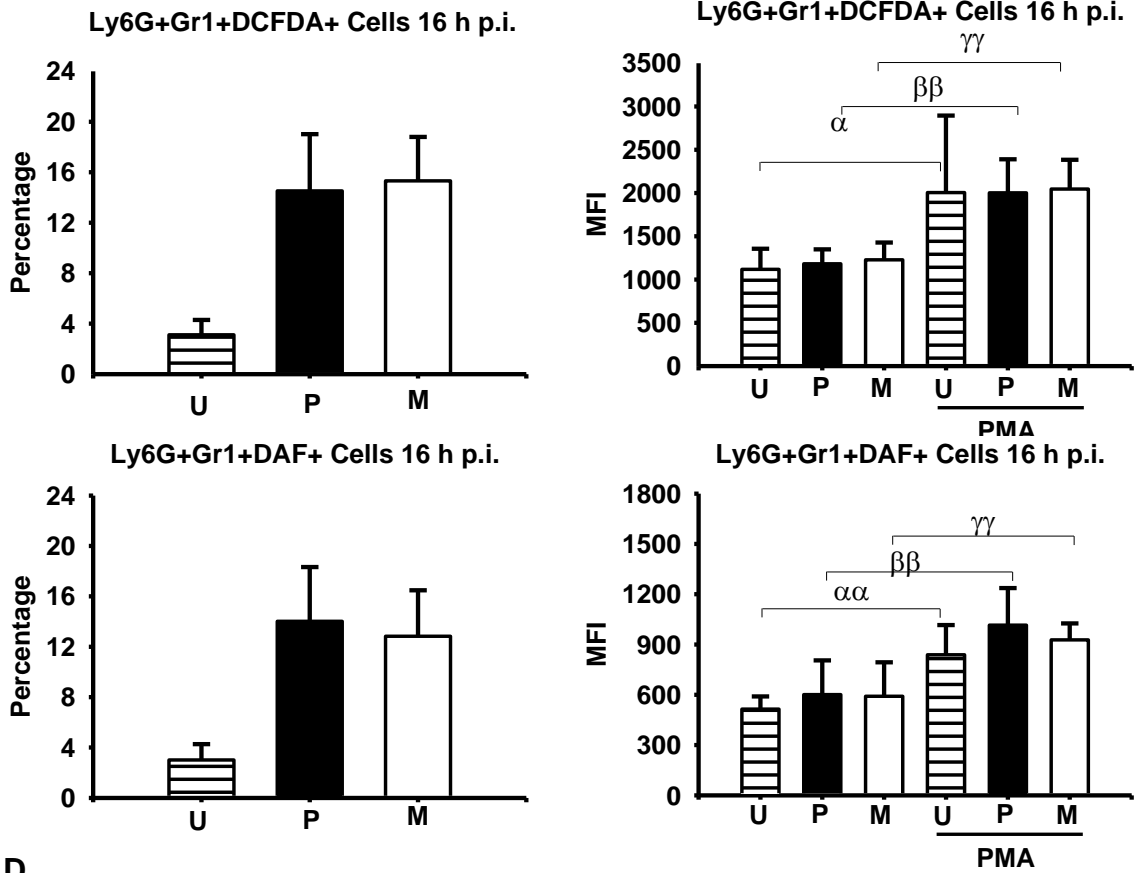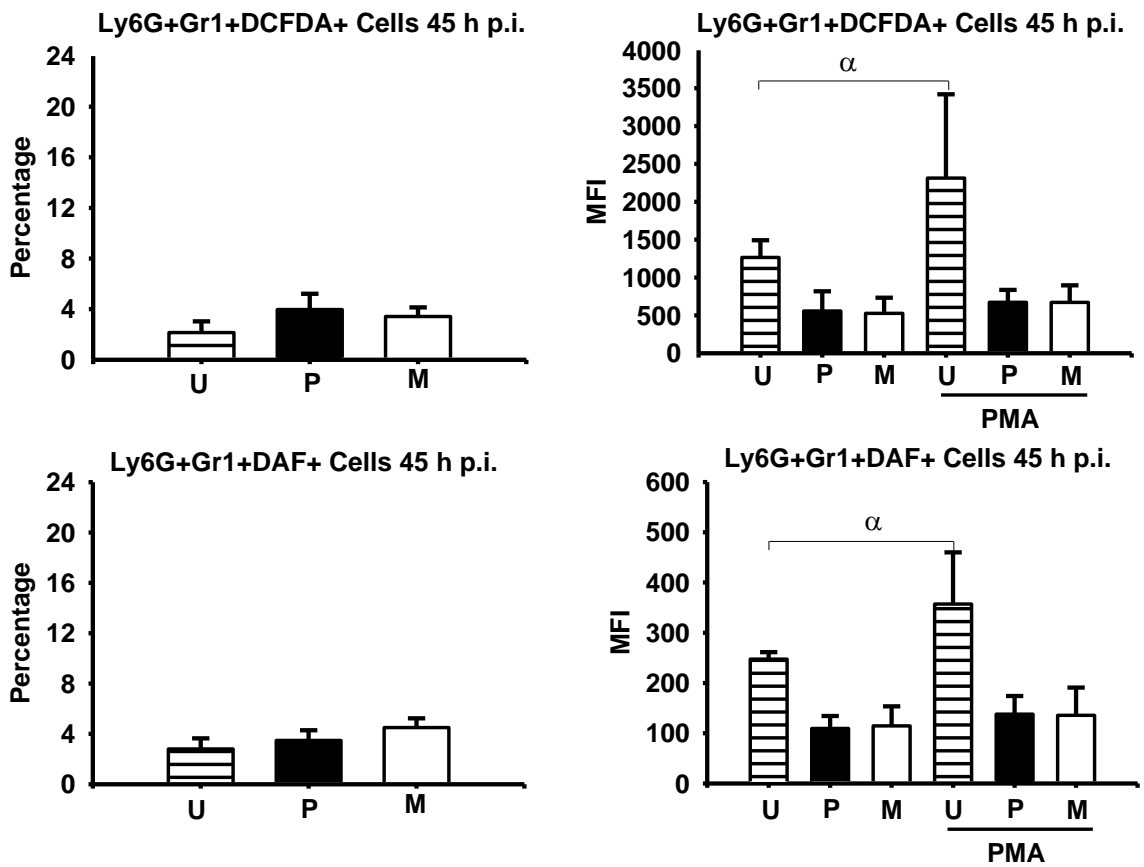
Mice were infected IV with 400 CFU of pre-induced KIM5-3002 or KIM5 *Y. pestis*. Panel A, experimental design. At 8, 16 and 45 h p.i., the percentages of Ly6G$^+$Gr1$^+$DCFDA$^+$ or Ly6G$^+$Gr1$^+$DAF$^+$ PMNs in the live leukocytes harvested from spleen, as well as MFI of DCFDA and DAF staining of those cells are shown in panels B, C and D, respectively. Horizontal-hatched bars, uninfected mice (U); filled bars, mice infected with parent *Y. pestis* KIM5 (P); open bars, mice infected with the *ΔyopM-1* mutant KIM5-3002 (M). PMA in the horizontal axis of the right panels of B, C and D indicates that the cells were stained by DCFDA and DAF after 1 hour incubation with PMA. Each datum point represents the average of values from 6 mice. The error bars indicate the standard deviations. To compare PMA treated and mock treated PMNs from uninfected mice, α, $P < 0.05$; αα, $P < 0.01$; from mice infected with *Y. pestis* KIM5, β, $P < 0.05$; ββ, $P < 0.01$; from mice infected with *Y. pestis* KIM5-3002, γ, $P < 0.05$; γγ, $P < 0.01$. In comparisons between mock-treated PMNs from mice infected with *Y. pestis* KIM5 and KIM5-3002, *, $P < 0.05$; **, $P < 0.01$; and #, $P < 0.05$; # #, $P < 0.01$ for PMA treated PMNs.

Figure 7.3 Influx of PMNs and macrophages into peritoneal cavity after IP infection of

C57BL/6 mice with *ΔyopM-1 Y. pestis* KIM5-3002 or the parent *Y. pestis* KIM5
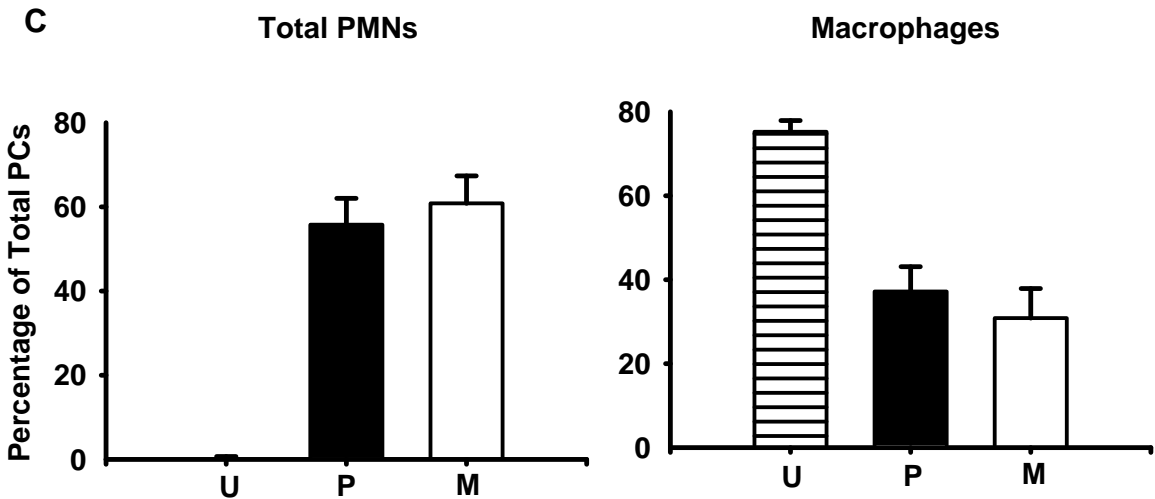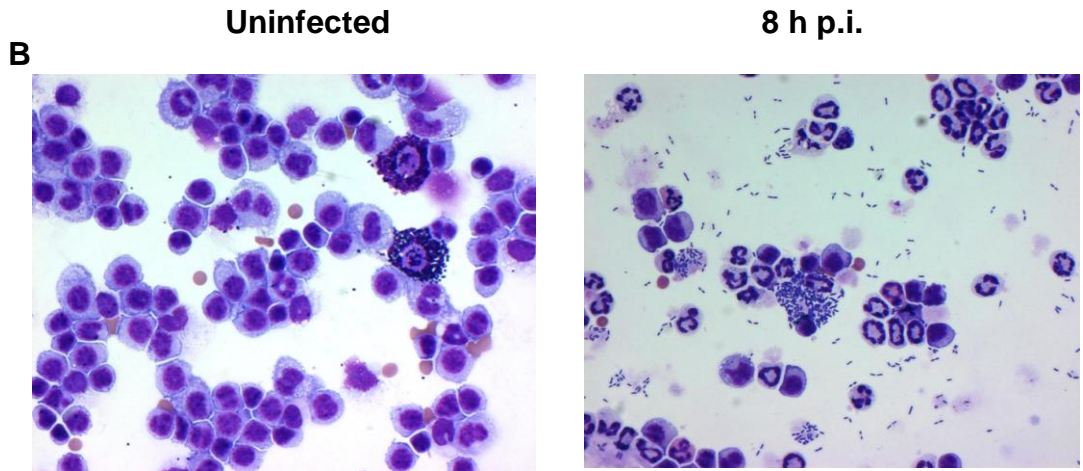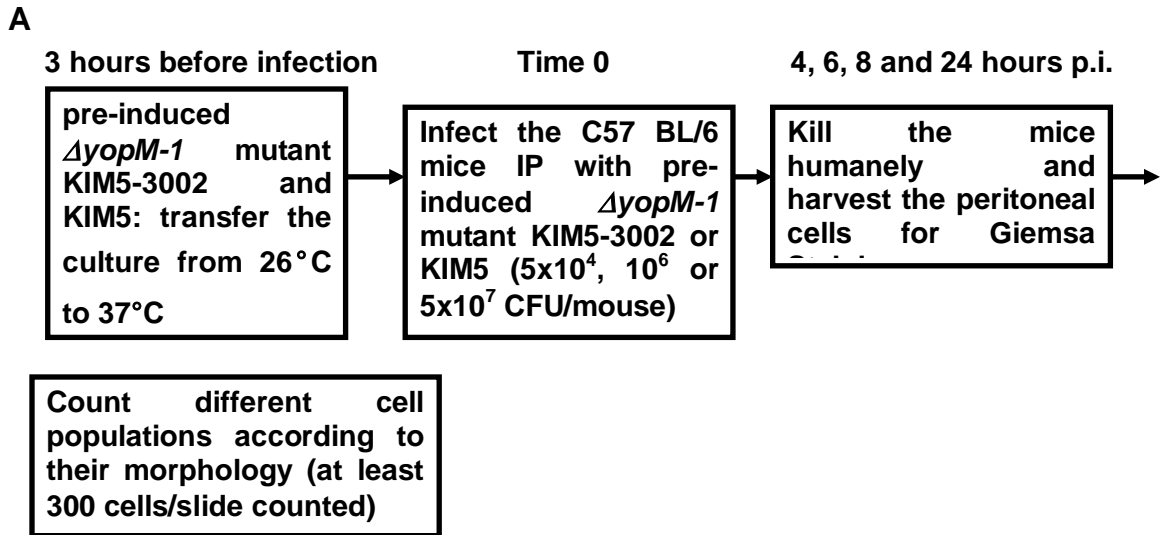
A

3 hours before infection	Time 0	4, 6, 8 and 24 hours p.i.
pre-induced *ΔyopM-1* mutant KIM5-3002 and KIM5: transfer the culture from 26°C to 37°C	Infect the C57 BL/6 mice IP with pre-induced *ΔyopM-1* mutant KIM5-3002 or KIM5 (5×10^4, 10^6 or 5×10^7 CFU/mouse)	Kill the mice humanely and harvest the peritoneal cells for Giemsa

Count different cell populations according to their morphology (at least 300 cells/slide counted)

B

| Uninfected | 8 h p.i. |

C

Total PMNs

Macrophages

126

Mice were infected IP with 5×10^4, 10^6 or 5×10^7 CFU of 26/37°C KIM5-3002 or KIM5 *Y. pestis*. At 4, 6, 8 and 24 h p.i., peritoneal cells (PCs) were harvested by peritoneal lavage. Panel A, experimental design. The PCs were spun down by Cytospin and stained by Diff-Quick. Panel B, representative pictures of stained PCs (dose: 5×10^7, harvest time: 8 h p.i. in this particular experiment). The percentages of PMNs and macrophages in the total PCs are shown in Panel C for two experiments with a dose of 10^6 CFU and harvest time of 6 h p.i.. Horizontal-hatched bars, uninfected mice (U); filled bars, mice infected with parent *Y. pestis* KIM5 (P); open bars, mice infected with the *ΔyopM-1* mutant KIM5-3002 (M). Each datum point represents the average of values from 8 mice. The error bars indicate the standard deviations.

Figure 7.4 Comparisons of ROS and NO production by the peritoneal cells harvested from mice IP-infected with $\Delta yopM$-1 *Y. pestis* KIM5-3002 or the parent *Y. pestis* KIM5

A

3 hours before infection   **Time 0**   **4, 6, 8 and 24 hours p.i.**

| Pre-induced $\Delta yopM$-1 mutant KIM5-3002 and KIM5: transfer the culture from 26°C to 37°C | → | Infect the C57BL/6 mice IP with pre-induced $\Delta yopM$-1 mutant KIM5-3002 or KIM5 (5×10^4, 10^6 or 5×10^7 CFU/mouse) | → | Kill the mice humanely and harvest PCs | → |

| Stained the PCs with DCFDA or DAF. Then read RFUs by microplate reader |

B

Mice were infected IP with 5×10^4, 10^6 or 5×10^7 CFU of 26/37°C KIM5-3002 or KIM5 *Y. pestis*. At 4, 6, 8 and 24 h p.i., the peritoneal cells (PCs) were harvested by peritoneal lavage. The PCs were stained with DCFDA or DAF for 30 min. Panel A, experimental design. RFUs of DCFDA and DAF staining of the PCs (dose: 10^6 CFU/mouse, harvested at 6 hours p.i.) are shown in panel B. Horizontal-hatched bars, uninfected mice (U); filled

bars, mice infected with parent *Y. pestis* KIM5 (P); open bars, mice infected with the

ΔyopM-1 mutant KIM5-3002 (M). Note that in uninfected mice, the PCs were 80% of

macrophages and lymphocytes and less than 1% PMNs, whereas in infected mice, the

PCs were 40% macrophages and lymphocytes and 60% PMNs. Each datum point

represents the average of values from 8 mice. The error bars indicate the standard

deviations.

Figure 7.5 Effect of PMN ablation on infection dynamics for of *ΔyopM-1* and parent *Y. pestis* KIM5.
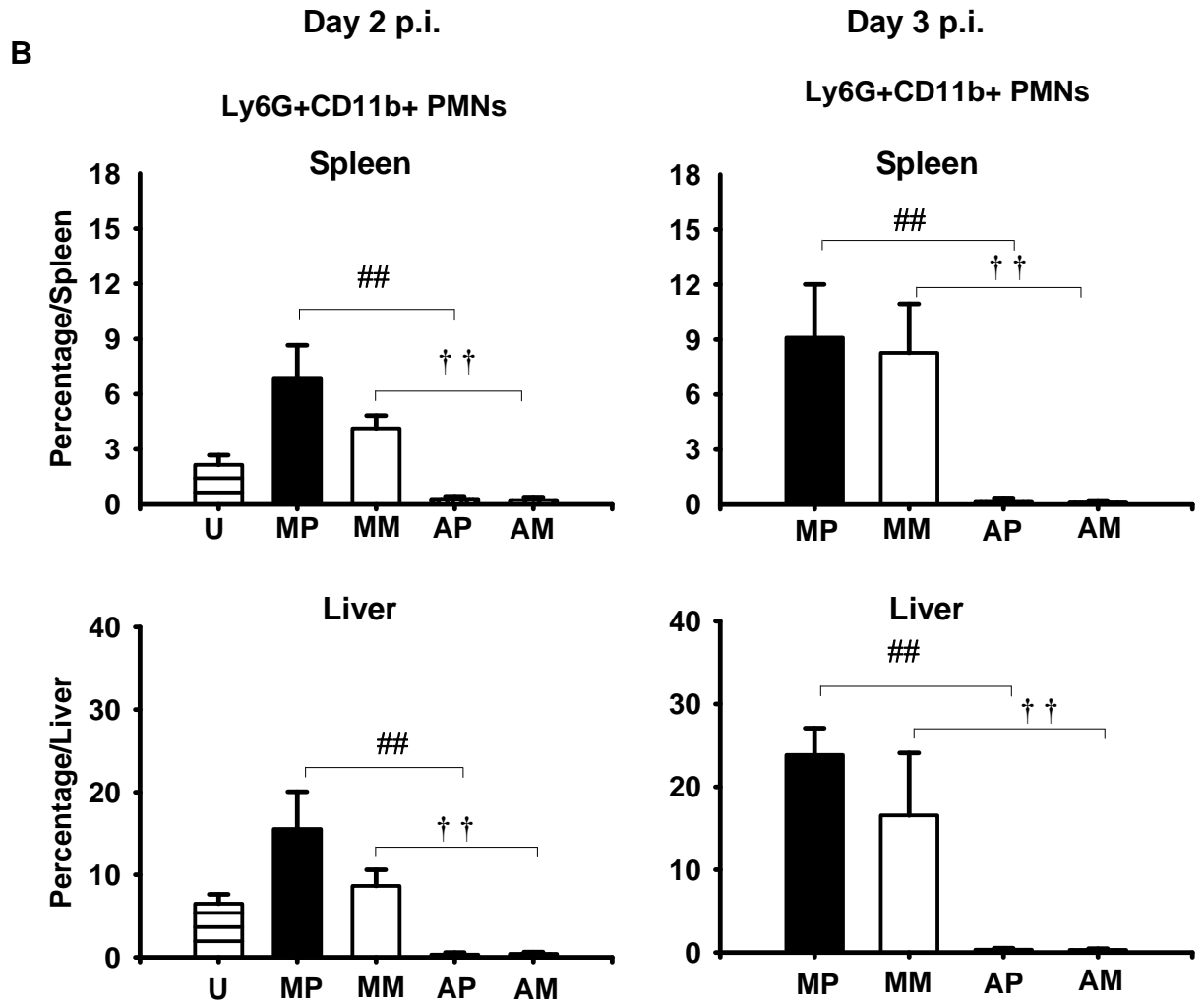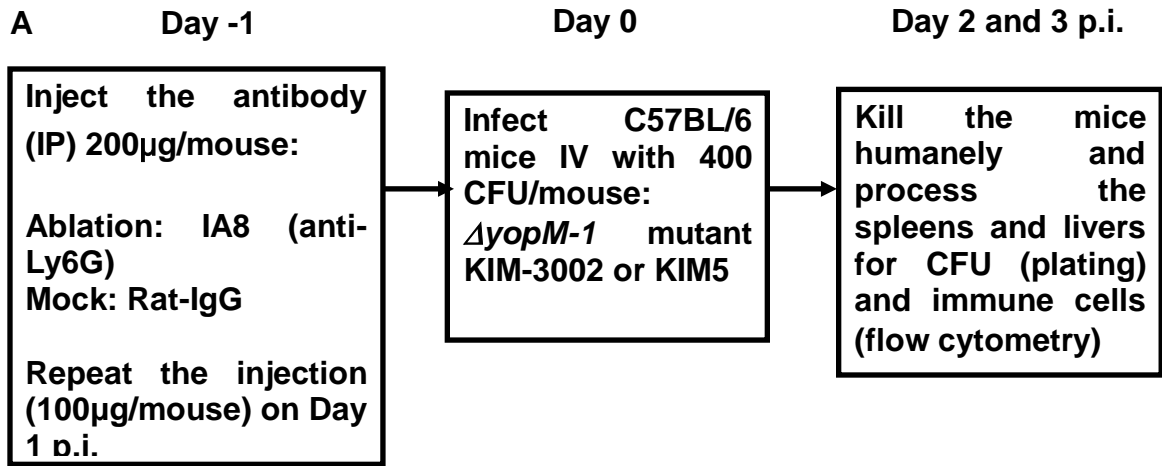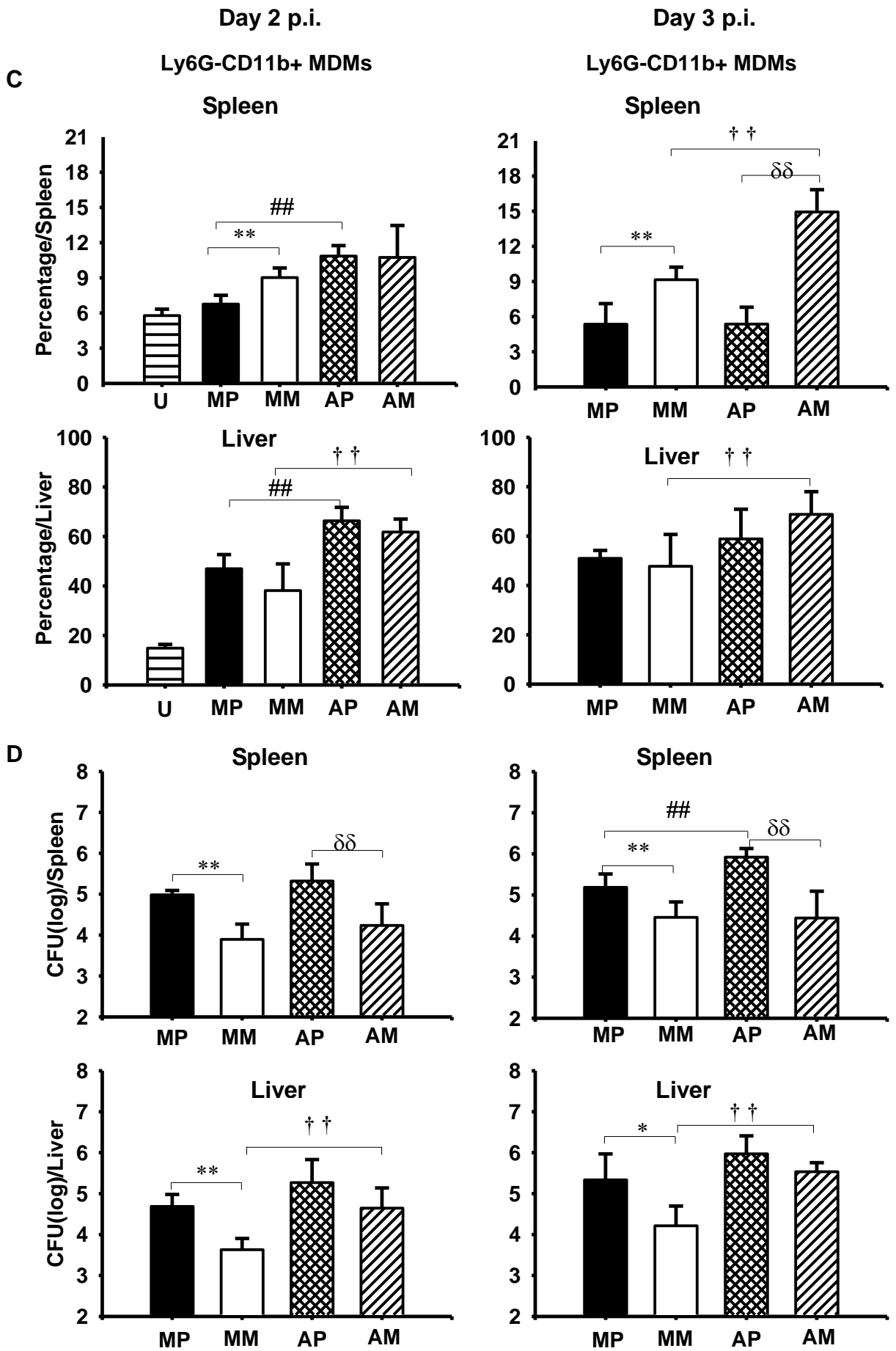
Day 2 p.i.

Ly6G-CD11b+ MDMs

Spleen

Liver

Day 3 p.i.

Ly6G-CD11b+ MDMs

Spleen

Liver

C

D

131

Mice treated with anti-Ly6G antibody to ablate PMNs or mock-treated with nonspecific rat IgG were infected and analyzed for bacterial burdens and inflammatory leukocyte populations in livers and spleens on days 2 and 3 p.i.. Horizontal-hatched bars, uninfected mice (U); filled bars, mock-treated mice infected with parent *Y. pestis* KIM5 (MP); open bars, mock-treated mice infected with the Δ*yopM-1* mutant KIM5-3002 (MM); cross-hatched bars, PMN-ablated mice infected with *Y. pestis* KIM5 (AP); diagonally-hatched bars, PMN-ablated mice infected with the Δ*yopM-1* strain KIM5-3002 (AM). Panel A, experimental design. Panels B and C, Ly6G$^+$CD11b$^+$ PMNs and Ly6G$^-$CD11b$^+$ MDMs, respectively, expressed as percent of total live leukocytes from spleen and liver. Panel D, CFU. Each datum point represents the average of values from 6 mice. The error bars indicate the standard deviations. To compare PMN-ablated and mock ablation groups for mice infected with the Δ*yopM-1* strain KIM5-3002, †, $P < 0.05$; ††, $P < 0.01$; for mice infected with the parent strain KIM5, #, $P < 0.05$; ##, $P < 0.01$. In comparisons between groups of mice infected with KIM5 and KIM5-3002, *, $P < 0.05$; **, $P < 0.01$ for mock-treated mice; δ, $P < 0.05$; δδ, $P < 0.01$ for PMN-ablated mice.

RESULTS

Chapter Eight: Distinct subsets of MDMs play different roles in controlling *Y. pestis* in spleen, and iDCs may be responsible for the growth limitation of *ΔyopM-1* mutant

Since Gr1$^+$ cells are the innate immune cells controlling the *ΔyopM-1* mutant in spleen and ablation of one of the major components in this population, PMNs, failed to relieve the growth defect of the *ΔyopM-1* mutant in spleen, we changed our focus to Gr1$^+$ MDMs, defined as Gr1$^+$Ly6G$^-$CD11b$^+$. Ly6G$^-$CD11b$^+$ MDMs include several subpopulations, such as resident MΦs/DCs, inflammatory monocytes and a newly discovered DC with pro-inflammatory function. Here we studied the recruitment of MDMs into spleens and livers and used KO mice and conditional ablation to test their role in the growth of infecting *Y. pestis* in systemic plague.

A. The accumulation of MDMs in spleens was compromised when YopM was present in the infecting strain

Through experiments designed as in Figure 7.1A, the recruitment of MDMs into spleens and livers was studied. In contrast to PMNs (Figure 7.1B), which were recruited similarly by parent and *ΔyopM-1* mutant, significantly greater numbers of MDMs were stably recruited to spleens when YopM was absent in the infecting strain. This effect was not observed in livers, which showed identical accumulations of these cells during infection by both *Y. pestis* strains (Figure 8.1A).

The cells in the peak population had high expression levels of CD11b, when analyzed as MFI, and thus likely were predominantly newly arrived monocytes (Figure 8.1B).

Accordingly, the increase in MDMs in mice infected with the *ΔyopM-1* mutant but not the parent *Y. pestis* may reflect an effect of YopM on monocyte influx into spleen but does not obviously explain the virulence effect of YopM in liver.

In contrast to Gr1$^+$ cell ablation, which abolished the influx of MDMs into infected spleens and delayed influx until d 3 p.i. in livers (Figure 6.1C), ablation only of PMNs did not abolish or even decrease influx of MDMs in either organ (Fig. 7.5C). This finding shows that PMNs are not essential for recruiting these cells from the bone marrow and peripheral circulation into infected organs. Further, either non-PMN Gr1$^+$ cells are responsible for recruiting MDMs in response to infection by *ΔyopM-1 Y. pestis* or the recruited MDMs themselves are Gr1$^+$.

B. Clodronate-mediated depletion inhibited the growth of both *ΔyopM-1* mutant and parent strains, indicating that an MDM subset may serve as the initial niche for *Y. pestis*

Resident macrophages and DCs are believed to provide an early intracellular niche for *Y. pestis* in spleen (192). Moreover, the presence of YopM in the infecting *Y. pestis* had previously been shown to be associated with decreased expression of proinflammatory cytokines like TNFα, IL-1, IL-12, IL-15, and IL-18 in F4/80$^+$ cells (macrophages and monocytes) by d 2 p.i. (159). Accordingly, it is possible that these resident cells are the initial target of YopM and those PMNs and inflammatory monocytes are affected secondarily. To test this hypothesis, as described in Figure 8.2A, we treated mice IV with 200 µL of clodronate-containing mannosylated liposomes 18 h prior to, and one day after, infection to specifically deplete MDMs, especially macrophages/DCs. The

mock-treated mice received 200 µL of liposome-encapsulated PBS. Organs were harvested on d 1, 2, and 3 p.i. for determination of bacterial load and flow cytometric analysis.

A series of preliminary experiments was performed to test the effect of clodronate on MDMs in spleen and liver without infection before the real experiments with *Y. pestis* infection. The experiments were designed similarly to that described in Figure 8.2A but without infection. For convenience, the time points in all experiments in this section were named according to the infection, no matter whether there was an infection. Therefore in Figure 8.2B, d -1 indicates the time to inject the liposomes and d 0 was 18 hours after injection. From Figure 8.2B, we found that the first clodronate treatment (injected on d-1) removed three fourths of the MDMs (CD11b$^+$Ly6G$^-$) from spleen and liver on d 0. Since there was no infection in these experiments, those ablated MDMs were considered to be resident cells. The second injection of clodronate maintained the low level of MDMs in these organs.

In the experiments with *Y. pestis*, mice were infected with 400 CFU/mouse of *Y. pestis* KIM5 or KIM5-3002 in addition to the liposome treatment. Similarly to the preliminary experiments, clodronate depleted ca. 80% of resident MDMs from spleen and prevented the net increase due to influx of inflammatory monocytes (Figure 8.2D). In liver, however, clodronate failed to reduce initial numbers of resident CD11b$^+$Ly6G$^-$ cells but did prevent or delay the influx of monocytes (Figure 8.2D). Flow cytometric analysis for total CD11c$^+$ DCs showed a depletion pattern similar to that of CD11b$^+$Ly6G$^-$ cells (Figure 8.2E). Nonetheless, the clodronate treatment strikingly curtailed the number of viable bacteria for both *Y. pestis* strains in both organs (Figure 8.2G). In liver, this effect

did not correlate with changes in numbers of hepatic PMNs (Figure 8.2F), indicating that PMNs were unlikely to be responsible for this growth pattern. However, a robust influx of splenic PMNs (Figure 8.2F) was found in clodronate-treated mice on d 3 p.i., correlating with the controlled growth of both strains in spleen (Figure 8.2G). It is reasonable to deduce that the bacterial growth in spleen was dampened by the increased number of PMNs, which resulted from clodronate treatment, as well as loss of amplification niches for the bacteria.

Lesions at d 3 p.i. in the mock-treated mice were similar in appearance to those of other mock-treated mice at the same time p.i. (compare Figure 8.2C upper panels to Figure 6.1E). However, in clodronate-treated mice, regardless of the strain they were infected with, only a few small lesions were found, and there was little or no necrosis present. These histopathological findings were consistent with a lower inflammatory status in the clodronate liposome-treated vs. PBS liposome-treated mice (Figure 8.2D). These data showed that clodronate-sensitive cells function to amplify bacterial numbers for *Y. pestis* with or without YopM, consistent with a previous study which suggested that macrophages serve as an intracellular reservoir during plague (192).

The liposomes per se are not completely benign, and the total numbers of MDMs were reduced on d 3 p.i. in spleens and livers and increased on d 0 in livers of mice that were mock-treated with PBS-liposomes (Figure 8.2B). A different method for ablation of MDMs was tested by two colleagues for its effect on infection by the parent *Y. pestis* KIM5 strain. MDMs can be conditionally depleted by treating transgenic MaFIA mice with a dimerizer drug that initiates Fas-induced apoptosis in these cell types without affecting mature PMNs (57). Groups of these mice were given dimerizer or were mock-

treated with injection solution, infected IV with 200 CFU of the parent *Y. pestis*, and analyzed for viable numbers of bacteria in liver and spleen on d 4 p.i.. The depletion of MDMs in dimerizer-treated MaFIA mice was about 95%, and PMNs were not depleted (data not shown). Figure 8.3 shows that ablation of MDMs by this alternative procedure again resulted in significantly lower bacterial burdens in organs.

Interestingly, in mice treated with clodronate-liposomes the *ΔyopM-1* mutant still showed restricted growth compared to the parent strain, most prominently in spleen (δ in Figure 8.2G). Because a portion of splenic MDMs always resisted the clodronate treatment and had a non-negligible number (ca. 4% of total live splenic leukocytes) (Figure 8.2D), it was hypothesized that these low numbers MDMs were responsible for the maintenance of growth limitation of the *ΔyopM-1* mutant bacteria after clodronate treatment.

C. The *ΔyopM-1* mutant and parent strain showed the same ability to elicit the efflux of MDMs from bone marrow into circulation only at a very early stage of the infection

The difference in recruitment of MDMs into spleen by parent and *ΔyopM-1* mutant raised a question: where was the recruitment of MDMs inhibited by YopM, efflux from bone marrow into blood or influx from circulation into spleen? Described in Figure 8.4A, mice were infected IV with the parent strain or *ΔyopM-1* mutant and bone marrow, spleens and blood were harvested on d 2 and 3 p.i. for flow cytometric analysis. In order to compare the numbers of cells from different organs, absolute numbers, instead of percentage per organ, are shown in the panels in Figure 8.4B and C.

As expected, we did not find any YopM-associated difference in the absolute number of PMNs in bone marrow, blood or spleen on both d 2 and 3 p.i. (Figure 8.4C). However, although the numbers of bone marrow MDMs in the mice infected with either strain were the same on d 2 p.i. (Figure 8.4B, left panel), the parent strain-infected mice contained ca. $2x10^6$/mouse more MDMs in the circulation than the *ΔyopM-1* mutant-infected ones (Figure 8.4B, middle panel), given that the total volume of blood in a mouse weighing 18 g, which is the average weight of the mice in our experiment, is ca. 1 mL (266). Meanwhile there were ca. $2x10^6$/mouse fewer MDMs recovered from parent strain-infected spleens than *ΔyopM-1* mutant-infected ones (Figure 8.4B, right panel) on d 2 p.i.. Therefore YopM produced by the parent strain did not affect the efflux of MDMs from bone marrow into blood, but it did inhibit the infiltration of those cells into spleen on d 2 p.i.

However, the above difference for MDMs in circulation disappeared on d 3 p.i. (Figure 8.4B, middle panel), while the difference in the accumulation of MDMs in spleen became greater than on d 2 p.i. (Figure 8.4B, right panel). Although on d 3 p.i. the *ΔyopM-1 Y. pestis* infection stimulated more bone marrow cells to differentiate into MDMs than did the parent strain infection (Figure 8.4B, left panel), that difference in absolute number was not large enough to result in the accumulation of MDMs in *ΔyopM-1* mutant-infected spleen. Thus, the compromised recruitment of MDMs into parent strain infected spleen on d 3 p.i. should be explained by YopM's negative effect on both the efflux of MDMs from bone marrow into blood and the influx of circulating MDMs into spleen.

D. CCR2 KO prevented the influx of MDMs into spleen and liver and specifically favored the growth of the *ΔyopM-1* mutant

As mentioned earlier, in the clodronate-mediated ablation model, the liposomes themselves are toxic to MDMs. A more important disadvantage is that clodronate removes resident macrophages and DCs as well as infiltrated inflammatory monocytes, and these cell types have distinct functions at different stage of infection. Thus, an animal model that only ablated infiltrating monocytes became necessary to further study the role of those cells in the YopM mechanism.

CCL2/MCP-1 is a member of the C-C chemokine family and a potent chemotactic factor recognized by CCR2 on the surface of inflammatory monocytes. Therefore, mice lacking the *ccr2* gene are susceptible to infectious pathogens because their monocytes fail to migrate to the infection sites. Although lacking CCR2 on the surface of their monocytes, NK cells, memory T cells, and PMNs (85, 144, 193), CCR2^{-/-} mice are not significantly different from WT mice under pathogen-free conditions, which indicates that those mice are not severely immunocompromised. Furthermore, since the CCL2-CCR2 chemokine pair functions mainly in the recruitment of monocytes, NK cells, and memory T cells, resident MDMs are not affected in CCR2^{-/-} mice, and NK cells and memory T cells are not Gr1^{+} and are not required for YopM to have its pathogenic effect. Meanwhile, PMNs would not be affected in recruitment because the CCR2 does not function in recruitment of that cell type (168). Therefore, all of these advantages make CCR2 KO mice a better model to study the role of inflammatory monocytes than clodronate-mediated ablation.

As described in Figure 8.5A, CCR2^{-/-} mice and C57BL/6 mice were infected IV with

the parent strain and the $\Delta yopM$-1 mutant. On d 3 p.i., spleens and livers were harvested to study leukocytes and bacterial burden. In CCR2$^{-/-}$ mice, significantly fewer Ly6G$^-$CD11b$^+$ MDMs were recruited to spleen and liver by the infection with both of the strains than in WT mice (Figure 8.5B). As expected, the MDMs were not completely abolished, because resident macrophages and DCs also are Ly6G$^-$CD11b$^+$ cells and their presence in organs is independent of the CCR2 signaling pathway (293). Further, the difference between parent and mutant strains in the residual MDMs in CCR2$^{-/-}$ mice was still significant in spleen (Figure 8.5B, left panel). This indicates that there are some CCR2$^-$ MDMs recruited into spleen with the YopM-associated pattern. The relief of growth limitation of the $\Delta yopM$-1 mutant strain in the spleens of CCR2$^{-/-}$ mice (Figure 8.5D, left panel) was not complete (although the difference from the parent strains growth was not significant statistically); the residual growth control might be mediated by these splenic CCR2$^-$ MDMs that were recruited through the signaling pathway of other chemokines and their receptors, such as CCL5/RANTES (regulated on activation, normal T cell expressed and secreted) and its receptor CCR3 (47, 123). Interestingly, infection by the $\Delta yopM$-1 mutant strain recruited significantly more Ly6G$^+$CD11b$^+$ PMNs into spleen than did the parent strain in CCR2$^{-/-}$ mice (Figure 8.5C, left panel), and those newly recruited PMNs apparently could not clear the $\Delta yopM$-1 strain, because the bacterial burden in spleen was significantly increased in $\Delta yopM$-1 strain-infected CCR2$^{-/-}$ mice (Figure 8.5D, left panel).

The accumulation of MDMs in liver showed no YopM-associated pattern in CCR2$^{-/-}$ mice (Figure 8.5B, right panel). In contrast, more PMNs were recruited in the livers of the $\Delta yopM$-1 strain-infected CCR2$^{-/-}$ mice than those of parent strain-infected ones

(Figure 8.5C, right panel), correlating with maintenance of the growth limitation of the *ΔyopM-1* strain. However, the *ΔyopM-1* KIM5-3002 actually grew much better in CCR2$^{-/-}$ mice than in WT mice in liver (Figure 8.5D, right panel). These data supported the importance of PMNs in liver, whose function in clearance of the *ΔyopM-1* mutant was likely compromised by CCR2 KO.

E. Absence of CCR2 favored the growth of *ΔyopM-2* mutant strain in skin

YopM was proven to be necessary for full lethality in the bubonic plague model by LD$_{50}$ measurement and histopathological analysis (Table 3.1) (363). However, the immune cells in skin controlling the *ΔyopM-2* mutant strain had not been characterized. Since the CCR2 KO favors the growth of the *ΔyopM-1* strain in the systemic plague model, it is reasonable to hypothesize that CCR2$^+$ cells mediate the decreased virulence of *ΔyopM-2 Y. pestis* in the bubonic plague model, in which a strong inflammatory response also occurs. To test this hypothesis, CCR2$^{-/-}$ mice and C57BL/6 mice were ID-infected with 200 CFU of *Y. pestis* CO92.S6 and *ΔyopM-2* mutant CO92.S19. On d 4 and d 5 p.i., spleens and the skin surrounding the infection sites were harvested to study bacterial growth in skin and dissemination to spleen (Figure 8.6).

In WT mice, the *ΔyopM-2* mutant *Y. pestis* showed a delayed growth compared to the parent strain. However, in the CCR2$^{-/-}$ mice the growth defect of the *ΔyopM-1* mutant strain in skin disappeared and the *ΔyopM-1* strain grew even better than the parent strain on d 5 p.i., while growth of the parent strain was not affected by CCR2 KO (Figure 8.6B, left panels). These findings suggest that CCR2$^+$ cells play a critical role in controlling *ΔyopM-2 Y. pestis* numbers in skin and YopM targets the protective function of CCR2$^+$

cells.

As shown in the right panels of Figure 8.6B, dissemination of parent *Y. pestis* to spleen showed no significant difference between WT and KO mice on d 4 p.i., but by d 5 p.i., 5 of the mice infected with the parent *Y. pestis* had died. In contrast to d 4 p.i., when CCR2 KO did not affect the colonization of *ΔyopM-2 Y. pestis* in spleen, a higher number of bacteria was recovered from the spleen of CCR2^{-/-} mice on d 5 p.i., although this difference was not statistically significant (P = 0.09). This finding suggested that CCR2^{+} cells may be one of the cell types inhibiting the dissemination of *ΔyopM-2 Y. pestis*, but their importance in this process still needs further investigation.

F. CCL2/MCP-1 KO favored both of the strains, consistent with the diversity of CCL2 functions in addition to recruiting MDMs

Although the major chemokine recognized by CCR2 is CCL2/MCP-1, CCR2 also interacts with other chemokines for macrophages, such as CCL8/MCP-2 and CCL7/MCP-3 (85). The growth of the *ΔyopM Y. pestis* in CCR2 KO mice could be enhanced by the absence of the CCL2-CCR2 interaction or of the CCL2-independent CCR2 signaling pathway.

Therefore, in addition to CCR2^{-/-} mice, we also tested the growth of parent and *ΔyopM-1* strains in CCL2^{-/-} mice. As described in Figure 8.7A, CCL2^{-/-} mice and C57BL/6 mice were IV-infected with the parent strain and the *ΔyopM-1* mutant. On d 3 p.i., spleens and livers were harvested to study bacterial burden. Unlike the enhanced growth of the *ΔyopM-1* mutant strain in the spleens of CCR2^{-/-} mice, there was no change in the relative growth yields between these two *Y. pestis* strains due to CCL2/MCP-1 KO,

although both of them grew much better in the spleens and livers from CCL2$^{-/-}$ mice than in those organs from WT ones (Figure 8.7B).

In addition to CCR2, CCL2/MCP-1 is also recognized by CCR4 (76). Meanwhile, in contrast to CCR2, which is restricted in expression to a few cell types, CCL2/MCP-1 is a potent chemoattractant for many cell types, such as monocytes, langerhan cells, memory T cells and NK cells (85, 209). Further, along with IL-8, MCP-1 has been shown to trigger the firm adhesion of monocytes to vascular endothelium under flow conditions (111). CCL2/MCP-1 also can induce the degranulation of basophils and mast cells as well as cell aggregation in rat peritoneal mast cells (37, 70). Therefore the KO of CCL2/MCP-1 compromises the immune system broadly and favors the growth of both strains whether they express YopM or not.

G. iDCs, one of the major subsets of MDMs, may be the key cells clearing the *ΔyopM-1* mutant in spleen

In Chapter 8D and 8E, we concluded that the CCR2$^+$ cells were the key cells to control the growth of the *ΔyopM Y. pestis* in spleen, liver and skin. Meanwhile, ablation of Gr1$^+$ cells from the infected mice made the *ΔyopM Y. pestis* grow like the parent strain in both spleen and liver, pointing towards Gr1$^+$ cells as the critical cellular component in the YopM virulence mechanism (Figure 6.1). Taken together, CCR2$^+$Gr1$^+$ cells were found to be responsible for the growth limitation of the *ΔyopM Y. pestis*. It was true for liver, in which PMNs controlled the growth of the *ΔyopM* mutant. PMNs express both Gr1 and CCR2 on their surface (144). Therefore, a subset of the CCR2$^+$Gr1$^+$ cells other than PMNs may be the critical cell for the *ΔyopM Y. pestis* phenotype in spleen.

Inflammatory monocytes no doubt are one of the major cell types whose recruitment depends on the CCL2-CCR2 chemokine pair (85). However, another cell type, inflammatory DCs (iDCs) or TipDCs (TNF alpha/iNOS producing DCs), which are derived from monocytes and recruited like inflammatory monocytes, i.e., depending on CCR2 signaling, into spleen (109, 294), was also studied. These TipDCs express both high level Gr1 (or more specific, Ly6C) and CCR2 on their surface (293) and act as a critical player to control some intracellular bacteria during infection (71, 294). Therefore it was necessary to test the role of these cells in the infection of parent *Y. pestis* and *ΔyopM-1* mutant.

a) Characterization of iDCs by flow cytometry and intracellular staining

Since there are only a few studies about TipDCs, there is not a consistent way to define them in terms of surface and intracellular markers. Currently there are three surface-staining combinations for TipDCs in the literature: $CD115^+Gr1^+$(17), $Ly6C^{high}CD11b^+$(71), $CD11b^{int} CD11c^{int}$(294). Meanwhile, combined with above surface marker detection, intracellular iNOS and TNF alpha staining are also important to define TipDCs. Since there is no literature reporting the definition of TipDCs in *Y. pestis* infection, we had to determine our own combination for these DCs.

In order to choose the correct staining plan for our study, the cells harvested from spleens d 3 post infection with the parent or mutant strains were stained for intracellular iNOS and TNF alpaha as well as surface markers. As showed in Figure 8.8A, we decided to use $CD11b^+ CD11c^{int}$ as our definition for TipDCs (Table 4.1) because this population was proven to make a high level intracellular iNOS. Since iDCs express CD11b but no Ly6G on their surface, they must be one major component of MDMs ($Ly6G^-CD11b^+$).

Interestingly, we did not detect TNF alpha production in those cells, whether the infecting bacteria contained YopM or not. However, that experiment lacked a positive control showing that the assay was working, so at present we cannot conclude that these iDCs are TNF$^-$. Therefore we decided to name those cells as iDCs (inflammatory DCs), instead of TipDCs. Apparently YopM from the parent strain inhibited the influx of those iNOS$^+$CD11b$^+$CD11c^{int} cells into spleens (Figure 8.8B).

b) YopM-related difference in iDC influx into spleen was dependent on CCR2 signaling, but not related to the presence of PMNs

Through experiments designed as shown in Figure 8.9A, the recruitment of iDCs into spleens and livers was studied. Similarly to MDMs (Figure 8.1A), there was a significant difference in the iDCs (CD11b$^+$ CD11c^{int}) in spleen starting on d 2 p.i., but this was not observed in liver (Figure 8.9B).

Meanwhile, CCR2$^{-/-}$ mice were used to study the relationship between the recruitment of iDCs and signaling through CCR2. As described in Figure 8.10A, CCR2$^{-/-}$ mice and C57BL/6 mice were IV-infected with the parent strain and the *ΔyopM-1* mutant. On d 3 p.i., spleens and livers were harvested to study leukocytes. In WT mice, similar to the result in Figure 8.8B, iDCs showed a YopM-associated pattern in the recruitment into spleen, but not in liver (Figure 8.10B). However, in CCR2$^{-/-}$ mice lacking CCR2-mediated chemotactic signals, the influx of iDCs into both spleen and liver was compromised, whether the infecting strain contained YopM or not. Consequently, the difference in recruitment of iDCs into spleen between mice infected with the parent and mutant strains disappeared (Figure 8.10B, left panel).

Although PMNs were confirmed not to be the major cells to clear the *ΔyopM-1*

145

mutant in systemic plague in spleen, the extensive crosstalk between them and MDMs raised the question as to whether PMNs affect the YopM-associated recruitment pattern of iDCs in spleen. By using a design similar to that described in Figure 7.5A, we compared the influx of iDCs into spleen and liver between the parent and $\Delta yopM$-1 mutant *Y. pestis* infection on d 2 and d 3 p.i.. As shown in Figure 8.11, absence of PMNs had no influence on the existing pattern of iDC influx into spleen and liver.

The studies in this section have shown that iDCs, a major component of MDMs, had exactly the same recruitment pattern as MDMs into spleen. Further, when the percentage of iDCs was subtracted from that of MDMs, the remaining MDMs were recruited similarly into spleen on d 2 p.i. (data not shown), indicating that the function of MDMs in the controlling the $\Delta yopM$-1 strain in spleen at the early stage of infection may be actually executed by this subset.

c) Co-infection of parent and *$\Delta yopM$-1 Y. pestis* relieves the growth defect of the *$\Delta yopM$-1* strain in spleen but not in liver

Since it was found that YopM produced by the parent strain inhibited the influx of iDCs into spleen and favored the growth of these bacteria in spleen, we hypothesized that co-infection of the parent and $\Delta yopM$-1 mutant should overcome the growth limitation of the $\Delta yopM$-1 strain because YopM produced by the parent strain would inhibit the recruitment of iDCs, which may be critical for controlling growth of $\Delta yopM$-1 *Y. pestis* in spleen.

In experiments designed as shown in Figure 8.12A, WT mice were infected with the parent strain $\Delta lacZ$ *Y. pestis* KIM5-3003, the $\Delta yopM$-1 strain KIM5-3002 or a 1:1 mixture of the two strains. To increase the likelihood of depositing bacteria of each strain in

infected splenic and hepatic sinusoids, a high infectious dose (5×10^3) was used in this experiment. The spleens and livers were harvested on d 2, 3 and 4 p.i.. To distinguish the two strains, we used a parent strain that lacked the *lacZ* gene (KIM5-3003) and used blue-white screening on agar medium containing X-Gal. As shown in Figure 8.12B, parent strain colonies were white and *ΔyopM-1* strain colony was blue.

Figure 8.12C shows that by d 2 p.i., the two *Y. pestis* strains in co-infected spleens showed the same viable numbers, which kept increasing and became significantly higher than that of spleen infected only with the *ΔyopM-1* strain on d 4 p.i.. Thus the YopM-related growth limitation in spleen was relieved by the presence of the parent strain. However in liver, there was little difference between the growth rates of the bacteria separately and together, and the YopM-associated difference between parent and mutant in bacterial numbers was maintained in the co-infected livers.

These results supported our hypothesis that the effect of YopM on recruitment of iDCs into spleen changes the whole microenvironment in spleen and thus protects the YopM producing *Y. pestis* as well as the nearby *ΔyopM-1* strain from clearance. In liver, the parent strain only promoted its own growth by a mechanism which may inhibit the bactericidal function of PMNs and did not favor the growth of nearby *ΔyopM-1* bacteria. It is worth noticing that the proinflammatory effects of the *ΔyopM-1* also compromised the growth of the parent strain, reflected in a lower viable number of the parent strain in co-infected organs than in the separate infection.

Figure 8.1 Effect of YopM on the accumulation of MDMs in spleens and livers
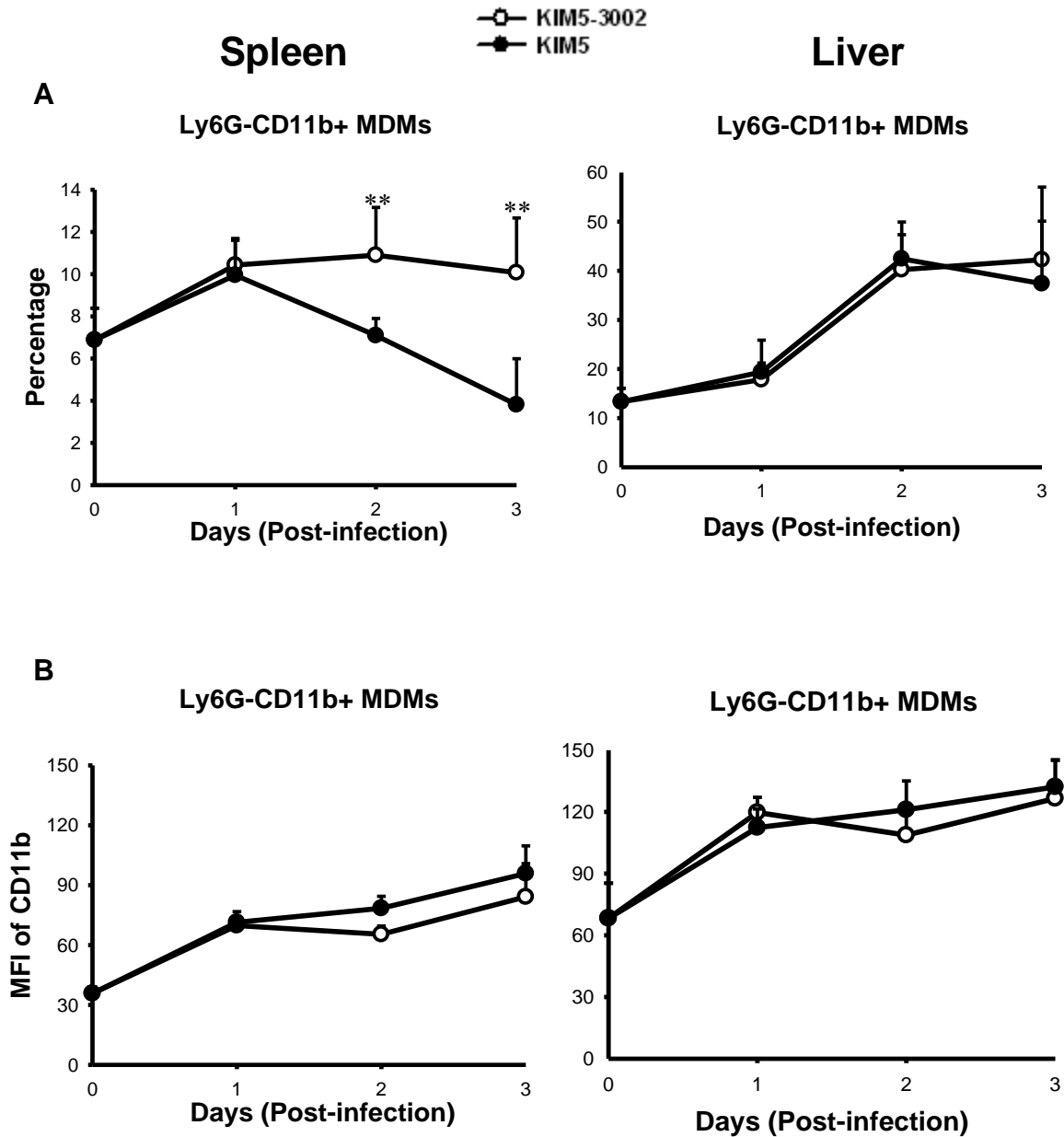
C57BL/6 mice were infected IV with 400 CFU KIM5 (parent strain, filled circles) or KIM5-3002 (*ΔyopM-1* mutant, open circles) strains that had been grown at 26°C. At the indicated times, groups of mice were analyzed for populations of live leukocytes in liver and spleen by flow cytometry. Panel A, Ly6G^{-}CD11b^{+} cells (MDMs) expressed as

percent of total live leukocytes in spleens and livers of mice infected with KIM5 or KIM5-3002. Panel B, MFI of the staining of CD11b in splenic and hepatic MDMs. Points at time 0 indicate the values for uninfected mice. In Panels A and B, each datum point represents the average of values from 26 mice and 9 mice, respectively. The error bars indicate the standard deviations. Significant differences by the unpaired Student's *t* test comparing data from mice infected with KIM5 and KIM5-3002 are indicated (*, $P < 0.05$; **, $P < 0.01$) .

Figure 8.2 Ablation of MDMs with clodronate-liposomes restricted growth of both *Y.*

pestis strains.

A | **18 h before Infection** | **Day 0** | **Day 1, 2 and 3 p.i.**

IV Injected the Liposome 200µL/mouse:

Ablation: Clodronate-containing liposome
Mock: liposome-encapsulated PBS

Repeat the injection on Day 1 p.i.

Infect C57BL/6 mice IV with 400 CFU/mouse: *ΔyopM-1* mutant KIM-3002 or KIM5

Kill the mice humanely and process the spleens and livers for CFU (plating) and immune cells (flow cytometry and H&E staining)

◆— Mock Ablation Uninfected
◇‧ MDM Ablation Uninfected

B

CD11b+Ly6G- MDMs — Spleen

CD11b+Ly6G- MDMs — Liver

C

KIM5 | KIM5-3002

Mock Ablation

MDM Ablation

150

D

Spleen

Liver

Legend:
- KIM5-3002 Mock Ablation (open circle, solid line)
- KIM5 Mock Ablation (filled circle, solid line)
- KIM5-3002 MDM Ablation (open triangle, dashed line)
- KIM5 MDM Ablation (filled triangle, dotted line)

CD11b+Ly6G- MDMs (Spleen)

CD11b+Ly6G- MDMs (Liver)

E

CD11c+ DCs (Spleen)

CD11c+ DCs (Liver)

F

CD11b+Ly6G+ PMNs (Spleen)

CD11b+Ly6G+ PMNs (Liver)

Days (Post-infection)

151

Mice were given clodronate-liposomes (ablation groups) or PBS-liposomes (mock ablation groups) IV 18 h before infection with 400 CFU of *ΔyopM-1 Y. pestis* (KIM5-3002) or the parent strain (KIM5) IV. The same doses of liposomes were also given to the mice on day 1 p.i.. Panel A, experimental design. Panel B, the percentages of MDMs in spleens and livers from uninfected mice treated with clodronate-liposomes or PBS-liposomes. Each datum point represents the average of values from 12 mice. Panel C, Histopathology on day 3 p.i. in the livers of the MDM-ablated and mock-treated mice infected with *Y. pestis* KIM5 or KIM5-3002. Bars, 50 μm. On days 1, 2, and 3 p.i., the percentages of MDMs (Panel D), CD11c$^+$DCs (Panel E), PMNs (Panel F), and numbers of CFU (Panel G) in spleens and livers from the mice infected with *Y. pestis* KIM5-3002 or KIM5 were determined. The data in the graphs represent the averages plus SDs (error bars) for six mice per datum point in panels B, D, E and F; and for nine and six mice per datum point from the spleen and liver, respectively, in panel G, pooled from replicate experiments. Values that are significantly different (P < 0.01) in the MDM-ablated and mock-treated groups of uninfected mice are indicated (φφ). Values that are significantly

152

different (P < 0.01) in the MDM-ablated and mock-treated groups of mice infected with *Y. pestis* KIM5-3002 are indicated (††). Values that are significantly different in the MDM-ablated and mock-treated groups of mice infected with *Y. pestis* KIM5 are indicated as follows: #, P < 0.05; ##, P < 0.01. Values that are significantly different (P < 0.01) in the mock-treated mice infected with *Y. pestis* KIM5 and KIM5-3002 are indicated (**). Values that are significantly different in the MDM-ablated mice infected with *Y. pestis* KIM5 and KIM5-3002 are indicated as follows: δ, P < 0.05; δδ, P < 0.01.

Figure 8.3 Conditional ablation of MDMs by Fas-induced apoptosis in transgenic MaFIA mice also restricted growth of *Y. pestis* KIM5.
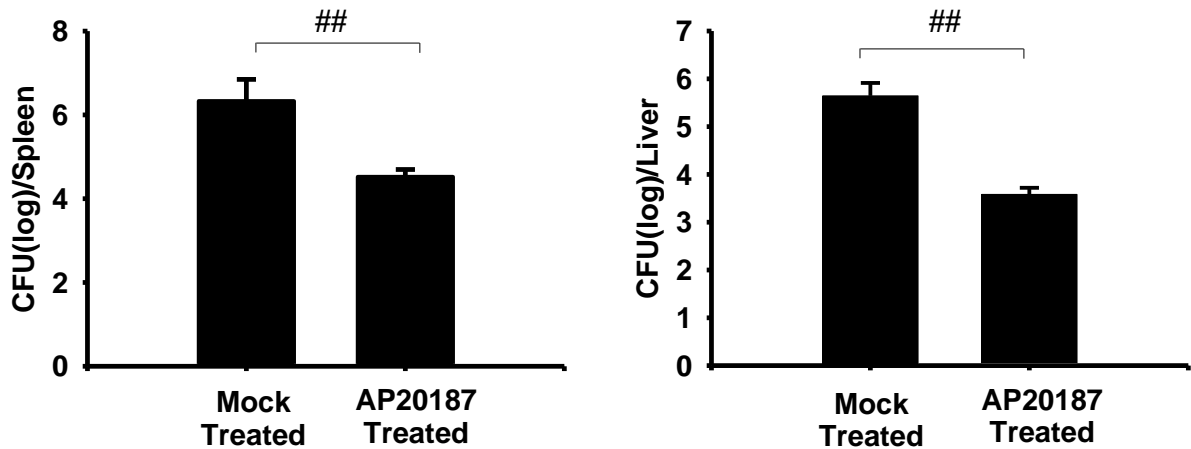
MaFIA mice were given daily i.v. injections of dimerizer drug AP20187 or mock injection solution for 5 days and then were allowed to rest two days before being infected with 200 CFU of the parent *Y. pestis* KIM5. The numbers of CFUs in liver and spleen on d 4 p.i. were measured. Data (average $\pm$ SD) are from 6 mice per treatment, pooled from replicate experiments. Differences between AP20187 and mock-treated groups (##, $P < 0.01$) are indicated. (This experiment was done by E. J. Kerschen Ph.D. in S. C. Straley's Lab and S. H. Burnett Ph.D. in D. A. Cohen's Lab in our Department)

Figure 8.4 Inhibition of MDM recruitment into spleen and into circulation by parent *Y. pestis* KIM5.

A

Day 0	Day 2 and 3 p.i.
Infect the C57 BL/6 mice IV with 400 CFU/mouse *ΔyopM-1* mutant KIM5-3002 or KIM5	Kill the mice humanely and harvest the bone marrow (from 2 femurs), spleens and blood (heart puncture, 200 µL/mouse) for flow cytometric analysis of MDMs and PMNs

B
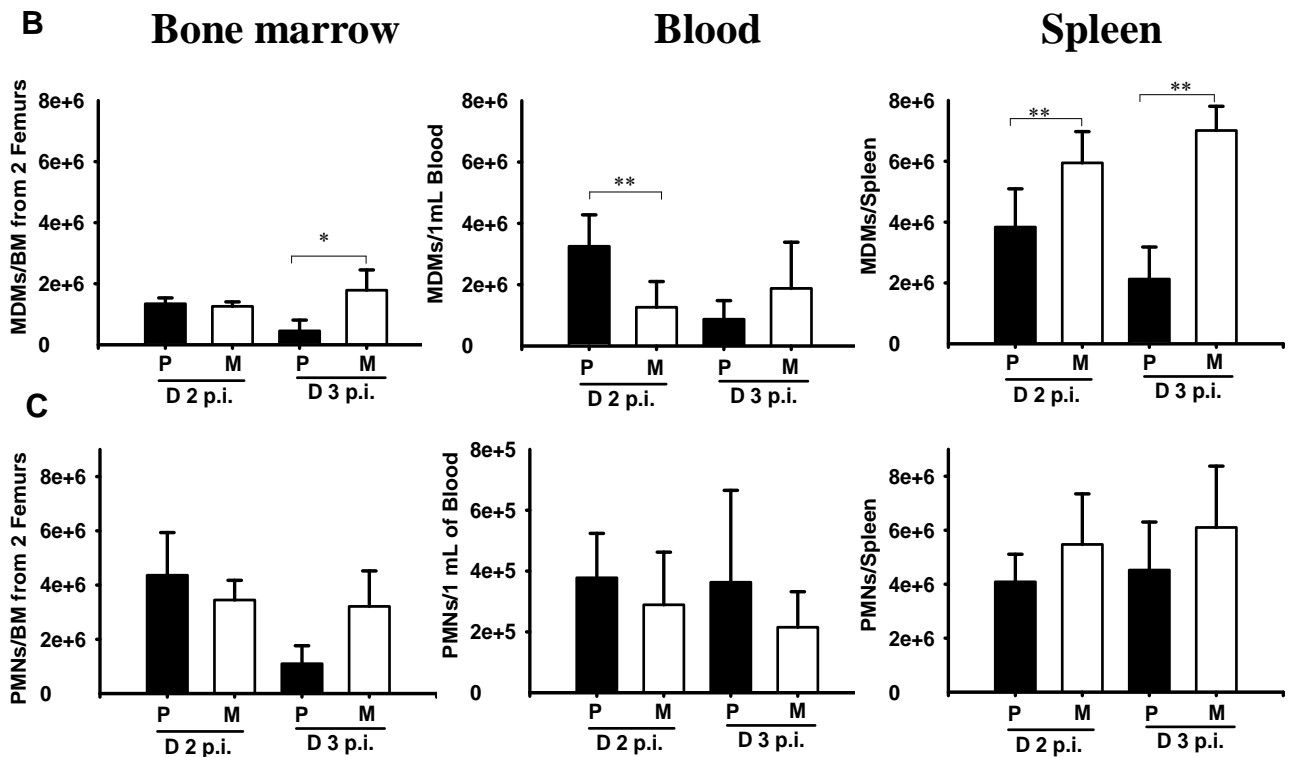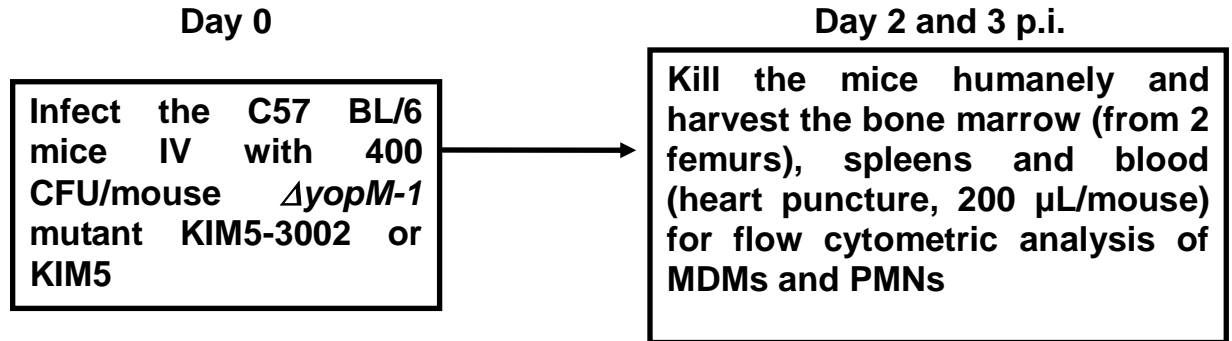
C57BL/6 mice were infected with the parent (KIM5) and *ΔyopM-1* (KIM5-3002) *Y. pestis* and analyzed by flow cytometry for populations of leukocytes in spleen, peripheral blood and bone marrow (BM) on days 2 and 3 p.i. Filled bars, mice infected with the parent strain; open bars, mice infected with the YopM- mutant. Panel A, experimental

design. Panel B, Ly6G⁻CD11b⁺ MDMs. Panel C, Ly6G⁺CD11b⁺ PMNs. The number of MDMs and PMNs is presented as absolute numbers of the cells harvested from whole spleen, 1mL blood or bone marrow from 2 femurs of one mouse. Each datum point represents the average of values from 9 mice. The error bars indicate the standard deviations. Significant differences by the unpaired Student's t test comparing data from mice infected with the parent and mutant strains are indicated (*, $P < 0.05$; **, $P < 0.01$).

Figure 8.5 CCR2 requirement for recruitment to selectively control growth of Δ*yopM-1 Y.*
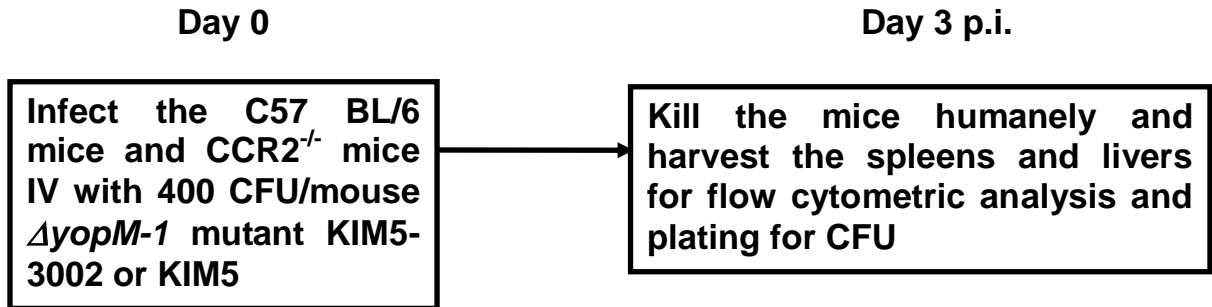
pestis KIM5-3002.

A

B
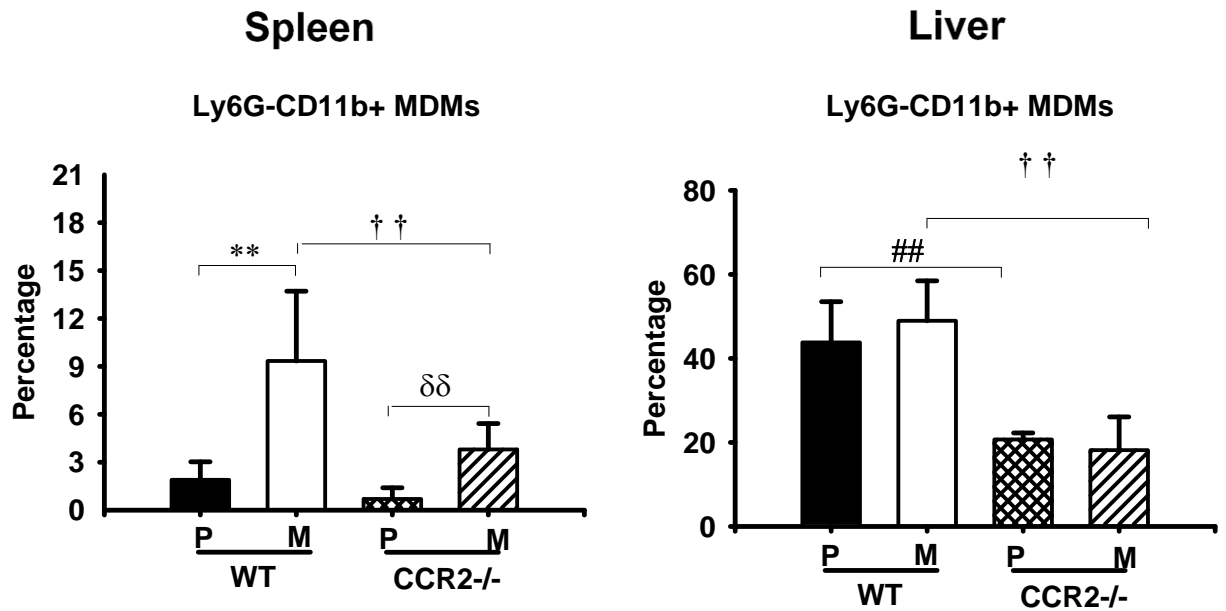
C
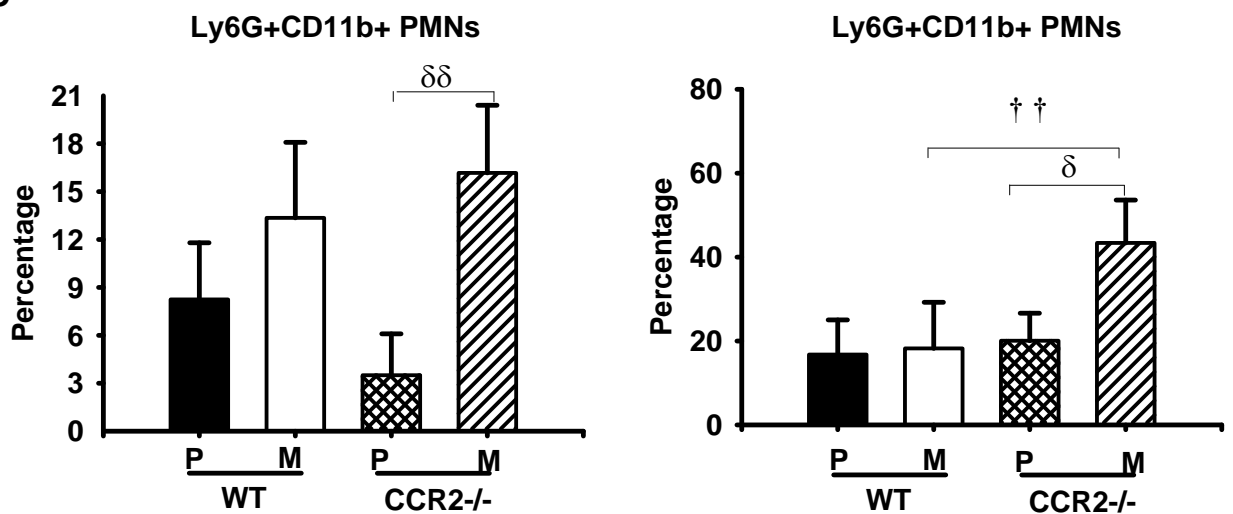
D
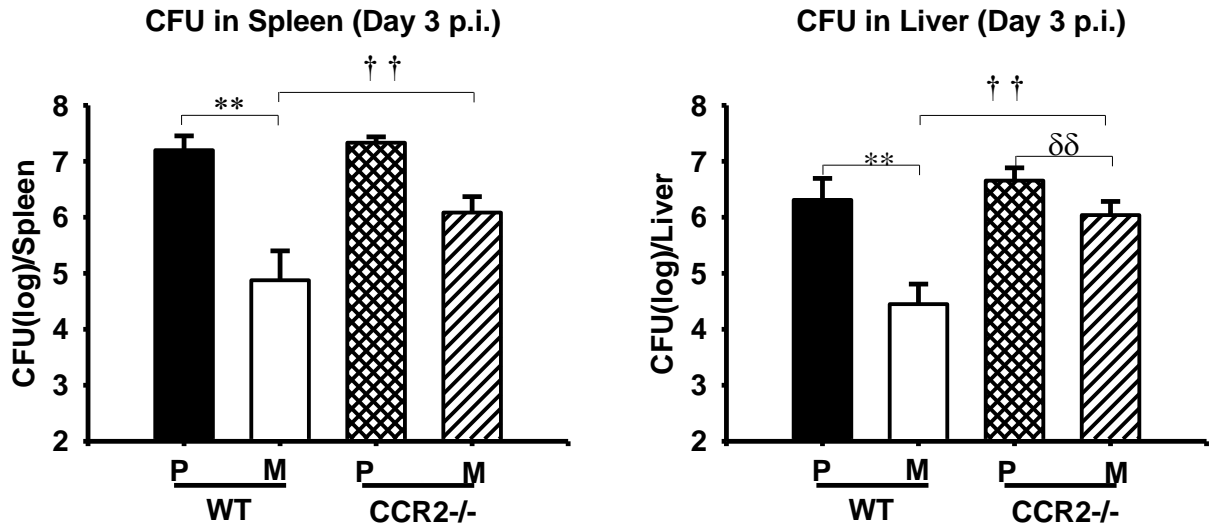
CFU in Spleen (Day 3 p.i.)

CFU in Liver (Day 3 p.i.)

WT and CCR2$^{-/-}$ C57BL/6 mice were infected and analyzed for bacterial burdens and inflammatory leukocyte populations in livers and spleens on d 3 p.i.. Panel A, experimental design. Panel B, Ly6G$^-$CD11b$^+$ MDMs and Panel C, PMNs (Ly6G$^+$CD11b$^+$ cells), expressed as percent of total live leukocytes. Panel D, CFU. Filled bars, WT mice infected with the parent *Y. pestis* KIM5 (P/WT); open bars, WT mice infected with the Δ*yopM-1* mutant KIM5-3002 (M/WT); cross-hatched bars, CCR2$^{-/-}$ mice infected with the parent strain KIM5 (P/CCR2$^{-/-}$); diagonally-hatched bars, CCR2-/- mice infected with the Δ*yopM-1* strain KIM5-3002 (M/CCR2$^{-/-}$). Each datum point represents the average of values from 9 mice. The error bars indicate the standard deviations. To compare WT and CCR2$^{-/-}$ mice infected with strain KIM5-3002, †, $P < 0.05$; ††, $P < 0.01$; for mice infected with *Y. pestis* KIM5, #, $P < 0.05$; ##, $P < 0.01$. In comparisons between groups of mice infected with strains KIM5 and KIM5-3002, *, $P < 0.05$; **, $P < 0.01$ for WT mice; δ, $P < 0.05$; δδ, $P < 0.01$ for CCR2$^{-/-}$ mice.

Figure 8.6 CCR2 requirement to control local growth of *ΔyopM-2* YopM- *Y. pestis* CO92

in bubonic plague.

A

Day 0

Day 4 and 5 p.i.

Infect the C57 BL/6 mice and CCR2-/- mice ID with 200 CFU/mouse *ΔyopM-2* mutant CO92.S19 or CO92.S6

Kill the mice humanely and harvest the spleen and the skin surrounding the infection sites for plating

B

159
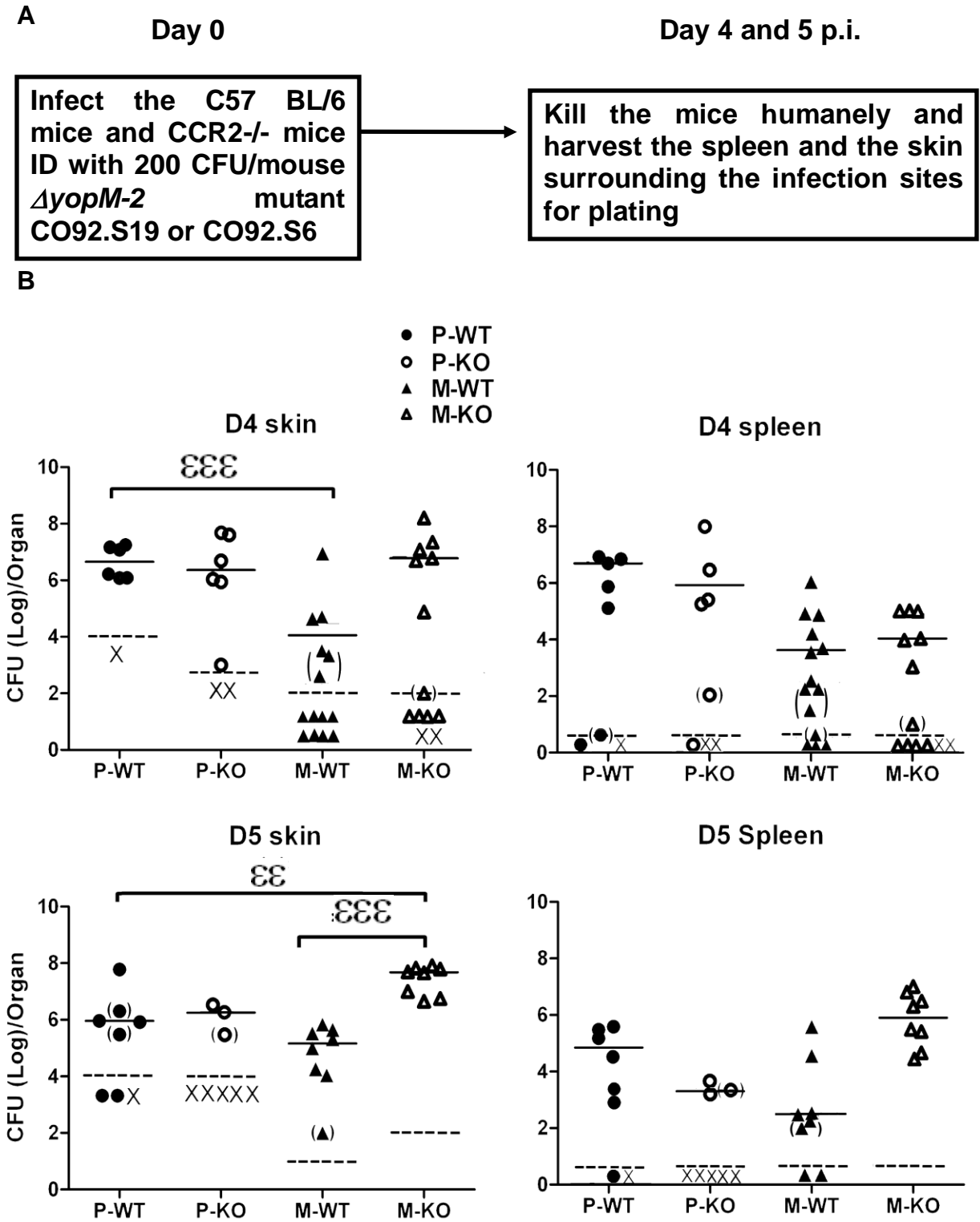
Groups of C57BL/6 and CCR2-/- mice were infected ID with 100-200 CFU of the parent *Y. pestis* CO92.S6 or 200-250 CFU of *ΔyopM-2 Y. pestis* CO92.S19, and skin and spleens were analyzed for CFU on days 4 and 5 p.i.. Because of the large number of mice involved, the infections for the two analysis times were done on different days. To improve the statistical power in the data for the *ΔyopM-2* mutant on d 4 p.i., that experiment was repeated and the data for the two experiments were pooled. Panel A, experimental design. Panel B, CFU on d 4 and d 5 p.i. Each symbol represents one mouse. Filled circles, parent strain and WT mice (P-WT; 8 mice in the group); filled triangles, *ΔyopM-2* mutant and WT mice (M-WT; 14 mice in the group on d 4 p.i. and 8 mice in the group on d 5 p.i.); open circles, parent strain and CCR2-/- mice (P-KO; 8 mice in the group); open triangles, *ΔyopM-2* mutant and CCR2-/- mice (M-KO; 14 mice in the group on d 4 p.i. and 8 mice in the group on d 5 p.i.); Xs, mice that died prior to analysis. Solid horizontal lines, median values of the data sets; dashed lines, limits of detection (a single colony on one of the duplicate plates); parentheses, data taken from plates with < 30 CFU. Significant differences of medians by the Wilcoxon two sample test are indicated: εε, P ≤ 0.01; εεε, P ≤ 0.001. On d 5 p.i. the number of P-KO mice that survived to be analyzed was too low for statistical evaluation, and the data for these mice likely underestimate those for the group. One sample of skin for P-WT on d 5 p.i. was lost, and one sample for spleen for M-KO on d 4 p.i. could not be enumerated (accounting for one less datum point for skin than spleen in those treatment groups).

Figure 8.7 Growth enhancement for both parent and YopM- mutant *Y. pestis* in mice lacking CCL2 (MCP-1).

A

Day 0		Day 3 p.i.
Infect the C57 BL/6 mice and CCL2-/- mice IV with 400 CFU/mouse *ΔyopM-1* mutant KIM5-3002 or KIM5	→	Kill the mice humanely and harvest the spleens and livers for flow cytometric analysis and plating for CFU

B
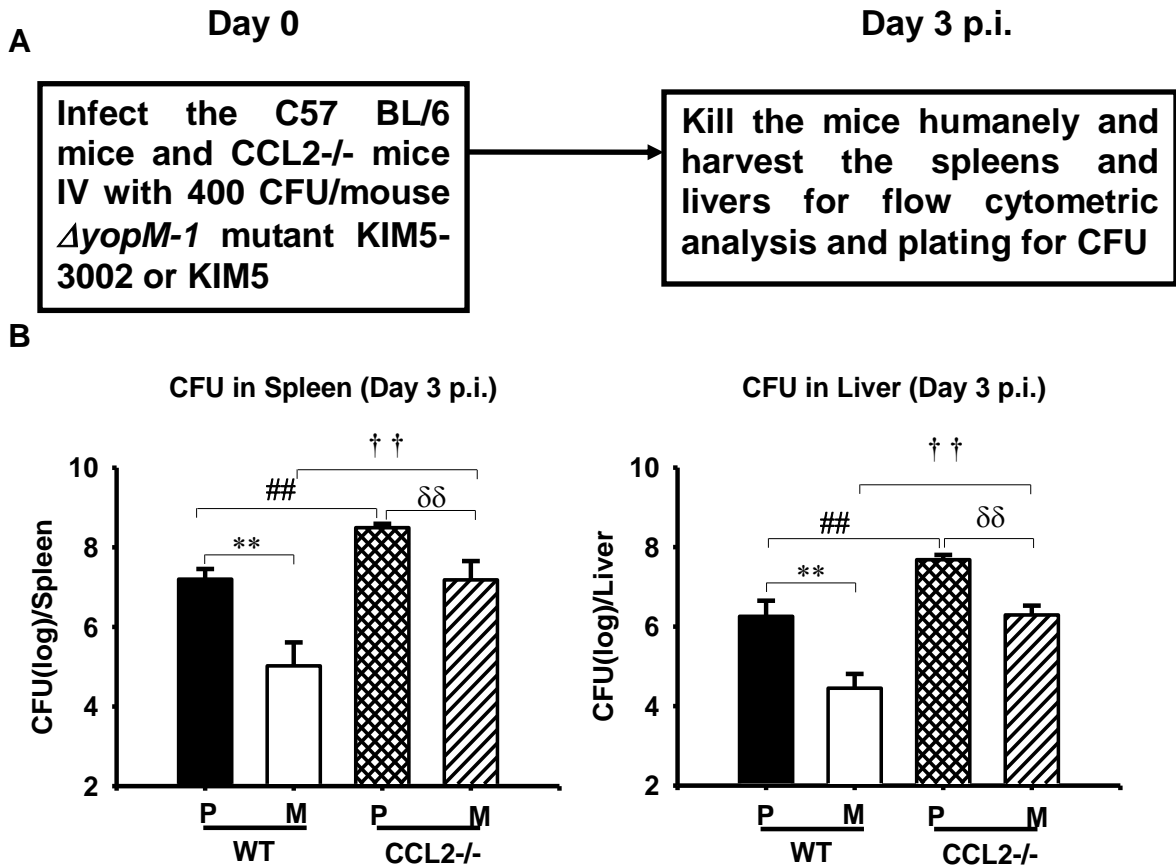
WT and CCL2-/- C57BL/6 mice were infected and analyzed for bacterial burdens on d 3 p.i.. Filled bars, WT mice infected with parent *Y. pestis* KIM5 (P-WT); open bars, WT mice infected with the *ΔyopM-1* mutant KIM5-3002 (M-WT); cross-hatched bars, CCL2-/- mice infected with the parent strain KIM5 (P-CCL2-/-); diagonally-hatched bars, CCL2$^{-/-}$ mice infected with the *ΔyopM-1* strain KIM5-3002 (M-CCL2-/-). Each datum point represents the average of values from 9 mice. The error bars indicate the standard deviations. To compare WT and CCL2-/- groups for mice infected with *Y. pestis* KIM5-3002, †, $P < 0.05$; ††, $P < 0.01$; for mice infected with strain KIM5, #, $P < 0.05$; ##, $P < 0.01$. In comparisons between groups of mice infected with *Y. pestis* KIM5 and KIM5-3002, *, $P < 0.05$; **, $P < 0.01$ for WT mice; δ, $P < 0.05$; δδ, $P < 0.01$ for CCL2-/- mice.

Figure 8.8 TipDC markers on inflammatory DCs preferentially recruited to spleens infected with YopM- *Y. pestis* KIM5-3002.
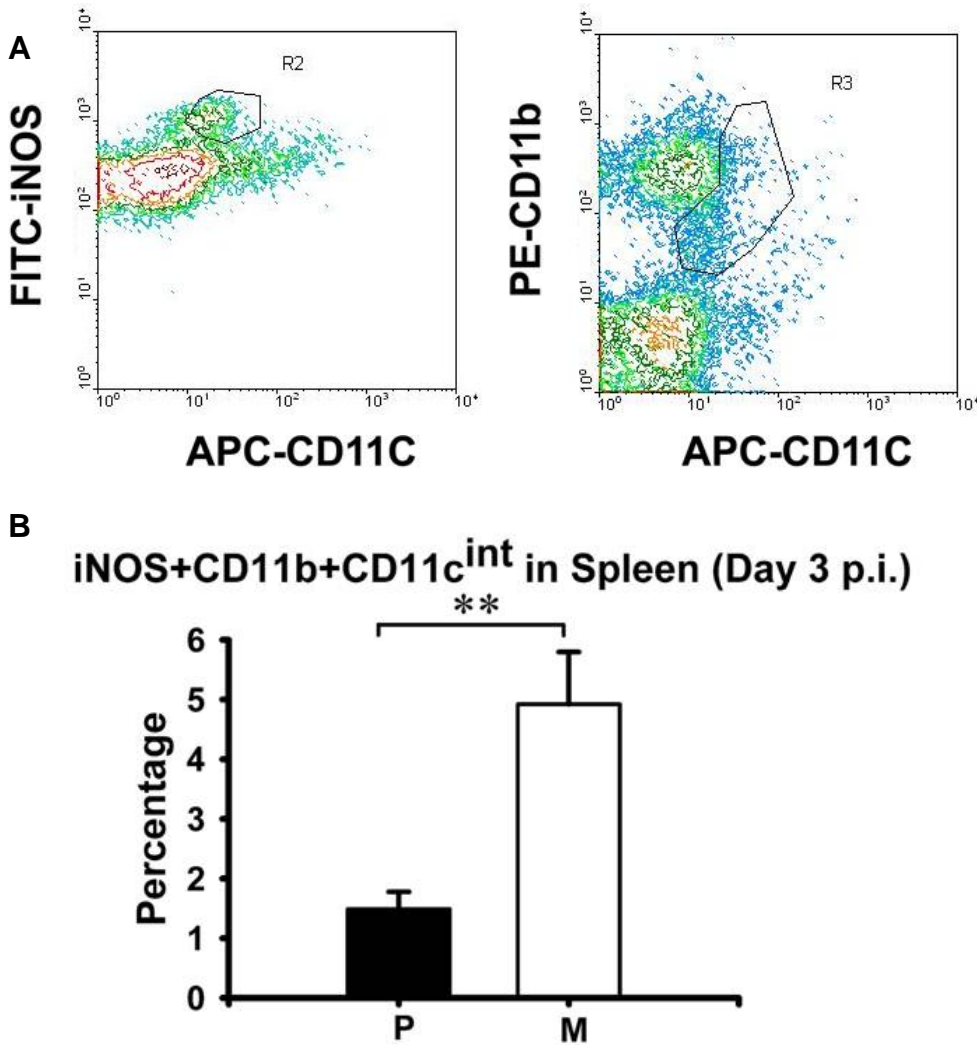
C57BL/6 mice were infected as in Figure 21A and analyzed for inflammatory leukocyte populations in spleens d 3 p.i.. Panel A, left, flow cytometric scatter plots defining a population of iNOS$^+$ CD11c^{int} cells recruited to spleen of a mouse infected by Δ*yopM-1* YopM- *Y. pestis* (demarcated by the surround). The right panel illustrates where those cells mapped in an analysis of that sample for CD11b$^+$ cells. Panel B compares the relative numbers of iNOS$^+$CD11b$^+$CD11c^{int} cells in spleens of mice infected with parent strain KIM5 (P, filled bars) and Δ*yopM-1* strain KIM5-3002 (M, open bars) *Y. pestis*.

Each datum point represents the average of values from 6 mice. The error bars indicate the standard deviations. Significant differences by the unpaired Student's *t* test comparing data from mice infected with the parent and mutant strains are indicated (*, $P < 0.05$; **, $P < 0.01$).

Figure 8.9 iNOS-producing CD11c^{int}CD11b$^+$ iDCs preferentially recruited to spleens infected with $\Delta yopM$-1 *Y. pestis* KIM5-3002.

A
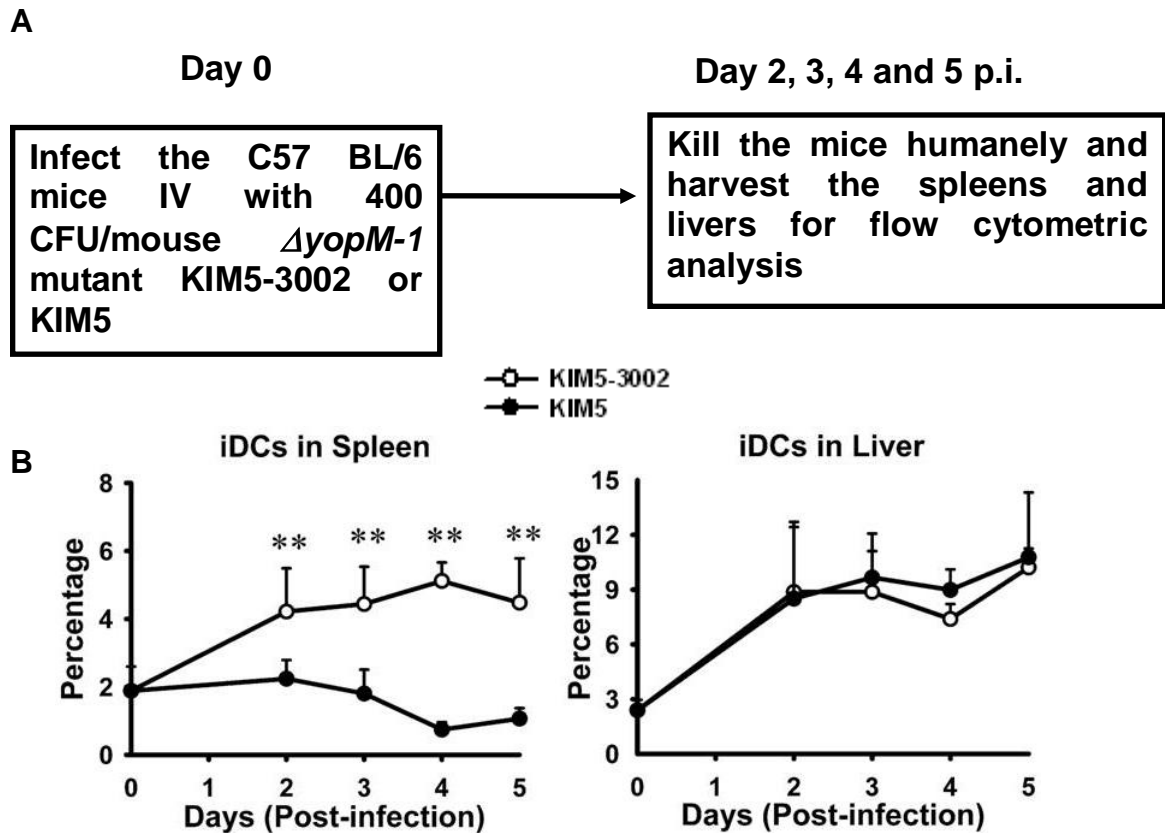
C57BL/6 mice were infected as described in Panel A and analyzed for inflammatory leukocyte populations in livers and spleens. Timecourses of changes in populations of iDCs in spleens and livers during infection with parent (KIM5, filled circles) and $\Delta yopM$-1 mutant *Y. pestis* (KIM5-3002, open circles). PMNs (Ly6G$^+$ cells) were gated out, and the remaining live cells were evaluated for presence of iDCs (CD11b$^+$ CD11c$^{low\text{-}int}$). The point at time 0 indicates the value for uninfected mice. Each datum point represents the average of values from 20 mice. The error bars indicate the standard deviations. Significant differences by the unpaired Student's *t* test comparing data from mice infected with the parent and mutant strains are indicated (*, $P < 0.05$; **, $P < 0.01$).

Figure 8.10 CCR2-dependence of iDC recruitment.

A

Day 0

Day 3 p.i.

| Infect the C57 BL/6 mice and CCR2-/- mice IV with 400 CFU/mouse *ΔyopM-1* mutant KIM5-3002 or KIM5 | → | Kill the mice humanely and harvest the spleens and livers for flow cytometric analysis |

B

iDCs in Spleen (Day 3 p.i.)

iDCs in Liver (Day 3 p.i.)
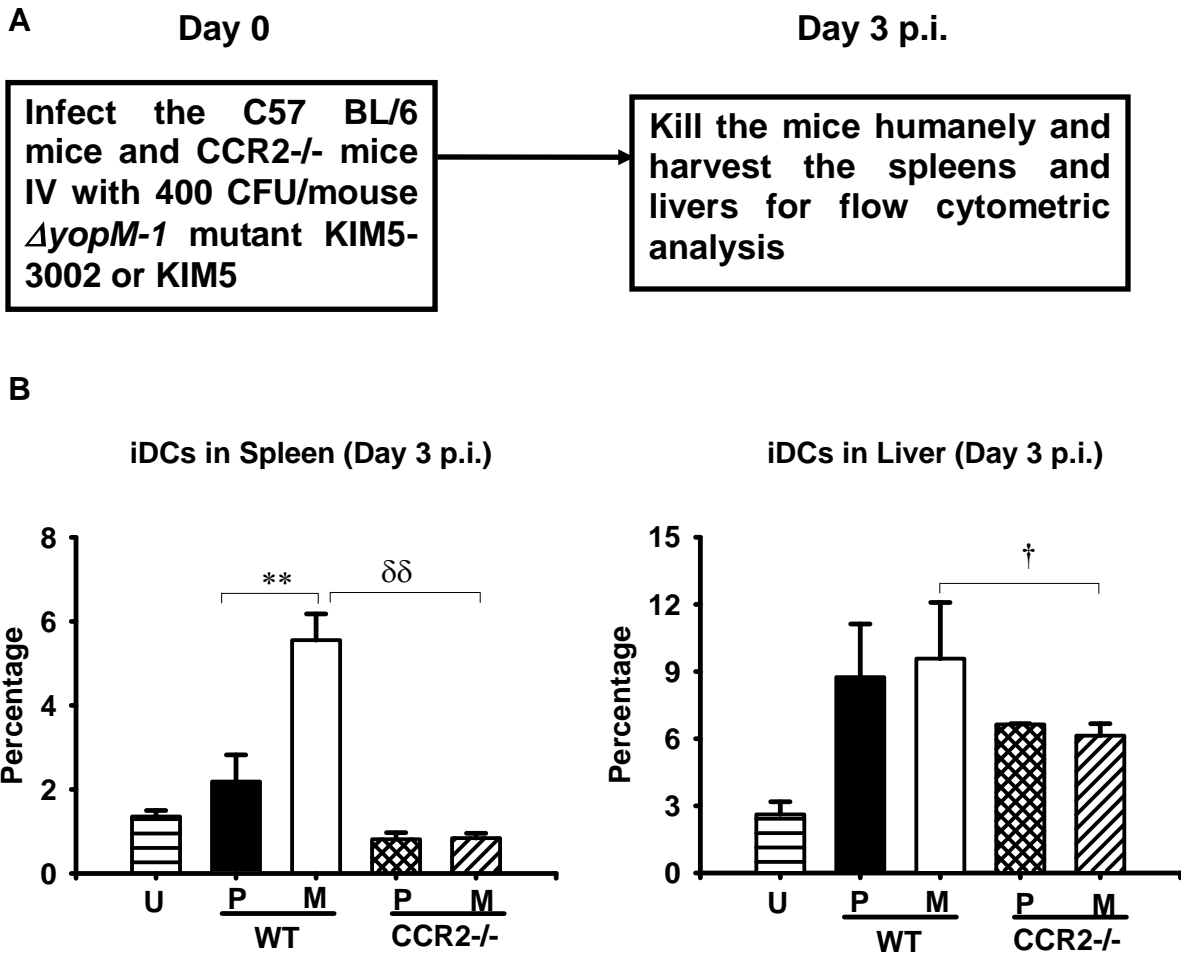
WT and CCR2-/- C57BL/6 mice were infected with parent and Δ*yopM-1 Y. pestis* and

analyzed for iDCs in spleens and livers on d 3 p.i.. Horizontally striped bars, uninfected

mice (U). Filled bars, WT mice infected with parent *Y. pestis* KIM5 (P/WT); open bars,

WT mice infected with the Δ*yopM-1* mutant KIM5-3002 (M/WT); cross-hatched bars,

CCR2-/- mice infected with the parent strain KIM5 (P/CCR2$^{-/-}$); diagonally-hatched bars,

CCR2-/- mice infected with the Δ*yopM-1* strain KIM5-3002 (M/CCR2-/-). Each datum

point represents the average of values from 19 mice. The error bars indicate the standard

deviations. To compare WT and CCR2-/- groups for mice infected with *Y. pestis* KIM5-

3002, †, P < 0.05; ††, P < 0.01; for mice infected with *Y. pestis* KIM5, #, P < 0.05; ##, P <

0.01. In comparisons between groups of mice infected with *Y. pestis* KIM5 and KIM5-3002, *, $P < 0.05$; **, $P < 0.01$ for WT mice; δ, $P < 0.05$;, δδ, $P < 0.01$ for CCR2-/- mice, if there was any.

Figure 8.11 Lack of dependence on PMNs of iDC recruitment.
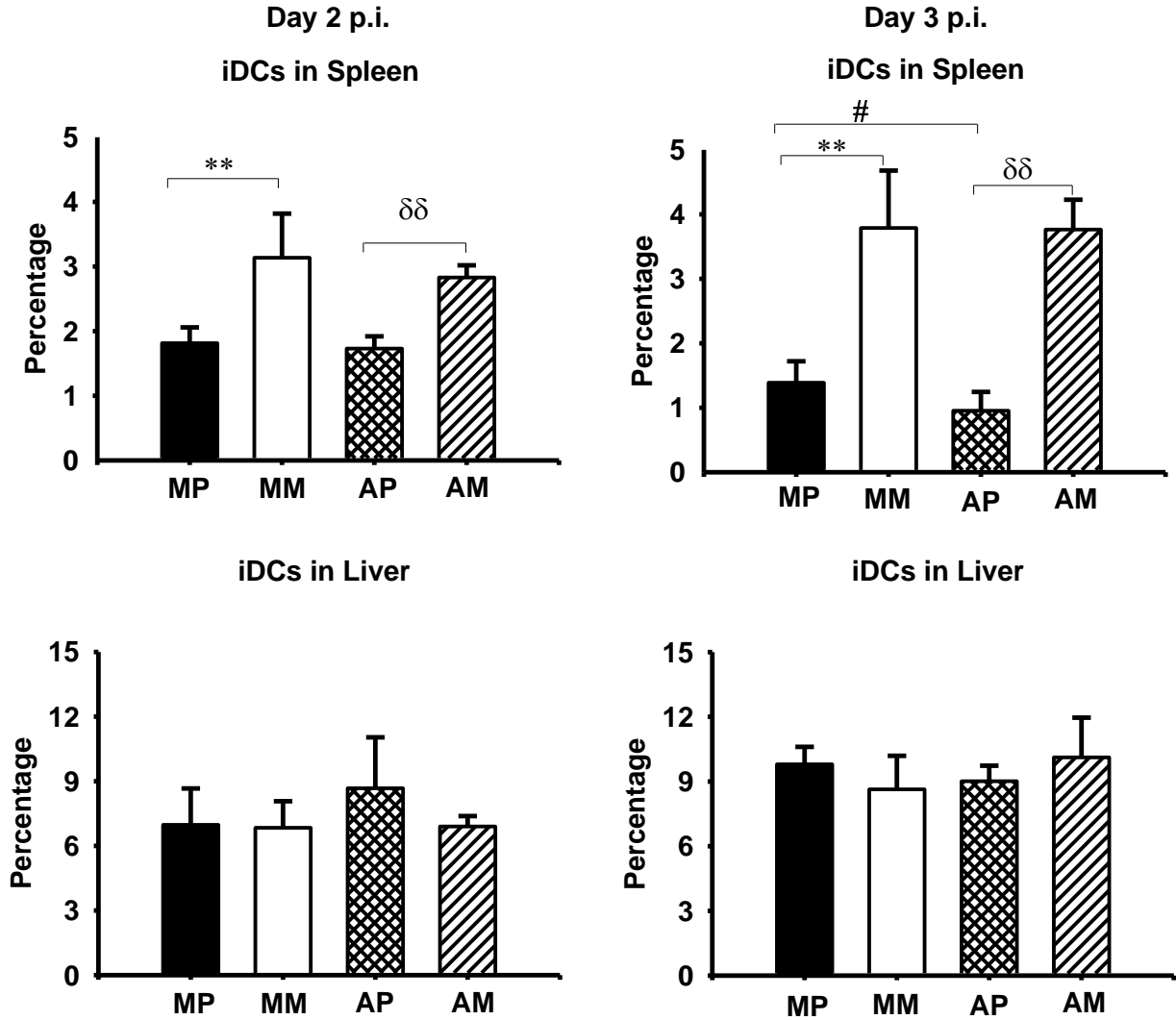
C57BL/6 mice treated with anti-Ly6G antibody to ablate PMNs or mock-treated with nonspecific rat IgG were infected and analyzed as in Figure 7.5A for populations of iDCs in spleens and livers on days 2 and 3 p.i.. Filled bars, mock-treated mice infected with parent *Y. pestis* KIM5 (MP); open bars, mock-treated mice infected with the Δ*yopM-1* mutant KIM5-3002 (MM); cross-hatched bars, PMN-ablated mice infected with the parent strain KIM5 (AP); diagonally-hatched bars, PMN-ablated mice infected with the Δ*yopM-1* strain KIM5-3002 (AM). Each datum point represents the average of values

from 6 mice. The error bars indicate the standard deviations. To compare PMN-ablated and mock ablation groups for mice infected with *Y. pestis* KIM5-3002, †, $P < 0.05$; ††, $P < 0.01$; for mice infected with *Y. pestis* KIM5, #, $P < 0.05$; ##, $P < 0.01$. In comparisons between groups of mice infected with strains KIM5 and KIM5-3002, *, $P < 0.05$; **, $P < 0.01$ for mock-treated mice; δ, $P < 0.05$;, δδ, $P < 0.01$ for PMN-ablated mice.

Figure 8.12 Trans complementation of the *ΔyopM-1* mutant in spleen but not in liver.

A
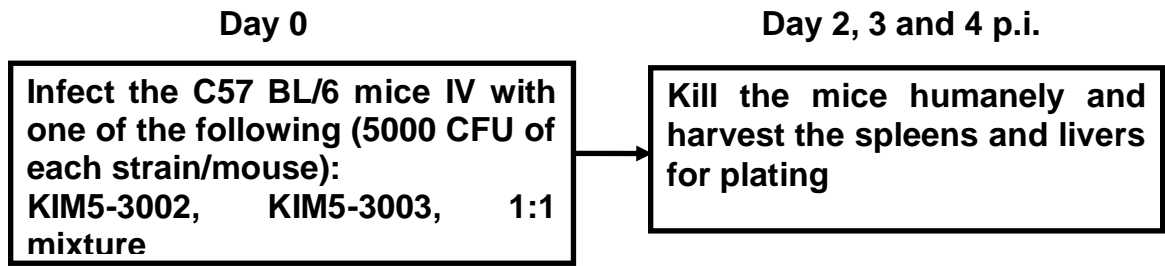
B
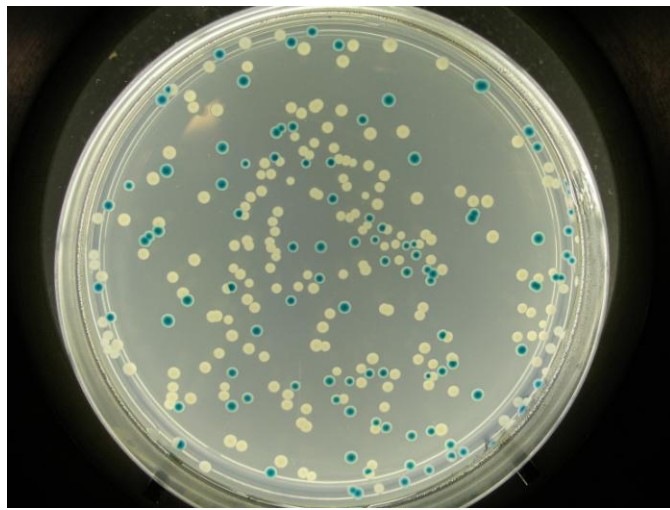
C
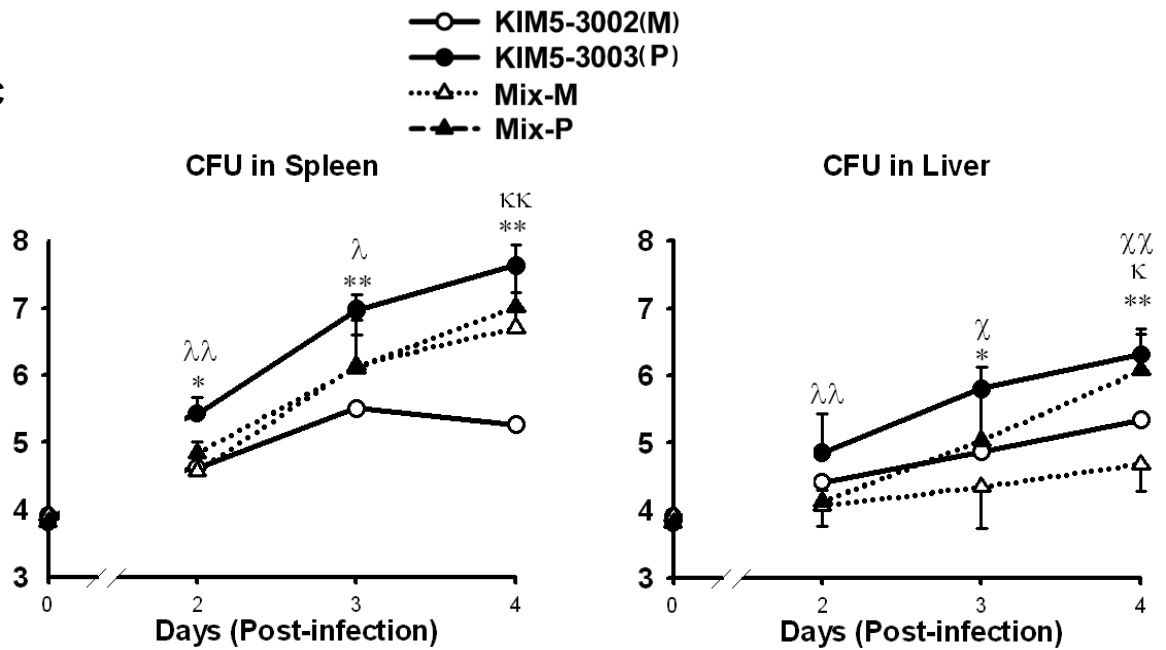
C57BL/6 mice were infected IV with 5 x 10^3 Δ*lacZ Y. pestis* KIM5-3003 (parent strain with intact *yopM* gene) and *ΔyopM-1* mutant *Y. pestis* KIM5-3002 separately or as a 1:1 mixture (Panel A, experimental design) and analyzed for CFU in spleen and liver on days 2, 3 and 4 p.i.. Panel B, photo of representative plate of 1:1 mixture. White colonies, Δ*lacZ* strain KIM5-3003; blue colonies, *ΔyopM-1* strain KIM5-3002. Panel C, CFUs in spleens and livers. Filled circles and solid lines, mice infected with the parent strain Δ*lacZ* KIM5-3003 (P); open circles and solid lines, mice infected with the *ΔyopM-1* strain KIM5-3002 (M); filled triangles and dotted line, parent strain KIM5-3003 CFU from mice infected with the mixture (Mix-P); open triangles and dashed lines, *ΔyopM-1* mutant CFU from mice infected with the mixture (Mix-M). The points at time 0 represent the doses given to the mice. Each datum point represents the average of values from 8 mice. To compare mice infected with Mix-P and P, λ, $P < 0.05$; λλ, $P < 0.01$; for mice infected with Mix-M and M, κ, $P < 0.05$; κκ, $P < 0.01$. In comparisons between mice infected with M and P, *, $P < 0.05$; **, $P < 0.01$; between mice infected with Mix-M and Mix-P; χ, $P < 0.05$;, χχ, $P < 0.01$.

RESULTS

Chapter Nine: the growth limitation of *ΔyopM-1* strain and YopM-mediated modulation in host defense were maintained in the infection with pre-induced *Y. pestis*, although the loss of YopM were compensated in spleen at early stage of infection by a pre-induction stimulated virulence mechanism

In most of the experiments described so far, we used *Y. pestis* cultured at 26°C to infect the mice. This is an appropriate choice for the bubonic plague model because *Y. pestis* in natural bubonic plague grows at ambient temperature in the flea gut.

The systemic plague model affords the use of a wide range of well-developed techniques for obtaining and characterizing the host response in reticuloendothelial organs after infection, and we used 26°C-grown *Yersinia pestis* in this model to develop a hypothesis for the innate defense that might also operate in skin to selectively control growth of *ΔyopM-1 Y. pestis* in bubonic plague.

However, natural systemic plague occurs usually secondarily to bubonic plague, which means the bacteria infecting liver and spleen have adapted to the internal environment in the mammalian host. At 37°C, the body temperature of the mammalian host, the T3SS of *Y. pestis* is present on the bacterial surface and Yops are present in the bacterial cytoplasm so that the Yops can be delivered into the host cells immediately upon contact.

It takes ca. 3-5 h at 37°C for ambient temperature-grown *Y. pestis* to become phagocytosis-resistant (63), which is equated with synthesis and assembly of the T3SS and Yops because this happens prior to the presence of adequate amounts of F1 fibrils,

which can block phagocytosis (which takes 5 h at 37°C in an macrophage infection model) (89). Therefore, we thought that 26°C-grown *Y. pestis* will require 3 h within the mammal before it can deliver Yops into host cells, and this may be enough time for the bacteria to be engulfed by resident macrophages (and grow) and by early responding PMNs (and be killed). We wanted to compare findings from a more realistic systemic plague model using 26/37°C-grown bacteria to those described so far. The 26/37°C *Y. pestis* would be able to deliver Yops and would not be coated with F1, which makes interactions with cells less efficient. The prediction was that these bacteria would slow Yops-dependent effect in infection because they would by pass the initial round of intracellular growth. We hoped that we might even be able to identify YopM-related effects much earlier in infection than previously possible and characterize YopM's initial, direct effects.

A. Three hours pre-induction postponed the appearance of the *ΔyopM-1* mutant phenotype from day 2 p.i. to day 3 p.i.

As shown in Figure 3.2B, when mice were infected with a low dose (400 CFU/mouse) of bacteria, the viable number of bacteria recovered from mice infected with the parent strain was significantly higher than that from mice infected with the *ΔyopM-1 Y. pestis* by d 2 p.i.. To test whether this pattern began earlier with the pre-induced bacteria, mice were infected with 400 CFU/mouse of parent or *ΔyopM-1* mutant strains with pre-induction or not. Spleens and livers were harvested on d 2 and d 3 p.i. for bacterial load measurement and flow cytometric analysis (Figure 9.1A). Although the growth limitation of *ΔyopM-1 Y. pestis* still existed when these bacteria had been pre-induced, a significant

difference between parent and mutant strains in bacterial burden of spleen appeared one day later than in the infection with non-induced bacteria, from d 2 p.i. to d 3 p.i. (Figure 9.1B, upper panels). However, the growth dynamic of both strains in liver was not affected by the pre-induction (Figure 9.1B, bottom panels).

B. The YopM-associated MDM and iDC influx was delayed in 26/37 _Y. pestis_ infected spleen

In chapter 8G, iDCs, one of the major subsets of MDMs, were found to be the key cell type to control the the growth of the _ΔyopM-1 Y. pestis_ in spleen. Therefore, we hypothesized that the virulence property of _Y. pestis_ induced by pre-induction may compensate for the loss of YopM in the _ΔyopM-1 Y. pestis_ at the early stage of infection by delaying the recruitment of iDCs into spleen.

To test this hypothesis, the leukocytes from experiments in Figure 9.1A were also studied by flow cytometry. We predicted that the recruitment of iDCs and MDMs into spleen by the _ΔyopM-1_ mutant would be delayed in the mice infected with the pre-induced _Y. pestis_. Indeed, we found the influx of MDMs and iDCs into the spleen of mice infected with pre-induced or non-induced _ΔyopM-1 Y. pestis_ exhibited a pattern that paralleled the ability of the host to control the bacterial growth (Figure 9.1C and D). As shown in the bottom panels of Figure 9.1C, pre-induction may help to recruit more MDMs into liver. However, this effect was so small that it is hardly worth mentioning, and YopM still had no effect on the recruitment of these cells into liver, whether or not the infecting bacteria had undergone pre-induction.

The influx of PMNs into spleens and livers was also studied in these experiments because PMNs were shown to be the major cells controlling *ΔyopM-1 Y. pestis* in liver. Here the data showed that the influx of PMNs into both organs was independent of YopM and pre-induction of the infecting bacteria did not change this pattern (Figure 9.1E). These findings are consistent with the results obtained so far that YopM does not influence the recruitment of PMNs.

C. LD$_{50}$ of 26/37°C *ΔyopM-1 Y. pestis* was lower than that of 26C *ΔyopM-1* mutant

Since pre-induction of the infecting bacteria delayed the appearance of the growth limitation on *ΔyopM-1 Y. pestis* and of the influx of MDMs and iDCs into spleen, it could affect the virulence of this strain in the systemic plague model, which can be measured by lethality (LD$_{50}$). As described previously, serial dilutions of pre-induced *ΔyopM-1* mutant *Y. pestis* were injected IV into C57BL/6 mice and those mice were observed closely for 2 weeks. The actual doses were determined by plating dilutions of the infecting suspensions and the death of mice was recorded. Through the software Biostat, we derived the LD$_{50}$ of the pre-induced *ΔyopM-1* mutant (26ºC, table 3.1). Compared to the known LD$_{50}$ of the non-induced *ΔyopM-1* mutant strain (26/37ºC, table 3.1), we found that pre-induction decreased the LD$_{50}$ of the *ΔyopM-1* mutant by 4 fold. These values indicate that although pre-induction does compensate for the growth defect of the *ΔyopM-1* mutant at the early stage of infection, the effect of this process on the lethality of this bacterium in mice is very limited.

D. Pre-induction did not change the effect of anti-Ly6G treatment on the growth of the *ΔyopM-1* mutant and parent strain in spleen and liver

In chapter 7, we concluded that PMNs were essential for controlling the *ΔyopM-1* mutant in liver, but not in spleen, if the infecting bacteria were cultured at ambient temperature. However, it was possible that PMNs had an indirect effect, such as mediating the recruitment of bactericidal monocytes (305), in controlling the *ΔyopM-1 Y. pestis* in spleen but this effect failed to be detected due to the YopM's early and strong effect on the influx of MDMs and iDCs.

In the infection by ambient-temperature-grown bacteria, the YopM-associated difference in iDC influx appeared on d 2 p.i.. However, this difference was delayed for at least one day when the infecting bacteria received 3 h pre-induction. Therefore, if there was any indirect effect of PMNs in controlling the *ΔyopM-1 Y. pestis*, it may appear in the infection by pre-induced bacteria. To test this hypothesis, we ablated PMNs from the mice infected with the pre-induced *Y. pestis*.

The experimental design (Figure 9.2A) was the same as described in Figure 7.5A except that the infecting bacteria were pre-induced. As shown in Figure 9.2B, anti-Ly6G treatment maintained Ly6G$^+$CD11b$^+$ PMNs at very low levels on d 2 and 3 p.i.. Similarly to the CFU data on spleen for non-ablated mice (Figure 9.1B), the appearance of the growth defect of the *ΔyopM-1* mutant in spleen was postponed to d 3 p.i. by pre-induction, and anti-Ly6G treatment did not change this pattern, although both of the strains grew better in PMN-ablated mice on d 2 p.i. than in mock-treated mice (Figure 9.2C, upper panels). However, PMN ablation favored the growth in liver of both of the strains, especially the *ΔyopM-1* mutant, and eventually relieved the growth limitation on the

175

ΔyopM-1 mutant on d 3 p.i.. These results further supported the conclusion that PMNs are not the major immune cells that control the *ΔyopM-1* mutant in spleen, even if the infecting bacteria are able to inject YopM into the host cells when they first contact those cells.

E. When infected with pre-induced *Y. pestis*, CCR2 KO still prevented the influx of MDMs into spleen and liver and specifically favored the growth of the *ΔyopM-1* mutant in spleen but both strains in liver

The *ΔyopM-1* mutant strain had been shown to grow uncontrolled in the spleen of CCR2^{-/-} mice (Figure 8.5D), correlating with the defective recruitment of MDMs to spleen (Figure 8.5B). However, the above data were gained from mice infected with non-induced bacteria. Pre-induction of infecting bacteria stimulated some *Y. pestis* virulence property to selectively favor the growth of *ΔyopM-1* mutant in spleen (Figure 9.1B), accompanied with a delayed influx of CCR2^{+} iDCs into spleen (Figure 9.1D). Therefore, the infection of CCR2^{-/-} mice with pre-induced bacteria was studied to see whether the uncontrolled growth of the *ΔyopM-1* mutant in spleen and liver, which occurred on d 3 p.i. in the infection of non-induced bacteria, could be reproduced.

As described in Figure 9.3A, CCR2^{-/-} mice and C57BL/6 mice were IV-infected with pre-induced parent strain and *ΔyopM-1* mutant *Y. pestis*. On d 3 p.i., spleens and livers were harvested to study leukocytes and bacterial burden. The influx of Ly6G^{-}CD11b^{+} MDMs into both spleen and liver was inhibited in CCR2 KO mice. This was especially striking in the *ΔyopM-1* mutant-infected spleen where this effect abolished the significant difference between two strains in CCR2^{-/-} mice (Figure 9.3B). The correlation between

compromised recruitment of MDMs and the uncontrolled growth of the *ΔyopM-1* mutant in spleen (Figure 9.3D) is similar to that in the infection with non-induced bacteria (Figure 8.5 B and D). Therefore, the role of CCR2⁺ MDMs in clearance of *ΔyopM-1* mutant is independent from the pre-induction of the infecting bacteria.

Similar to the infection with non-induced bacteria (Figure 8.5), the impact of the CCR2 KO on the MDM influx into liver was also not YopM-associated in the infection with pre-induced *Y. pestis* (Figure 9.3 B, right panel). The growth limitation of the *ΔyopM-1* mutant was kept in CCR2$^{-/-}$ mice whether the infecting bacteria were pre-induced or not (Figure 9.3D and Figure 8.5D, right panels). However, only the growth of the *ΔyopM-1* mutant was enhanced significantly by the CCR2 KO in the infection with ambient-temperature-grown bacteria (Figure 8.5D, right panel), whereas both of the parent and mutant strains grew uncontrolled when the infecting bacteria received 3 h pre-induction (Figure 9.3D, right panel), indicating that some property of Y. pestis induced by pre-induction favored their growth in a YopM-independent manner in the absence of CCR2 signaling pathway.

The only YopM-associated difference in PMN influx appeared in the spleen of CCR2$^{-/-}$ mice; however, the growth limitation of the *ΔyopM-1* mutant was relieved in those spleens. This result is consistent with our data from the PMN ablation experiments and helped to exclude PMNs from the major cells controlling the *ΔyopM-1* mutant in spleen.

Overall, these findings with pre-induced *Y. pestis* agreed qualitatively with those obtained with 26°C-grown bacteria. However, this infection model failed to provide the hoped-for insight on earlier times in infection. Apparently, a property that compensated for loss of YopM before d 3 of infection was induced in expression in addition to the

T3SS and Yops. This property influenced the infection dynamics most strongly in spleen, where it caused a delay in influx of MDMs and a corresponding delay in control over the growth of the *ΔyopM-1* mutant.

Figure 9.1 Effect of 3 hour pre-indcution on infection dynamics for of *ΔyopM-1* and parent *Y. pestis* KIM5.

A

3 hours before infection	Time 0	D 2 and 3 p.i.
pre-induced *ΔyopM-1* mutant KIM5-3002 and KIM5: transfer the culture from 26°C to 37°C	Infect the C57BL/6 mice IV with pre-induced *ΔyopM-1* mutant KIM5-3002 or KIM5 (400 CFU/mouse)	Kill the mice humanely and harvest spleens and livers for plating and flow cytometric analysis
Non-induced *ΔyopM-1* mutant KIM5-3002 and KIM5: keep growing at 26°C	Infect the C57BL/6 mice IV with non-induced *ΔyopM-1* mutant KIM5-3002 or KIM5 (400 CFU/mouse)	Kill the mice humanely and harvest spleens and livers for plating and flow cytometric analysis

B

C Day 2 p.i. Ly6G-CD11b+ MDMs Day 3 p.i. Ly6G-CD11b+ MDMs

D CD11b+CD11c^int iDCs CD11b+CD11c^int iDCs

180

E

Day 2 p.i.   Day 3 p.i.

Ly6G+CD11b+ PMNs   **Ly6G+CD11b+ PMNs**

Mice were infected with pre-induced or non-induced $\Delta yopM$-1 (KIM5-3002) and parent $Y.$
$pestis$ (KIM5), and analyzed for bacterial burdens and inflammatory leukocyte
populations in livers and spleens on days 2 and 3 p.i.. Panel A, experimental design.
Panel B, CFU. Each datum point represents the average of values from 25 mice. Panels C,
D and E, Ly6G$^-$CD11b$^+$ MDMs, CD11b$^+$CD11c^{int} iDCs and Ly6G$^+$CD11b$^+$ PMNs
expressed as percent of total live leukocytes from spleen and liver, respectively. Each
datum point represents the average of values from 8 mice (pooled from two experiments).
The error bars indicate the standard deviations. Filled bars, mice infected with parent $Y.$

pestis KIM5 (P); open bars, mice infected with the Δ*yopM-1* mutant KIM5-3002 (M). 26C and 26/37 in the horizontal axis indicate the growth conditions of the infecting bacteria, non-induced and pre-induced, respectively. To compare mice infected with non-induced and pre-induced Δ*yopM-1Y. pestis* KIM5-3002, θ, $P < 0.05$; θθ, $P < 0.01$; for mice infected with non-induced and pre-induced parent strain KIM5, ω, $P < 0.05$; ωω, $P < 0.01$. In comparisons between groups of mice infected with *Y. pestis* KIM5 and KIM5-3002, *, $P < 0.05$; **, $P < 0.01$.

Figure 9.2 Pre-induction of the infecting bacteria does not change the effect of PMN ablation on the infection dynamics for *Y. pestis*.
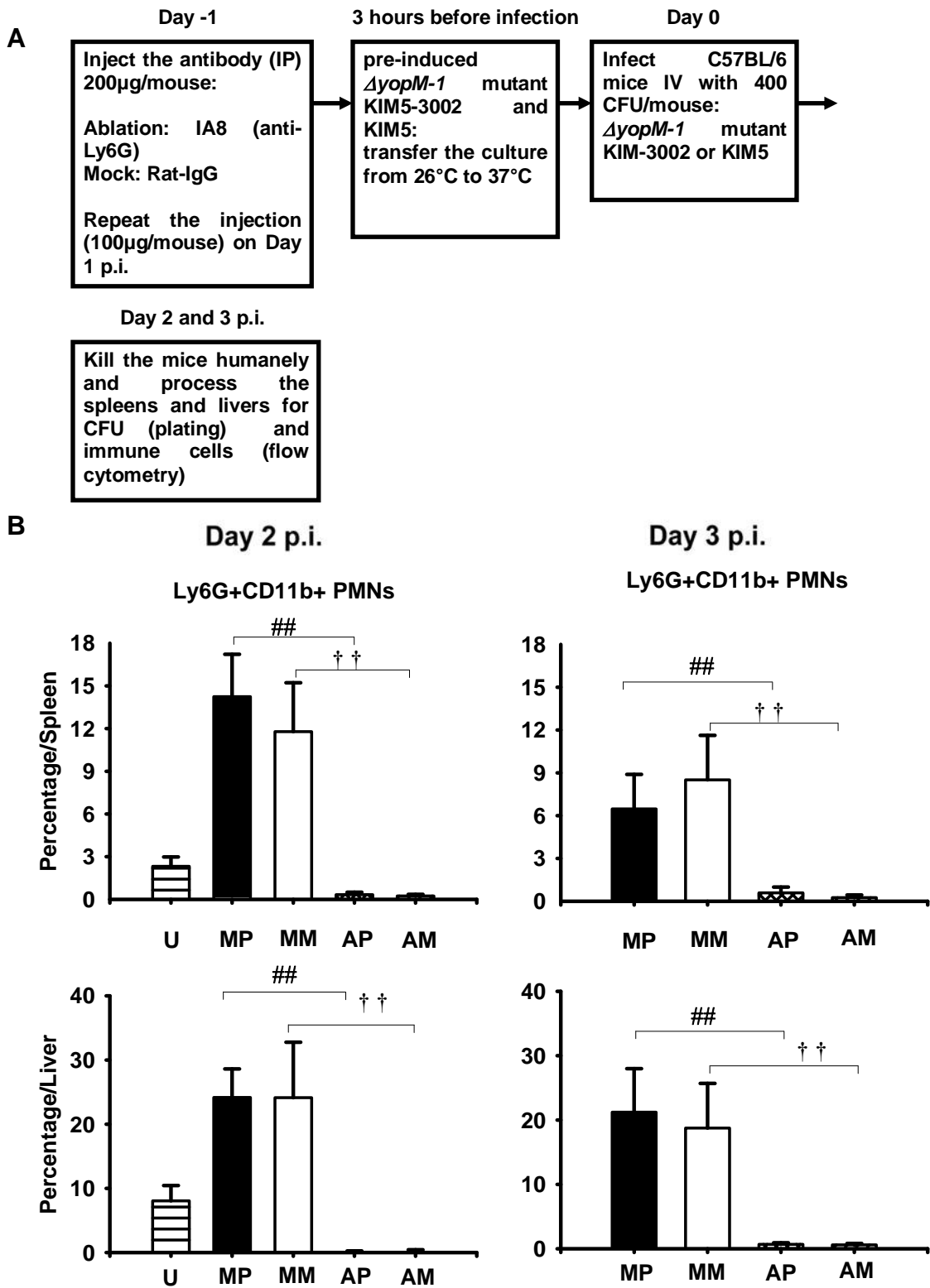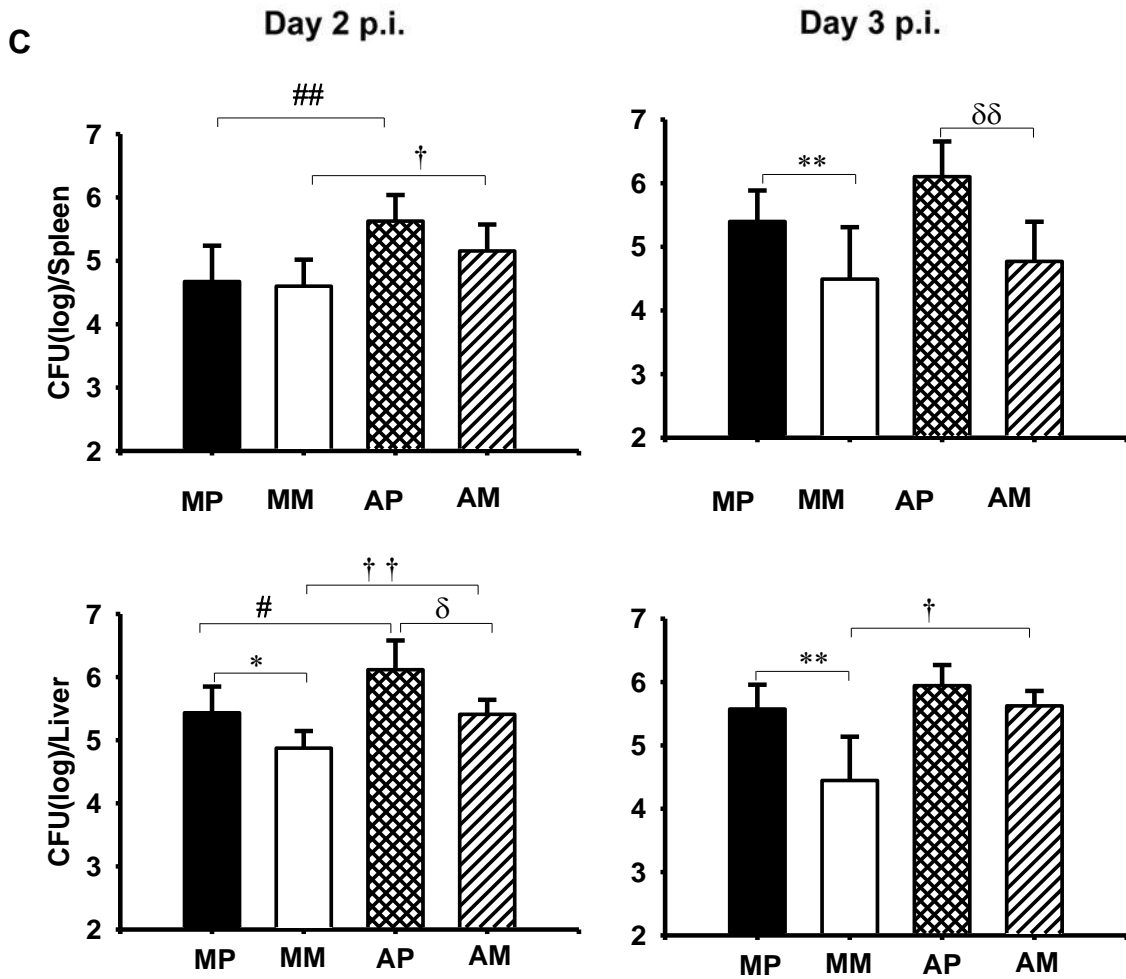
C

Day 2 p.i.

Day 3 p.i.

Mice treated with anti-Ly6G antibody to ablate PMNs or mock-treated with nonspecific rat IgG were infected with pre-induced *Y. pestis* and analyzed for bacterial burdens and inflammatory leukocyte populations in livers and spleens on days 2 and 3 post-infection (p.i.). Horizontal-hatched bars, uninfected mice (U); filled bars, mock-treated mice infected with the parent *Y. pestis* KIM5 (MP); open bars, mock-treated mice infected with the Δ*yopM-1* mutant KIM5-3002 (MM); cross-hatched bars, PMN-ablated mice infected with the parent *Y. pestis* KIM5 (AP); diagonally-hatched bars, PMN-ablated mice infected with the Δ*yopM-1* strain KIM5-3002 (AM). Panel A, experimental design. Panel B, Ly6G$^+$CD11b$^+$ PMNs expressed as percent of total live leukocytes from spleen and liver. Panel C, CFU. Each datum point represents the average of values from 6 mice. The

error bars indicate the standard deviations. To compare PMN-ablated and mock ablation groups for mice infected with the $\Delta yopM$-1 strain KIM5-3002, †, $P < 0.05$; ††, $P < 0.01$; for mice infected with the parent strain KIM5, #, $P < 0.05$; ##, $P < 0.01$. In comparisons between groups of mice infected with *Y. pestis* KIM5 and KIM5-3002, *, $P < 0.05$; **, $P < 0.01$ for mock-treated mice; δ, $P < 0.05$; δδ, $P < 0.01$ for PMN-ablated mice.

Figure 9.3 Pre-induction of the infecting bacteria changed infection dynamics for *Y. pestis* in the liver but not in the spleen of CCR2^{-/-} mice.
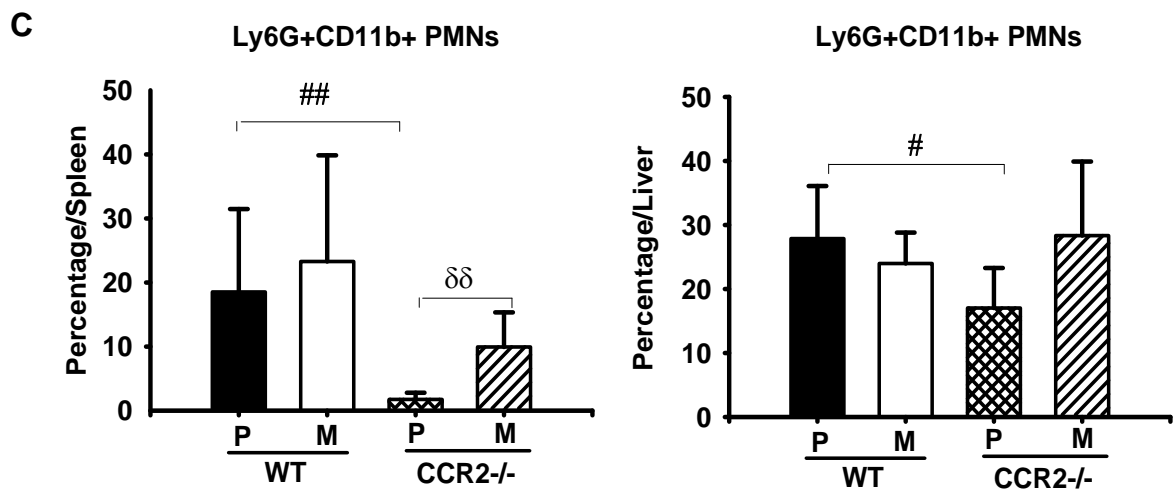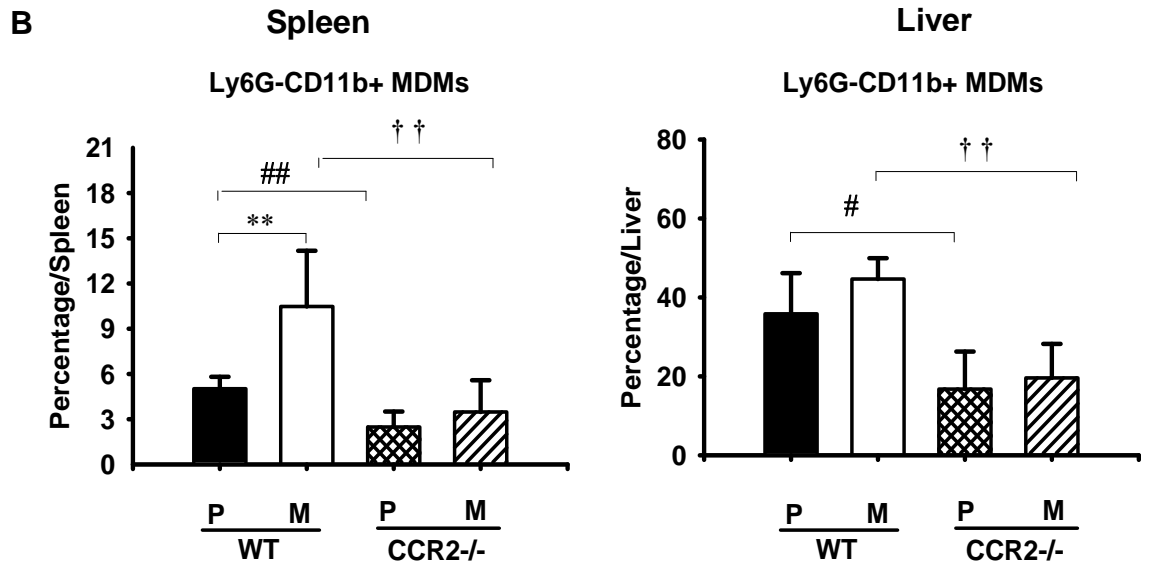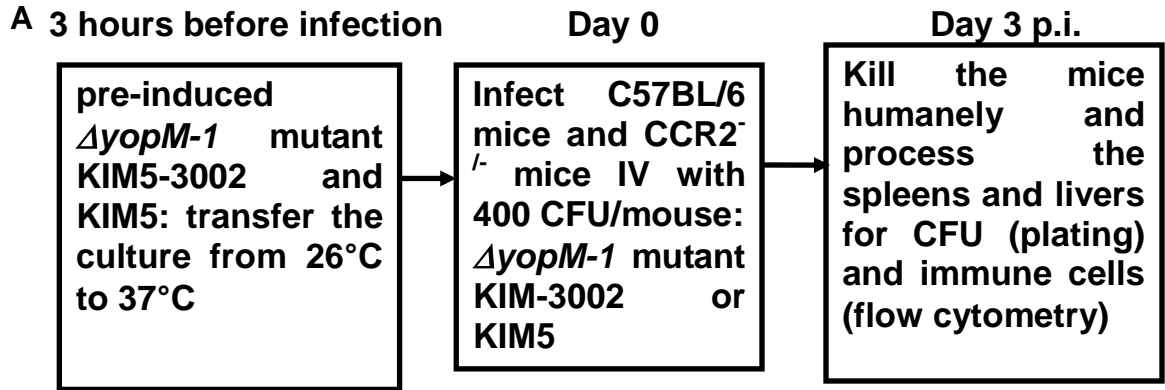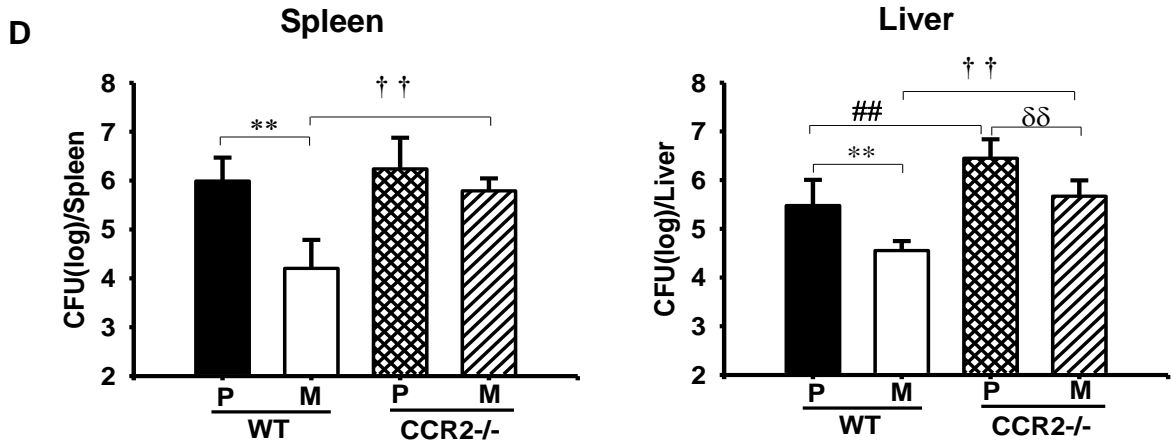
A

3 hours before infection	Day 0	Day 3 p.i.
pre-induced *ΔyopM-1* mutant KIM5-3002 and KIM5: transfer the culture from 26°C to 37°C	Infect C57BL/6 mice and CCR2^{-/-} mice IV with 400 CFU/mouse: *ΔyopM-1* mutant KIM-3002 or KIM5	Kill the mice humanely and process the spleens and livers for CFU (plating) and immune cells (flow cytometry)

B

Spleen — Ly6G-CD11b+ MDMs; Liver — Ly6G-CD11b+ MDMs

C

Ly6G+CD11b+ PMNs (Spleen); Ly6G+CD11b+ PMNs (Liver)

D

WT and CCR2$^{-/-}$ C57BL/6 mice were infected with pre-induced *Y. pestis* and analyzed for bacterial burdens and inflammatory leukocyte populations in livers and spleens on d 3 p.i.. Panel A, experimental design. Filled bars, WT mice infected with parent *Y. pestis* KIM5 (P/WT); open bars, WT mice infected with the Δ*yopM-1* mutant KIM5-3002 (M/WT); cross-hatched bars, CCR2$^{-/-}$ mice infected with the parent strain KIM5 (P/CCR2-/-); diagonally-hatched bars, CCR2$^{-/-}$ mice infected with the Δ*yopM-1*strain KIM5-3002 (M/CCR2-/-). Panel B, Ly6G$^-$CD11b$^+$ MDMs and Panel C, PMNs (Ly6G$^+$CD11b$^+$ cells), expressed as percent of total live leukocytes. Panel D, CFU. Each datum point for CCR2$^{-/-}$ and WT represents the average of values from 6 and 12 mice, respectively. The error bars indicate the standard deviations. To compare WT and CCR2$^{-/-}$ mice infected with strain KIM5-3002, †, P < 0.05; ††, P < 0.01; for mice infected with *Y. pestis* KIM5, #, P < 0.05; ##, P < 0.01. In comparisons between groups of mice infected with strains KIM5 and KIM5-3002, *, P < 0.05; **, P < 0.01 for WT mice; δ, P < 0.05; δδ, P < 0.01 for CCR2-/- mice.

Chapter Ten: Discussion

As one of effector Yops, the major virulence factors in *Y. pestis*, YopM is known to be delivered into the nucleus of host cells and presumed to counteract host defenses through regulating gene expression in major cellular components in the immune system. However, this protein has been refractory to *in vitro* attempts to identify a phenotype resulting from its delivery. In contrast, YopM has a strong virulence phenotype *in vivo*, in which parent *Y. pestis* KIM5 and the *ΔyopM-1* mutant KIM5-3002 show distinct dynamics for viable numbers in organs of mice infected systemically. By using the systemic plague model which displays the *in vivo* phenotype of YopM, we studied how YopM modulates the host immune defense by identifying the cells that are critical for imposing a growth limitation selectively on *ΔyopM Y. pestis*. These cells would be direct or indirect *in vivo* targets of YopM produced by the infecting parent strain.

A. Recapitulation of the main findings in this work

Previous *in vivo* studies done in our laboratory excluded the importance of the adaptive immune system in the YopM virulence mechanism and revealed a YopM-associated depletion of NK cells from the spleen and blood accompanied by decreased production of several proinflammatory cytokines (159). However, in the present study the absence of NK cells in mice exerted no influence on growth of either the parent *Y. pestis* or the *ΔyopM* mutant strain, and YopM did not cause NK cells to be depleted in liver. In contrast, ablation of Gr1$^+$ cells significantly relieved the growth defect of the *ΔyopM* mutant in both spleen and liver, and the mutant and parent strains caused similar necrotic

lesions in livers of Gr1-depleted mice. These findings pointed toward Gr1$^+$ cells, which include PMNs and MDMs (macrophages/monocytes/DCs), as the true cellular targets of YopM *in vivo*, instead of NK cells.

However, YopM in the infecting bacteria had no effect on the recruitment of PMNs into organs, or ROS and NO production by splenic or peritoneal PMNs. Further, ablation of PMNs from *Y. pestis*-infected mice relieved the growth limitation of the *ΔyopM* mutant only in liver, instead of both spleen and liver, indicating that YopM modulates the immune responses differently in spleen and liver, and PMNs are the major cell type counteracted by YopM in liver but not in spleen.

In addition to the different effects of YopM on the accumulation of NK cells in spleen and liver, we also found that YopM compromised recruitment of MDMs into the spleen, but not in liver. The greater recruitment of splenic MDMs in mice infected with the *ΔyopM* mutant disappeared when the mice were treated with anti-Gr1 antibody, accompanied by uncontrolled growth of the *ΔyopM* mutant in spleen. Therefore Gr1$^+$ cells (potentially inflammatory monocytes and inflammatory DCs) became promising candidates modulated by YopM to favor bacterial growth in spleen.

Clodronate treatment, which depleted both resident macrophages/DCs as well as circulating monocytes from mice (4, 321), compromised the growth of both parent and mutant strains in the mice, but the growth limitation of the *ΔyopM-1* mutant was maintained. Therefore the clodronate-sensitive resident macrophages/DCs could act as a niche to protect both the parent and mutant strains from the immune attack, whereas the MDMs resistant to clodronate may be responsible for the maintenance of growth limitation of the *ΔyopM-1* mutant.

However, the growth limitation of the *ΔyopM* mutant was relieved in spleen and liver of mice lacking CCR2, the receptor recognizing CCL2/MCP-1 and mediating the recruitment of inflammatory monocytes and TipDCs (151), indicating that $CCR2^+$ $Gr1^+$ inflammatory monocytes and DCs are critical for the control of the *ΔyopM* mutant in spleen. Meanwhile, studies of the distribution of these cells in bone marrow, blood and spleen showed that YopM inhibited their recruitment at the level of infiltration from blood into spleen. Further, the uncontrolled growth of the *ΔyopM* mutant in the liver of $CCR2^{-/-}$ mice could be explained by a compromised function of PMNs because PMNs are also $Gr1^+CCR2^+$ and their differentiation and adherence are enhanced by CCR2 (144, 262). This finding is consistent with the PMN ablation data in liver. In the bubonic plague model, in which YopM is also necessary for the full virulence of *Y. pestis*, absence of CCR2 in mice relieved the growth limitation of the *ΔyopM* mutant in skin at an early stage of infection, indicating that YopM's capacity to disable host defenses in skin is mediated by CCR2.

A model with different innate immune cell types modulated by YopM in spleen and liver was supported further by the outcome of co-infection experiment of the parent and *ΔyopM* mutant strains. The growth defect of the *ΔyopM* mutant was relieved in the spleen, but not in liver, of the mice infected with the mixture of the two strains, because YopM in the parent *Y. pestis* protected both strains in spleen despite inhibiting the influx of iDCs into the whole spleen. In livers, however, the parent strain favored only its own growth by compromising the function of immediately adjacent PMNs.

In most of the experiments in this study, the infecting bacteria were grown at a temperature mimicking that in the flea gut (26ºC). However, when the bacteria received 3

hours of pre-induction at mammalian temperature (37ºC), an unexpected delay in the appearance of the growth defect of the *ΔyopM* mutant strain as well as the attenuated virulence of this mutant were found, accompanied by postponed *ΔyopM*-associated influx of inflammatory monocytes and iDC into spleen. These findings supported further the importance of these cells in the YopM mechanism in spleen, without changing the model for 26ºC grown bacteria, because the effects of PMN ablation and CCR2 KO on the infection of pre-induced bacteria were the same as those of non-induced *Y. pestis*.

In conclusion, CCR2$^+$Gr1$^+$ PMNs and CCR2$^+$Gr1$^+$ inflammatory monocytes/DCs were identified as the major cell types affected by YopM in spleen and liver, respectively, in the systemic plague model. Meanwhile, signals mediated by the chemokine receptor CCR2 are critical in YopM-mediated virulence in both systemic and bubonic plague. Thus, these findings provide a framework for focusing future research to identify the direct molecular targets of YopM.

B. The adaptive immune system is not critical in the YopM virulence mechanism

There is *in vitro* evidence that *Y. pestis* can inhibit T cell activation and induce apoptosis of T cells, probably through YopH, an effector Yop with tyrosine phosphatase activity (6, 52). Meanwhile, *in vivo* studies showed the possible importance of T cells in the defense against *Y. pestis* (239, 247). Serum collected from mice inoculated IP showed protective function against plague in mice (240); and two major immunogenic proteins, F1 antigen and LcrV, were shown to provide a high degree of protection in small animal models (11, 184, 227), which indicates that antibodies secreted by plasma cells play an important role against *Y. pestis*.

In previous work done in our lab, infection in lymphocyte-deficient SCID mice (C57BL/6 background) were compared to that in WT mice to determine whether YopM functions primarily at the level of the adaptive immune system or on innate immune defenses (159). After infection with a low dose (100CFU) of either KIM5 or *ΔyopM-1 Y. pestis*, SCID and C57BL/6 mice displayed similar patterns of bacterial burden in both spleen and liver (159) (Figure 10.1), as well as similar histopathological manifestations in liver until day 4 p.i. (159), indicating that YopM only counteracts innate immunity at the early stage of infection. However, after day 4 p.i. the number of *ΔyopM-1 Y. pestis* remained at high levels in the liver and declined slightly in the spleen of SCID mice, whereas *ΔyopM-1 Y. pestis* were cleared in C57BL/6 mice by day 10. Both of the mouse strains infected with parent strain *Y. pestis* were killed by day 5 p.i., and no differences were found between the two mouse strains (159) (Figure 10.1). Therefore, the adaptive immune response is only required for efficient clearance of the *ΔyopM-1* mutant beyond day 4 p.i.. The presence of YopM in the KIM5 strain renders the infecting bacteria fully virulent to kill the mice before the adaptive immune system exhibits the ability to clear *Y. pestis*. Thus, the modulation of the immune response by YopM must occur at the early phase of the infection and the innate immune system would be the primary target of YopM.

C. YopM does not modulate innate immune responses through NK cells

a) NK cell function and previous model about the role of NK cells in YopM-mediated immune modulation

When our lab initially tried to identify the innate immune cell types that may be

affected by YopM, a YopM-associated depletion of NK cells from spleen and blood of mice infected IV was found by flow cytometric analysis (159). NK1.1$^+$ cells were depleted dramatically from day 3 p.i. in spleen from mice infected with *Y. pestis* KIM5, but not in mice infected with the *ΔyopM-1* mutant. Staining with another pan-NK marker, CD49b, similarly showed YopM-associated depletion. Meanwhile, staining of blood leukocytes showed that the percentage of NK1.1$^+$ lymphocytes was reduced 5-fold at day 5 p.i. in mice infected with parent strain KIM5, while no change in NK cell percentage was found in mice infected with the *ΔyopM-1* mutant. Further, the mice infected with a *Y. pestis* strain lacking another major effector Yop, YopH, displayed the same depression of NK cell numbers that was seen in mice infected with the parent strain KIM5. Therefore, it is YopM, not other effector Yops, in the infecting *Y. pestis* that causes a systemic reduction in NK cells during infection, instead of a localized inhibition of the infiltration of NK cells into spleen.

As one of the major cell types to form the first line of defense against infection, NK cells function as an interface between the innate and adaptive immune systems. They originate in the bone marrow and are derived from the same lymphoid progenitor as T and B cells. They comprise 5–10% of the lymphocyte population in the blood, spleen and liver (189).

There are two sets of cytokines that induce the proliferation and activation of NK cells. The first set is IL-2 and IL-15. It was believed that both of IL-2 (127) and IL-15 (216, 355) were critical for NK development. However, studies on mice lacking the IL-2R γ-chain, which is shared by the IL-2R and IL-15R, and on IL-2 KO mice showed that IL-15, but not IL-2, played the critical role in NK cell development (88, 166). Meanwhile,

differentiation of bone-marrow-derived precursors of murine uterine NK (uNK) cells into mature cells, which expressed NK surface markers and effector molecules, was found to depend on IL-15, instead of IL-2 (362).

Another set of cytokines related to NK cell proliferation includes IL-12 and IL-18, for which importance was proven by the impaired NK cell activity in IL-18 and IL-12 KO mice (327). In addition to a strong synergistic proliferation and activation of NK cells induced by IL-12 and IL-18, three major differences in NK development between IL-12/IL-18 and IL-2/IL-15 treatment were also found (176). As shown in Table 10.1, IL2/IL15 treatment induced the proliferation of both NK and NKT cells, as well as the expression of NK1.1 on the cell surface. However, although IL-12/IL-18 treatment failed to induce differentiation of NKT cells and expression of NK1.1, it did stimulate the production of cytokines, such as IFN-γ, IL-3, IL-6 and TNF, which were absent in IL2/IL15 treatment (176). NK cells derived in response to IL-12/IL-18 were much more cytotoxic than NK cells grown in IL-2 or IL-15, which may be explained by a Fas-independent pathway in the first NK cell group (175).

Current theory about the activation of NK cells is the "missing-self" hypothesis: NK cells are activated when their potential target cells have downregulated MHC-I as well as some abnormal surface molecules, which frequently happens in cells infected with certain viruses (156, 189). That means that NK cells use two sets of cell surface receptors, inhibitory and activating receptors, to distinguish between normal healthy cells and abnormal cells and control their activation, proliferation, and effector functions.

Inhibitory receptors, whose ligand is self-MHC class I on potential targets, function to inhibit the activation of NK cells. These receptors include Ly49 receptors (rodent), killer

cell immunoglobulin-like receptors (KIR, human), and conserved heterodimers of the CD94/NKG2 receptor family (expressed by both species) (128). Activating receptors, whose function is to activate NK cells, are more diverse than inhibitory receptors. The best studied activating receptor, NKG2D, recognizes MHC-I-like surface glycoproteins, most of which are not encoded by genes in the MHC complex and do not function as peptide-binding structures for the presentation of antigens (260). Other activating receptors such as the NKR-P1 Receptors, CD244 and CD226, whose ligands are not MHC related, cannot directly trigger cytotoxicity and cytokine production but appear to function primarily as "costimulatory" receptors or to overcome the inhibitory NK cell receptors (189, 225).

After being activated, NK cells share a common killing mechanism with CTL (i.e., using perforin and granzymes) to lyse infected cells directly, as well as secrete many cytokines, such as IFN-γ, which can activate macrophages (189). The previous studies about production of proinflammatory cytokines in our lab also pointed toward NK cells as the major target of YopM (159). mRNA expression of the pro-inflammatory and Th1 cytokines IL-1β, IL-6, TNF-α, IFN-γ, IL-12 and IL-18, especially the last two, in spleen as early as d 2 p.i. was compromised by YopM in the infecting bacteria. This was a direct effect on expression, as opposed to being an indirect effect of increased expression of suppressive Th2 cytokines such as IL-10 and IL-4, which in fact were not detectable until d 4 p.i.. Expression of mRNA for these cytokines in purified splenic F4/80$^+$ macrophages and monocytes (IL-1β, IL-6, TNF-α, IL-12 and IL-18) and NK cells (IFN-γ only) showed a pattern similar to that in the whole spleen, indicating that YopM was modulating immune function early in infection and that macrophages and monocytes as well as NK

cells were important sources for the observed changes in whole spleen. Meanwhile, the levels of IL-15 mRNA in purified F4/80$^+$ macrophages/monocytes and IL-15R mRNA in purified NK1.1$^+$ NK cells were much lower in mice infected by *Y. pestis* KIM5 than ones infected by the *ΔyopM-1* mutant. Therefore, YopM could inhibit the proliferation of both NK and NKT cells, as well as their functions in cytotoxicity and cytokine production. And lacking the signal from NK cell-secreted IFN-γ, macrophages failed to be fully activated, and the growth of the YopM containing *Y. pestis* would be unchecked (Figure 10.2) (159).

b) NK cell ablation did not relieve the growth defect of the *ΔyopM-1* mutant

If the above hypothesis reflects the true role of NK cells in the YopM mechanism, the growth limitation of the *ΔyopM-1* mutant should be relieved if NK cells are depleted from the infected mice. There are two traditional antibodies to deplete NK cell *in vivo*, anti-NK1.1 (PK136) and anti-asialo-GM1 (157, 158), which are usually used to ablate NK cells from NK1.1 expressing mouse strain such as C57BL/6 mice and other mice strains, respectively.

As described in Table 10.1, NK cells induced by IL-12/IL-18 express no NK1.1 as well as produce large amount of IFN-γ; and the IL-2 or IL-15-induced NK cells act in the opposite way. These observations raised a concern that the anti-NK1.1 susceptible NK1.1$^+$ cells were not responsible for the IFN-γ production on days 2-4 of infection by the *ΔyopM* Y. pestis, and thus not important in the YopM virulence mechanism. However, the above results about cytokine-induced NK cell development came from *in vitro* cytokine-treated splenocytes, and the failure in expression of IFN-γ by those IL2/IL-15

196

induced NK1.1$^+$ cells could be due to the absence of stimulation from activating receptor ligands (175, 176). Meanwhile, there is compelling evidence from anti-NK1.1 mediated NK depletion that NK1.1$^+$ cells play a central role in early IFN-γ synthesis in response to infection by a number of protozoal and bacterial pathogens (83, 90, 172), and purified splenic NK1.1$^+$ cells show robust production of IFN-γ after anti-NK1.1 treatment (14).

Since it is reported that a freshly isolated murine spleen CD8+ T cell population contains 20% to 30% asialo-GM1$^+$ cells, which were distinct from asialo-GM1$^+$ NK1.1$^+$ NK cells (179), we utilized anti-NK1.1 to deplete NK cells in our experiments. Actually, our preliminary experiments showed that both anti-NK1.1 (PK136) and anti-asialo-GM1 displayed similar ability to ablate NK cells (data not shown). However, although 90% of the NK1.1$^+$ NK cells were depleted from spleen and liver, anti-NK1.1 antibody treatment in the present study failed to cause any change in the bacterial growth and histopathological appearance in infections by either strain until day 5 p.i. (Figure 4.3).

c) YopM depletes traditional splenic NK cells, but not hepatic NK cells or NKT cells in either organs

This unexpected result made us check our model again. In previous work, we used anti-NK1.1 to stain NK cells as a single cell type. However, NK cells contain several subgroups which may have different functions and YopM may not affect all of them. To address this issue, we used three antibodies to define NK subgroups. NK1.1 or NKR-P1C (natural killer cell receptor P1C) is a type II transmembrane C-type lectin receptor belonging to the family of activating NK receptors (112, 277) and is only expressed by some mouse strains, including C57BL/6 (292). The antigen recognized by mAb DX5 is

CD49b (15), belonging to α2 integrin, which is known to bind to collagen or laminin (249). DX5 is a useful reagent because it stains NK cells from all mouse strains examined; however, the cells detected by DX5 include a small group of T cells (224), which are not NKT cells (243). Therefore, DX5 is only used as a supplemental antibody in the identification of NK cells in this study. The third antibody was anti-CD3, which is not specific for NK cell detection. Always associating with the TCR, CD3 is a member of a complex comprised of 5 proteins, which transduce activation signals to the cell following antigen interaction with the TCR. This surface marker was used to define a subgroup of NK cells, NKT cells. NKT cells are narrowly defined as a T cell lineage expressing NK lineage receptors, including NK1.1 in the C57BL/6 background, in addition to semi-invariant (Vα14-Jα18) CD1d-restricted αβ TCRs (34, 113). The traditional way to define NKT cells is that they are $CD3^+NK1.1^+$ (or $DX5^+$) cells (175) and the newest definition is that they are CD1d-dependent and $Vα14-Jα18^+$ ($NK1.1^+$ or $NK1.1^-$)$CD3^+$ cells (113). Upon stimulation, $NK1.1^+$ NKT cells express high levels of IFN-γ and TNF, some IL-4, IL-13, granulocyte–macrophage colony-stimulating factor (GM-CSF) and IL-2; whereas $NK1.1^-$ NKT cells produce higher levels of IL-4 and lower levels of IFN-γ than their $NK1.1^+$ counterparts (113). In our study, a simple combination of CD3 and NK1.1 markers was used to define NKT cells, i.e., as $NK1.1^+CD3^+$ cells, because IFN-γ producing $NK1.1^+$ NKT cells were our interest in defense against *Y. pestis*, and mCD1d-$PBS57^+$ cells were mainly $CD3^+NK1.1^+$ in our study (Figure 4.1B). Our studies of the effects of YopM on the subgroups of NK cells in spleen showed that YopM only depleted $NK1.1^+CD3^-$ cells, but had no effect on the $NK1.1^-DX5^+$ cells or NKT cells, which would remain as potentially a great source of IFN-γ in the infection.

Our previous work had mainly analyzed immune cell populations in spleen. However, liver is the other organ predominantly infected in the first 3 days of systemic plague, and growth dynamics in liver for *Y. pestis* are similar to those in spleen despite the distinct immune microenvironments in these two organs. For example, liver, more than spleen, is a focus for immune surveillance by NKT cells, which can release IL-4 explosively and other key Th2 cytokines such as IL-13, in addition to massive amounts of IFN-γ, as described previously (34, 113, 219). In our previous study (159), we had not evaluated leukocyte population dynamics in liver, due to the difficulty of separating leukocytes from hepatocytes. In this work, we combined and modified protocols originally developed for obtaining leukocytes from colon (257) to obtain high-purity preparations of leukocytes from liver, and these were analyzed by flow cytometry alongside leukocytes from spleen in mice infected with *Y. pestis* KIM5 or KIM5-3002. Several tissue-specific changes were found. Contrary to the depletion of NK1.1$^+$CD3$^-$ NK cells in spleen by YopM-containing *Y. pestis*, there was little to no depletion of either classic NK cells (NK1.1$^+$ CD3$^-$) or NKT cells in liver of mice infected by either the parent or *ΔyopM-1 Y. pestis* strains. This finding indicated that the virulence effect of YopM in liver was not manifested as a net loss of NK cells but did not rule out the possibility that these cells were lost and rapidly replenished. Combined with the results from NK cell ablation experiments, we concluded that NK cells are redundant for YopM's pathogenic mechanism or that NK cell depletion by YopM is an irrelevant secondary effect of YopM.

D. YopM affects the dynamics of DCs in both spleen and liver, but does not compromise host defense through DCs

We next examined populations of DCs for changes that might correlate with YopM's effect on bacterial growth, because of the well-established frontline surveillance function of DCs for invading microorganisms or microbial products (24). It was reported that human monocytes could differentiate into mature DCs, which expressed IFN-α and stimulated cytotoxic T cell responses, after *in vitro* infection with *Y. pestis* strain CO92 (*Δpgm Δpla*) (279). There is evidence that *Y. pestis* selectively engages macrophages, DCs and PMNs for Yops injection through the T3SS (197), and the migration of DCs to draining lymph nodes is inhibited when the infecting *Y. pestis* strain contains the Yops-encoding virulence plasmid (347).

We monitored the numbers of all major subgroups of DCs in mice infected by the parent or the *ΔyopM-1 Y. pestis*. There are at least three subtypes of DCs in mouse spleen: CD8$^+$DCs (lymphoid DCs), CD11b$^+$DCs (myeloid DCs, mDCs), and B220$^+$DCs (pDCs) (16, 299). Although it was believed that CD8$^+$DCs derived from lymphoid-restricted precursors, and all CD8$^-$DCs derived from myeloid-restricted precursors, recent evidence showed that both precursors could produce all the mature splenic and thymic DC subtypes (299). The distribution, development and function in innate immunity of the three subsets are listed in Table 10.2.

In spleen, only the numbers of CD8$^+$ DCs displayed a YopM-specific change, decreasing 4-fold by d 4 p.i.. These DCs are located in the T cell area, where they can internalize apoptotic cells, selectively present antigens to both CD4$^+$ and CD8$^+$ T cells, and elicit a Th-1 response through production of IL-12 and IFN-gamma (16, 147). In liver, all three subgroups of DCs decreased in numbers when the infecting *Y. pestis* strain contained YopM. However, the YopM-related changes in numbers of CD8$^+$DCs in spleen

or DCs in liver only became significant relatively late in infection (d 4 to 5 p.i.) compared to the time when the growth difference between the two *Y. pestis* strains was significant (d 2 or 3 p.i.). Meanwhile, the mean fluorescence intensity (MFI) of CD86 and MHC-II, two major DC maturation and activation markers (187), showed no difference between the infection of two strains.

There is cross-talk between NK cells and DCs, especially pDCs. As listed in Table 10.2, after activation by virus or CpG-ODN, pDCs expressed the ligand for the glucocorticoid-induced TNF receptor (GITRL), which was shown to promote NK cell cytotoxicity and IFN-γ production in synergy with IL-2, IFN-α and NKG2D triggering (124). Further, a B220^{+}CD11c^{+}NK1.1^{+} population, which is capable of producing higher levels of IFN-γ than conventional NK cells, was identified recently to functionally overlap with NK cells and pDCs (38). Therefore, the dynamics of all three DC subsets in NK cell-ablated mice were studied, but no effect of NK cell ablation on the distribution of these DCs in either spleen or liver was found (Figure 5.2). Meanwhile, our preliminary DC ablation experiments by using CD11c-DTR transgenic mice (155) also did not support CD11c^{+} DCs as the target cells for YopM, despite that both the parent and *ΔyopM-1* mutant strains grew much better in DC-ablated mice (done by Annette Uittenbogaard, data not shown). Accordingly, although DCs likely are important in plague and YopM may have a role in modulating the function of these cells, an inhibitory effect of YopM on another cell type is likely to be responsible for promoting early bacterial growth.

E. Gr1$^+$ cells are responsible for controlling the *ΔyopM-1* mutant

Since both NK cells and DCs are unlikely to be early cellular targets of YopM *in vivo*, we turned our focus to other cell types in innate immunity. In previous studies, there was no YopM-associated recruitment of PMNs (Gr1$^+$ cells) and macrophages (F4/80$^+$ cells) found in the systemic plague model (159). However, defining PMNs as Gr1$^+$ only is not correct since the anti-Gr1 antibody detects not only Ly6G, a PMN surface marker, but also Ly6C (229), which is expressed on monocytes and pDCs in addition to PMNs. Meanwhile, F4/80 is highly expressed on macrophages but low or intermediate on monocytes (325, 329). These cells not only differentiate into macrophages and DCs but also produce cytokines including TNF and IFN-γ (293).

Unlike PK136, which successfully ablated NK cells *in vivo* but exhibited no effect on growth of either the parent *Y. pestis* or the *ΔyopM-1* mutant strain, RB6-8C5 (anti-Gr1) depleted Gr1$^+$ cells and showed strong effects on bacterial growth. 90% of the Ly6G$^+$ PMNs were ablated from spleen and liver, the growth defect of the *ΔyopM-1* mutant was significantly relieved, and the mutant and parent strains caused similarly necrotic lesions in liver. These findings showed that Gr1$^+$ cells are important in restricting the growth of *ΔyopM-1 Y. pestis*. Depletion of these cells also allowed some increased growth of the parent *Y. pestis*, likely because even the YopM-containing parent strain does not neutralize 100% of the Gr1$^+$ cells.

Initially we thought that PMNs were the single key cellular player in the YopM virulence mechanism because the specificity of anti-Gr1 (RB6-8C5) was misunderstood for a long time. RB6-8C5 was believed to detect PMNs only and had been used extensively to deplete PMNs in murine disease models, and even was called anti-Ly6G in

some papers (93, 206, 208, 332, 373). However, RB6-8C5 also depletes Ly6C$^+$ cells *in vivo*. It has been determined that Ly6C$^+$ blood monocytes are precursors of inflammatory macrophages (110, 320, 321). RB6-8C5 detects this subpopulation of blood monocytes as well as monocytes from early peritoneal exudates, which maintain Gr-1 expression as they differentiate into macrophages (130). Therefore, systemic administration of this antibody could eliminate these cells along with PMNs. In addition, *in vivo* administration of RB6-8C5 has already been shown to deplete pDCs (25). Thus, results of our studies with RB6-8C5 treatment reflected not only the loss of PMNs but also the loss of other Gr-1-expressing cells.

F. YopM favors the growth of *Y. pestis* in liver through inhibiting the function of PMNs

a) YopM does not affect the recruitment of PMNs into infected tissue

PMNs and inflammatory monocytes have received little *in vitro* study compared to macrophages for their role in the pathogenic mechanisms of Yops, although PMNs are thought to be important in controlling bacterial numbers early in plague (146, 290)**.** *In vitro*, *Y. pestis* KIM5 selectively injects Yops into PMNs as well as macrophages and DCs among splenic leukocytes (197). We already knew that Gr1$^+$ cells are dominant in restricting the growth of *ΔyopM-1 Y. pestis*. Since PMNs were strongly depleted by the anti-Gr1 treatment, they became a prime candidate for a cell type that is important for controlling bacterial proliferation in both liver and spleen.

The recruitment of PMNs under normal homeostatic and inflammatory conditions involves a multistep process (310) (Figure 10.3 A). In an initial step, PMNs adhere

weakly to the endothelial cell layer but are still allowed to roll along the venular wall. This rolling is promoted by vasodilation and by expression of selectins on PMNs (L-selectin; CD62L) and endothelial cells (E and P-selectins; CD62P and CD62E). Then these PMNs are stimulated by many mediators, which include TNF-α, IL-1, complement fragment C5a, platelet-activating factor (PAF), leukotriene B4 (LTB4), and chemokines (286). These stimulated PMNs attach firmly to the endothelial layer and change in shape through interaction of their surface integrins, mainly Mac-1 (CD11b/CD18) with adhesion molecules on the endothelial cell (Figure 10.3 B). Integrin adhesiveness is enhanced by chemokines produced by leukocytes (e.g., IL-8) as well as by endothelial and tissue cells. Chemoattractive mediators, such as C5a, PAF, chemokines and the bacterial mediator fMLP, activate PMNs through specific recognition of their corresponding G protein-coupled receptor (GPCR) so that PMNs migrate through the endothelial cell layer into the underlying tissue to the chemoattractant source. Activation of PMNs by chemokines also provokes the secretion of proteases, such as gelatinases (matrix metalloproteinase-2 and -9 (MMP-2 and -9)) which can degrade the subendothelial extracellular matrix and facilitate the migration of leukocytes (263).

Members of the chemokine family fall into two major groups, based on the position of one or two cysteine residues located near the N terminus of the protein: CC chemokine ligands (CCL) with two adjacent cysteines, e.g., MCP-1/CCL2, and CXC chemokine ligands (CXCL), for which the two cysteine residues are separated by another amino acid, e.g., IL-8/CXCL8 (207, 274). All chemokine receptors are integral membrane proteins containing seven membrane-spanning helices and belong to the family of GPCR.

IL-8, a CXC chemokine, is the major human chemokine to induce recruitment and

activation of PMNs by binding CXCR1 and CXCR2 expressed on the PMN surface (274, 291). However, murine PMNs express only CXCR2, and the rodents lack a direct homologue of IL-8; but the chemokines CXCL1/KC, CXCL2/MIP-2, and CXCL5-6/LIX are regarded as murine functional homologues of IL-8 (140, 200). CC chemokines, e.g. macrophage-inflammatory protein-1α (MIP-1α), may also participate in PMN migration in different models of inflammation (45, 259, 313). MIP-1α promotes PMN recruitment by interacting with CCR1 probably on CD4$^+$ T cells and inducing the sequential release of TNF-α and LTB4, which are potent chemoattractants for PMNs (259).

We found no difference in numbers of PMNs in livers and spleens of mice infected with the parent strain of *Y. pestis* or the *ΔyopM-1* mutant (Figure 7.1), indicating that YopM does not affect the recruitment of PMNs in the systemic plague model. Meanwhile, study of the PMNs in blood and spleen in the early stage of infection in this model also showed that YopM did not affect efflux of PMNs into circulation or their infiltration into spleen (Figure 8.4). This result is consistent with our observations from liver and spleen infected with *Y. pestis* KIM5 or the *ΔyopM-1* strains and also with studies using a peritoneal infection model to quantify PMN influx (Figure 7.3).

In pneumonic plague, recruitment of PMNs to the lungs and local production of proinflammatory cytokines and chemokines are delayed and do not occur for 36 to 48 h (53). We confirmed this result for influx of inflammatory cells (Figure 3.3). In contrast, we found that there was a robust inflammatory response in skin as early as 8 h following ID infection mimicking fleabite. Consistent with an early difference in inflammatory character between the two types of plague, there is a growing number of pathogenic properties that are required for full virulence in bubonic, but not pneumonic, plague (61,

79, 104). YopM also was required for virulence of *Y. pestis* CO92 in experimental bubonic, but not pneumonic, plague in mice (LD$_{50}$ data, Table 4, CO92.S6 and CO92.S19, ID and IN routes), consistent with our hypothesis that YopM functions to counteract the effect of PMNs on bacterial growth. However, there was no large difference in the magnitude of PMN recruitment to the infected dermis between mice infected with the parent strain or the Δ*yopM-2* mutant.

Accordingly, we thought that YopM's major effect on PMNs, if there was any, was not on their influx into infected organs but on their inflammatory function. A recent study has shown that *in vitro*, *Y. pestis* KIM5 shows the same timecourse of killing by human PMNs as does *Y. pestis* KIM6 (lacking the virulence plasmid that encodes the T3SS and Yops) (308), indicating that YopM and other Yops may not function directly to enhance survival within PMNs.

b) YopM dose not compromise the activation of PMNs

In response to pathogens, PMNs move from the bloodstream into infected tissues, where they are activated and start to produce ROS, a response which is known as the oxidative burst (20, 64). The generation of microbicidal oxidants by PMNs starts from the activation of NADPH oxidase, which reduces O_2 to an oxygen free radical and then H_2O_2. PMNs and monocytes utilize myeloperoxidase to further combine H_2O_2 with Cl^- to produce hypochlorite, which plays a critical role in destroying bacteria (64).

This multicomponent enzyme system is inactive in resting cells, in which various components are distributed between the cytosol and membranes. The major membrane component, cytochrome b558, is located in specific granules or the plasma membrane of

resting PMNs. The cytosolic components consist of four major proteins: p47^{phox}, p67^{phox}, p40^{phox} and Rac 2 (19). When PMNs are activated by stimuli such as N-formyl peptide derived from bacteria (fMLP) or PMA, some of the cytosolic components, especially p47^{phox}, become phosphorylated and migrate to the membrane, where they assemble as an active complex (19).

PMNs can exist in three different activation states, namely, the resting, primed, and activated states. The priming process occurs upon stimulation of PMNs by a number of inflammatory mediators, including TNF-α, GM-CSF, and LPS, and subsequently enhances the PMN response to a second stimulus such as fMLP (78, 81, 86). The mechanisms underlying the priming process may include partial p47^{phox} phosphorylation induced by priming agents such as TNF-α, GM-CSF, and LPS (78, 81, 86), increased membrane expression of cytochrome b558 (81), as well as up-regulation of fMLP receptors (331).

Another sign of the activation in PMNs is the production of NO. Derived from the oxidation of the terminal guanidine nitrogen atom of LI-arginine by the enzyme NO synthase (NOS), NO has been implicated in various physiological and pathological processes including cell injury and apoptosis. Two general classes of NOS have been identified (220, 221). Constitutive NO synthase (cNOS) is a Ca^{2+}/calmodulin and NADPH-dependent enzyme. Mainly involved in physiological processes in the cardiovascular and nervous systems, cNOS is expressed in vascular endothelium, brain and platelets.

We used two models to analyze the production of ROS and NO by PMNs. The staining reagents used in both models were the same: DCFDA, which becomes

fluorescent when acetate groups are removed by intracellular esterases and oxidation by ROS occurs within the cell, and DAF, which becomes fluorescent when it reacts with NO. The first model was IV infection (systemic plague model), and the production of ROS and NO by the splenocytes was measured by flow cytometric analysis. The advantage of this model was that the cell types, such as macrophages and PMNs which made ROS and NO, could be distinguished by their surface markers from DCFDA- and DAF-negative cells, e.g. lymphocytes.

However, only ca. 10% of leukocytes in spleen are cell types related to the YopM virulence mechanism. Therefore, we used the IP infection model as an alternative approach. A high dose of bacteria was injected IP, peritoneal cells were harvested after several hours, and ROS and NO production were measured immediately by microplate reader. Most of the peritoneal cells were relevant, being PMNs (60% of total peritoneal cells) and macrophages (40% of total peritoneal cells). The infecting bacteria (*Y. pestis* KIM5 and *ΔyopM-1* KIM5) were *Δpgm* and they needed iron from blood to support extensive growth. Therefore we infected the mice with a high dose (10^6CFU/mouse, between the LD_{50}s of the two strains) of pre-induced bacteria, which could inject Yops into the host cells as soon as stable contact was established. Peritoneal cells were harvested at a very early stage of infection (before the bacteria would have depleted their iron stores) and the early responses of these cells to YopM could be captured.

However, as with the systemic model, there were still some concerns about the IP model. This model was not a mimic of any natural plague model, although YopM was required for the full virulence of *Y. pestis* (Table 3.1, LD_{50} of IP). This IP model exhibited the MDR, best documented as a physiological response to both acute nonspecific

208

inflammatory and specific delayed immune hypersensitivity processes (26). This phenomenon enriched these peritoneal cells for PMNs at the expense of ca. half of the macrophages and probably accounted for our inability to recover even 10% of the bacteria form the peritoneal cavity. The lost *Y. pestis* could attach to the peritoneal wall or be conveyed as intracellular bacteria via the migrating macrophages. Under either condition, those bacteria failed to contact and deliver the Yops into the harvested PCs. Therefore, we may have lost some signals of DCFDA and DAF by losing these bacteria.

Another disadvantage of peritoneal infection is the presence of B1 cells, which constitute a minor fraction of the spleen but are enriched in the peritoneal and pleural cavities (125, 171) and express IL-10, an anti-inflammatory cytokine (121). However, the main drawback of this method was that the source of ROS and NO, i.e., PMNs and macrophages, cannot be distinguished because these cells were not stained with antibodies against surface markers. Therefore, the amount of ROS and NO detected in this model reflected the activation of all recoverable peritoneal cells.

Although neither model was perfect, they were complementary to each other and no YopM-dependent activation was found either in splenic PMNs or peritoneal cells (Figure 7.2 and 13). To test whether YopM affected the priming process of these cells, their stimulability was measured after one hour of *in vitro* treatment with PMA or pCD1-negative *Y. pestis*, which lacks the T3SS and all of the effector Yops. YopM showed no effect on the stimulation of cells in either model (Figure 7.2 and 13, and data not shown for the *in vitro* infection).

Another possible effect of YopM on PMN function was to inhibit the directed migration of PMNs. Two *in vitro* migration experiments were done with peritoneal cells

after IP infection; the migration of neither PMNs nor macrophages toward the bacterial-derived chemoattractant fMLP was influenced by the presence of YopM in the infecting *Y. pestis* (done by Annette Uittenbogaard and data not shown).

Therefore, we concluded that YopM does not modulate the host immune responses through inhibiting the function or recruitment of splenic or peritoneal PMNs. However, PMNs from infected liver were not tested for effects of YopM on function because their *in vivo* status would have decayed by the time they could be obtained.

c) PMN ablation only relieved the growth limitation of the *ΔyopM-1* strain in liver, but not in spleen

A commercial anti-Ly6G (IA8) was developed recently and made selectively *in vivo* depletion of PMNs possible. It was reported that unlike anti-Gr1 antibody (RB6-8C5), which ablates blood PMNs and Gr-1$^+$ monocytes, *in vivo* administration of 1A8 only reduced blood PMNs but not Gr-1$^+$ monocytes (77). In our experiments, IA8 depleted over 90% of the Ly6G$^+$CD11b$^+$ PMNs from both spleen and liver, and growth of *ΔyopM-1 Y. pestis* was disproportionately enhanced in liver compared to the parent strain, showing that PMNs are selectively involved in controlling growth of the mutant in that organ. In contrast, there was no effect of the ablation on growth of the *ΔyopM-1* strain in spleen (Figure 7.5). These findings indicate that YopM directly or indirectly undermines a function of PMNs in liver, but not in spleen where these cells are not a critical target of YopM's pathogenic mechanism, or they are a redundant target.

It needs to be noted that the PMNs investigated here were defined as Ly6G$^+$CD11b$^+$ cells, which represent the major portion of PMNs. However, according to recent studies,

PMNs can be divided into several subgroups by two different ways. Where PMNs were distinguished based on patterns of cytokine and chemokine production, TLR expression, and surface CD49d and CD11b expression, three subsets were identified as PMN-I, PMN-II, and PMN-N (Table 10.3) (340). PMN-Ns are quiescent circulating PMNs and can convert to the other two subsets under certain circumstances (340). Another way to classify PMNs depends on the expression of the surface marker Gr1. Both Gr1^{high} and Gr1^{low} cells were harvested from the peritoneal cavity in C57BL/6 mice that were infected IP with *Haemophilus influenzae*. The Gr1^{high} cells were found to be the major source of IL-15, which is important in the clearance of intracellular bacteria through activating NK cells (218). However, the expression of Gr-1 surface marker on PMNs is not correlated to the properties that distinguish PMN-I, PMN-II, and PMN-N cells (217) and therefore Gr-1 PMNs cannot be classified as any of those three PMN subsets. Thus, in our work only the importance of Ly6G$^+$CD11b$^+$ PMNs, which may belong to the CD11b$^+$ PMN-II or Gr1^{high} PMN classification, was studied. Further investigation of the role of other PMN subsets in the YopM virulence mechanism can be done in the future. However, the importance of these PMN subsets in the control of *ΔyopM-1 Y. pestis* will not be determined until efficient methods to specifically ablate these PMN subsets are developed.

G. Subgroups of MDMs play different roles in the YopM-mediated virulence mechanism

a) YopM inhibits the recruitment of MDMs into spleen but not liver through a PMN-independent pathway

We already identified Gr1$^+$ PMNs in liver as the major cell type whose function is modulated by YopM. However, the cellular target of YopM in spleen still needed to be determined. Early in infection, the first immune cells encountered in spleen by *Y. pestis* are resident macrophages and myeloid DCs at the infection site. Within a short time, PMNs also are involved. These cell types express CD11b on their surface. CD11b, also known as macrophage-1 antigen (Mac-1) or complement receptor 3 (CR3), is expressed at low or undetectable levels in myeloid precursors, and its expression increases steadily during myeloid differentiation, reaching highest levels in mature phagocytes, such as PMNs, monocytes, and macrophages (120, 273, 335). Upon exposure to degranulation stimuli such as the bacterial peptide fMLP, stored Mac-l, an integrin heterodimer, rapidly mobilizes to the cell surface and serves as an important adhesion molecule mediating many functions, including firm adhesion of these leukocytes onto the endothelium (Figure 10.3) (352).

Combined with the PMN-specific marker Ly6G, CD11b was used to distinguish PMNs from other phagocytes. PMNs were defined as Ly6G$^+$CD11b$^+$, whereas the rest of the phagocytes are Ly6G$^-$CD11b$^+$. Since Ly6G$^-$CD11b$^+$ cells include macrophages, monocytes and some DCs, we named them MDMs.

Interestingly, MDMs failed to be recruited as robustly into spleens of mice infected with parent *Y. pestis* as in mice infected by the *ΔyopM-1* mutant after d 2 p.i.. This effect did not occur in liver (Figure 8.1). However, the same number of MDMs was induced by both strains in bone marrow and they effused into the circulation equally by d 2 p.i.. Taken together, these findings indicated that YopM produced by the parent strain acts locally to prevent those MDMs from reaching extravascular tissue in spleen at an early

212

stage of infection.

The anti-Gr1 treatment eliminated the *ΔyopM-1 Y. pestis*-induced influx of MDMs into spleen and delayed that influx into liver, accompanied by relief of the growth defect of *ΔyopM-1 Y. pestis* in both organs (Figure 6.1). This anti-Gr1-mediated effect on the MDM infiltration could be due to the depletion of inflammatory monocytes in MDMs directly by this antibody because of the robust expression of Ly6C on these cells (110, 321).

Meanwhile, the absence of PMNs caused by anti-Gr1 treatment may be responsible for inhibiting recruitment of MDMs since in inflammatory situations where PMNs serve as early responders; and the cytokines and chemokines they produce elicit the influx of monocytes as a secondary wave of the acute inflammatory response (143, 305, 306). However, the role of PMNs in the recruitment of MDMs is questionable in plague models. In a rat model of bubonic plague, macrophages began to appear in primary swollen lymph nodes (bubo) 18 h before PMN numbers increased; and in spleen, PMNs and macrophages were noted to appear at about the same time (287). In our systemic plague model, influx of PMNs and MDMs peaks at the same time in both spleen and liver (Figure 7.1 and 15). The depletion of PMNs by anti-Ly6G did not delay or diminish the influx of MDMs (Figure 7.5). These findings indicate that recruitment of MDMs in plague is independent of PMNs, raising the potential for YopM directed modulation of influx of MDMs through pathways not involving PMNs.

b) Clodronate-sensitive resident macrophages and DCs provide a protective environment for *Y. pestis* in a YopM-independent manner

We previously showed that there is a YopM-associated decrease in net message expression for pro-inflammatory cytokines in splenic F4/80$^+$ cells (macrophages/monocytes) as early as d 2 p.i. (159). This could have reflected a smaller contribution of inflammatory monocytes to the F4/80$^+$ population analyzed from mice infected by the parent *Y. pestis* KIM5 compared to the *ΔyopM-1* mutant. However, it may also reflect an early effect of YopM delivered to resident macrophages/DCs. In a sterile peritonitis model in rat, it was reported that mobilization and chemotaxis of PMNs were regulated by macrophages (162). Thus, YopM could favor the growth of the parent strain in liver through indirectly affecting the function of PMNs by compromising cytokine production of macrophages and DCs.

In order to determine whether those MDMs played a critical role in YopM-mediated virulence, we used clodronate-liposomes to deplete macrophages/DCs. Dichloromethylene-bisphosphonate (CI2MBP or clodronate) is not a toxic drug in itself because the free drug does not easily cross cell membranes and has an extremely short half life in circulation and body fluids. However, after being delivered into phagocytes by liposomes, which enter by phagocytosis, clodronate is released because the phospholipid bilayers of the liposomes are disrupted under the influence of lysosomal phospholipases. The intracellular free clodronate accumulates in the phagocytes and induces apoptosis of these cells probably through depletion of intracellular iron (222, 345) or a direct effect on the ATP metabolism (269, 345).

Clodronate is safe to non-phagocytic cells because it cannot enter those cells and has an extremely short half life in the circulation and body fluids when released into the circulation from dead macrophages or by leakage from liposomes (346). In our

experiments, 80% of the MDMs were depleted in spleen and liver after clodronate treatment 18 h prior to the infection; and MDMs and DCs remained at the same level in spleen, or their influx was delayed in liver, after infection (Figure 8.2). However, in contrast to the effect of anti-Gr1, treatment of mice with clodronate-liposomes to deplete MDMs curtailed growth of both *Y. pestis* strains accompanied by significantly fewer, smaller, and less necrotic lesion sites in liver. As reported by other groups (31, 154) and shown in our result (Figure 8.2), treatment with clodronate-liposomes did not deplete PMNs.

Since MDMs include resident macrophages/DCs and Gr1$^+$ inflammatory monocytes and all of them could be susceptible to clodronate treatment, it was difficult to determine which cell type(s) favored the growth of *Y. pestis*. Considering that the growth limitation of *ΔyopM-1 Y. pestis* was relieved in the mice lacking CCR2, a chemokine receptor which mediates the recruitment of inflammatory monocytes into organs, we concluded that during the first few days of systemic plague resident macrophages/DCs provide a protected environment for the *Y. pestis* to survive and proliferate, in which the bacteria avoid contact with other components of the host immune system, as previously suggested (192, 253, 254, 319).

Although the growth of both strains was inhibited in clodronate-treated mice compared to the mock treated groups, the bacteria kept multiplying in the first two days in both organs (Figure 8.2, panel G). This could have been due to the incomplete ablation of the resident macrophages and DCs. Ca. 20% of this population was left at the time of infection (Figure 8.2, panel G), and these cells may offer enough protective niches for early growth.

c) CCR2$^+$ cells played a critical role in YopM-mediated virulence in spleen

Inflammatory monocytes became the next candidate among MDMs as cells may that play an essential role in controlling growth of *ΔyopM Y. pestis*.

In humans, circulating monocytes are divided into two subsets based on their surface expression of CD14, a component of the LPS receptor complex, and CD16, the FcγRIII receptor (242). 90% of the circulating monocytes are CD14$^+$, whereas CD16$^+$ monocytes only constitute 10% of circulating monocytes. The CD16$^+$ population expands during infections (102, 333) and produces high levels of proinflammatory cytokines such as TNF (32), and is therefore referred to as proinflammatory monocytes.

Monocytes in mice fall into two subsets, which are distinguished by differences in expression of their surface markers Ly6C, CCR2 and CX3CR1 (110, 238, 321) (Table 10.4 and Figure 10.4). The CX3CR1^{low}CCR2$^+$Ly6C$^+$ are most similar to human CD16$^+$ monocytes, whereas CX3CR1$^+$CCR2$^-$ Ly6C^{low} monocytes are most similar to human CD14$^+$ monocytes according to their morphological characters and surface chemokine receptors (293).

CX3CR1$^+$ (CX3CR1$^+$CCR2$^-$ Ly6C^{low}) monocytes remain in the circulation for longer periods than Ly6C$^+$ (CX3CR1^{low}CCR2$^+$Ly6C$^+$) and traffic into peripheral tissues under noninflammatory conditions (110). These cells, referred to as resident monocytes, serve as the major precursor for tissue macrophages and DCs (110), except in spleen where MDPs (macrophage-DC progenitor) and pre-DCs reconstitute resident macrophages and conventional DCs most effectively (293) (Figure 10.5). Although CX3CR1$^+$ monocytes may descend from Ly6C$^+$ monocytes (321, 326), their recruitment is mediated by a CX3CR1 signal and independent from the CCR2-mediated pathway by which Ly6C$^+$

cells are recruited into tissues (110, 256).

Ly6C$^+$ monocytes have a short transit time in the bloodstream and are not recovered from peripheral tissues in the absence of inflammation (110). In response to inflammatory stimuli, Ly6C$^+$ monocytes home to peripheral tissues, produce high levels of TNF-α and IL-1β during infection or tissue damage, and thus are named inflammatory monocytes (18, 110). These monocytes differentiates into active macrophages. Another destiny of Ly6C$^+$ monocytes is to become DCs. However, they develop into different DCs under different conditions. In adoptive transfer experiments, the recipient mice are irradiated, and transferred Ly6C$^+$ bone marrow monocytes give rise to splenic CD11c^{high} conventional DCs as well as F4/80$^+$ splenic macrophages (181). In the setting of systemic inflammation Ly6C$^+$ monocytes differentiate into splenic CD11b$^+$CD11c^{int}Mac-3$^+$ cells (230), which are similar to TNF- and iNOS-producing DCs (TipDCs) in systemic listeriosis (294) (Figure 10.5).

We already knew that Gr1 (Ly6G/Ly6C)$^+$ cells were critical in the control of *ΔyopM-1 Y. pestis* in both spleen and liver (Figure 6.1). The stable accumulation of Ly6G$^-$CD11b$^+$ MDMs in spleen was also found to be inhibited in the infection by the parent *Y. pestis*, in contrast to infection by the *ΔyopM-1* mutant (Figure 8.1). When Gr1$^+$ cells were ablated, the influx of Ly6G$^-$ CD11b$^+$ MDMs was abolished in the infection by both strains (Figure 6.1), indicating that those cells potentially were Gr1 (or Ly6C)$^+$ cells. Once we found that PMNs were not required to control the *ΔyopM-1* mutant in spleen (Figure 7.5) and excluded resident macrophages and DCs as cells that control growth of *ΔyopM Y. pestis* (Figure 8.2), Ly6C$^+$ inflammatory monocytes/DCs became the prime candidates for Gr1$^+$ cells that selectively control the growth of the *ΔyopM-1 Y. pestis* in spleen.

The recruitment of those Ly6C^{+} inflammatory monocytes depends primarily on the signaling pathway mediated by the chemokine receptor CCR2 on their surface (293). The major ligand of CCR2 is CCL2/MCP-1, a member of the C-C chemokine family and a potent chemotactic factor for monocytes. There are additional CCL family members that signal through CCR2 in mice (CCL8, CCL7, CCL12/MCP-5). These peptides are approximately 70% homologous with CCL2/MCP-1 (344).

The expression of CCL2/MCP-1 can be induced in many cell types, including endothelial, fibroblasts, epithelial, smooth muscle, mesangial, astrocytic, monocytic, and microglial cells (85, 270). However, monocyte/macrophages are found to be the major source of CCL2/MCP-1 (365, 366). CCL2/MCP-1 is a potent chemoattractant for monocytes in vitro. CCL2/MCP-1 binds to its receptor, CCR2, and produces directional cell motion through several signaling pathways (Figure 10.6) (207). Meanwhile, as part of its migration program in monocytes, CCL2/MCP-1 induces the expression of integrins required for chemotaxis (152, 342). In addition, CCL2/MCP-1 attracts memory T lymphocytes, DCs, NK cells, and even activates NK cells and CD8^{+} T cells (60, 190, 194, 293).

As shown in Figure 10.6, CCL2/MCP-1 mediates its effects through its receptor CCR2, a G-protein coupled receptor (207). After binding to their ligand, CCR2 undergoes a conformational change, which modifies its function to that of a GEF. Then the associated G-protein is activated by exchanging its bound GDP for a GTP, which causes the dissociation of its α subunit from the β and γ subunits. The α subunit activates phospholipase C and hydrolyzes phosphatidylinositol-bisphosphate (PIP2) in the cytoplasmic membrane. Two products from this reaction, diacylglycerol (DAG) and

218

inositol trisphosphate (IP3) activate intracellular calcium release and protein kinase C (PKC)-dependent NF-κB pathways, respectively. The released intracellular calcium activates calmodulin (CaM) kinase pathway, in which CaM binds calcium and activates CaM kinase II. This kinase then phosphorylates target enzymes and regulates their activities. This GPCR signaling pathway ultimately regulates directional motion of the cell. Meanwhile, Rho family proteins, which are GTP-binding proteins with the capacity to influence cell motility through regulation of actin-dependent processes, are also activated by CCR2-mediated signal.

Because inflammatory monocytes/DCs largely depend on CCR2 for recruitment to foci of infection, we could test their involvement by comparing growth of parent and mutant *Y. pestis* in CCR2$^{-/-}$ mice. It is reported that KO mice for CCL2/MCP-1 or its receptor CCR2 are viable but have abnormalities in monocyte recruitment and cytokine expression (167, 191). Indeed, spleens of CCR2$^{-/-}$ mice had greatly reduced recruitment of Ly6G$^-$CD11b$^+$ cells, and the *ΔyopM-1* mutant grew nearly as well as the parent strain (Figure 8.5), thereby directly implicating cells recruited through CCR2 in controlling growth of *ΔyopM-1 Y. pestis*. We concluded that YopM selectively inhibits recruitment of inflammatory monocytes/DCs into spleen; when YopM is absent, those cells accumulate at foci of infection and limit growth of the bacteria.

In contrast to CCR2 KO, parent and *ΔyopM-1 Y. pestis* strains were similarly enhanced in growth in mice lacking CCL2/MCP-1, although the growth difference between the parent and mutant *Y. pestis* strains was slightly decreased (Figure 8.7). CCL2/MCP-1 acts on many cell types, including monocytes, memory T lymphocytes, natural killer (NK) cells and PMNs (85, 264), as well as interacting with receptors other

than CCR2 (284). Therefore, CCL2/MCP-1 KO may favor the growth of both parent and mutant strains by compromising the immune system broadly. Meanwhile, CCR2$^+$ cells could still be recruited or activated via other ligands of CCR2 such as CCL3 and CCL7 (85, 151, 235). Thus, this finding supports that CCR2$^+$ cells, other than the cells recruited by CCL2/MCP-1, play the key role in YopM-mediated virulence mechanism.

d) CCR2$^+$ PMNs played a critical role in the YopM-mediated virulence in liver

Gr1$^+$ cells dependent on CCR2 function were required to control growth of the $\Delta yopM$-1 mutant in liver (Figure 6.1). We have identified PMNs as critical cells that control growth of $\Delta yopM$-1 *Y. pestis* in liver, and these cells should be Gr1$^+$ and CCR2$^+$. However, although there has been little information about the expression and function of CCRs in PMNs, it was reported that bone marrow PMNs are capable of expressing functional CCR2 under the stimulation of G-CSF (144). The role of CCR2-mediated signals on the recruitment of PMNs is controversial. Christoph Reichel et al. found a CCR2-mediated PMN recruitment to postischemic tissue (262), whereas another group reported that in CCR2 KO mice early accumulation and delay clearance of PMNs in the peritoneal cavity after thioglycollate injection could be enhanced (168), and we may have observed this latter effect in livers of CCR2$^{-/-}$ mice (Figure 8.5 C, right panel). A possible explanation for the different findings may come from a difference in the isoforms of CCR2 in these experiments.

Unlike CCL2/MCP-1, CCR2 expression is relatively restricted to certain types of cells, mainly monocytes. There are two alternatively spliced forms of CCR2, namely, CCR2A and CCR2B, which differ only in their C-terminal tails (270). In addition to their

amino acid sequences, these two isoforms are also different in their tissue distribution and signaling pathway. For example, CCR2A was found to be expressed by vascular smooth muscle cells and some mononuclear cells (27), and Ca^{2+} flux was not stimulated when CCL2/MCP-1 interacted with CCR2A (280). It has been reported that activated monocytes, NK cells, and dendritic cells expressed abundant amounts of the CCR2B isoform and, to a lesser extent, the CCR2A isoform (250), and Ca^{2+} flux was induced in the CCR2B-positive cells (280). Thus, the CCR2 mediating PMN recruitment to postischemic tissue may be CCR2A isoform, whereas the one in peritoneal inflammation model is CCR2B.

Currently there is no information about the CCR2 isoform on PMNs; however, it would be reasonable to assume that it is CCR2B, because CCR2B mainly appears on inflammatory cells. Therefore, it is unlikely that the CCR2-mediated signaling pathway governs PMN recruitment into infection sites. However, it does promote PMN differentiation and adherence (144, 264).

Therefore, YopM's mechanism in liver, like that in spleen, results in downregulation of expression of ligands for CCR2 but not of other chemokines, e.g. KC/IL-8, that are sufficient for recruitment of inflammatory cells. During capture of PMNs from circulation, signaling through CCR2 by chemokines bound to proteoglycans on endothelial cells (354) might promote subsequent PMN antibacterial function. Consistent with this speculation, even though CCR2$^{-/-}$ mice responded to infection by *ΔyopM-1 Y. pestis* with enhanced recruitment of PMNs (Figure 8.5C), these PMNs apparently were not functional, because the *ΔyopM-1* mutant grew better in these mice than in WT mice in which fewer PMNs were present in organs (Figure 8.5D).

In the co-infection experiment (Figure 8.12), the presence of the parent strain (i.e., YopM being delivered to cells in the infection sites) in liver did not relieve the growth limitation of the *ΔyopM-1* mutant, despite the fact that both of the strains grew similarly in the co-infected spleen. The importance of CCR2-mediated PMN function in YopM virulence in liver may explain this difference. It is likely that parent and mutant *Y. pestis* would bind to different Kupffer cells (KCs), and only the KCs that bind the *ΔyopM-1 Y. pestis* could retain their ability to present CCR2-binding chemokines to activate surrounding PMNs, which in turn could kill some of the bacteria. However, the parent *Y. pestis* modulated nearby KCs and protected itself from PMN anti-bacterial activity. Thus, the parent strain would maintain its growth advantage over the *ΔyopM-1* mutant after d 2 p.i.

e) CCR2^{+} cells played a critical role in the YopM-mediated virulence in the bubonic plague model

In our studies, *Y. pestis* was grown at ambient temperature (26 $^{\circ}$C) so that the host responses might resemble those in skin during bubonic plague, in which the infecting bacteria grow at 26 $^{\circ}$C in the flea gut. Meanwhile, the major innate defense cells in skin are Langerhans cells (DCs) and macrophages, which are differentiated from Ly6C^{+}CCR2^{+} inflammatory monocytes (Figure 10.5) (293). Because CCR2 function was critical for limiting growth of the *ΔyopM-1* mutant in both liver and spleen, we hypothesized that this would also be the case when mice were challenged ID with ambient-temperature-grown *Y. pestis*.

Indeed, the *ΔyopM-2 Y. pestis* CO92.S19 showed delayed growth in skin compared to

the fully virulent parent *Y. pestis* CO92.S6 in WT mice at d 4 p.i. (Figure 8.6). Further, the *ΔyopM-2* mutant grew as well in CCR2$^{-/-}$ mice as the parent strain did in skin of WT mice. As seen in liver and spleen in systemic plague, growth of the parent strain in skin was not altered in the CCR2$^{-/-}$ mice compared to in WT mice, likely because YopM was present to neutralize CCR2-related functions in WT mice. Therefore, our findings show that signals through CCR2 are important for defense against both bubonic and systemic plague.

f) CD11b$^+$CD11c^{int}CCR2$^+$ Gr1$^+$ inflammatory DCs are the key cell type in controlling the *ΔyopM-1 Y. pestis* in spleen

According to the Figure 10.5, in response to infection, blood inflammatory monocytes in spleen differentiate into DCs with a CD11b$^+$CD11c^{int}Mac-3$^+$ phenotype, distinct from the conventional DC subsets (CD11c^{high}). In the spleen of *ΔyopM-1* infected mice, we identified a population of inflammation-induced DCs whose phenotype, Gr1$^+$ CD11b$^+$CD11c^{int} iNOS$^+$ Mac3$^+$ (Figure 8.8), is similar to TNF- and iNOS-producing DCs (TipDCs) that infiltrate the spleen of *Listeria monocytogenes*-infected mice (17, 294). As the downstream differentiation product of Gr1 (Ly6C)$^+$ monocytes, TipDCs only exist in peripheral organs and their presence depends on the CCR2-mediated recruitment of blood inflammatory monocytes (293, 328), which was also confirmed in our experiments with CCR2$^{-/-}$ mice (Figure 8.10).

These inflammatory DCs were differentially recruited into spleen by *ΔyopM-1* and parent *Y. pestis* and may underlie at least part of the mechanism for the growth limitation of the *ΔyopM-1* mutant (Figure 8.9). At foci of infection their major bactericidal product,

NO, could be responsible for limiting net growth of the *ΔyopM-1* mutant. Even though the bacteria would be predominantly extracellularly located in spleens by 2 d of infection (192), NO can be an effective antibacterial mechanism, as indicated in studies of bubonic and septicemic plague where free NO is available for killing extracellular bacteria and nitrosative stress is a prominent driving force shaping *Y. pestis* gene expression and metabolism (290).

The parent *Y. pestis* could decrease its exposure to this antibacterial agent by limiting influx of the NO-producing cells into spleen, and all the bacteria growing in this spleen should benefit from this microenvironment. Consistent with this idea, the presence of the parent strain conferred partial protection on the *ΔyopM-1* mutant in spleen after d 2 in the co-infection experiment. Interestingly, there was a reciprocal but detrimental effect of the mutant strain on net growth of the parent strain prior to d 3 of infection (Figure 8.12). This likely is a distinct phenomenon, as it happened in both liver and spleen. We speculate that resident and early-responding inflammatory cells are stimulated in the focus of infection by pro-inflammatory cytokines induced in expression by the *ΔyopM-1* strain (159), and these cells have heightened anti-bacterial activity that affects both *Y. pestis* strains in the co-infection.

H. The molecular targets of YopM

In mice infected with the *ΔyopM-1* mutant, inflammatory DCs were recruited and retained by spleen (Figure 8.9). In contrast, PMNs were captured in similar numbers by the two strains in spleen (Figure 7.1). These findings imply that YopM affects recruitment mechanisms in spleen, which are distinct between PMNs and inflammatory monocytes

(the circulating precursors of inflammatory DCs). The greatest distinction between the two cell types in the recruitment process lies in the chemokines that bind corresponding GPCRs.

Two prominent chemokines that elicit migration of monocytes but not PMNs are CCL2/MCP-1 and CCL5/RANTES, which are produced by cytokine-stimulated platelets, endothelial cells, mast cells and resident macrophages (85, 151, 168, 236, 293, 351) as well as stimulated PMNs (305). Current evidence points toward the signaling pathway of CCR2, the receptor for CCL2/MCP-1, CCL7/MCP-3, and CCL13/MCP-4 (85) as one of the major molecular target of YopM. In our studies, absence of CCR2 was sufficient to relieve the growth defect of *ΔyopM-1 Y. pestis* (Figure 8.5). Inflammatory DCs, which we found to be selectively accumulated in spleens infected with *ΔyopM-1 Y. pestis*, are defective for recruitment to spleen in CCR2$^{-/-}$ mice (Figure 8.9 and 8.10). YopM could indirectly influence production of chemokines that signal through CCR2 in spleen by downregulating expression of cytokines such as IL-1β and TNFα (159) that activate endothelial cells (196, 271) or by directly downregulating a cell biological pathway that leads to chemokine expression.

Our recent mRNA expression analysis also supports the importance of the CCR2 signaling pathway in YopM-mediated virulence. Harvested 1 hour after high-dose IV infection, splenic CD11b^{+}Ly6G^{-}CD5^{-} macrophages were purified by magnetic beads, and their mRNA was subjected to microarray analysis. We found that the expression of CCL2/MCP-1 and CCL3 in the *ΔyopM-1* strain infection was higher than that in parent strain infection. This difference was even larger when we analyzed those mRNA samples by quantitative real-time RT-PCR. (Done by Tanya Myers and Annette Uittenbogaard,

data not shown).

There are new findings about the molecular targets of YopM in host cell cytosol. Reported by two independent groups, YopM was confirmed to bind RSK1 through its C-terminal domain (from LRR12 to the C-terminus), and such binding contributes to virulence in a systemic infection model of *Y. pseudotuberculosis* grown at ambient temperature (201, 204).

Because of numerous differences in surface molecules expressed by *Y. pseudotuberculosis* and *Y. pestis* grown at 26°C (e.g., the former has flagella and the latter does not), the cell-biological context in which YopM acts will be different in infections by the two *Yersinia* species. We do not yet know whether this interaction is involved in the CCR2 mediated pathways in spleen discussed earlier.

I. 3 hour pre-induction at 37 °C induces some virulence property of *Y. pestis* to compensate the loss of YopM in the Δ*yopM* strain in the spleen at an early stage of the infection

We observed an interesting phenomenon in spleen when we tried to improve our systemic model by pre-inducing the infecting bacteria, which had been cultured at ambient temperature, for 3 hours at 37°C, the internal temperature of a mammal. Pre-induction initiated the expression of thermo-regulated virulence factors, including the T3SS and Yops. Therefore, the infecting bacteria encountered the microenvironment in the spleen and liver with a status close to that in natural septicemic plague.

The length of time for the pre-induction was decided based on our current understanding of the phenotypic changes of *Y. pestis* during temperature transition.

Once shifted to 37°C, expression of T3SS and Yops, encoded by the virulence plasmid pCD1, is upregulated. The injectisomes start to be assembled and the synthesis of Yops is upregulated, probably via thermoinduction of the pCD-encoded transcriptional activator LcrF (6, 226). *yopM* is one of genes expressed at the highest level discovered among the components of the T3SS during thermoregulation (226).

Another important factor regulated by temperature is the F1 pilus capsule, which contributes to the ability of *Y. pestis* to block uptake by phagocytes in concert with the T3SS. The anti-phagocytosis function of the F1 capsule was seen only after 4-5 h pre-induction at 37°C (89) but the phagocytosis-resistance was gained by ambient temperature-grown *Y. pestis* 3-5 h after temperature shifting (21, 63) and correlated with detectable production of V antigen (i.e., LcrV a component of the T3SS) (21) .

Therefore, we chose 3 hours for the pre-induction because the T3SS would be strongly expressed, the anti-phagocytosis function of the F1 capsule would not be strong and the bacteria could efficiently bind to host cells and delivers Yops. The idea was to maximize the early delivery of Yops and (hopefully) produce a stronger YopM phenotype that could be analyzed earlier than d 2 of infection.

Although the growth limitation of the *ΔyopM-1* mutant strain was retained in the infection with the pre-induced bacteria, its appearance was postponed by the 3 hours pre-induction from d 2 p.i. to d 3 p.i., accompanied by similarly delayed YopM-associated influx of MDMs and iDCs into spleen (Figure 9.1). Influx of PMNs into spleen was not affected by the pre-induction. Meanwhile, the effects of YopM on the dynamics of infection and the recruitment of relevant leukocytes in liver were not affected by this pre-

induction (Figure 9.1). Further, the pre-induction showed very little effect on the lethality of the *ΔyopM-1*mutant strain (Table 3.1), or on the pattern of bacterial growth in PMN-ablated (Figure 9.2) or CCR2-KO mice (Figure 9.3).

The observation that the pre-induction could relieve the growth defect of the *ΔyopM-1* mutant in spleen on day 2 p.i. therefore indicated that the temperature transition of *Y. pestis* induced some early thermo-regulated properties of the infecting bacteria that compromise the immune system in spleen in a manner that is similar to that used by YopM. However, this compensation for the loss of YopM held only until d 2 p.i.. This means that the accumulation of the immune responses specifically evoked by the *ΔyopM-1* mutant, as opposed to the YopM$^+$ strain, eventually overcame the negative effects on host defenses from those unknown thermo-induced properties. After d 2 p.i., the infection dynamics of pre-induced *Y. pestis* were similar to those of ambient temperature-grown bacteria. This observation supported our conclusion that different immune responses were responsible for the control of *ΔyopM-1* mutant in spleen and liver.

The entire genome of *Yersinia pestis* has been studied by DNA microarrays to characterize global regulatory changes during temperature transition (226). 235 chromosomal genes and open reading frames (ORFs) were thermally upregulated and 274 were thermally downregulated, most of which are related to the metabolism of the bacteria. The changes of these genes may influence the growth of the bacteria but would not obviously affect the modulation of host immune system.

Fifty one, four, and thirteen ORFs on major virulence plasmids, pCD1, pPCP, and pMT, respectively, were thermoinduced. These genes are strongly induced by the temperature transition, for example, the *caf* operon encoding the F1 capsule components and the

transcriptional regulator (*caf1R*) became upregulated by 100-fold at 10 h and is the strongest upregulation value in the entire genome. However, the only immunomodulatory effect of F1 capsule documented so far is to activate peritoneal macrophages (297). The activated macrophages should control the growth of *Y. pestis*. It is unlikely that thermoinduced expression of F1 capsule would compensate the loss of YopM in *ΔyopM Y. pestis*.

LPS is a potential candidate to explain this compensation. LPS is found in the outer membrane of Gram-negative bacteria, acts as an endotoxin and elicits rapid and strong innate immune responses in animals. LPS consists of three portions: O-antigen, core oligosaccharide and lipid A. O-antigen is a repetitive glycan polymer attached to the core oligosaccharide, and comprises the outermost domain of the LPS molecule. The presence or absence of O chains determines whether the LPS is considered rough or smooth, terms that derive from the appearance of colonies on agar medium. Full-length O-chains would render the LPS smooth, whereas the absence or reduction of O-chains would make the LPS rough (267). *Y. pestis* has a rough-type LPS that lacks an O-specific chain (301), which favors efficient plasminogen activation by Pla (165). The lipid A component is a phosphorylated glucosamine disaccharide decorated with multiple fatty acids. These hydrophobic fatty acid chains anchor the LPS into the bacterial membrane. The lipid A domain is the endotoxic part of LPS and is responsible for much of the toxicity of Gram-negative bacteria. When bacterial cells are lysed by the immune system, fragments of membrane containing lipid A are released into the circulation, causing fever, diarrhea, and possibly fatal endotoxic shock (also called septic shock). Lipid A interacts with the host LPS receptor complex consisting of TLR4 and its coreceptor MD-2 to induce cellular

responses.

The number and length of acyl side chains are critical for TLR4 signaling in humans and mice. Hexa-acylated Lipid A maximally stimulates immunological responses, whereas altering the number or length of the attached fatty acids reduces the magnitude of the signal (215). Lipid A of *Y. pestis* differs in the degree of acylation, depending on the temperature at which *Y. pestis* is grown. The lipid A obtained from bacteria cultivated at ambient temperature is normally a typical hexa-acylated LPS, which is a strong activator for the TLR-4 mediated signaling pathway for TNF-α production in macrophages.

TNF-α, a cytokine involved in systemic inflammation, is mainly produced by macrophages, but also by a broad variety of other cell types including TipDCs. TNF-α is a multi-functional cytokine which is able to activate macrophages, to induce apoptotic cell death, and to inhibit tumorigenesis and viral replication. It is also a potent chemoattractant for PMNs, and helps them to stick to the endothelial cells for migration.

After the temperature transition from 26°C to 37°C, *Y. pestis* immediately begins to produce LPS with tetra-acylated Lipid A, which is not only nonstimulatory for TLR4 but also acts as an antagonist for the stimulatory hexa-acylated form of LPS (91, 223). It is also reported that tetra-acylated LPS (37°C) can inhibit stimulation of DCs not only via TLR4 signaling but also via TLR2 and TLR9 (330).

The change of LPS from the hexa-acylated to the tetra-acylated form occurs rapidly after the temperature transition. The modification of Lipid A stimulated by a 3-h pre-induction might not seem like much, but the TLR-mediated anti-bacterial response is potent: *Y. pestis* that is modified to stably produce hexa-acylated due to a plasmid-borne E. coli acyltransferase is completely avirulent (223). We hypothesize that the

downregulation of cytokine and chemokine production caused by the inhibition of TLRs via tetra-acylated Lipid A favors the growth of the *ΔyopM-1* mutant in spleen before d 3 p.i..

J. Current Model of the YopM virulence Mechanism

a) Spleen and liver respond differently to YopM

Due to difficulty in separating leukocytes from hepatocytes, the immune responses to *Y. pestis* in liver has not been studied as much as in spleen. In our systemic plague studies, we found that spleen and liver respond to *Y. pestis* infection differently with regard to recruitment of NK cells (Figure 4.1) and pDCs (Figure 5.1) as well as $Ly6G^-CD11b^+$ MDMs (Figure 8.1). Meanwhile, in contrast to spleen, liver did not respond with differential inflammatory DC recruitment in mice infected with parent and *ΔyopM Y. pestis* (Figure 8.9), and the parent strain did not complement the *ΔyopM* mutant in trans after d 2 p.i. in liver (Figure 8.12). These findings suggest that YopM does not exert a dominant effect on chemokine pathways in liver; or, that YopM's effect on chemokine pathways is redundant for recruitment of inflammatory cells. The importance of CCR2 for recruitment of cells into spleen but not liver during systemic plague and a selective inhibitory effect of $YopM^+$ *Y. pestis* on this recruitment may explain our previous finding that NK cells, which are also recruited via CCR2 (190, 250), are differentially recruited to spleen by the parent and YopM- strains, whereas there is no difference in recruitment of NK cells by the two *Y. pestis* strains in liver (Figure 4.1).

In the spleen, the blood-borne pathogens leave the bloodstream and enter the external rim of the white pulp through a transit area called the marginal zone and reach the venous

sinus of the red pulp from the penicillar arteries that form terminal branches of the central arterioles. The marginal zone contains a large number of resident cells including macrophages and DCs. Two subsets of macrophages, marginal zone-macrophages and marginal-zone metallophillic macrophages, can be found there. Marginal zone-macrophages form the outer macrophage ring and express specific ICAM-3 grabbing nonintegrin-related 1 (SIGNR1), a C-type lectin, and macrophage receptor with a collagenous structure (MARCO), a type I scavenger receptor. Marginal-zone metallophillic macrophages are close to the white pulp to form the inner macrophage ring. The adhesion molecule sialic-acid-binding immunoglobulin-like lectin 1 (SIGLEC1) is present on the surface of these cells. Marginal zone B cells and DCs are located between these two rings (Figure 10.7) (205).

In addition to TLR-4, the specific receptors on those macrophages play a critical role in the trapping of blood-borne pathogens. The SIGNR1 and MARCO on marginal-zone macrophages synergistically mediate uptake of pathogens through recognition of their surface molecules, such as mannosylated lipoarabinomannan on the surface of *Mycobacterium tuberculosis*. SIGLEC1 on the marginal-zone metallophilic macrophages can bind sialic-acid residues at the cell surface of some pathogens, which may concentrate blood-borne pathogens in this area, leading to their subsequent clearance through phagocytosis (205). In response to the ingested pathogens, these macrophages produce different proinflammatory cytokines, e.g., IFN, TNF and IL-1. In the red pulp, macrophages actively migrate in and out of the venous sinuses and phagocytose pathogens they encounter there.

Liver structure, function, and response to infection are distinct from those in spleen

(145, 232). As the largest reticulo-endothelial cell network in the body, the liver is a major source of many components of the innate immune response including acute-phase and complement proteins as well as inflammatory cytokines and chemokines. The liver receives a dual blood supply from the hepatic portal vein and hepatic arteries. Supplying approximately 75% of the liver's blood supply, the hepatic portal vein carries venous blood drained from the spleen, gastrointestinal tract, and its associated organs. The hepatic arteries supply arterial blood to the liver, accounting for the remainder of its blood flow. The reticulo-endothelial cell network in liver displays a sinusoidal structure with fenestrated, discontinuous endothelium and serves as a mixing chamber for the oxygen-rich blood from the hepatic artery and the nutrient-rich blood from the portal vein.

Endothelial cells, KCs, hepatic stellate cells, Pit cells and some DCs are located in sinusoids and called as "hepatic sinusoidal cells". As shown in Figure 10.8, the endothelial cells have pores or fenestrations through which solutes can apparently move freely into the perisinusoidal space.

Unlike most of the splenic macrophages which are localized in the marginal zone and splenic cords and trap pathogens that filter out of the central arterioles, KCs are located within the lumen of the sinusoids (145). KCs are the first defense line to be exposed to pathogens that come with blood. Actually, liver sinusoidal KCs constitute 80~90% of the tissue macrophages in the body. As the resident macrophages, KCs are the principal liver cells for phagocytosis, antigen presentation, and production of pro-inflammatory cytokines.

KCs express a variety of TLRs, including TLR4 which is involved in uptake and clearance of LPS and production of cytokines, as well as TLR2 that leads to production

of pro-inflammatory cytokines (145). In response to LPS or some pro-inflammatory bacterial products, KCs are activated and produce large amount of inflammatory mediators including cytokines (e.g. TNF-α and IFN-α), ROS and NO, and chemokines (CCL2/MCP-I, IL-8), while KCs in the non-inflamed liver secrete anti-inflammatory mediators, such as IL-10 and TGF-β (161, 258).

The interaction between KCs and PMNs is prominent in the response to bacterial infection (117, 119, 141). KCs themselves are not potent antibacterial cells, but they bind bacteria avidly and present them to PMNs for killing (117-119, 182). In response to stimulation of TLRs, KCs do produce IL-1β, IL-6, and TNFα (119) that activate endothelial cells to produce CCL2/MCP-1. KCs also produce CCL3/MIP-1α, which recruits DC precursors to liver (364).

b) Model of ambient-temperature grown YopM-mediated immune modulation in spleen

As shown on Figure 10.7, our findings for spleen in systemic plague are incorporated to generate a model for the sequence of events in wt mice. ❶, the IV-injected ambient-temperature grown *Y. pestis* reach the marginal zone sinus and pass through discontinuous endothelium and interact with resident DCs and macrophages. Initially, hexa-acylated lipid A (flea version) stimulates resident cells through TLR4-mediated pathways (223, 261) and creates a local pro-inflammatory environment. Meanwhile, the phagocytosis resistance and other inhibitory effects on host defense caused by major virulence factors, such as T3SS, Caf1, and PsaA, are not manifested yet because the expression of these genes has not been fully induced. *Y. pestis* could bind to and be

ingested by resident macrophages and DCs through Pla and Ail, the adhesions expressed at both 26 ^{o}C and 37 ^{o}C. Within the phagocytosome, the bacteria inhibit acidification (255) and may have access to the cytosol (254), where they potentially promote proinflammatory cytokine expression through stimulation of intracellular molecular pattern receptors such as NOD1 and NOD2 (213, 298). This intracellular incubation step is critical for the growth of the *Y. pestis in vivo* because removal of these resident phagocytes by clodronate caused the failure of both strains to multiply. The thermoregulated genes of *Y. pestis* start to be expressed while the bacterium resides intracellularly and support the survival of bacterium by dampening the bactericidal function of those phagocytes. Once released, the bacterium would be fully adapted to 37 ^{o}C and able to resist phagocytosis by PMNs.

❷, YopM delivered to resident cells by extracellular *Yersinia* would curtail expression of proinflammatory cytokines and some chemokines that may already exist and would have been activating cells locally or serving as homing factors for inflammatory monocytes. This downregulation constitutes the induction phase of YopM's pathogenic effect. It is the outcome of molecular cell biological interactions mediated by YopM within resident cells that have yet to be defined. If the infecting *Y. pestis* are pre-induced for 3 hours, their lipid A changed from the hexa-acylated form to the tetra-acylated form, which is not only nonstimulatory for TLR4 but also acts as an antagonist for the stimulatory hexa-acylated form of LPS. Pre-induction is assumed to inhibit some early immune responses that overlap with those compromised by YopM in spleen because the pre-induction compensates for the loss of YopM in the very early stage of the infection of the *ΔyopM* mutant in spleen.

❸, before YopM carries out its inhibitory effects on the resident cells, the initial proinflammatory condition would have attracted PMNs and inflammatory monocytes (iMOs)/DCs from blood by activating local endothelial cells and more of these cells would have been recruited from the bone marrow. They are recruited in parallel, through separate chemokine pathways.

❹, YopM compromises the accumulation of $CCR2^+$ iDCs in spleen; however, PMNs are recruited similarly whether YopM is present or absent from the infecting *Y. pestis*. Therefore, the initial capture and rolling steps mediated on endothelial cells by selectins are unlikely affected by YopM because those selectins interact with both PMNs and inflammatory monocytes. The defective influx of $CCR2^+$ iMOs and $CCR2^+$ NK cells into spleen infected by the YopM-containing parent strain could result from YopM's inhibitory effect on activation of the endothelial cells (ECs) and nearby resident cells to express chemokines such as CCL2/MCP-1 (❷) that support recruitment of $CCR2^+$ cells to the focus of infection.

If the infecting *Y. pestis* strain lacks YopM, $CCR2^+$ iMOs develop into $CCR2^+$ iDCs that persist in spleen and reduce net growth of the bacteria by releasing NO (❺). Neither the recruitment nor activation of PMNs, in which the signal from CXCL1(❷) may be critical, is affected in spleen by the presence of YopM in the infecting bacteria, which indicates that YopM does not modulate the innate immune responses in spleen through affecting PMNs. Although YopM inhibits the recruitment of NK cells into spleen, NK cells are not critical in the YopM mediated virulence (❺).

c) Model of ambient-temperature grown YopM-mediated immune modulation in liver

236

Figure 10.8 describes a possible model for the sequence of events in liver of systemic plague of WT mice. ❶, the input ambient-temperature grown *Y. pestis* reach the sinusoid of liver via the blood and interact with KCs in liver. The hexa-acylated lipid A of the infecting bacteria may induce early pro-inflammmatory responses by stimulating KCs through the same mechanism as in splenic resident macrophages. However, after pre-induction, YopM injected into host cells does not compromise this early pro-inflammatory response (❷) because the growth limitation of the *ΔyopM* mutant in liver was maintained despite the dampening effect on pro-inflammmatory responses due to the nonstimulatory LPS with tetra-acylated Lipid A.

Although YopM uses the same molecular mechanisms to modulate immune responses in spleen and liver, the affected pathways have different cellular components between spleen and liver. However, the global systemic responses to the infecting *Y. pestis* is universal and YopM plays no important role in these responses (❸).

❹, CCR2$^+$ PMNs, CCR2$^+$ iMOs/iDCs and CCR2$^+$ NK cells are recruited similarly into liver between the parent and *ΔyopM Y. pestis*, indicating that the recruitment of those cells is independent of the CCR2-CCL2 signaling pathway. However, PMN function is undermined by YopM in some CCR2-related way, perhaps indirectly at the level of an interaction of PMNs with KCs or endothelial cells. This is a downstream response to YopM in liver. If YopM is not present in the infecting strain, PMNs reduce net growth of the bacteria (❺) through production of bactericidal compounds probably including ROS and defensins.

K. conclusion

In this study, we used a systemic plague model to identify the cells and pathways that are undermined by the virulence protein YopM of the plague bacterium *Yersinia pestis*. YopM favors the growth of *Y. pestis* through modulating the innate immune responses. Gr1$^+$ cells are required to selectively limit growth of YopM- *Y. pestis*, and the virulence mechanism of YopM involves different subsets of Gr1$^+$ cells in spleen and liver. Gr1$^+$ PMN ablation relieved the growth defect of YopM- *Y. pestis* only in liver, showing that PMNs are critical for controlling growth of YopM- *Y. pestis* in liver but not spleen. In spleen, the Gr1$^+$ CD11b$^+$ CD11c^{lo-int} MAC3$^+$ iNOS$^+$ iDCs are differentially recruited by parent and YopM- *Y. pestis* infections, and their recruitment to spleen from blood was blocked when YopM was present in the infecting strain.

Both Gr1$^+$ PMNs and Gr1$^+$ iDCs express CCR2, the chemokine receptor for CCL2/MCP-1, on their surface and YopM- *Y. pestis* grows as well as the parent strain if mice lack CCR2. Therefore, CCR2 is identified as a critical node in the chemokine communications network that YopM disables. Taken together, the data show that YopM modulates the host immune system by disabling the recruitment of CCR2$^+$ Gr1$^+$ iDCs into spleen, while undermining the function of CCR2$^+$ Gr1$^+$ PMNs in liver.

Meanwhile, YopM is indispensable for the full virulence of *Y. pestis* in bubonic plague because the absence of YopM significantly increased the LD$_{50}$ in the ID infection model. CCR2 was found to be responsible for controlling growth of YopM- *Y. pestis* in skin, indicating that YopM's molecular targets in skin ultimately act through CCR2 and showing that CCR2-mediated functions are important in host defense against bubonic plague. Thus, the findings provide a framework for focusing future research to identify

YopM's direct molecular targets.

Table 10.1 Differences between NK cells derived from splenocytes in response to IL-12/IL-18 and those derived in the presence of IL-2 or IL-15 （Summarized from References (175, 176)）

	IL12/IL18 treatment	IL2 treatment	IL15 treatment
Cell type(s) produced	NK	NK and NKT	NK and NKT
Expression of Surface NK1.1	None	Yes	Yes
Cytokine production	IFN-γ IL-3 IL-6 TNF	IL-4 and IL-10 IL-5 IL-9 IL-13	none
Cytotoxicity	Strong	weak	weak

Table 10.2 Characteristics of DC subsets

	CD11b+DC (Myeloid DCs)	CD8+DCs (Lymphoid DCs)	B220+DCs (Plasmacytoid DCs)
Early Haematopoietic Precursors	Although there are myeloid-restricted and lymphoid-restricted precursors, they can develop to all of the three subsets (299)		
Factors that Promote Differentiation	Transcription Factor RelB (361)	Transcription Factor Id2 (122) and ICSBP (IFN consensus sequence binding protein) (5)	Flt3L (68) (CD135 ligand)
Chemokines or their Receptors	CCR1 and 5 (recognize MIP-1α from Kuffer Cells) (364) CCL19 and CCL21(69) CCL3	CCL19 and CCL21(69)	CXCR3 (68), CCR7 (244) CCR1, CCR2 and CCR5 (68)
Distribution in Spleen	Marginal zone (migrate into T-cell zones on stimulation with microbial products) (299)	T cell zone	T cell zone and scattered in marginal zone and red pulp (68)
Maturation Markers	CD80, CD86, CD40, MHC-II (187, 295)		
Major Surface Markers	High CD11c CD11b(299)	High CD11c CD8 CD205(299)	Moderate CD11c B220 (CD45RA) Ly6C (68)
Function in Innate Immunity	Induce a TH2-biased response (299) IL-12p40 and TNF-α ?(153)	Produce IL-12 and IFN-γ to induce a TH1-biased cytokine response (16) IL-12p40 and TNF-α (153)	Produce IFN-α and β (upon bacterial or viral infection) (68) IFN-γ (upon IL-4 stimulation) (324) Activate NK cells through GITRL (124)

Table 10.3 Characters of PMN subsets

	PMN-I	PMN-II	PMN-N
Source	MRSA[a]- resistant hosts (SCIDbg mice with mild SIRS[b])	MRSAsusceptible hosts (SCIDbg mice with severe SIRS)	SCIDbg mice without SIRS
Shape of the nucleus	Multilobular	Ring-form	Round
MPO positive granules in cytosol	High Level	Minimal Level	Minimal Level
Surface Antigen Expression	CD49d$^+$ CD11b$^-$	CD49d$^-$ CD11b$^+$	CD49d$^-$ CD11b$^-$
TLR Expression	TLR 2,4,5 and 8	TLR 2,4,7 and 9	TLR 2,4 and 9
Cytokine Production	IL-12 TNF-α IL-1β	IL-10 TNF-α IL-1β	No
Chemokine Production	CCL3 CXCL1	CCL2 CXCL1	No
H_2O_2 production	Yes	Yes	No
Activate Macrophage	Classically Activated Macrophage (anti-bacteria effector cells)	Alternatively Activated Macrophage (promote fibrosis, wound healing, neovascularization and granuloma formation (336))	No

a. MRSA, methicillin-resistant *Staphylococcus aureus*; b. SIRS, systemic inflammatory response syndrome
All the information comes from reference (340) unless denoted.

Table 10.4 Characteristics of monocytes subsets (Summarized from References (18, 293)

	Ly6C$^+$ (human: CD14$^+$, 90% in circulation)	CX3CR1$^+$ (human: CD16+,10% in circulation)
Chemokine Receptor	CCR2 (ligand: CCL2, 7, 8, 13 and 16) (CCL2 produced by endothelial, fibroblast, epithelial, smooth muscle cells) (85)	CX3CR1 (ligand: CX3CL1/fractalkine: produced by endothelial cells, monocytes, T cells and NK cells)
% in Circulation	50%	50%
Surface Marker at High Level	CD11b, CD62L	MHC-II, CD11c
Size	Large (10-14uM)	Small (8-12uM)
Development	Inflammatory monocyte (highly phagocytic) ↓ DCs, macrophages	Long lived in blood ↓ Steady-state Resident Macrophages and DCs

Common markers of bone marrow and blood monocytes: CD115 (M-CSF-R), CD11b and F4/80 (low)

Figure 10.1 the relationship between YopM and adaptive immunity
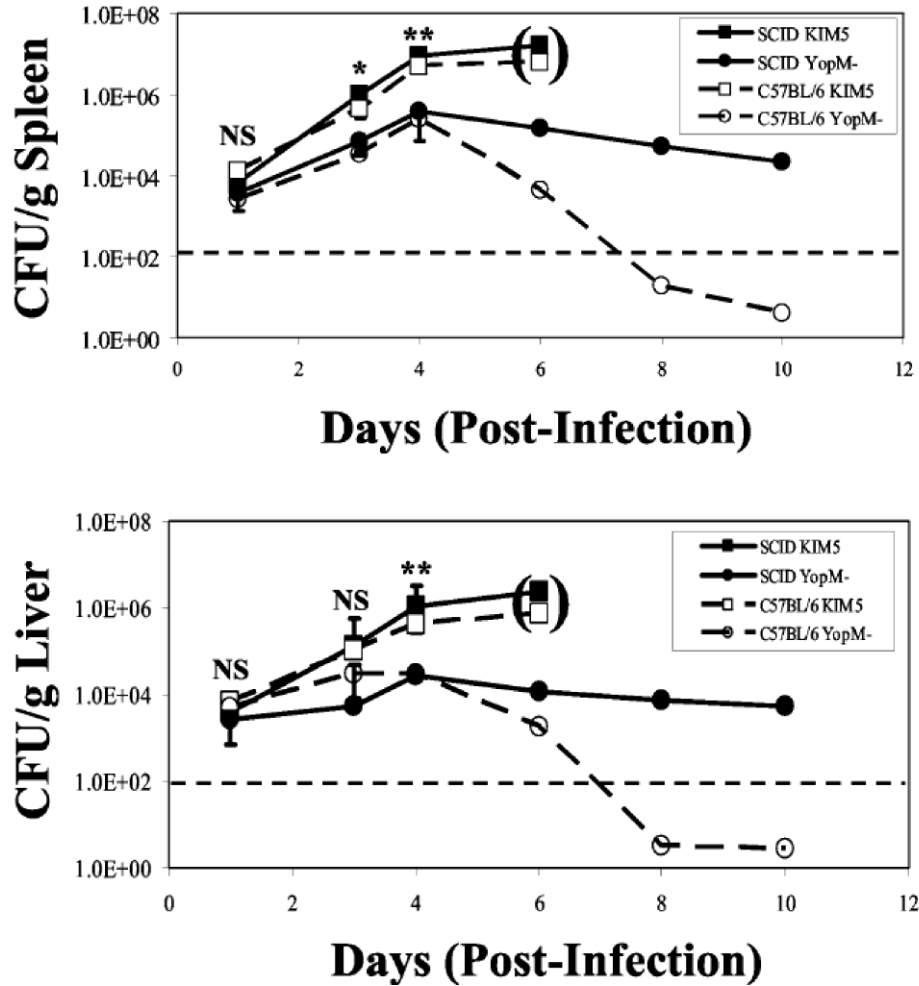
Time course of infection with *Y. pestis* KIM5 and the *ΔyopM-1* mutant in BL/6 and SCID mice. BL/6 mice (open symbols) and SCID mice (solid symbols) were infected with 100 CFU of *Y. pestis* KIM5 (squares) or *Y. pestis* KIM5-3002 (*ΔyopM-1*, circles). A, CFU in spleens and B, CFU in livers. The horizontal dotted lines indicate the lowest numbers of CFU per organ detected with at least 30 CFU per plate. The mice infected with the parent strain KIM5 were all morbid by day 5 and had died several hours prior to preparation for CFU analysis (indicated by the parentheses). (NS, not significantly different; *, $P \leq 0.05$; **, significantly different at $P \leq 0.01$). (159)

Figure 10.2 Previous model of virulence mechanism of YopM
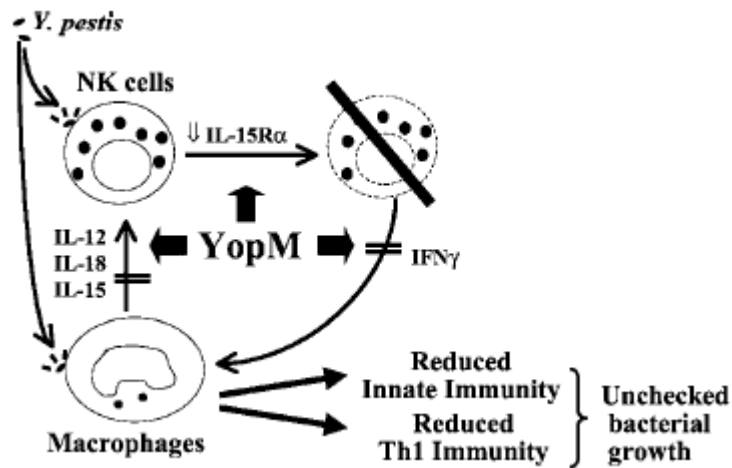
YopM injected into macrophages by the T3SS inhibits the expression of all three major cytokines for NK cell development, IL-12, IL-18, and IL-15. Meanwhile, IL-15R expression on the NK cell surface is also inhibited by the YopM delivered into NK cells. The effects of YopM on both cell types promote systemic depletion of NK cells and compromise the production of IFN-γ by NK cells, which causes deficient activation of macrophages. The growth of the *ΔyopM-1* mutant is limited because of the subsequently reduced innate and Th1 immunity. (159)

Figure 10.3 Leukocyte Extravasation

A.

B.

Neutrophil - Endothelial Cell Ligands
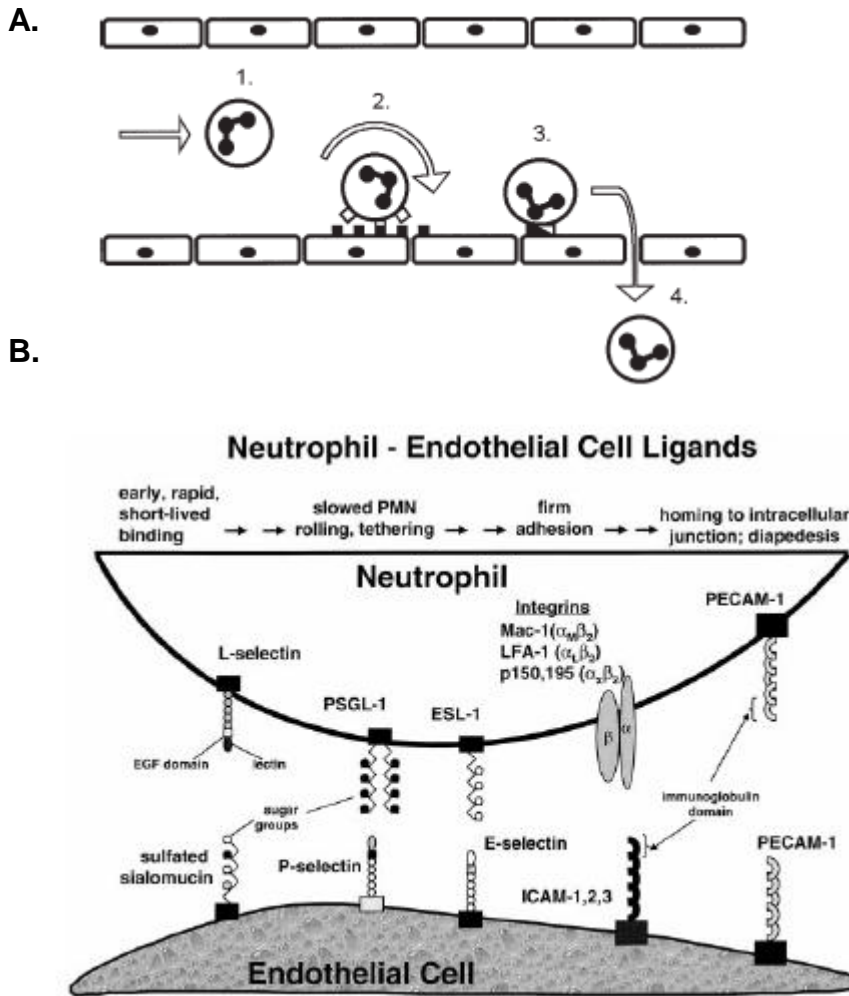
A. the model for leukocyte recruitment (285). Blood flow is from the left to the right as indicated. Free flowing leukocytes (1) are captured by activated endothelial cells and begin to roll along the vessel wall on endothelial selectins (2). The rolling leukocytes sense chemoattractive signals, i.e. chemokines, and become activated for firm adherence to the endothelium mediated by $b2$ integrins (3). Firmly adhering leukoctyes transit into the extravasacular space through intercellular endothelial gaps (4), where they migrate along chemoattractive gradients to the inflammatory focus. B. adhesion molecules and respective ligands involved in transendothelial migration of PMNs (352). PSGL-1, P-

selectin glycoprotein ligand-1; ESL-1, E-selectin ligand 1; LFA-1, lymphocyte associated function antigen-1; PECAM, platelet-endothelial cell adhesion molecule, Mac-1, macrophage antigen-1.

Figure 10.4 Phenotype of monocyte subsets
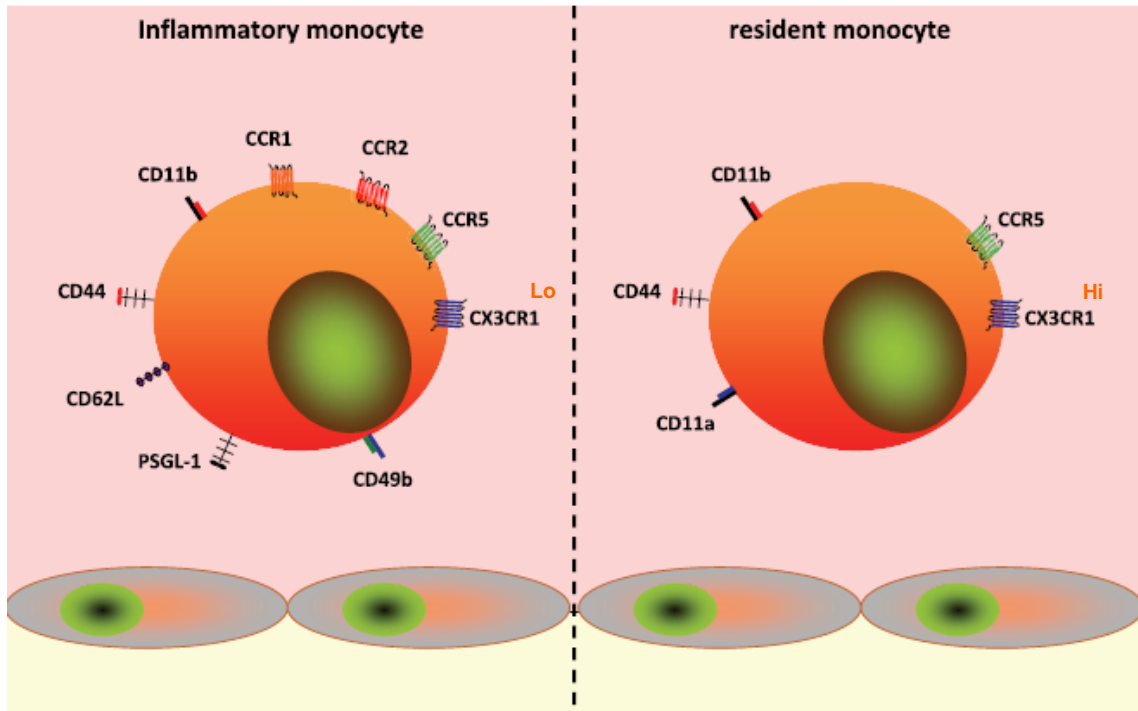
Inflammatory (left) and resident (right) monocytes differentially express cell adhesion molecules and chemokine receptors, thus implying distinct recruitment mechanisms(305).

Figure 10.5 Development of monocytes (Summarized from Reference (18, 293)

A. Spleen

| Bone Marrow |

| Common myeloid progenitor cells (**CMP**) (CD117$^+$ Lin$^-$(linage associated marker, e.g. CD3, NK1.1)) |

MDP (macrophage-DC

Steady state

Inflammation

Ly6C$^+$

| **Ly6C$^+$** (after depletion of circulating monocytes, 3-4 day to replenish) | **CX3CR1$^+$** (after depletion of circulating monocyte , 7 day to replenish) |

| **Blood** |

| **Spleen** |

recruited by CCL2-CCR2

MDP

Local Pre-DCs

| **TipDCs** **macrophage** |

| **Resident macrophages and DCs** |

B. Skin

| Steady State |

| Tissue damage (e.g. UV light, inflammation) Need circulation myeloid precursor |

| **Local pre-DC** |

Ly6C$^+$

| **LCs** (Langerhans cells) |

| **LCs** |

| **F4/80$^+$ macrophage** |

Inflammation induces the release of MCP-1, which binds to skin-draining lymph nodes and recruits Ly6C$^+$CCR2$^+$ monocytes

Figure 10.6 The signaling pathways activated upon CCL2/MCP-1 ligation to CCR2
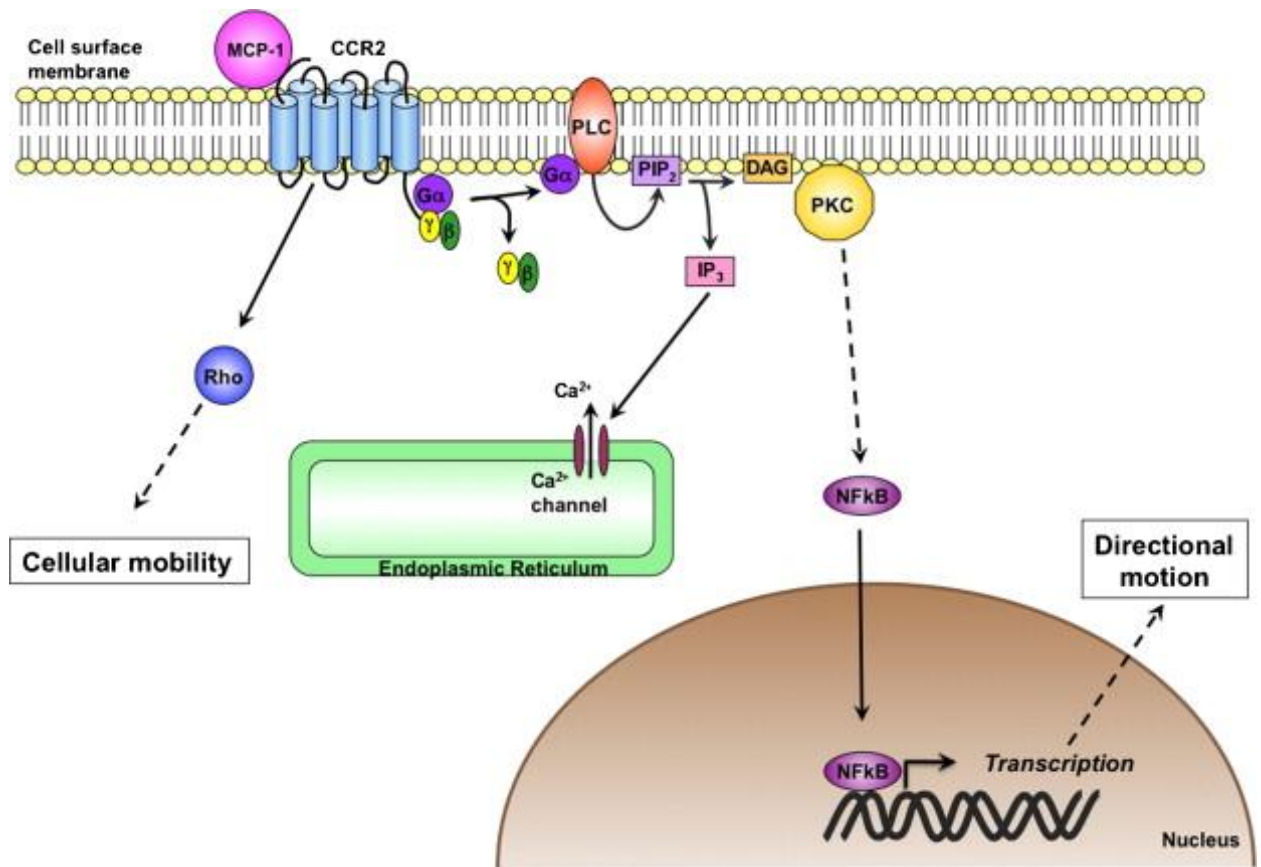
CCR2 is a GPCR. Interaction between CCL2 and CCR2 activates the G protein and induces the PLC-IP3 pathway, which stimulates intracellular calcium release. In addition to inducing IP3, PLC causes the activation of PKC that activates PKC-dependent NF-κB. NF-κB upregulates several genes that produce directional cell motion. Rho is also activated, which results in induction of cell mobility. DAG, diacylglycerol; IP3, inositol trisphosphate; NF-κB, nuclear factor-kappa B; PIP_2, phosphatidylinositol-bisphosphate; PKC, protein kinase C; PLC, phospholipase C. (207)

Figure 10.7 Model for how YopM affects cells and cytokines in systemic plague caused by *Y. pestis* (Spleen)
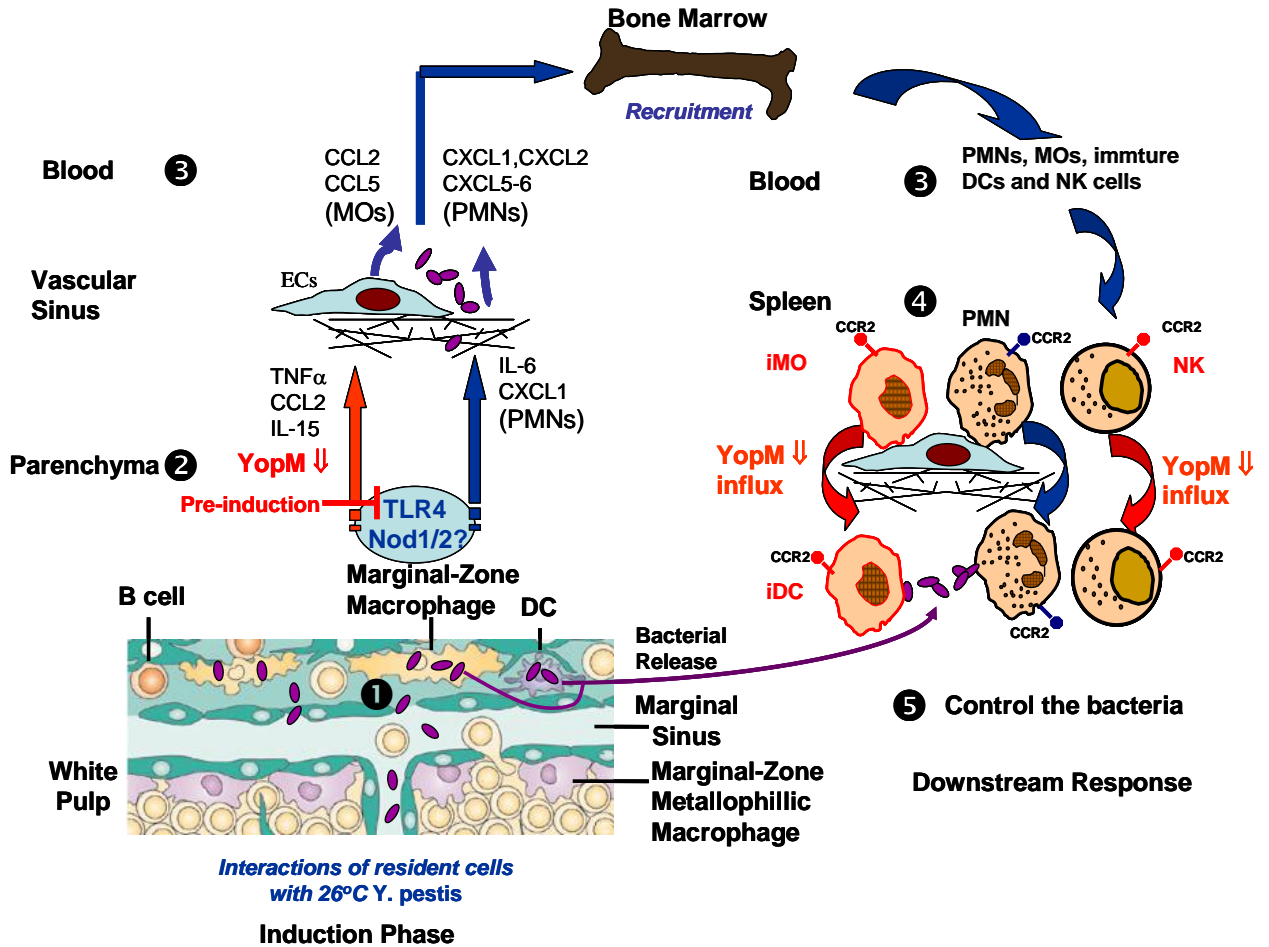
The flow of events following IV infection of WT mice is indicated by the numbers. Red arrows and text denote YopM-specific effects. See the Discussion for a narrative description. (The cartoon of the structure of the spleen marginal zone is modified from reference (205))

Figure 10.8 Model for how YopM affects cells and cytokines in systemic plague caused by *Y. pestis* (Liver)
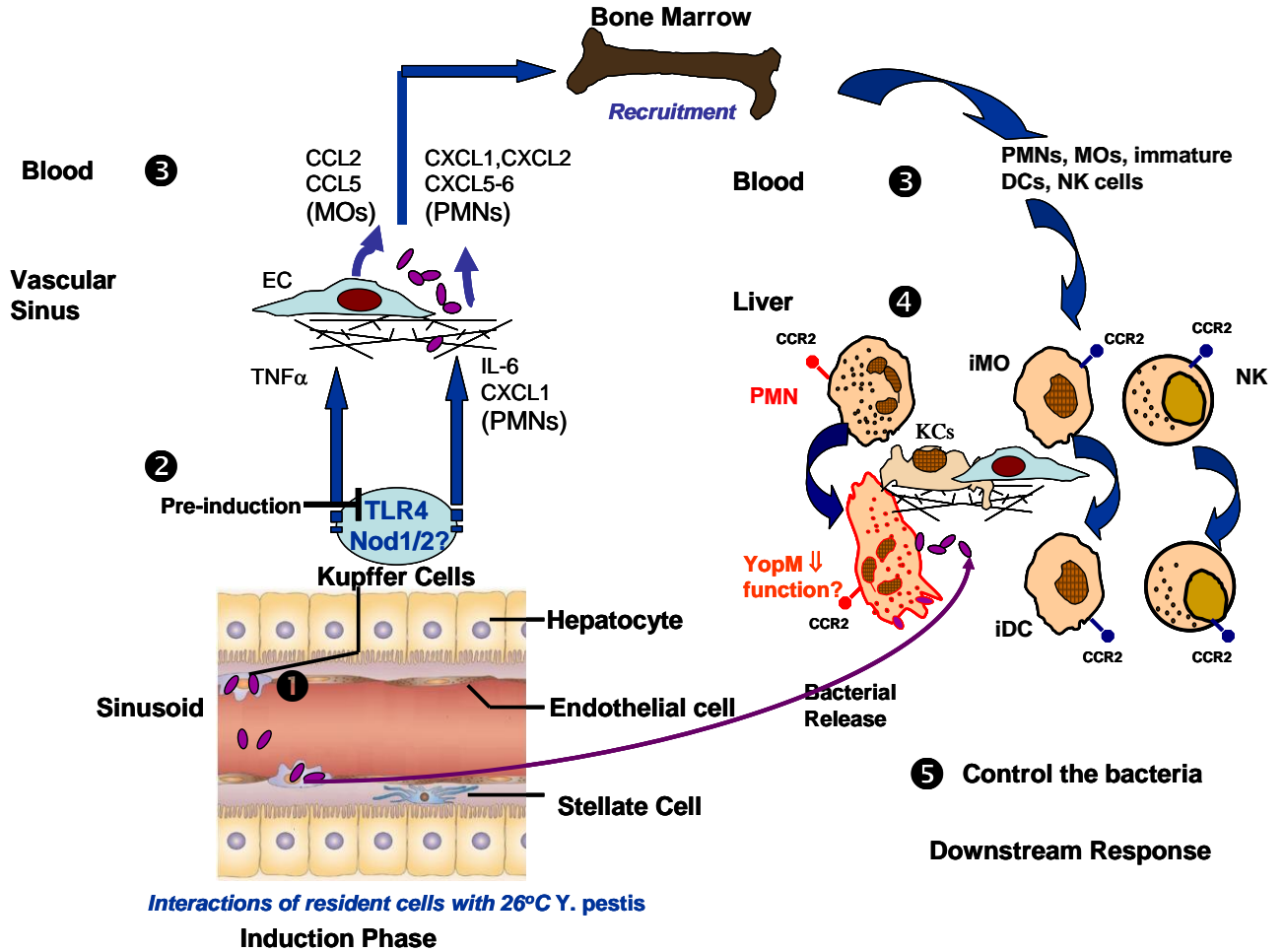
The flow of events following IV infection of WT mice is indicated by the numbers. Red arrows and text denote YopM-specific effects. See the Discussion for a narrative description. （The cartoon of the structure of the sinusoid in liver is modified from reference (252)）

Copyright © Zhan Ye 2010

APPENDICES

(LIST OF ABBREVIATIONS)

ABC   ATP-binding cassette

Ail   attachment-invasion locus

APC   allophycocyanin

apoB   apolipoprotein B

CaM   calmodulin

Cb   carbenicillin

CCL2   Chemokine (C-C motif) ligand 2

CCR2   Chemokine (C-C motif) Receptor 2

CFU   colony forming unit

cNOS   constitutive nitric oxide synthase

DAF   4-amino-5-methylamino-2',7'-difluorofluorescein

DC   Dendritic cell

DCF   2',7'-dichlorofluorescein

DCFDA   2',7'-dichlorodihydrofluorescein diacetate

EMA   ethidium monoazide

ERK   extracellular signal-related kinase

ESL-1   E-selectin ligand 1

F1 protein   fraction 1 proteins

FITC   fluorescein isothiocyanate

Fur   ferric uptake regulation

GAP	GTPase-activating protein
GEF	Guanine nucleotide-Exchange Factors
GITRL	ligand for the glucocorticoid-induced TNF receptor
GM-CSF	granulocyte–macrophage colony-stimulating factor
GPCR	G protein-coupled receptor
HIB	Heart Infusion Broth
hms	hemin storage locus
HPI	high-pathogenicity island
ICAM-1	intercellular adhesion molecule-1
ID	intradermal
IKK	inhibitor-κB kinase
IN	intranasal
IP	intraperitoneal
irp	iron-regulated proteins
KC	Kupffer cells
KO	knock-out
LcrV	low calcium response protein V
LFA-1	lymphocyte associated function antigen-1
LPS	lipopolysaccharide
LRR	leucine-rich repeat
Mac-1	macrophage antigen-1
MaFIA	Macrophage Fas-induced apoptosis
MAPK	mitogen-activated protein kinase

MARCO   macrophage receptor with a collagenous structure

MCP-1   Monocyte Chemoattractant Protein-1

mDC   myeloid DC

MDM   inflammatory monocytes/DC, myeloid DC and macrophage

MDP   macrophage-DC progenitor

MDR   macrophage disappearance reaction

MFI   mean fluorescence intensity

MHC   major histocompatibility complex

MKK   mitogen-activated protein kinase kinase

MT   Murine Toxin

NF-κB   nuclear factor-κB

NK cell   natural killer cell

NO   nitric oxide

NOS   NO synthase

ORF   open reading frames

PC   peritoneal cell

pCD1   Calcium Dependence

pDC   plamacytoid DC

PE   phycoerythrin

PECAM   platelet-endothelial cell adhesion molecule

pgm   the pigmentation locus

p.i.   post infection

Pim   pesticin immunity protein

Pla   plasminogen activator

Plg   plasminogen

Pln   plasmin

PMA   Phorbol Myristate Acetate

PMN   polymorphonuclear leukocyte

pPCP1   Pesticin, Coagulase, Plasminogen activator

PRK2   protein kinase C-related kinase 2

PSGL-1   P-selectin glycoprotein ligand-1

Pst   bacteriocin pesticin

PTP   protein tyrosine phosphatase

RANTES   regulated on activation, normal T cell expressed and secreted

RFU   relative fluorescence unit

ROS   Reactive Oxygen Species

RSK1   ribosomal S6 protein kinase 1

SC   subcutaneous

SCID mice   severe combined immunodeficiency mice

SIGLEC1   sialic-acid-binding immunoglobulin-like lectin 1

SIGNR1   specific ICAM-3 grabbing nonintegrin-related 1

TBA   tryptose blood agar

TCR   T cell antigen receptor

TLR   Toll-like receptor

TNF-α   tumor necrosis factor-α

T3SS   Type III Secretion System

WT   wild-type

Yap   *Yersinia* Autotransporter Protein

Yop   *Yersinia* outer protein

YSA   *Yersinia* selective agar

Ysc   Yop secretion

REFERENCES

1.   **Achtman, M., G. Morelli, P. Zhu, T. Wirth, I. Diehl, B. Kusecek, A. J. Vogler, D. M. Wagner, C. J. Allender, W. R. Easterday, V. Chenal-Francisque, P. Worsham, N. R. Thomson, J. Parkhill, L. E. Lindler, E. Carniel, and P. Keim.** 2004. Microevolution and history of the plague bacillus, Yersinia pestis. Proc Natl Acad Sci U S A **101:**17837-17842.

2.   **Achtman, M., K. Zurth, G. Morelli, G. Torrea, A. Guiyoule, and E. Carniel.** 1999. Yersinia pestis, the cause of plague, is a recently emerged clone of Yersinia pseudotuberculosis. Proc Natl Acad Sci U S A **96:**14043-14048.

3.   **Agar, S. L., J. Sha, S. M. Foltz, T. E. Erova, K. G. Walberg, T. E. Parham, W. B. Baze, G. Suarez, J. W. Peterson, and A. K. Chopra.** 2008. Characterization of a mouse model of plague after aerosolization of Yersinia pestis CO92. Microbiology **154:**1939-1948.

4.   **Aichele, P., J. Zinke, L. Grode, R. A. Schwendener, S. H. Kaufmann, and P. Seiler.** 2003. Macrophages of the splenic marginal zone are essential for trapping of blood-borne particulate antigen but dispensable for induction of specific T cell responses. J Immunol **171:**1148-1155.

5.   **Aliberti, J., O. Schulz, D. J. Pennington, H. Tsujimura, C. Reis e Sousa, K. Ozato, and A. Sher.** 2003. Essential role for ICSBP in the in vivo development of murine CD8alpha + dendritic cells. Blood **101:**305-310.

6.   **Alonso, A., N. Bottini, S. Bruckner, S. Rahmouni, S. Williams, S. P. Schoenberger, and T. Mustelin.** 2004. Lck dephosphorylation at Tyr-394 and inhibition of T cell antigen receptor signaling by Yersinia phosphatase YopH. J Biol Chem **279:**4922-4928.

7.   **Ambati, J., A. Anand, S. Fernandez, E. Sakurai, B. C. Lynn, W. A. Kuziel, B. J. Rollins, and B. K. Ambati.** 2003. An animal model of age-related macular degeneration in senescent Ccl-2- or Ccr-2-deficient mice. Nat Med **9:**1390-1397.

8.   **Anderson, D. M., and O. Schneewind.** 1997. A mRNA signal for the type III secretion of Yop proteins by Yersinia enterocolitica. Science **278:**1140-1143.

9.   **Anderson, D. M., and O. Schneewind.** 1999. Yersinia enterocolitica type III secretion: an mRNA signal that couples translation and secretion of YopQ. Mol Microbiol **31:**1139-1148.

10. **Anderson, G. W., Jr., S. E. Leary, E. D. Williamson, R. W. Titball, S. L. Welkos, P. L. Worsham, and A. M. Friedlander.** 1996. Recombinant V antigen protects mice against pneumonic and bubonic plague caused by F1-capsule-positive and -negative strains of Yersinia pestis. Infect Immun **64:**4580-4585.

11. **Andrews, G. P., D. G. Heath, G. W. Anderson, Jr., S. L. Welkos, and A. M. Friedlander.** 1996. Fraction 1 capsular antigen (F1) purification from Yersinia pestis CO92 and from an Escherichia coli recombinant strain and efficacy against lethal plague challenge. Infect Immun **64:**2180-2187.

12. **Anisimov, A. P., S. V. Dentovskaya, G. M. Titareva, I. V. Bakhteeva, R. Z. Shaikhutdinova, S. V. Balakhonov, B. Lindner, N. A. Kocharova, S. N. Senchenkova, O. Holst, G. B. Pier, and Y. A. Knirel.** 2005. Intraspecies and temperature-dependent variations in susceptibility of Yersinia pestis to the

bactericidal action of serum and to polymyxin B. Infect Immun **73:**7324-7331.

13. **Anisimov, A. P., L. E. Lindler, and G. B. Pier.** 2004. Intraspecific diversity of Yersinia pestis. Clin Microbiol Rev **17:**434-464.

14. **Arase, H., N. Arase, and T. Saito.** 1996. Interferon gamma production by natural killer (NK) cells and NK1.1+ T cells upon NKR-P1 cross-linking. J Exp Med **183:**2391-2396.

15. **Arase, H., T. Saito, J. H. Phillips, and L. L. Lanier.** 2001. Cutting edge: the mouse NK cell-associated antigen recognized by DX5 monoclonal antibody is CD49b (alpha 2 integrin, very late antigen-2). J Immunol **167:**1141-1144.

16. **Ardavin, C.** 2003. Origin, precursors and differentiation of mouse dendritic cells. Nat Rev Immunol **3:**582-590.

17. **Auffray, C., D. K. Fogg, E. Narni-Mancinelli, B. Senechal, C. Trouillet, N. Saederup, J. Leemput, K. Bigot, L. Campisi, M. Abitbol, T. Molina, I. Charo, D. A. Hume, A. Cumano, G. Lauvau, and F. Geissmann.** 2009. CX3CR1+ CD115+ CD135+ common macrophage/DC precursors and the role of CX3CR1 in their response to inflammation. J Exp Med **206:**595-606.

18. **Auffray, C., M. H. Sieweke, and F. Geissmann.** 2009. Blood monocytes: development, heterogeneity, and relationship with dendritic cells. Annu Rev Immunol **27:**669-692.

19. **Babior, B. M.** 1999. NADPH oxidase: an update. Blood **93:**1464-1476.

20. **Babior, B. M.** 1984. Oxidants from phagocytes: agents of defense and destruction. Blood **64:**959-966.

21. **Bacon, G. A., and T. W. Burrows.** 1956. The basis of virulence in Pasteurella pestis: an antigen determining virulence. Br J Exp Pathol **37:**481-493.

22. **Bacot, A. W., and C. J. Martin.** 1914. LXVII. Observations on the mechanism of the transmission of plague by fleas. J Hyg (Lond) **13:**423-439.

23. **Banchereau, J., F. Briere, C. Caux, J. Davoust, S. Lebecque, Y. J. Liu, B. Pulendran, and K. Palucka.** 2000. Immunobiology of dendritic cells. Annu Rev Immunol **18:**767-811.

24. **Banchereau, J., and R. M. Steinman.** 1998. Dendritic cells and the control of immunity. Nature **392:**245-252.

25. **Barchet, W., M. Cella, B. Odermatt, C. Asselin-Paturel, M. Colonna, and U. Kalinke.** 2002. Virus-induced interferon alpha production by a dendritic cell subset in the absence of feedback signaling in vivo. J Exp Med **195:**507-516.

26. **Barth, M. W., J. A. Hendrzak, M. J. Melnicoff, and P. S. Morahan.** 1995. Review of the macrophage disappearance reaction. J Leukoc Biol **57:**361-367.

27. **Bartoli, C., M. Civatte, J. F. Pellissier, and D. Figarella-Branger.** 2001. CCR2A and CCR2B, the two isoforms of the monocyte chemoattractant protein-1 receptor are up-regulated and expressed by different cell subsets in idiopathic inflammatory myopathies. Acta Neuropathol **102:**385-392.

28. **Bartra, S. S., K. L. Styer, D. M. O'Bryant, M. L. Nilles, B. J. Hinnebusch, A. Aballay, and G. V. Plano.** 2008. Resistance of Yersinia pestis to complement-dependent killing is mediated by the Ail outer membrane protein. Infect Immun **76:**612-622.

29. **Bearden, S. W., J. D. Fetherston, and R. D. Perry.** 1997. Genetic organization of the yersiniabactin biosynthetic region and construction of avirulent mutants in

Yersinia pestis. Infect Immun **65:**1659-1668.

30. **Bearden, S. W., and R. D. Perry.** 1999. The Yfe system of Yersinia pestis transports iron and manganese and is required for full virulence of plague. Mol Microbiol **32:**403-414.

31. **Beck-Schimmer, B., R. Schwendener, T. Pasch, L. Reyes, C. Booy, and R. C. Schimmer.** 2005. Alveolar macrophages regulate neutrophil recruitment in endotoxin-induced lung injury. Respir Res **6:**61.

32. **Belge, K. U., F. Dayyani, A. Horelt, M. Siedlar, M. Frankenberger, B. Frankenberger, T. Espevik, and L. Ziegler-Heitbrock.** 2002. The proinflammatory CD14+CD16+DR++ monocytes are a major source of TNF. J Immunol **168:**3536-3542.

33. **Beller, D. I., T. A. Springer, and R. D. Schreiber.** 1982. Anti-Mac-1 selectively inhibits the mouse and human type three complement receptor. J Exp Med **156:**1000-1009.

34. **Bendelac, A., P. B. Savage, and L. Teyton.** 2007. The biology of NKT cells. Annu Rev Immunol **25:**297-336.

35. **Biedzka-Sarek, M., R. Venho, and M. Skurnik.** 2005. Role of YadA, Ail, and Lipopolysaccharide in Serum Resistance of Yersinia enterocolitica Serotype O:3. Infect Immun **73:**2232-2244.

36. **Birtalan, S. C., R. M. Phillips, and P. Ghosh.** 2002. Three-dimensional secretion signals in chaperone-effector complexes of bacterial pathogens. Mol Cell **9:**971-980.

37. **Bischoff, S. C., M. Krieger, T. Brunner, and C. A. Dahinden.** 1992. Monocyte chemotactic protein 1 is a potent activator of human basophils. J Exp Med **175:**1271-1275.

38. **Blasius, A. L., W. Barchet, M. Cella, and M. Colonna.** 2007. Development and function of murine B220+CD11c+NK1.1+ cells identify them as a subset of NK cells. J Exp Med **204:**2561-2568.

39. **Bliska, J. B., and D. S. Black.** 1995. Inhibition of the Fc receptor-mediated oxidative burst in macrophages by the Yersinia pseudotuberculosis tyrosine phosphatase. Infect Immun **63:**681-685.

40. **Bliska, J. B., and S. Falkow.** 1992. Bacterial resistance to complement killing mediated by the Ail protein of Yersinia enterocolitica. Proc Natl Acad Sci U S A **89:**3561-3565.

41. **Blocker, A., N. Jouihri, E. Larquet, P. Gounon, F. Ebel, C. Parsot, P. Sansonetti, and A. Allaoui.** 2001. Structure and composition of the Shigella flexneri "needle complex", a part of its type III secreton. Mol Microbiol **39:**652-663.

42. **Bobrov, A. G., and R. D. Perry.** 2006. Yersinia pestis lacZ expresses a beta-galactosidase with low enzymatic activity. FEMS Microbiol Lett **255:**43-51.

43. **Bohn, E., S. Muller, J. Lauber, R. Geffers, N. Speer, C. Spieth, J. Krejci, B. Manncke, J. Buer, A. Zell, and I. B. Autenrieth.** 2004. Gene expression patterns of epithelial cells modulated by pathogenicity factors of Yersinia enterocolitica. Cell Microbiol **6:**129-141.

44. **Boland, A., and G. R. Cornelis.** 1998. Role of YopP in suppression of tumor necrosis factor alpha release by macrophages during Yersinia infection. Infect

Immun **66:**1878-1884.

45. **Bonecchi, R., N. Polentarutti, W. Luini, A. Borsatti, S. Bernasconi, M. Locati, C. Power, A. Proudfoot, T. N. Wells, C. Mackay, A. Mantovani, and S. Sozzani.** 1999. Up-regulation of CCR1 and CCR3 and induction of chemotaxis to CC chemokines by IFN-gamma in human neutrophils. J Immunol **162:**474-479.

46. **Bosio, C. M., A. W. Goodyear, and S. W. Dow.** 2005. Early interaction of Yersinia pestis with APCs in the lung. J Immunol **175:**6750-6756.

47. **Braciak, T. A., K. Bacon, Z. Xing, D. J. Torry, F. L. Graham, T. J. Schall, C. D. Richards, K. Croitoru, and J. Gauldie.** 1996. Overexpression of RANTES using a recombinant adenovirus vector induces the tissue-directed recruitment of monocytes to the lung. J Immunol **157:**5076-5084.

48. **Brown, S. D., and T. C. Montie.** 1977. Beta-adrenergic blocking activity of Yersinia pestis murine toxin. Infect Immun **18:**85-93.

49. **Brubaker, R. R.** 1991. Factors promoting acute and chronic diseases caused by yersiniae. Clin Microbiol Rev **4:**309-324.

50. **Brubaker, R. R.** 2003. Interleukin-10 and inhibition of innate immunity to Yersiniae: roles of Yops and LcrV (V antigen). Infect Immun **71:**3673-3681.

51. **Brubaker, R. R., E. D. Beesley, and M. J. Surgalla.** 1965. Pasteurella pestis: Role of Pesticin I and Iron in Experimental Plague. Science **149:**422-424.

52. **Bruckner, S., S. Rhamouni, L. Tautz, J. B. Denault, A. Alonso, B. Becattini, G. S. Salvesen, and T. Mustelin.** 2005. Yersinia phosphatase induces mitochondrially dependent apoptosis of T cells. J Biol Chem **280:**10388-10394.

53. **Bubeck, S. S., A. M. Cantwell, and P. H. Dube.** 2007. Delayed inflammatory response to primary pneumonic plague occurs in both outbred and inbred mice. Infect Immun **75:**697-705.

54. **Bubeck, S. S., and P. H. Dube.** 2007. Yersinia pestis CO92 delta yopH is a potent live, attenuated plague vaccine. Clin Vaccine Immunol **14:**1235-1238.

55. **Buchrieser, C., M. Prentice, and E. Carniel.** 1998. The 102-kilobase unstable region of Yersinia pestis comprises a high-pathogenicity island linked to a pigmentation segment which undergoes internal rearrangement. J Bacteriol **180:**2321-2329.

56. **Bullen, J. J.** 1981. The significance of iron in infection. Rev Infect Dis **3:**1127-1138.

57. **Burnett, S. H., E. J. Kershen, J. Zhang, L. Zeng, S. C. Straley, A. M. Kaplan, and D. A. Cohen.** 2004. Conditional macrophage ablation in transgenic mice expressing a Fas-based suicide gene. J Leukoc Biol **75:**612-623.

58. **Carniel, E.** 2003. Evolution of pathogenic Yersinia, some lights in the dark. Adv Exp Med Biol **529:**3-12.

59. **Carniel, E.** 2001. The Yersinia high-pathogenicity island: an iron-uptake island. Microbes Infect **3:**561-569.

60. **Carr, M. W., S. J. Roth, E. Luther, S. S. Rose, and T. A. Springer.** 1994. Monocyte chemoattractant protein 1 acts as a T-lymphocyte chemoattractant. Proc Natl Acad Sci U S A **91:**3652-3656.

61. **Cathelyn, J. S., S. D. Crosby, W. W. Lathem, W. E. Goldman, and V. L. Miller.** 2006. RovA, a global regulator of Yersinia pestis, specifically required for bubonic plague. Proc Natl Acad Sci U S A **103:**13514-13519.

62. **Cavanaugh, D. C., B. L. Elisberg, C. H. Llewellyn, J. D. Marshall, Jr., J. H. Rust, Jr., J. E. Williams, and K. F. Meyer.** 1974. Plague immunization. V. Indirect evidence for the efficacy of plague vaccine. J Infect Dis **129:**Suppl:S37-40.

63. **Cavanaugh, D. C., and R. Randall.** 1959. The role of multiplication of Pasteurella pestis in mononuclear phagocytes in the pathogenesis of flea-borne plague. J Immunol **83:**348-363.

64. **Chanock, S. J., J. el Benna, R. M. Smith, and B. M. Babior.** 1994. The respiratory burst oxidase. J Biol Chem **269:**24519-24522.

65. **Chanteau, S., L. Rabarijaona, T. O'Brien, L. Rahalison, J. Hager, P. Boisier, J. Burans, and M. Rasolomaharo.** 1998. F1 antigenaemia in bubonic plague patients, a marker of gravity and efficacy of therapy. Trans R Soc Trop Med Hyg **92:**572-573.

66. **Chen, T. H., and S. S. Elberg.** 1977. Scanning electron microscopic study of virulent Yersinia pestis and Yersinia pseudotuberculosis type 1. Infect Immun **15:**972-977.

67. **Cohen, R. J., and J. L. Stockard.** 1967. Pneumonic plague in an untreated plague-vaccinated individual. Jama **202:**365-366.

68. **Colonna, M., G. Trinchieri, and Y. J. Liu.** 2004. Plasmacytoid dendritic cells in immunity. Nat Immunol **5:**1219-1226.

69. **Colvin, B. L., A. E. Morelli, A. J. Logar, A. H. Lau, and A. W. Thomson.** 2004. Comparative evaluation of CC chemokine-induced migration of murine CD8alpha+ and CD8alpha- dendritic cells and their in vivo trafficking. J Leukoc Biol **75:**275-285.

70. **Conti, P., W. Boucher, R. Letourneau, C. Feliciani, M. Reale, R. C. Barbacane, P. Vlagopoulos, G. Bruneau, J. Thibault, and T. C. Theoharides.** 1995. Monocyte chemotactic protein-1 provokes mast cell aggregation and [3H]5HT release. Immunology **86:**434-440.

71. **Copin, R., P. De Baetselier, Y. Carlier, J. J. Letesson, and E. Muraille.** 2007. MyD88-dependent activation of B220-CD11b+LY-6C+ dendritic cells during Brucella melitensis infection. J Immunol **178:**5182-5191.

72. **Cornelis, G., J. C. Vanootegem, and C. Sluiters.** 1987. Transcription of the yop regulon from Y. enterocolitica requires trans acting pYV and chromosomal genes. Microb Pathog **2:**367-379.

73. **Cornelis, G. R.** 2002. Yersinia type III secretion: send in the effectors. J Cell Biol **158:**401-408.

74. **Cornelis, G. R.** 2002. The Yersinia Ysc-Yop 'type III' weaponry. Nat Rev Mol Cell Biol **3:**742-752.

75. **Cowan, C., H. A. Jones, Y. H. Kaya, R. D. Perry, and S. C. Straley.** 2000. Invasion of epithelial cells by Yersinia pestis: evidence for a Y. pestis-specific invasin. Infect Immun **68:**4523-4530.

76. **Craig, M. J., and R. D. Loberg.** 2006. CCL2 (Monocyte Chemoattractant Protein-1) in cancer bone metastases. Cancer Metastasis Rev **25:**611-619.

77. **Daley, J. M., A. A. Thomay, M. D. Connolly, J. S. Reichner, and J. E. Albina.** 2008. Use of Ly6G-specific monoclonal antibody to deplete neutrophils in mice. J Leukoc Biol **83:**64-70.

78. **Dang, P. M., C. Dewas, M. Gaudry, M. Fay, E. Pedruzzi, M. A. Gougerot-Pocidalo, and J. El Benna.** 1999. Priming of human neutrophil respiratory burst by granulocyte/macrophage colony-stimulating factor (GM-CSF) involves partial phosphorylation of p47(phox). J Biol Chem **274:**20704-20708.

79. **Davis, K. J., D. L. Fritz, M. L. Pitt, S. L. Welkos, P. L. Worsham, and A. M. Friedlander.** 1996. Pathology of experimental pneumonic plague produced by fraction 1-positive and fraction 1-negative Yersinia pestis in African green monkeys (Cercopithecus aethiops). Arch Pathol Lab Med **120:**156-163.

80. **Degen, J. L., T. H. Bugge, and J. D. Goguen.** 2007. Fibrin and fibrinolysis in infection and host defense. J Thromb Haemost **5 Suppl 1:**24-31.

81. **DeLeo, F. R., J. Renee, S. McCormick, M. Nakamura, M. Apicella, J. P. Weiss, and W. M. Nauseef.** 1998. Neutrophils exposed to bacterial lipopolysaccharide upregulate NADPH oxidase assembly. J Clin Invest **101:**455-463.

82. **Deng, W., V. Burland, G. Plunkett, 3rd, A. Boutin, G. F. Mayhew, P. Liss, N. T. Perna, D. J. Rose, B. Mau, S. Zhou, D. C. Schwartz, J. D. Fetherston, L. E. Lindler, R. R. Brubaker, G. V. Plano, S. C. Straley, K. A. McDonough, M. L. Nilles, J. S. Matson, F. R. Blattner, and R. D. Perry.** 2002. Genome sequence of Yersinia pestis KIM. J Bacteriol **184:**4601-4611.

83. **Denkers, E. Y., R. T. Gazzinelli, D. Martin, and A. Sher.** 1993. Emergence of NK1.1+ cells as effectors of IFN-gamma dependent immunity to Toxoplasma gondii in MHC class I-deficient mice. J Exp Med **178:**1465-1472.

84. **Depaolo, R. W., F. Tang, I. Kim, M. Han, N. Levin, N. Ciletti, A. Lin, D. Anderson, O. Schneewind, and B. Jabri.** 2008. Toll-like receptor 6 drives differentiation of tolerogenic dendritic cells and contributes to LcrV-mediated plague pathogenesis. Cell Host Microbe **4:**350-361.

85. **Deshmane, S. L., S. Kremlev, S. Amini, and B. E. Sawaya.** 2009. Monocyte chemoattractant protein-1 (MCP-1): an overview. J Interferon Cytokine Res **29:**313-326.

86. **Dewas, C., P. M. Dang, M. A. Gougerot-Pocidalo, and J. El-Benna.** 2003. TNF-alpha induces phosphorylation of p47(phox) in human neutrophils: partial phosphorylation of p47phox is a common event of priming of human neutrophils by TNF-alpha and granulocyte-macrophage colony-stimulating factor. J Immunol **171:**4392-4398.

87. **DiMezzo, T. L., G. Ruthel, E. E. Brueggemann, H. B. Hines, W. J. Ribot, C. E. Chapman, B. S. Powell, and S. L. Welkos.** 2009. In vitro intracellular trafficking of virulence antigen during infection by Yersinia pestis. PLoS One **4:**e6281.

88. **DiSanto, J. P., W. Muller, D. Guy-Grand, A. Fischer, and K. Rajewsky.** 1995. Lymphoid development in mice with a targeted deletion of the interleukin 2 receptor gamma chain. Proc Natl Acad Sci U S A **92:**377-381.

89. **Du, Y., R. Rosqvist, and A. Forsberg.** 2002. Role of fraction 1 antigen of Yersinia pestis in inhibition of phagocytosis. Infect Immun **70:**1453-1460.

90. **Dunn, P. L., and R. J. North.** 1991. Early gamma interferon production by natural killer cells is important in defense against murine listeriosis. Infect Immun **59:**2892-2900.

91. **Dziarski, R.** 2006. Deadly plague versus mild-mannered TLR4. Nat Immunol **7:**1017-1019.

92. **Eisen, R. J., S. W. Bearden, A. P. Wilder, J. A. Montenieri, M. F. Antolin, and K. L. Gage.** 2006. Early-phase transmission of Yersinia pestis by unblocked fleas as a mechanism explaining rapidly spreading plague epizootics. Proc Natl Acad Sci U S A **103:**15380-15385.

93. **Endlich, B., D. Armstrong, J. Brodsky, M. Novotny, and T. A. Hamilton.** 2002. Distinct temporal patterns of macrophage-inflammatory protein-2 and KC chemokine gene expression in surgical injury. J Immunol **168:**3586-3594.

94. **Erfurth, S. E., S. Grobner, U. Kramer, D. S. Gunst, I. Soldanova, M. Schaller, I. B. Autenrieth, and S. Borgmann.** 2004. Yersinia enterocolitica induces apoptosis and inhibits surface molecule expression and cytokine production in murine dendritic cells. Infect Immun **72:**7045-7054.

95. **Erickson, D. L., C. O. Jarrett, J. A. Callison, E. R. Fischer, and B. J. Hinnebusch.** 2008. Loss of a biofilm-inhibiting glycosyl hydrolase during the emergence of Yersinia pestis. J Bacteriol **190:**8163-8170.

96. **Evdokimov, A. G., D. E. Anderson, K. M. Routzahn, and D. S. Waugh.** 2001. Unusual molecular architecture of the Yersinia pestis cytotoxin YopM: a leucine-rich repeat protein with the shortest repeating unit. J Mol Biol **312:**807-821.

97. **Fallman, M., C. Persson, and H. Wolf-Watz.** 1997. Yersinia proteins that target host cell signaling pathways. J Clin Invest **99:**1153-1157.

98. **Felek, S., and E. S. Krukonis.** 2009. The Yersinia pestis Ail protein mediates binding and Yop delivery to host cells required for plague virulence. Infect Immun **77:**825-836.

99. **Fetherston, J. D., P. Schuetze, and R. D. Perry.** 1992. Loss of the pigmentation phenotype in Yersinia pestis is due to the spontaneous deletion of 102 kb of chromosomal DNA which is flanked by a repetitive element. Mol Microbiol **6:**2693-2704.

100. **Fields, K. A., and S. C. Straley.** 1999. LcrV of Yersinia pestis enters infected eukaryotic cells by a virulence plasmid-independent mechanism. Infect Immun **67:**4801-4813.

101. **Fierro, I. M., C. Barja-Fidalgo, R. M. Canedo, F. Q. Cunha, and S. H. Ferreira.** 1995. An increase in nitric oxide produced by rat peritoneal neutrophils is not involved in cell apoptosis. Mediators Inflamm **4:**222-228.

102. **Fingerle, G., A. Pforte, B. Passlick, M. Blumenstein, M. Strobel, and H. W. Ziegler-Heitbrock.** 1993. The novel subset of CD14+/CD16+ blood monocytes is expanded in sepsis patients. Blood **82:**3170-3176.

103. **Forman, S., J. T. Paulley, J. D. Fetherston, Y. Q. Cheng, and R. D. Perry.** Yersinia ironomics: comparison of iron transporters among Yersinia pestis biotypes and its nearest neighbor, Yersinia pseudotuberculosis. Biometals **23:**275-294.

104. **Forman, S., C. R. Wulff, T. Myers-Morales, C. Cowan, R. D. Perry, and S. C. Straley.** 2008. yadBC of Yersinia pestis, a new virulence determinant for bubonic plague. Infect Immun **76:**578-587.

105. **Frodin, M., and S. Gammeltoft.** 1999. Role and regulation of 90 kDa ribosomal S6 kinase (RSK) in signal transduction. Mol Cell Endocrinol **151:**65-77.

106. **Gage, K. L., and M. Y. Kosoy.** 2005. Natural history of plague: perspectives from more than a century of research. Annu Rev Entomol **50:**505-528.

107. **Galan, J. E., and H. Wolf-Watz.** 2006. Protein delivery into eukaryotic cells by type III secretion machines. Nature **444:**567-573.

108. **Galvan, E. M., H. Chen, and D. M. Schifferli.** 2007. The Psa fimbriae of Yersinia pestis interact with phosphatidylcholine on alveolar epithelial cells and pulmonary surfactant. Infect Immun **75:**1272-1279.

109. **Geissmann, F., C. Auffray, R. Palframan, C. Wirrig, A. Ciocca, L. Campisi, E. Narni-Mancinelli, and G. Lauvau.** 2008. Blood monocytes: distinct subsets, how they relate to dendritic cells, and their possible roles in the regulation of T-cell responses. Immunol Cell Biol **86:**398-408.

110. **Geissmann, F., S. Jung, and D. R. Littman.** 2003. Blood monocytes consist of two principal subsets with distinct migratory properties. Immunity **19:**71-82.

111. **Gerszten, R. E., E. A. Garcia-Zepeda, Y. C. Lim, M. Yoshida, H. A. Ding, M. A. Gimbrone, Jr., A. D. Luster, F. W. Luscinskas, and A. Rosenzweig.** 1999. MCP-1 and IL-8 trigger firm adhesion of monocytes to vascular endothelium under flow conditions. Nature **398:**718-723.

112. **Giorda, R., and M. Trucco.** 1991. Mouse NKR-P1. A family of genes selectively coexpressed in adherent lymphokine-activated killer cells. J Immunol **147:**1701-1708.

113. **Godfrey, D. I., H. R. MacDonald, M. Kronenberg, M. J. Smyth, and L. Van Kaer.** 2004. NKT cells: what's in a name? Nat Rev Immunol **4:**231-237.

114. **Goguen, J. D., W. S. Walker, T. P. Hatch, and J. Yother.** 1986. Plasmid-determined cytotoxicity in Yersinia pestis and Yersinia pseudotuberculosis. Infect Immun **51:**788-794.

115. **Gong, S., S. W. Bearden, V. A. Geoffroy, J. D. Fetherston, and R. D. Perry.** 2001. Characterization of the Yersinia pestis Yfu ABC inorganic iron transport system. Infect Immun **69:**2829-2837.

116. **Green, S. P., E. L. Hartland, R. M. Robins-Browne, and W. A. Phillips.** 1995. Role of YopH in the suppression of tyrosine phosphorylation and respiratory burst activity in murine macrophages infected with Yersinia enterocolitica. J Leukoc Biol **57:**972-977.

117. **Gregory, S. H., L. P. Cousens, N. van Rooijen, E. A. Dopp, T. M. Carlos, and E. J. Wing.** 2002. Complementary adhesion molecules promote neutrophil-Kupffer cell interaction and the elimination of bacteria taken up by the liver. J Immunol **168:**308-315.

118. **Gregory, S. H., A. J. Sagnimeni, and E. J. Wing.** 1996. Bacteria in the bloodstream are trapped in the liver and killed by immigrating neutrophils. J Immunol **157:**2514-2520.

119. **Gregory, S. H., and E. J. Wing.** 2002. Neutrophil-Kupffer cell interaction: a critical component of host defenses to systemic bacterial infections. J Leukoc Biol **72:**239-248.

120. **Griffin, J. D., J. Ritz, L. M. Nadler, and S. F. Schlossman.** 1981. Expression of myeloid differentiation antigens on normal and malignant myeloid cells. J Clin Invest **68:**932-941.

121. **Groux, H., and F. Cottrez.** 2003. The complex role of interleukin-10 in autoimmunity. J Autoimmun **20:**281-285.

122. **Hacker, C., R. D. Kirsch, X. S. Ju, T. Hieronymus, T. C. Gust, C. Kuhl, T.**

Jorgas, S. M. Kurz, S. Rose-John, Y. Yokota, and M. Zenke. 2003. Transcriptional profiling identifies Id2 function in dendritic cell development. Nat Immunol **4:**380-386.

123. **Haley, K. J., C. M. Lilly, J. H. Yang, Y. Feng, S. P. Kennedy, T. G. Turi, J. F. Thompson, G. H. Sukhova, P. Libby, and R. T. Lee.** 2000. Overexpression of eotaxin and the CCR3 receptor in human atherosclerosis: using genomic technology to identify a potential novel pathway of vascular inflammation. Circulation **102:**2185-2189.

124. **Hanabuchi, S., N. Watanabe, Y. H. Wang, Y. H. Wang, T. Ito, J. Shaw, W. Cao, F. X. Qin, and Y. J. Liu.** 2006. Human plasmacytoid predendritic cells activate NK cells through glucocorticoid-induced tumor necrosis factor receptor-ligand (GITRL). Blood **107:**3617-3623.

125. **Hayakawa, K., R. R. Hardy, L. A. Herzenberg, and L. A. Herzenberg.** 1985. Progenitors for Ly-1 B cells are distinct from progenitors for other B cells. J Exp Med **161:**1554-1568.

126. **Heath, D. G., G. W. Anderson, Jr., J. M. Mauro, S. L. Welkos, G. P. Andrews, J. Adamovicz, and A. M. Friedlander.** 1998. Protection against experimental bubonic and pneumonic plague by a recombinant capsular F1-V antigen fusion protein vaccine. Vaccine **16:**1131-1137.

127. **Hefeneider, S. H., P. J. Conlon, C. S. Henney, and S. Gillis.** 1983. In vivo interleukin 2 administration augments the generation of alloreactive cytolytic T lymphocytes and resident natural killer cells. J Immunol **130:**222-227.

128. **Held, W., J. D. Coudert, and J. Zimmer.** 2003. The NK cell receptor repertoire: formation, adaptation and exploitation. Curr Opin Immunol **15:**233-237.

129. **Henderson, I. R., F. Navarro-Garcia, M. Desvaux, R. C. Fernandez, and D. Ala'Aldeen.** 2004. Type V protein secretion pathway: the autotransporter story. Microbiol Mol Biol Rev **68:**692-744.

130. **Henderson, R. B., J. A. Hobbs, M. Mathies, and N. Hogg.** 2003. Rapid recruitment of inflammatory monocytes is independent of neutrophil migration. Blood **102:**328-335.

131. **Heusipp, G., K. Spekker, S. Brast, S. Falker, and M. A. Schmidt.** 2006. YopM of Yersinia enterocolitica specifically interacts with alpha1-antitrypsin without affecting the anti-protease activity. Microbiology **152:**1327-1335.

132. **Hilbi, H., J. E. Moss, D. Hersh, Y. Chen, J. Arondel, S. Banerjee, R. A. Flavell, J. Yuan, P. J. Sansonetti, and A. Zychlinsky.** 1998. Shigella-induced apoptosis is dependent on caspase-1 which binds to IpaB. J Biol Chem **273:**32895-32900.

133. **Hinnebusch, B. J.** 2005. The evolution of flea-borne transmission in Yersinia pestis. Curr Issues Mol Biol **7:**197-212.

134. **Hinnebusch, B. J., and D. L. Erickson.** 2008. Yersinia pestis biofilm in the flea vector and its role in the transmission of plague. Curr Top Microbiol Immunol **322:**229-248.

135. **Hinnebusch, B. J., R. D. Perry, and T. G. Schwan.** 1996. Role of the Yersinia pestis hemin storage (hms) locus in the transmission of plague by fleas. Science **273:**367-370.

136. **Hinnebusch, B. J., A. E. Rudolph, P. Cherepanov, J. E. Dixon, T. G. Schwan, and A. Forsberg.** 2002. Role of Yersinia murine toxin in survival of Yersinia

pestis in the midgut of the flea vector. Science **296:**733-735.

137. **Hinnebusch, J., P. Cherepanov, Y. Du, A. Rudolph, J. D. Dixon, T. Schwan, and A. Forsberg.** 2000. Murine toxin of Yersinia pestis shows phospholipase D activity but is not required for virulence in mice. Int J Med Microbiol **290:**483-487.

138. **Hoffman, S. L.** 1980. Plague in the United States: the "black death" is still alive. Ann Emerg Med **9:**319-322.

139. **Hoffmann, R., K. van Erp, K. Trulzsch, and J. Heesemann.** 2004. Transcriptional responses of murine macrophages to infection with Yersinia enterocolitica. Cell Microbiol **6:**377-390.

140. **Hol, J., L. Wilhelmsen, and G. Haraldsen.** The murine IL-8 homologues KC, MIP-2, and LIX are found in endothelial cytoplasmic granules but not in Weibel-Palade bodies. J Leukoc Biol **87:**501-508.

141. **Holub, M., C. W. Cheng, S. Mott, P. Wintermeyer, N. van Rooijen, and S. H. Gregory.** 2009. Neutrophils sequestered in the liver suppress the proinflammatory response of Kupffer cells to systemic bacterial infection. J Immunol **183:**3309-3316.

142. **Hull, H. F., J. M. Montes, and J. M. Mann.** 1987. Septicemic plague in New Mexico. J Infect Dis **155:**113-118.

143. **Hurst, S. M., T. S. Wilkinson, R. M. McLoughlin, S. Jones, S. Horiuchi, N. Yamamoto, S. Rose-John, G. M. Fuller, N. Topley, and S. A. Jones.** 2001. Il-6 and its soluble receptor orchestrate a temporal switch in the pattern of leukocyte recruitment seen during acute inflammation. Immunity **14:**705-714.

144. **Iida, S., T. Kohro, T. Kodama, S. Nagata, and R. Fukunaga.** 2005. Identification of CCR2, flotillin, and gp49B genes as new G-CSF targets during neutrophilic differentiation. J Leukoc Biol **78:**481-490.

145. **Ishibashi, H., M. Nakamura, A. Komori, K. Migita, and S. Shimoda.** 2009. Liver architecture, cell function, and disease. Semin Immunopathol **31:**399-409.

146. **Isin Zh, M., and B. M. Suleimenov.** 1987. Comparative investigation of PMN leucocyte antimicrobial potential in animals of different species susceptibility to the plague agent. J Hyg Epidemiol Microbiol Immunol **31:**307-312.

147. **Iyoda, T., S. Shimoyama, K. Liu, Y. Omatsu, Y. Akiyama, Y. Maeda, K. Takahara, R. M. Steinman, and K. Inaba.** 2002. The CD8+ dendritic cell subset selectively endocytoses dying cells in culture and in vivo. J Exp Med **195:**1289-1302.

148. **Jakubowski, W., and G. Bartosz.** 2000. 2,7-dichlorofluorescin oxidation and reactive oxygen species: what does it measure? Cell Biol Int **24:**757-760.

149. **Jarrett, C. O., E. Deak, K. E. Isherwood, P. C. Oyston, E. R. Fischer, A. R. Whitney, S. D. Kobayashi, F. R. DeLeo, and B. J. Hinnebusch.** 2004. Transmission of Yersinia pestis from an infectious biofilm in the flea vector. J Infect Dis **190:**783-792.

150. **Jarrett, C. O., F. Sebbane, J. J. Adamovicz, G. P. Andrews, and B. J. Hinnebusch.** 2004. Flea-borne transmission model to evaluate vaccine efficacy against naturally acquired bubonic plague. Infect Immun **72:**2052-2056.

151. **Jia, T., N. V. Serbina, K. Brandl, M. X. Zhong, I. M. Leiner, I. F. Charo, and E. G. Pamer.** 2008. Additive roles for MCP-1 and MCP-3 in CCR2-mediated

recruitment of inflammatory monocytes during Listeria monocytogenes infection. J Immunol **180:**6846-6853.

152. **Jiang, Y., D. I. Beller, G. Frendl, and D. T. Graves.** 1992. Monocyte chemoattractant protein-1 regulates adhesion molecule expression and cytokine production in human monocytes. J Immunol **148:**2423-2428.

153. **Johansson, C., and M. J. Wick.** 2004. Liver dendritic cells present bacterial antigens and produce cytokines upon Salmonella encounter. J Immunol **172:**2496-2503.

154. **Jordan, M. B., N. van Rooijen, S. Izui, J. Kappler, and P. Marrack.** 2003. Liposomal clodronate as a novel agent for treating autoimmune hemolytic anemia in a mouse model. Blood **101:**594-601.

155. **Jung, S., D. Unutmaz, P. Wong, G. Sano, K. De los Santos, T. Sparwasser, S. Wu, S. Vuthoori, K. Ko, F. Zavala, E. G. Pamer, D. R. Littman, and R. A. Lang.** 2002. In vivo depletion of CD11c+ dendritic cells abrogates priming of CD8+ T cells by exogenous cell-associated antigens. Immunity **17:**211-220.

156. **Karre, K., H. G. Ljunggren, G. Piontek, and R. Kiessling.** 1986. Selective rejection of H-2-deficient lymphoma variants suggests alternative immune defence strategy. Nature **319:**675-678.

157. **Kasai, M., M. Iwamori, Y. Nagai, K. Okumura, and T. Tada.** 1980. A glycolipid on the surface of mouse natural killer cells. Eur J Immunol **10:**175-180.

158. **Kawase, I., D. L. Urdal, C. G. Brooks, and C. S. Henney.** 1982. Selective depletion of NK cell activity in vivo and its effect on the growth of NK-sensitive and NK-resistant tumor cell variants. Int J Cancer **29:**567-574.

159. **Kerschen, E. J., D. A. Cohen, A. M. Kaplan, and S. C. Straley.** 2004. The plague virulence protein YopM targets the innate immune response by causing a global depletion of NK cells. Infect Immun **72:**4589-4602.

160. **Kirillina, O., A. G. Bobrov, J. D. Fetherston, and R. D. Perry.** 2006. Hierarchy of iron uptake systems: Yfu and Yiu are functional in Yersinia pestis. Infect Immun **74:**6171-6178.

161. **Kmiec, Z.** 2001. Cooperation of liver cells in health and disease. Adv Anat Embryol Cell Biol **161:**III-XIII, 1-151.

162. **Knudsen, E., P. O. Iversen, N. Van Rooijen, and H. B. Benestad.** 2002. Macrophage-dependent regulation of neutrophil mobilization and chemotaxis during development of sterile peritonitis in the rat. Eur J Haematol **69:**284-296.

163. **Kojima, H., N. Nakatsubo, K. Kikuchi, S. Kawahara, Y. Kirino, H. Nagoshi, Y. Hirata, and T. Nagano.** 1998. Detection and imaging of nitric oxide with novel fluorescent indicators: diaminofluoresceins. Anal Chem **70:**2446-2453.

164. **Kukkonen, M., K. Lahteenmaki, M. Suomalainen, N. Kalkkinen, L. Emody, H. Lang, and T. K. Korhonen.** 2001. Protein regions important for plasminogen activation and inactivation of alpha2-antiplasmin in the surface protease Pla of Yersinia pestis. Mol Microbiol **40:**1097-1111.

165. **Kukkonen, M., M. Suomalainen, P. Kyllonen, K. Lahteenmaki, H. Lang, R. Virkola, I. M. Helander, O. Holst, and T. K. Korhonen.** 2004. Lack of O-antigen is essential for plasminogen activation by Yersinia pestis and Salmonella enterica. Mol Microbiol **51:**215-225.

166. **Kundig, T. M., H. Schorle, M. F. Bachmann, H. Hengartner, R. M.**

Zinkernagel, and I. Horak. 1993. Immune responses in interleukin-2-deficient mice. Science **262:**1059-1061.

167. **Kurihara, T., G. Warr, J. Loy, and R. Bravo.** 1997. Defects in macrophage recruitment and host defense in mice lacking the CCR2 chemokine receptor. J Exp Med **186:**1757-1762.

168. **Kuziel, W. A., S. J. Morgan, T. C. Dawson, S. Griffin, O. Smithies, K. Ley, and N. Maeda.** 1997. Severe reduction in leukocyte adhesion and monocyte extravasation in mice deficient in CC chemokine receptor 2. Proc Natl Acad Sci U S A **94:**12053-12058.

169. **Lahteenmaki, K., S. Edelman, and T. K. Korhonen.** 2005. Bacterial metastasis: the host plasminogen system in bacterial invasion. Trends Microbiol **13:**79-85.

170. **Lahteenmaki, K., R. Virkola, A. Saren, L. Emody, and T. K. Korhonen.** 1998. Expression of plasminogen activator pla of Yersinia pestis enhances bacterial attachment to the mammalian extracellular matrix. Infect Immun **66:**5755-5762.

171. **Lalor, P. A., A. M. Stall, S. Adams, and L. A. Herzenberg.** 1989. Permanent alteration of the murine Ly-1 B repertoire due to selective depletion of Ly-1 B cells in neonatal animals. Eur J Immunol **19:**501-506.

172. **Laskay, T., M. Rollinghoff, and W. Solbach.** 1993. Natural killer cells participate in the early defense against Leishmania major infection in mice. Eur J Immunol **23:**2237-2241.

173. **Lathem, W. W., S. D. Crosby, V. L. Miller, and W. E. Goldman.** 2005. Progression of primary pneumonic plague: a mouse model of infection, pathology, and bacterial transcriptional activity. Proc Natl Acad Sci U S A **102:**17786-17791.

174. **Lathem, W. W., P. A. Price, V. L. Miller, and W. E. Goldman.** 2007. A plasminogen-activating protease specifically controls the development of primary pneumonic plague. Science **315:**509-513.

175. **Lauwerys, B. R., N. Garot, J. C. Renauld, and F. A. Houssiau.** 2000. Cytokine production and killer activity of NK/T-NK cells derived with IL-2, IL-15, or the combination of IL-12 and IL-18. J Immunol **165:**1847-1853.

176. **Lauwerys, B. R., J. C. Renauld, and F. A. Houssiau.** 1999. Synergistic proliferation and activation of natural killer cells by interleukin 12 and interleukin 18. Cytokine **11:**822-830.

177. **Lawrenz, M. B., J. D. Lenz, and V. L. Miller.** 2009. A novel autotransporter adhesin is required for efficient colonization during bubonic plague. Infect Immun **77:**317-326.

178. **Lee, H. K., and A. Iwasaki.** 2007. Innate control of adaptive immunity: dendritic cells and beyond. Semin Immunol **19:**48-55.

179. **Lee, U., K. Santa, S. Habu, and T. Nishimura.** 1996. Murine asialo GM1+CD8+ T cells as novel interleukin-12-responsive killer T cell precursors. Jpn J Cancer Res **87:**429-432.

180. **Lemaitre, N., F. Sebbane, D. Long, and B. J. Hinnebusch.** 2006. Yersinia pestis YopJ suppresses tumor necrosis factor alpha induction and contributes to apoptosis of immune cells in the lymph node but is not required for virulence in a rat model of bubonic plague. Infect Immun **74:**5126-5131.

181. **Leon, B., G. Martinez del Hoyo, V. Parrillas, H. H. Vargas, P. Sanchez-Mateos, N. Longo, M. Lopez-Bravo, and C. Ardavin.** 2004. Dendritic cell differentiation

potential of mouse monocytes: monocytes represent immediate precursors of CD8- and CD8+ splenic dendritic cells. Blood **103:**2668-2676.

182. **Lepay, D. A., C. F. Nathan, R. M. Steinman, H. W. Murray, and Z. A. Cohn.** 1985. Murine Kupffer cells. Mononuclear phagocytes deficient in the generation of reactive oxygen intermediates. J Exp Med **161:**1079-1096.

183. **Leung, K. Y., B. S. Reisner, and S. C. Straley.** 1990. YopM inhibits platelet aggregation and is necessary for virulence of Yersinia pestis in mice. Infect Immun **58:**3262-3271.

184. **Leung, K. Y., and S. C. Straley.** 1989. The yopM gene of Yersinia pestis encodes a released protein having homology with the human platelet surface protein GPIb alpha. J Bacteriol **171:**4623-4632.

185. **Li, B., and R. Yang.** 2008. Interaction between Yersinia pestis and the host immune system. Infect Immun **76:**1804-1811.

186. **Lindler, L. E., M. S. Klempner, and S. C. Straley.** 1990. Yersinia pestis pH 6 antigen: genetic, biochemical, and virulence characterization of a protein involved in the pathogenesis of bubonic plague. Infect Immun **58:**2569-2577.

187. **Lipscomb, M. F., and B. J. Masten.** 2002. Dendritic cells: immune regulators in health and disease. Physiol Rev **82:**97-130.

188. **Lloyd, S. A., M. Norman, R. Rosqvist, and H. Wolf-Watz.** 2001. Yersinia YopE is targeted for type III secretion by N-terminal, not mRNA, signals. Mol Microbiol **39:**520-531.

189. **Lodoen, M. B., and L. L. Lanier.** 2005. Viral modulation of NK cell immunity. Nat Rev Microbiol **3:**59-69.

190. **Loetscher, P., M. Seitz, I. Clark-Lewis, M. Baggiolini, and B. Moser.** 1996. Activation of NK cells by CC chemokines. Chemotaxis, Ca2+ mobilization, and enzyme release. J Immunol **156:**322-327.

191. **Lu, B., B. J. Rutledge, L. Gu, J. Fiorillo, N. W. Lukacs, S. L. Kunkel, R. North, C. Gerard, and B. J. Rollins.** 1998. Abnormalities in monocyte recruitment and cytokine expression in monocyte chemoattractant protein 1-deficient mice. J Exp Med **187:**601-608.

192. **Lukaszewski, R. A., D. J. Kenny, R. Taylor, D. G. Rees, M. G. Hartley, and P. C. Oyston.** 2005. Pathogenesis of Yersinia pestis infection in BALB/c mice: effects on host macrophages and neutrophils. Infect Immun **73:**7142-7150.

193. **Mack, M., J. Cihak, C. Simonis, B. Luckow, A. E. Proudfoot, J. Plachy, H. Bruhl, M. Frink, H. J. Anders, V. Vielhauer, J. Pfirstinger, M. Stangassinger, and D. Schlondorff.** 2001. Expression and characterization of the chemokine receptors CCR2 and CCR5 in mice. J Immunol **166:**4697-4704.

194. **Maghazachi, A. A., A. Al-Aoukaty, and T. J. Schall.** 1996. CC chemokines induce the generation of killer cells from CD56+ cells. Eur J Immunol **26:**315-319.

195. **Makoveichuk, E., P. Cherepanov, S. Lundberg, A. Forsberg, and G. Olivecrona.** 2003. pH6 antigen of Yersinia pestis interacts with plasma lipoproteins and cell membranes. J Lipid Res **44:**320-330.

196. **Mantovani, A., C. Garlanda, M. Introna, and A. Vecchi.** 1998. Regulation of endothelial cell function by pro- and anti-inflammatory cytokines. Transplant Proc **30:**4239-4243.

197. **Marketon, M. M., R. W. DePaolo, K. L. DeBord, B. Jabri, and O. Schneewind.** 2005. Plague bacteria target immune cells during infection. Science **309:**1739-1741.

198. **Marshall, J. D., Jr., P. J. Bartelloni, D. C. Cavanaugh, P. J. Kadull, and K. F. Meyer.** 1974. Plague immunization. II. Relation of adverse clinical reactions to multiple immunizations with killed vaccine. J Infect Dis **129:**Suppl:S19-25.

199. **Matson, J. S., and M. L. Nilles.** 2001. LcrG-LcrV interaction is required for control of Yops secretion in Yersinia pestis. J Bacteriol **183:**5082-5091.

200. **McColl, S. R., and I. Clark-Lewis.** 1999. Inhibition of murine neutrophil recruitment in vivo by CXC chemokine receptor antagonists. J Immunol **163:**2829-2835.

201. **McCoy, M. W., M. L. Marre, C. F. Lesser, and J. Mecsas.** The C-terminal tail of Yersinia pseudotuberculosis YopM is critical for interacting with RSK1 and for virulence. Infect Immun **78:**2584-2598.

202. **McDonald, C., P. O. Vacratsis, J. B. Bliska, and J. E. Dixon.** 2003. The yersinia virulence factor YopM forms a novel protein complex with two cellular kinases. J Biol Chem **278:**18514-18523.

203. **McDonough, K. A., and S. Falkow.** 1989. A Yersinia pestis-specific DNA fragment encodes temperature-dependent coagulase and fibrinolysin-associated phenotypes. Mol Microbiol **3:**767-775.

204. **McPhee, J. B., P. Mena, and J. B. Bliska.** Delineation of regions of the Yersinia YopM protein required for interaction with the RSK1 and PRK2 host kinases and their requirement for interleukin-10 production and virulence. Infect Immun.

205. **Mebius, R. E., and G. Kraal.** 2005. Structure and function of the spleen. Nat Rev Immunol **5:**606-616.

206. **Mednick, A. J., M. Feldmesser, J. Rivera, and A. Casadevall.** 2003. Neutropenia alters lung cytokine production in mice and reduces their susceptibility to pulmonary cryptococcosis. Eur J Immunol **33:**1744-1753.

207. **Melgarejo, E., M. A. Medina, F. Sanchez-Jimenez, and J. L. Urdiales.** 2009. Monocyte chemoattractant protein-1: a key mediator in inflammatory processes. Int J Biochem Cell Biol **41:**998-1001.

208. **Melnikov, V. Y., S. Faubel, B. Siegmund, M. S. Lucia, D. Ljubanovic, and C. L. Edelstein.** 2002. Neutrophil-independent mechanisms of caspase-1- and IL-18-mediated ischemic acute tubular necrosis in mice. J Clin Invest **110:**1083-1091.

209. **Merad, M., M. G. Manz, H. Karsunky, A. Wagers, W. Peters, I. Charo, I. L. Weissman, J. G. Cyster, and E. G. Engleman.** 2002. Langerhans cells renew in the skin throughout life under steady-state conditions. Nat Immunol **3:**1135-1141.

210. **Metcalf, W. W., W. Jiang, L. L. Daniels, S. K. Kim, A. Haldimann, and B. L. Wanner.** 1996. Conditionally replicative and conjugative plasmids carrying lacZ alpha for cloning, mutagenesis, and allele replacement in bacteria. Plasmid **35:**1-13.

211. **Meyer, K. F.** 1950. Modern therapy of plague. J Am Med Assoc **144:**982-985.

212. **Meyer, K. F., J. A. Hightower, and F. R. McCrumb.** 1974. Plague immunization. VI. Vaccination with the fraction I antigen of Yersinia pestis. J Infect Dis **129:**Suppl:S41-45.

213. **Meylan, E., J. Tschopp, and M. Karin.** 2006. Intracellular pattern recognition

receptors in the host response. Nature **442:**39-44.

214. **Michiels, T., P. Wattiau, R. Brasseur, J. M. Ruysschaert, and G. Cornelis.** 1990. Secretion of Yop proteins by Yersiniae. Infect Immun **58:**2840-2849.

215. **Miller, S. I., R. K. Ernst, and M. W. Bader.** 2005. LPS, TLR4 and infectious disease diversity. Nat Rev Microbiol **3:**36-46.

216. **Mingari, M. C., C. Vitale, C. Cantoni, R. Bellomo, M. Ponte, F. Schiavetti, S. Bertone, A. Moretta, and L. Moretta.** 1997. Interleukin-15-induced maturation of human natural killer cells from early thymic precursors: selective expression of CD94/NKG2-A as the only HLA class I-specific inhibitory receptor. Eur J Immunol **27:**1374-1380.

217. **Miyazaki, S., F. Ishikawa, T. Fujikawa, S. Nagata, and K. Yamaguchi.** 2004. Intraperitoneal injection of lipopolysaccharide induces dynamic migration of Gr-1high polymorphonuclear neutrophils in the murine abdominal cavity. Clin Diagn Lab Immunol **11:**452-457.

218. **Miyazaki, S., F. Ishikawa, K. Shimizu, T. Ubagai, P. H. Edelstein, and K. Yamaguchi.** 2007. Gr-1high polymorphonuclear leukocytes and NK cells act via IL-15 to clear intracellular Haemophilus influenzae in experimental murine peritonitis and pneumonia. J Immunol **179:**5407-5414.

219. **Mocchegiani, E., and M. Malavolta.** 2004. NK and NKT cell functions in immunosenescence. Aging Cell **3:**177-184.

220. **Moncada, S., and E. A. Higgs.** 1991. Endogenous nitric oxide: physiology, pathology and clinical relevance. Eur J Clin Invest **21:**361-374.

221. **Moncada, S., R. M. Palmer, and E. A. Higgs.** 1991. Nitric oxide: physiology, pathophysiology, and pharmacology. Pharmacol Rev **43:**109-142.

222. **Monkkonen, J., and T. D. Heath.** 1993. The effects of liposome-encapsulated and free clodronate on the growth of macrophage-like cells in vitro: the role of calcium and iron. Calcif Tissue Int **53:**139-146.

223. **Montminy, S. W., N. Khan, S. McGrath, M. J. Walkowicz, F. Sharp, J. E. Conlon, K. Fukase, S. Kusumoto, C. Sweet, K. Miyake, S. Akira, R. J. Cotter, J. D. Goguen, and E. Lien.** 2006. Virulence factors of Yersinia pestis are overcome by a strong lipopolysaccharide response. Nat Immunol **7:**1066-1073.

224. **Moore, T. A., U. von Freeden-Jeffry, R. Murray, and A. Zlotnik.** 1996. Inhibition of gamma delta T cell development and early thymocyte maturation in IL-7 -/- mice. J Immunol **157:**2366-2373.

225. **Moretta, L., and A. Moretta.** 2004. Unravelling natural killer cell function: triggering and inhibitory human NK receptors. Embo J **23:**255-259.

226. **Motin, V. L., A. M. Georgescu, J. P. Fitch, P. P. Gu, D. O. Nelson, S. L. Mabery, J. B. Garnham, B. A. Sokhansanj, L. L. Ott, M. A. Coleman, J. M. Elliott, L. M. Kegelmeyer, A. J. Wyrobek, T. R. Slezak, R. R. Brubaker, and E. Garcia.** 2004. Temporal global changes in gene expression during temperature transition in Yersinia pestis. J Bacteriol **186:**6298-6305.

227. **Motin, V. L., R. Nakajima, G. B. Smirnov, and R. R. Brubaker.** 1994. Passive immunity to yersiniae mediated by anti-recombinant V antigen and protein A-V antigen fusion peptide. Infect Immun **62:**4192-4201.

228. **Mukherjee, S., G. Keitany, Y. Li, Y. Wang, H. L. Ball, E. J. Goldsmith, and K. Orth.** 2006. Yersinia YopJ acetylates and inhibits kinase activation by blocking

phosphorylation. Science **312:**1211-1214.

229. **Nagendra, S., and A. J. Schlueter.** 2004. Absence of cross-reactivity between murine Ly-6C and Ly-6G. Cytometry A **58:**195-200.

230. **Naik, S. H., D. Metcalf, A. van Nieuwenhuijze, I. Wicks, L. Wu, M. O'Keeffe, and K. Shortman.** 2006. Intrasplenic steady-state dendritic cell precursors that are distinct from monocytes. Nat Immunol **7:**663-671.

231. **Nakajima, R., V. L. Motin, and R. R. Brubaker.** 1995. Suppression of cytokines in mice by protein A-V antigen fusion peptide and restoration of synthesis by active immunization. Infect Immun **63:**3021-3029.

232. **Nemeth, E., A. W. Baird, and C. O'Farrelly.** 2009. Microanatomy of the liver immune system. Semin Immunopathol **31:**333-343.

233. **Nilles, M. L., K. A. Fields, and S. C. Straley.** 1998. The V antigen of Yersinia pestis regulates Yop vectorial targeting as well as Yop secretion through effects on YopB and LcrG. J Bacteriol **180:**3410-3420.

234. **Orth, K., Z. Xu, M. B. Mudgett, Z. Q. Bao, L. E. Palmer, J. B. Bliska, W. F. Mangel, B. Staskawicz, and J. E. Dixon.** 2000. Disruption of signaling by Yersinia effector YopJ, a ubiquitin-like protein protease. Science **290:**1594-1597.

235. **Osterholzer, J. J., J. L. Curtis, T. Polak, T. Ames, G. H. Chen, R. McDonald, G. B. Huffnagle, and G. B. Toews.** 2008. CCR2 mediates conventional dendritic cell recruitment and the formation of bronchovascular mononuclear cell infiltrates in the lungs of mice infected with Cryptococcus neoformans. J Immunol **181:**610-620.

236. **Oynebraten, I., O. Bakke, P. Brandtzaeg, F. E. Johansen, and G. Haraldsen.** 2004. Rapid chemokine secretion from endothelial cells originates from 2 distinct compartments. Blood **104:**314-320.

237. **Oyston, P. C., N. Dorrell, K. Williams, S. R. Li, M. Green, R. W. Titball, and B. W. Wren.** 2000. The response regulator PhoP is important for survival under conditions of macrophage-induced stress and virulence in Yersinia pestis. Infect Immun **68:**3419-3425.

238. **Palframan, R. T., S. Jung, G. Cheng, W. Weninger, Y. Luo, M. Dorf, D. R. Littman, B. J. Rollins, H. Zweerink, A. Rot, and U. H. von Andrian.** 2001. Inflammatory chemokine transport and presentation in HEV: a remote control mechanism for monocyte recruitment to lymph nodes in inflamed tissues. J Exp Med **194:**1361-1373.

239. **Parent, M. A., K. N. Berggren, L. W. Kummer, L. B. Wilhelm, F. M. Szaba, I. K. Mullarky, and S. T. Smiley.** 2005. Cell-mediated protection against pulmonary Yersinia pestis infection. Infect Immun **73:**7304-7310.

240. **Parent, M. A., L. B. Wilhelm, L. W. Kummer, F. M. Szaba, I. K. Mullarky, and S. T. Smiley.** 2006. Gamma interferon, tumor necrosis factor alpha, and nitric oxide synthase 2, key elements of cellular immunity, perform critical protective functions during humoral defense against lethal pulmonary Yersinia pestis infection. Infect Immun **74:**3381-3386.

241. **Parkhill, J., B. W. Wren, N. R. Thomson, R. W. Titball, M. T. Holden, M. B. Prentice, M. Sebaihia, K. D. James, C. Churcher, K. L. Mungall, S. Baker, D. Basham, S. D. Bentley, K. Brooks, A. M. Cerdeno-Tarraga, T. Chillingworth, A. Cronin, R. M. Davies, P. Davis, G. Dougan, T. Feltwell, N. Hamlin, S.**

Holroyd, K. Jagels, A. V. Karlyshev, S. Leather, S. Moule, P. C. Oyston, M. Quail, K. Rutherford, M. Simmonds, J. Skelton, K. Stevens, S. Whitehead, and B. G. Barrell. 2001. Genome sequence of Yersinia pestis, the causative agent of plague. Nature **413:**523-527.

242. **Passlick, B., D. Flieger, and H. W. Ziegler-Heitbrock.** 1989. Identification and characterization of a novel monocyte subpopulation in human peripheral blood. Blood **74:**2527-2534.

243. **Pellicci, D. G., K. J. Hammond, J. Coquet, K. Kyparissoudis, A. G. Brooks, K. Kedzierska, R. Keating, S. Turner, S. Berzins, M. J. Smyth, and D. I. Godfrey.** 2005. DX5/CD49b-positive T cells are not synonymous with CD1d-dependent NKT cells. J Immunol **175:**4416-4425.

244. **Penna, G., S. Sozzani, and L. Adorini.** 2001. Cutting edge: selective usage of chemokine receptors by plasmacytoid dendritic cells. J Immunol **167:**1862-1866.

245. **Perry, R. D., and J. D. Fetherston.** 1997. Yersinia pestis--etiologic agent of plague. Clin Microbiol Rev **10:**35-66.

246. **Pettersson, J., A. Holmstrom, J. Hill, S. Leary, E. Frithz-Lindsten, A. von Euler-Matell, E. Carlsson, R. Titball, A. Forsberg, and H. Wolf-Watz.** 1999. The V-antigen of Yersinia is surface exposed before target cell contact and involved in virulence protein translocation. Mol Microbiol **32:**961-976.

247. **Philipovskiy, A. V., and S. T. Smiley.** 2007. Vaccination with live Yersinia pestis primes CD4 and CD8 T cells that synergistically protect against lethal pulmonary Y. pestis infection. Infect Immun **75:**878-885.

248. **Pilsl, H., H. Killmann, K. Hantke, and V. Braun.** 1996. Periplasmic location of the pesticin immunity protein suggests inactivation of pesticin in the periplasm. J Bacteriol **178:**2431-2435.

249. **Plow, E. F., T. A. Haas, L. Zhang, J. Loftus, and J. W. Smith.** 2000. Ligand binding to integrins. J Biol Chem **275:**21785-21788.

250. **Polentarutti, N., P. Allavena, G. Bianchi, G. Giardina, A. Basile, S. Sozzani, A. Mantovani, and M. Introna.** 1997. IL-2-regulated expression of the monocyte chemotactic protein-1 receptor (CCR2) in human NK cells: characterization of a predominant 3.4-kilobase transcript containing CCR2B and CCR2A sequences. J Immunol **158:**2689-2694.

251. **Pollitzer, R.** 1954. Plague. World Health Organization, Geneva,.

252. **Prudencio, M., A. Rodriguez, and M. M. Mota.** 2006. The silent path to thousands of merozoites: the Plasmodium liver stage. Nat Rev Microbiol **4:**849-856.

253. **Pujol, C., and J. B. Bliska.** 2003. The ability to replicate in macrophages is conserved between Yersinia pestis and Yersinia pseudotuberculosis. Infect Immun **71:**5892-5899.

254. **Pujol, C., and J. B. Bliska.** 2005. Turning Yersinia pathogenesis outside in: subversion of macrophage function by intracellular yersiniae. Clin Immunol **114:**216-226.

255. **Pujol, C., K. A. Klein, G. A. Romanov, L. E. Palmer, C. Cirota, Z. Zhao, and J. B. Bliska.** 2009. Yersinia pestis can reside in autophagosomes and avoid xenophagy in murine macrophages by preventing vacuole acidification. Infect Immun **77:**2251-2261.

256. **Qu, C., E. W. Edwards, F. Tacke, V. Angeli, J. Llodra, G. Sanchez-Schmitz, A. Garin, N. S. Haque, W. Peters, N. van Rooijen, C. Sanchez-Torres, J. Bromberg, I. F. Charo, S. Jung, S. A. Lira, and G. J. Randolph.** 2004. Role of CCR8 and other chemokine pathways in the migration of monocyte-derived dendritic cells to lymph nodes. J Exp Med **200:**1231-1241.

257. **Qualls, J. E., A. M. Kaplan, N. van Rooijen, and D. A. Cohen.** 2006. Suppression of experimental colitis by intestinal mononuclear phagocytes. J Leukoc Biol **80:**802-815.

258. **Racanelli, V., and B. Rehermann.** 2006. The liver as an immunological organ. Hepatology **43:**S54-62.

259. **Ramos, C. D., C. Canetti, J. T. Souto, J. S. Silva, C. M. Hogaboam, S. H. Ferreira, and F. Q. Cunha.** 2005. MIP-1alpha[CCL3] acting on the CCR1 receptor mediates neutrophil migration in immune inflammation via sequential release of TNF-alpha and LTB4. J Leukoc Biol **78:**167-177.

260. **Raulet, D. H.** 2003. Roles of the NKG2D immunoreceptor and its ligands. Nat Rev Immunol **3:**781-790.

261. **Rebeil, R., R. K. Ernst, B. B. Gowen, S. I. Miller, and B. J. Hinnebusch.** 2004. Variation in lipid A structure in the pathogenic yersiniae. Mol Microbiol **52:**1363-1373.

262. **Reichel, C. A., A. Khandoga, H. J. Anders, D. Schlondorff, B. Luckow, and F. Krombach.** 2006. Chemokine receptors Ccr1, Ccr2, and Ccr5 mediate neutrophil migration to postischemic tissue. J Leukoc Biol **79:**114-122.

263. **Reichel, C. A., M. Rehberg, P. Bihari, C. M. Moser, S. Linder, A. Khandoga, and F. Krombach.** 2008. Gelatinases mediate neutrophil recruitment in vivo: evidence for stimulus specificity and a critical role in collagen IV remodeling. J Leukoc Biol **83:**864-874.

264. **Reichel, C. A., M. Rehberg, M. Lerchenberger, N. Berberich, P. Bihari, A. G. Khandoga, S. Zahler, and F. Krombach.** 2009. Ccl2 and Ccl3 mediate neutrophil recruitment via induction of protein synthesis and generation of lipid mediators. Arterioscler Thromb Vasc Biol **29:**1787-1793.

265. **Reisner, B. S., and S. C. Straley.** 1992. Yersinia pestis YopM: thrombin binding and overexpression. Infect Immun **60:**5242-5252.

266. **Riches, A. C., J. G. Sharp, D. B. Thomas, and S. V. Smith.** 1973. Blood volume determination in the mouse. J Physiol **228:**279-284.

267. **Rittig, M. G., A. Kaufmann, A. Robins, B. Shaw, H. Sprenger, D. Gemsa, V. Foulongne, B. Rouot, and J. Dornand.** 2003. Smooth and rough lipopolysaccharide phenotypes of Brucella induce different intracellular trafficking and cytokine/chemokine release in human monocytes. J Leukoc Biol **74:**1045-1055.

268. **Robinson, R. T., S. A. Khader, R. M. Locksley, E. Lien, S. T. Smiley, and A. M. Cooper.** 2008. Yersinia pestis evades TLR4-dependent induction of IL-12(p40)2 by dendritic cells and subsequent cell migration. J Immunol **181:**5560-5567.

269. **Rogers, M. J., R. G. Russell, G. M. Blackburn, M. P. Williamson, and D. J. Watts.** 1992. Metabolism of halogenated bisphosphonates by the cellular slime mould Dictyostelium discoideum. Biochem Biophys Res Commun **189:**414-423.

270. **Rollins, B. J.** 1997. Chemokines. Blood **90:**909-928.

271. **Rollins, B. J., T. Yoshimura, E. J. Leonard, and J. S. Pober.** 1990. Cytokine-activated human endothelial cells synthesize and secrete a monocyte chemoattractant, MCP-1/JE. Am J Pathol **136:**1229-1233.

272. **Romani, L., A. Mencacci, E. Cenci, G. Del Sero, F. Bistoni, and P. Puccetti.** 1997. An immunoregulatory role for neutrophils in CD4+ T helper subset selection in mice with candidiasis. J Immunol **158:**2356-2362.

273. **Rosmarin, A. G., S. C. Weil, G. L. Rosner, J. D. Griffin, M. A. Arnaout, and D. G. Tenen.** 1989. Differential expression of CD11b/CD18 (Mo1) and myeloperoxidase genes during myeloid differentiation. Blood **73:**131-136.

274. **Rot, A., and U. H. von Andrian.** 2004. Chemokines in innate and adaptive host defense: basic chemokinese grammar for immune cells. Annu Rev Immunol **22:**891-928.

275. **Russell, P., S. M. Eley, S. E. Hibbs, R. J. Manchee, A. J. Stagg, and R. W. Titball.** 1995. A comparison of Plague vaccine, USP and EV76 vaccine induced protection against Yersinia pestis in a murine model. Vaccine **13:**1551-1556.

276. **Ruter, C., C. Buss, J. Scharnert, G. Heusipp, and M. A. Schmidt.** A newly identified bacterial cell-penetrating peptide that reduces the transcription of pro-inflammatory cytokines. J Cell Sci **123:**2190-2198.

277. **Ryan, J. C., J. Turck, E. C. Niemi, W. M. Yokoyama, and W. E. Seaman.** 1992. Molecular cloning of the NK1.1 antigen, a member of the NKR-P1 family of natural killer cell activation molecules. J Immunol **149:**1631-1635.

278. **Saikh, K. U., T. L. Kissner, B. Dyas, J. E. Tropea, D. S. Waugh, and R. G. Ulrich.** 2006. Human cytolytic T cell recognition of Yersinia pestis virulence proteins that target innate immune responses. J Infect Dis **194:**1753-1760.

279. **Saikh, K. U., T. L. Kissner, A. Sultana, G. Ruthel, and R. G. Ulrich.** 2004. Human monocytes infected with Yersinia pestis express cell surface TLR9 and differentiate into dendritic cells. J Immunol **173:**7426-7434.

280. **Sanders, S. K., S. M. Crean, P. A. Boxer, D. Kellner, G. J. LaRosa, and S. W. Hunt, 3rd.** 2000. Functional differences between monocyte chemotactic protein-1 receptor A and monocyte chemotactic protein-1 receptor B expressed in a Jurkat T cell. J Immunol **165:**4877-4883.

281. **Sauvonnet, N., I. Lambermont, P. van der Bruggen, and G. R. Cornelis.** 2002. YopH prevents monocyte chemoattractant protein 1 expression in macrophages and T-cell proliferation through inactivation of the phosphatidylinositol 3-kinase pathway. Mol Microbiol **45:**805-815.

282. **Sauvonnet, N., B. Pradet-Balade, J. A. Garcia-Sanz, and G. R. Cornelis.** 2002. Regulation of mRNA expression in macrophages after Yersinia enterocolitica infection. Role of different Yop effectors. J Biol Chem **277:**25133-25142.

283. **Schar, M., and K. F. Meyer.** 1956. Studies on immunization against plague. XV. The pathophysiologic action of the toxin of Pasteurella pestis in experimental animals. Schweiz Z Pathol Bakteriol **19:**51-70.

284. **Schecter, A. D., B. J. Rollins, Y. J. Zhang, I. F. Charo, J. T. Fallon, M. Rossikhina, P. L. Giesen, Y. Nemerson, and M. B. Taubman.** 1997. Tissue factor is induced by monocyte chemoattractant protein-1 in human aortic smooth muscle and THP-1 cells. J Biol Chem **272:**28568-28573.

285. **Schramm, R., and H. Thorlacius.** 2004. Neutrophil recruitment in mast cell-

dependent inflammation: inhibitory mechanisms of glucocorticoids. Inflamm Res **53:**644-652.

286. **Schroder, J. M.** 2000. Chemoattractants as mediators of neutrophilic tissue recruitment. Clin Dermatol **18:**245-263.

287. **Sebbane, F., D. Gardner, D. Long, B. B. Gowen, and B. J. Hinnebusch.** 2005. Kinetics of disease progression and host response in a rat model of bubonic plague. Am J Pathol **166:**1427-1439.

288. **Sebbane, F., C. Jarrett, D. Gardner, D. Long, and B. J. Hinnebusch.** 2009. The Yersinia pestis caf1M1A1 fimbrial capsule operon promotes transmission by flea bite in a mouse model of bubonic plague. Infect Immun **77:**1222-1229.

289. **Sebbane, F., C. O. Jarrett, D. Gardner, D. Long, and B. J. Hinnebusch.** 2006. Role of the Yersinia pestis plasminogen activator in the incidence of distinct septicemic and bubonic forms of flea-borne plague. Proc Natl Acad Sci U S A **103:**5526-5530.

290. **Sebbane, F., N. Lemaitre, D. E. Sturdevant, R. Rebeil, K. Virtaneva, S. F. Porcella, and B. J. Hinnebusch.** 2006. Adaptive response of Yersinia pestis to extracellular effectors of innate immunity during bubonic plague. Proc Natl Acad Sci U S A **103:**11766-11771.

291. **Sekido, N., N. Mukaida, A. Harada, I. Nakanishi, Y. Watanabe, and K. Matsushima.** 1993. Prevention of lung reperfusion injury in rabbits by a monoclonal antibody against interleukin-8. Nature **365:**654-657.

292. **Sentman, C. L., J. Hackett, Jr., T. A. Moore, M. M. Tutt, M. Bennett, and V. Kumar.** 1989. Pan natural killer cell monoclonal antibodies and their relationship to the NK1.1 antigen. Hybridoma **8:**605-614.

293. **Serbina, N. V., T. Jia, T. M. Hohl, and E. G. Pamer.** 2008. Monocyte-mediated defense against microbial pathogens. Annu Rev Immunol **26:**421-452.

294. **Serbina, N. V., T. P. Salazar-Mather, C. A. Biron, W. A. Kuziel, and E. G. Pamer.** 2003. TNF/iNOS-producing dendritic cells mediate innate immune defense against bacterial infection. Immunity **19:**59-70.

295. **Sevko, A. L., N. Barysik, L. Perez, M. R. Shurin, and V. Gerein.** 2007. Differences in dendritic cell activation and distribution after intravenous, intraperitoneal, and subcutaneous injection of lymphoma cells in mice. Adv Exp Med Biol **601:**257-264.

296. **Shao, F., P. M. Merritt, Z. Bao, R. W. Innes, and J. E. Dixon.** 2002. A Yersinia effector and a Pseudomonas avirulence protein define a family of cysteine proteases functioning in bacterial pathogenesis. Cell **109:**575-588.

297. **Sharma, R. K., A. Sodhi, and H. V. Batra.** 2005. Involvement of c-Jun N-terminal kinase in rF1 mediated activation of murine peritoneal macrophages in vitro. J Clin Immunol **25:**215-223.

298. **Shaw, M. H., T. Reimer, Y. G. Kim, and G. Nunez.** 2008. NOD-like receptors (NLRs): bona fide intracellular microbial sensors. Curr Opin Immunol **20:**377-382.

299. **Shortman, K., and Y. J. Liu.** 2002. Mouse and human dendritic cell subtypes. Nat Rev Immunol **2:**151-161.

300. **Skrzypek, E., C. Cowan, and S. C. Straley.** 1998. Targeting of the Yersinia pestis YopM protein into HeLa cells and intracellular trafficking to the nucleus.

Mol Microbiol **30:**1051-1065.

301. **Skurnik, M., and J. A. Bengoechea.** 2003. The biosynthesis and biological role of lipopolysaccharide O-antigens of pathogenic Yersiniae. Carbohydr Res **338:**2521-2529.

302. **Skurnik, M., and H. Wolf-Watz.** 1989. Analysis of the yopA gene encoding the Yop1 virulence determinants of Yersinia spp. Mol Microbiol **3:**517-529.

303. **Sodeinde, O. A., and J. D. Goguen.** 1988. Genetic analysis of the 9.5-kilobase virulence plasmid of Yersinia pestis. Infect Immun **56:**2743-2748.

304. **Sodeinde, O. A., Y. V. Subrahmanyam, K. Stark, T. Quan, Y. Bao, and J. D. Goguen.** 1992. A surface protease and the invasive character of plague. Science **258:**1004-1007.

305. **Soehnlein, O., L. Lindbom, and C. Weber.** 2009. Mechanisms underlying neutrophil-mediated monocyte recruitment. Blood **114:**4613-4623.

306. **Soehnlein, O., A. Zernecke, and C. Weber.** 2009. Neutrophils launch monocyte extravasation by release of granule proteins. Thromb Haemost **102:**198-205.

307. **Sory, M. P., A. Boland, I. Lambermont, and G. R. Cornelis.** 1995. Identification of the YopE and YopH domains required for secretion and internalization into the cytosol of macrophages, using the cyaA gene fusion approach. Proc Natl Acad Sci U S A **92:**11998-12002.

308. **Spinner, J. L., J. A. Cundiff, and S. D. Kobayashi.** 2008. Yersinia pestis type-three secretion system-dependent inhibition of human polymorphonuclear leukocyte function. Infect Immun.

309. **Springer, T., G. Galfre, D. S. Secher, and C. Milstein.** 1979. Mac-1: a macrophage differentiation antigen identified by monoclonal antibody. Eur J Immunol **9:**301-306.

310. **Springer, T. A.** 1994. Traffic signals for lymphocyte recirculation and leukocyte emigration: the multistep paradigm. Cell **76:**301-314.

311. **Springer, T. A., D. Davignon, M. K. Ho, K. Kurzinger, E. Martz, and F. Sanchez-Madrid.** 1982. LFA-1 and Lyt-2,3, molecules associated with T lymphocyte-mediated killing; and Mac-1, an LFA-1 homologue associated with complement receptor function. Immunol Rev **68:**171-195.

312. **Staggs, T. M., and R. D. Perry.** 1992. Fur regulation in Yersinia species. Mol Microbiol **6:**2507-2516.

313. **Standiford, T. J., S. L. Kunkel, N. W. Lukacs, M. J. Greenberger, J. M. Danforth, R. G. Kunkel, and R. M. Strieter.** 1995. Macrophage inflammatory protein-1 alpha mediates lung leukocyte recruitment, lung capillary leak, and early mortality in murine endotoxemia. J Immunol **155:**1515-1524.

314. **Stebbins, C. E., and J. E. Galan.** 2001. Maintenance of an unfolded polypeptide by a cognate chaperone in bacterial type III secretion. Nature **414:**77-81.

315. **Stenseth, N. C., N. I. Samia, H. Viljugrein, K. L. Kausrud, M. Begon, S. Davis, H. Leirs, V. M. Dubyanskiy, J. Esper, V. S. Ageyev, N. L. Klassovskiy, S. B. Pole, and K. S. Chan.** 2006. Plague dynamics are driven by climate variation. Proc Natl Acad Sci U S A **103:**13110-13115.

316. **Straley, S. C.** 1993. Adhesins in Yersinia pestis. Trends Microbiol **1:**285-286.

317. **Straley, S. C., and W. S. Bowmer.** 1986. Virulence genes regulated at the transcriptional level by Ca2+ in Yersinia pestis include structural genes for outer

membrane proteins. Infect Immun **51:**445-454.

318. **Straley, S. C., and M. L. Cibull.** 1989. Differential clearance and host-pathogen interactions of YopE- and YopK- YopL- Yersinia pestis in BALB/c mice. Infect Immun **57:**1200-1210.

319. **Straley, S. C., and P. A. Harmon.** 1984. Yersinia pestis grows within phagolysosomes in mouse peritoneal macrophages. Infect Immun **45:**655-659.

320. **Strauss-Ayali, D., S. M. Conrad, and D. M. Mosser.** 2007. Monocyte subpopulations and their differentiation patterns during infection. J Leukoc Biol **82:**244-252.

321. **Sunderkotter, C., T. Nikolic, M. J. Dillon, N. Van Rooijen, M. Stehling, D. A. Drevets, and P. J. Leenen.** 2004. Subpopulations of mouse blood monocytes differ in maturation stage and inflammatory response. J Immunol **172:**4410-4417.

322. **Suomalainen, M., J. Haiko, P. Ramu, L. Lobo, M. Kukkonen, B. Westerlund-Wikstrom, R. Virkola, K. Lahteenmaki, and T. K. Korhonen.** 2007. Using every trick in the book: the Pla surface protease of Yersinia pestis. Adv Exp Med Biol **603:**268-278.

323. **Surgalla, M. J., and E. D. Beesley.** 1969. Congo red-agar plating medium for detecting pigmentation in Pasteurella pestis. Appl Microbiol **18:**834-837.

324. **Suto, A., H. Nakajima, N. Tokumasa, H. Takatori, S. Kagami, K. Suzuki, and I. Iwamoto.** 2005. Murine plasmacytoid dendritic cells produce IFN-gamma upon IL-4 stimulation. J Immunol **175:**5681-5689.

325. **Swirski, F. K., M. Nahrendorf, M. Etzrodt, M. Wildgruber, V. Cortez-Retamozo, P. Panizzi, J. L. Figueiredo, R. H. Kohler, A. Chudnovskiy, P. Waterman, E. Aikawa, T. R. Mempel, P. Libby, R. Weissleder, and M. J. Pittet.** 2009. Identification of splenic reservoir monocytes and their deployment to inflammatory sites. Science **325:**612-616.

326. **Tacke, F., and G. J. Randolph.** 2006. Migratory fate and differentiation of blood monocyte subsets. Immunobiology **211:**609-618.

327. **Takeda, K., H. Tsutsui, T. Yoshimoto, O. Adachi, N. Yoshida, T. Kishimoto, H. Okamura, K. Nakanishi, and S. Akira.** 1998. Defective NK cell activity and Th1 response in IL-18-deficient mice. Immunity **8:**383-390.

328. **Tam, M. A., and M. J. Wick.** 2004. Dendritic cells and immunity to Listeria: TipDCs are a new recruit. Trends Immunol **25:**335-339.

329. **Taylor, P. R., G. D. Brown, A. B. Geldhof, L. Martinez-Pomares, and S. Gordon.** 2003. Pattern recognition receptors and differentiation antigens define murine myeloid cell heterogeneity ex vivo. Eur J Immunol **33:**2090-2097.

330. **Telepnev, M. V., G. R. Klimpel, J. Haithcoat, Y. A. Knirel, A. P. Anisimov, and V. L. Motin.** 2009. Tetraacylated lipopolysaccharide of Yersinia pestis can inhibit multiple Toll-like receptor-mediated signaling pathways in human dendritic cells. J Infect Dis **200:**1694-1702.

331. **Tennenberg, S. D., and J. S. Solomkin.** 1990. Activation of neutrophils by cachectin/tumor necrosis factor: priming of N-formyl-methionyl-leucyl-phenylalanine-induced oxidative responsiveness via receptor mobilization without degranulation. J Leukoc Biol **47:**217-223.

332. **Tepper, R. I., R. L. Coffman, and P. Leder.** 1992. An eosinophil-dependent mechanism for the antitumor effect of interleukin-4. Science **257:**548-551.

333. **Thieblemont, N., L. Weiss, H. M. Sadeghi, C. Estcourt, and N. Haeffner-Cavaillon.** 1995. CD14lowCD16high: a cytokine-producing monocyte subset which expands during human immunodeficiency virus infection. Eur J Immunol **25:**3418-3424.

334. **Thompson, J. M., H. A. Jones, and R. D. Perry.** 1999. Molecular characterization of the hemin uptake locus (hmu) from Yersinia pestis and analysis of hmu mutants for hemin and hemoprotein utilization. Infect Immun **67:**3879-3892.

335. **Todd, R. F., 3rd, L. M. Nadler, and S. F. Schlossman.** 1981. Antigens on human monocytes identified by monoclonal antibodies. J Immunol **126:**1435-1442.

336. **Troidl, C., H. Mollmann, H. Nef, F. Masseli, S. Voss, S. Szardien, M. Willmer, A. Rolf, J. Rixe, K. Troidl, S. Kostin, C. Hamm, and A. Elsasser.** 2009. Classically and alternatively activated macrophages contribute to tissue remodelling after myocardial infarction. J Cell Mol Med **13:**3485-3496.

337. **Trosky, J. E., A. D. Liverman, and K. Orth.** 2008. Yersinia outer proteins: Yops. Cell Microbiol **10:**557-565.

338. **Trulzsch, K., T. Sporleder, E. I. Igwe, H. Russmann, and J. Heesemann.** 2004. Contribution of the major secreted yops of Yersinia enterocolitica O:8 to pathogenicity in the mouse infection model. Infect Immun **72:**5227-5234.

339. **Tsang, T. M., S. Felek, and E. S. Krukonis.** Ail binding to fibronectin facilitates Yersinia pestis binding to host cells and Yop delivery. Infect Immun **78:**3358-3368.

340. **Tsuda, Y., H. Takahashi, M. Kobayashi, T. Hanafusa, D. N. Herndon, and F. Suzuki.** 2004. Three different neutrophil subsets exhibited in mice with different susceptibilities to infection by methicillin-resistant Staphylococcus aureus. Immunity **21:**215-226.

341. **Une, T., and R. R. Brubaker.** 1984. In vivo comparison of avirulent Vwa- and Pgm- or Pstr phenotypes of yersiniae. Infect Immun **43:**895-900.

342. **Vaddi, K., and R. C. Newton.** 1994. Regulation of monocyte integrin expression by beta-family chemokines. J Immunol **153:**4721-4732.

343. **Vadyvaloo, V., C. Jarrett, D. E. Sturdevant, F. Sebbane, and B. J. Hinnebusch.** Transit through the flea vector induces a pretransmission innate immunity resistance phenotype in Yersinia pestis. PLoS Pathog **6:**e1000783.

344. **Van Coillie, E., J. Van Damme, and G. Opdenakker.** 1999. The MCP/eotaxin subfamily of CC chemokines. Cytokine Growth Factor Rev **10:**61-86.

345. **van Rooijen, N.** 1993. Extracellular and intracellular action of clodronate in osteolytic bone diseases? A hypothesis. Calcif Tissue Int **52:**407-410.

346. **Van Rooijen, N., and A. Sanders.** 1994. Liposome mediated depletion of macrophages: mechanism of action, preparation of liposomes and applications. J Immunol Methods **174:**83-93.

347. **Velan, B., E. Bar-Haim, A. Zauberman, E. Mamroud, A. Shafferman, and S. Cohen.** 2006. Discordance in the effects of Yersinia pestis on the dendritic cell functions manifested by induction of maturation and paralysis of migration. Infect Immun **74:**6365-6376.

348. **Viboud, G. I., and J. B. Bliska.** 2001. A bacterial type III secretion system inhibits actin polymerization to prevent pore formation in host cell membranes.

Embo J **20:**5373-5382.

349. **Viboud, G. I., and J. B. Bliska.** 2005. Yersinia outer proteins: role in modulation of host cell signaling responses and pathogenesis. Annu Rev Microbiol **59:**69-89.

350. **Vollmer, W., H. Pilsl, K. Hantke, J. V. Holtje, and V. Braun.** 1997. Pesticin displays muramidase activity. J Bacteriol **179:**1580-1583.

351. **von Hundelshausen, P., F. Petersen, and E. Brandt.** 2007. Platelet-derived chemokines in vascular biology. Thromb Haemost **97:**704-713.

352. **Wagner, J. G., and R. A. Roth.** 2000. Neutrophil migration mechanisms, with an emphasis on the pulmonary vasculature. Pharmacol Rev **52:**349-374.

353. **Walzer, T., M. Dalod, S. H. Robbins, L. Zitvogel, and E. Vivier.** 2005. Natural-killer cells and dendritic cells: "l'union fait la force". Blood **106:**2252-2258.

354. **Wang, L., M. Fuster, P. Sriramarao, and J. D. Esko.** 2005. Endothelial heparan sulfate deficiency impairs L-selectin- and chemokine-mediated neutrophil trafficking during inflammatory responses. Nat Immunol **6:**902-910.

355. **Warren, H. S., B. F. Kinnear, R. L. Kastelein, and L. L. Lanier.** 1996. Analysis of the costimulatory role of IL-2 and IL-15 in initiating proliferation of resting (CD56dim) human NK cells. J Immunol **156:**3254-3259.

356. **Wattiau, P., B. Bernier, P. Deslee, T. Michiels, and G. R. Cornelis.** 1994. Individual chaperones required for Yop secretion by Yersinia. Proc Natl Acad Sci U S A **91:**10493-10497.

357. **Wattiau, P., and G. R. Cornelis.** 1993. SycE, a chaperone-like protein of Yersinia enterocolitica involved in Ohe secretion of YopE. Mol Microbiol **8:**123-131.

358. **Williamson, E. D., S. M. Eley, K. F. Griffin, M. Green, P. Russell, S. E. Leary, P. C. Oyston, T. Easterbrook, K. M. Reddin, A. Robinson, and et al.** 1995. A new improved sub-unit vaccine for plague: the basis of protection. FEMS Immunol Med Microbiol **12:**223-230.

359. **Williamson, E. D., S. M. Eley, A. J. Stagg, M. Green, P. Russell, and R. W. Titball.** 1997. A sub-unit vaccine elicits IgG in serum, spleen cell cultures and bronchial washings and protects immunized animals against pneumonic plague. Vaccine **15:**1079-1084.

360. **Winfield, M. D., T. Latifi, and E. A. Groisman.** 2005. Transcriptional regulation of the 4-amino-4-deoxy-L-arabinose biosynthetic genes in Yersinia pestis. J Biol Chem **280:**14765-14772.

361. **Wu, L., A. D'Amico, K. D. Winkel, M. Suter, D. Lo, and K. Shortman.** 1998. RelB is essential for the development of myeloid-related CD8alpha- dendritic cells but not of lymphoid-related CD8alpha+ dendritic cells. Immunity **9:**839-847.

362. **Ye, W., L. M. Zheng, J. D. Young, and C. C. Liu.** 1996. The involvement of interleukin (IL)-15 in regulating the differentiation of granulated metrial gland cells in mouse pregnant uterus. J Exp Med **184:**2405-2410.

363. **Ye, Z., E. J. Kerschen, D. A. Cohen, A. M. Kaplan, N. van Rooijen, and S. C. Straley.** 2009. Gr1+ cells control growth of YopM-negative yersinia pestis during systemic plague. Infect Immun **77:**3791-3806.

364. **Yoneyama, H., and T. Ichida.** 2005. Recruitment of dendritic cells to pathological niches in inflamed liver. Med Mol Morphol **38:**136-141.

365. **Yoshimura, T., E. A. Robinson, S. Tanaka, E. Appella, and E. J. Leonard.** 1989. Purification and amino acid analysis of two human monocyte

chemoattractants produced by phytohemagglutinin-stimulated human blood mononuclear leukocytes. J Immunol **142:**1956-1962.

366. **Yoshimura, T., N. Yuhki, S. K. Moore, E. Appella, M. I. Lerman, and E. J. Leonard.** 1989. Human monocyte chemoattractant protein-1 (MCP-1). Full-length cDNA cloning, expression in mitogen-stimulated blood mononuclear leukocytes, and sequence similarity to mouse competence gene JE. FEBS Lett **244:**487-493.

367. **Zauberman, A., S. Cohen, E. Mamroud, Y. Flashner, A. Tidhar, R. Ber, E. Elhanany, A. Shafferman, and B. Velan.** 2006. Interaction of Yersinia pestis with macrophages: limitations in YopJ-dependent apoptosis. Infect Immun **74:**3239-3250.

368. **Zauberman, A., A. Tidhar, Y. Levy, E. Bar-Haim, G. Halperin, Y. Flashner, S. Cohen, A. Shafferman, and E. Mamroud.** 2009. Yersinia pestis endowed with increased cytotoxicity is avirulent in a bubonic plague model and induces rapid protection against pneumonic plague. PLoS One **4:**e5938.

369. **Zauberman, A., B. Velan, E. Mamroud, Y. Flashner, A. Shafferman, and S. Cohen.** 2007. Disparity between Yersinia pestis and Yersinia enterocolitica O:8 in YopJ/YopP-dependent functions. Adv Exp Med Biol **603:**312-320.

370. **Zhang, P., M. Skurnik, S. S. Zhang, O. Schwartz, R. Kalyanasundaram, S. Bulgheresi, J. J. He, J. D. Klena, B. J. Hinnebusch, and T. Chen.** 2008. Human dendritic cell-specific intercellular adhesion molecule-grabbing nonintegrin (CD209) is a receptor for Yersinia pestis that promotes phagocytosis by dendritic cells. Infect Immun **76:**2070-2079.

371. **Zhang, S. S., C. G. Park, P. Zhang, S. S. Bartra, G. V. Plano, J. D. Klena, M. Skurnik, B. J. Hinnebusch, and T. Chen.** 2008. Plasminogen activator Pla of Yersinia pestis utilizes murine DEC-205 (CD205) as a receptor to promote dissemination. J Biol Chem **283:**31511-31521.

372. **Zhou, D., Z. Tong, Y. Song, Y. Han, D. Pei, X. Pang, J. Zhai, M. Li, B. Cui, Z. Qi, L. Jin, R. Dai, Z. Du, J. Wang, Z. Guo, J. Wang, P. Huang, and R. Yang.** 2004. Genetics of metabolic variations between Yersinia pestis biovars and the proposal of a new biovar, microtus. J Bacteriol **186:**5147-5152.

373. **Zhou, J., S. A. Stohlman, D. R. Hinton, and N. W. Marten.** 2003. Neutrophils promote mononuclear cell infiltration during viral-induced encephalitis. J Immunol **170:**3331-3336.

VITA

Zhan Ye

Personal Information

Date of Birth   **07/01/1974, Zhengzhou, China**

Education

2004~Present   **Graduate Student**
Department of Microbiology, Immunology and Molecular Genetics
University of Kentucky, USA

1999~ 2002   **Master of Science**
Department of Biochemistry and Molecular Biology
Shanghai Jiao Tong University, School of medicine, China

1994~1999   **Bachelor of Medicine in Medicine**
Zhengzhou University Medical School, China

Professional Experience

2002~2003   **Project Manager,**
Shanghai Genomics, INC., Shanghai, China

Awards and Honor

2009~2010   **Dissertation Year Fellowship,**
University of Kentucky

2008~2009   **Presidential Fellowship Award,**
University of Kentucky

June, 2008   **ASM (American Society for Microbiology)**
Corporate Activities Program Student Travel Grants

Publication and Manuscript

Z. Ye, E.J. Kerschen, D.A. Cohen, A.M. Kaplan, N.V. Rooijen and S.C. Straley Gr1+ Cells Control Growth of YopM-Negative *Yersinia pestis* during Systemic Plague. Infect Immune. 2009 September; 77(9):3791-3806

Cowan, C., A.V. Philipovskiy, C.R. Wulff-Strobel, **Z. Ye**, and S.C. Straley Anti-LcrV antibody inhibits delivery of Yops by Yersinia pestis KIM5 by directly promoting phagocytosis. Infect Immune. 2005 September; 73(9):6127-37

Z. Ye, J. Li, H. Zhao, S. Chen. Preparation and identification of hVEGF modified genetically monoclonal engineering cell. Journal of Surgery Concepts and Practice, 2006 January; 11(1): 49-53

J. Li, **Z. Ye**, H. Zhao, S. Chen. Transfection of foreign DNA into NIH3T3 cell mediated by cationic liposome. Academic Journal of Shanghai Second Medical University, 2005 October; 25(10):1025-1029

Z. Ye, J. Li, H. Zhao, G. Qian. The structure and function of FGFRs. (Review) Academic Journal of Shanghai Second Medical University, 2003 March; 23(2):176-179

X. Li, Y. Xu, **Z. Ye**, Z. Wang, A. Xia, S. Chen, G. Qian. The expression of GFP reporter gene driven by different promoters in tumor cells regulated by ionizing radiation. Academic Journal of Shanghai Second Medical University, 2003 January; 23(1):5-9

Conference and Presentation

Z. Ye, D.A. Cohen, A.M. Kaplan, and S.C. Straley. Yersinia pestis YopM targets PMNs early in systemic plague. 108th General meeting of ASM (American Society for Microbiology), Jun 1st-5th 2008, Boston, MA

Z. Ye, D.A. Cohen, A.M. Kaplan, and S.C. Straley. Hunting the immune cell targets of YopM in early-stage systemic plague. Autumn Immunology Conference, Nov. 16th-19th 2007, Chicago, IL

Z. Ye, J. Li, H. Zhao, G. Qian. Preparation and Identification of hVEGF Monoclonal Cell Clone and Research of Its Application in Gene Therapy for Burns (in Chinese) The 8th National Conference of the Gene Structure, Expression and Regulation, July 26th-29th 2002, Harbin, China